

# UNIVERSITÉ DE STRASBOURG



#### ÉCOLE DOCTORALE DES SCIENCES CHIMIQUES

UPR 3572 – Immunologie, Immunopathologie et Chimie Thérapeutique

# THÈSE présentée par :

### Chloé GUILBAUD-CHÉREAU

soutenue le : 23 Octobre 2020

pour obtenir le grade de : Docteur de l'université de Strasbourg

Discipline/ Spécialité: Chimie biologique et thérapeutique

# Development of supramolecular medical hydrogels based on amino acids and dipeptides in combination with carbon nanomaterials

THÈSE dirigée par :

M. BIANCO Alberto Directeur de recherche, CNRS, Strasbourg Mme. MENARD-MOYON Cécilia Chargée de recherche, CNRS, Strasbourg

**RAPPORTEURS:** 

Mme. AUZELY-VELTY Rachel Professeure, Université de Grenoble Alpes Mme. LE VISAGE Catherine Directrice de recherche, INSERM, Nantes

**AUTRES MEMBRES DU JURY:** 

Mme. BOULMEDAIS Fouzia Directrice de recherche, CNRS, Strasbourg Chargé de recherche, CNRS, Nancy

#### **ACKNOWLEDGMENTS**

In my opinion, the choice of a laboratory to do a Ph.D. should depend on several criteria: a subject dear and close to our heart, a good working atmosphere and good supervisors. For my part, I was very lucky, I managed to have all three. All this work, and my learning, would never have been possible without all people who have crossed my path over the last few years. I would like to thank them here.

First of all, I'm grateful to Prof. Rachel Auzely-Velty, Dr. Catherine Le Visage, Dr. Fouzia Boulmedaïs and Dr. Loïc Stefan, for accepting to be members of my defense commission and for reading the manuscript.

I would like to thank the Labex CSC (Chemistry of Complex Systems) for funding my Ph.D.

I would especially like to thank my supervisors Dr. Alberto Bianco and Dr. Cécilia Ménard-Moyon, I couldn't have found better supervisors.

Alberto, thank you for allowing me to pursue my Master's project to this Ph.D. in your team and for believing in me for this project. You have given me the space I needed to learn how to manage a project while making yourself available in the difficult moments when I needed your advice and support.

Cécilia, thank you for your eternal enthusiasm and positivism. Your passion for research is communicative and you have been able to give me back the desire and the motivation when needed. Thank you also for your daily support and your many suggestions during the evolution of this project.

I would like to thank the unit research director Dr. Hélène Dumortier and the past unit research director, prof. Sylviane Muller as well as the Isis director Dr. Paolo Samorì for allowing me to complete my final year of Ph.D. in the new ISIS-2 extension.

I want to thank all the members of the I<sup>2</sup>CT unit, past and present for every moment I have shared with them and who have made these years at the IBMC a wonderful adventure. I would especially like to thank the entire research team:

Olivier Chaloin for your eternal humor, you have succeeded in making me laugh even during the difficult days; to Dinesh for your help during my beginnings and all your kind advices; to Kim, Boajin, Hazel, and Zengmei for the nice moments spent together and the help in case of need; to Tengfei and Shyiuan thanks for this wonderful year at Isis you are super office neighbors; to Lucas thanks for the many nice discussions we had in the office or in the "irradiation room" I know you are going to rock these last two years; a special thank to Shi with whom I shared these three years of Ph.D., thank for your ideas and scientific advice as well as you good mood and the Chinese meal you cooked for us, I send you all my courage for this end of thesis next month.

Many thanks to those who became my friends rather than colleagues, Cristina and Matteo for all the laugh and happy moments spent together. I especially thank Giacomo Reina for our numerous scientific and personal discussions and who made the fluorescence spectroscopy real moments of pleasure!

Last but not least, Ma Rymou, much more than a colleague and a friend, with whom I can share everything. These last two years would never have been the same without you. Thank you for all our moments of laugh in the laboratory between unsuccessful experiments, for our lunches at your home when I needed a break, for all the moments when you knew how to cheer me up and for your daily encouragement.

My thanks also go to Cathy Royer from the *in vitro* imaging platform of the Neurochemistry Center of the University of Strasbourg for her help with the transmission electron microscopy images and her good mood during each of our meetings. I want also to express my gratitude to the Dr. Rachel Schurhammer, Dr. Dominique Collin, Dr. Didier Lievremont, Dr. Catherine Grosdemange, and the Dr. Christopher Mueller, Dr. Vincent Flacher, Dr. Quentin Muller and Astrid Hoste with which I collaborated during these years. I would also like to thank Martine Heinrich and Noémie Bourgeois for their kind help for the dichroism.

Thanks to Laurène Wagner who has been a terrific intern and who has shown incredible autonomy and super positivism during these few weeks working by my side.

Going back a little further into the past, I would like to thank Dr. Nicole Grobert, for having welcomed me in her laboratory when I was a young student and with whom I discovered my passion for carbon nanomaterials. Those few months in your laboratory were one of the most beautiful experiences of my young life as a researcher and our discussions at this time motivated me to continue until my Ph.D. in this research area.

I would also like to thank Dr. Pierre-Arnaud Artola, with whom I could have pursued a career as a thermodynamic theorist if destiny had not drawn me elsewhere. It is teachers like you who make the beauty of the university. Thank you for your teaching, your piece of advice, and your friendship.

Thanks also to Dr. Valérie Berl-Bauder with whom I had the chance to teach metabolic chemistry for a whole semester. Thank you for all our discussions, for the freedom you gave me for these teachings, it was one of the most beautiful experiences of my thesis!

Many thanks to my Mom for all her support during all these years. Thank you for always believing in me, especially when I didn't. Thank you for all your love, for all your trips between Paris and Strasbourg and for being present at my side every day.

Finally, I give the biggest thanks of all to my wife, Ingrid, whose support has been spectacular. None of this would have been possible without your patience, understanding and love. Thanks for always believe in me as you do and, especially for all the patience you have shown during these last months. Thanks for making all this possible and for giving me the greatest gift during this thesis, our Arthur.

To my Mom, my source of inspiration.
(Suffering of Spasticity from December 2018)

& to my Wife. It is only through your eyes that it is important for me to shine.

#### **ABSTRACT**

Molecular self-assembly is a powerful method for the development of new supramolecular materials. Particularly, self-assembled hydrogels made of amino acids or short peptides have gained great attention in biomedical applications for drug delivery. However, supramolecular hydrogels suffer from low mechanical strength due to the non-covalent interactions within the hydrogels, which severely limit their practical applications. One solution for improving the physical and mechanical properties of physical hydrogels is to create covalent bonds within the supramolecular structure. Another possible way of reinforcing supramolecular hydrogels is to combine the physical network with a polymeric one to construct a double network (DN) hydrogel.

In this study, we have investigated the capacity of aromatic amino acid derivatives to self-assemble into hydrogels. Single and binary amino acids mixture hydrogels were obtained and oxidized carbon nanotubes or graphene oxide were incorporated in the most stable hydrogels, gel 1 (made of Fmoc-Tyr-OH/Fmoc-Tyr(Bzl)-OH) and gel 2 (Fmoc-Phe-OH/Fmoc-Tyr(Bzl)-OH). The structural and physical properties of the gels were assessed using electron microscopy and rheology. Different drug models were loaded into the hybrid hydrogels at high concentration and release studies were performed taking advantages of the photothermal properties of carbon nanomaterials under near-infrared (NIR) irradiation.

We have also extended our study to assess the capacity of Boc-diphenylananine and Boc-dityrosine and their  $\beta$  and  $\gamma$  homologues to form hydrogels. We have applied several distinct protocols to obtain hydrogels with the different dipeptides and one method based on pH variation allowed the formation of hydrogels for the three Boc-diphenylalanine homologues. We also studied their structural and physical properties as well as the incorporation of carbon nanomaterials and L-ascorbic acid as drug model and its release under NIR irradiation. In addition, preliminary tests concerning the toxicity of the dipeptide hydrogels developed on human skin samples have been performed by topical application with no apparent inflammation or sensibilization of the skin.

Finally, a series of cross-linking protocols were tested on tyrosine derivatives in order to apply the procedure to gel 1 and gel 2. All the tests suggested that the presence of a protecting group such as the Fmoc moiety prevents enzymatic or chemical cross-linking reactions. As an alternative, we designed two polymer/supramolecular double network hydrogels with polyacrylamide or agarose. Oxidized carbon nanomaterials were added to the DN hydrogels to study the release properties of baclofen, prescribed against muscle spasticity, under NIR irradiation. These new classes of DN hydrogels could find applications in the development of new treatment for spasticity to complement or replace current treatment methods.

## **INDEX**

ACKNO	WLEDGI	MENTS	I
ABSTRA	<b>\CT</b>		V
INDEX.			VII
ACRON	YMS AN	D ABBREVIATIONS	XI
RESUM	E DE THI	SE	XIII
СНАРТЕ	ER 1. INT	RODUCTION	1
1.1	Hydro	gels for drug delivery	1
1.1 1.2 1.2 1.2	1.2 Phy 1.3 Supral 2.1 Influ 2.2 Influ 2.3 Hor Charal 3.1 The 3.2 pH-	mically cross-linked hydrogels	
		trical sensitive hydrogels	
1.4	Strate	gies for the rigidification of supramolecular amino acid- and sma	II peptide-
based	d hydrog	els	19
1.4 1.5 1.5 1.5	4.2 Ford Hybrid 5.1 Hyb 5.2 Pro	mical cross linking of amino acids	
1.6		tives of the Thesis	
1.7	•	ences	
		IINO ACID-BASED SUPRAMOLECULAR HYDROGELS IN COMBINAIS	
		MATERIALS	
2.1	Introd	uction	38

2.2	Objectives	39
2.3	Results and discussion	39
2.3	3.1 Self-assembly of aromatic amino acids	39
2.3	3.2 Hydrogel formation	
2.3	3.3 Formation of hybrid hydrogels containing carbon nanomaterials	46
2.3	3.4 Structural characterization	47
2.3	3.5 Circular dichroism	50
2.3	3.6 Mechanical properties	
	3.7 Computational analysis	
	3.8 Photothermal properties	
	3.9 Drug loading properties	
	2.3.9.1 Incorporation of hydrophobic drug models: rhodamine B or	
	blue2.3.9.2 Incorporation of hydrophilic drug model: L-ascorbic acid	
	3.10 Drug release	
	2.3.10.1 Release of hydrophobic drug models: rhodamine B and methylen	
	2.3.10.2 Release of a hydrophilic drug model: L-ascorbic acid	
	, , ,	
2.4	Conclusion	
2.5	References	70
CHAPTI	ER 3. PREPARATION OF HYDROGELS BASED ON DIPEPTIDES	75
3.1	Introduction	75
3.2	Objectives	76
3.3	Results and discussion	76
3.5	3.1 Self-assembly	76
	3.2 Hydrogels synthesis	
	3.3 Formation of hybrid hydrogels containing carbon nanomaterials	
	3.4 Structural characterization	
3.3	3.5 Circular dichroism	86
<b>3.</b> 3	3.6 Photothermal properties	88
3.3	3.7 Drug loading	89
3.3	3.8 Drug release	
<i>3.</i> 3	3.9 Skin sensibility for topical application	
3.4	Conclusion	93
3.5	References	93
СНАРТІ	ER 4. STRATEGIES FOR HYDROGEL RIGIDIFICATION: TYROSINE CROSS-LIN	IKING AND
DOUBL	E NETWORK HYDROGELS	96
4.1	Introduction	96
4.2	Objectives	97
4.3	Results and discussion	97

	4.3.1	Cross-linking using horseradish peroxidase	97
	4.3.2	Cross-linking using Fenton, Fenton-like and photo-Fenton reactions	
	4.3.3	Cross-linking using Fremy's salt	105
	4.3.4	Cross-linking using tyrosinase	106
	4.3.5	Photo cross-linking using phenylalanine and tyrosine derivatives	109
	4.3.6	Synthesis of double network hydrogel based on amino acids	and
	polyac	rylamide	112
	4.3.7	Synthesis of double network hydrogel based on amino acids and agarose	114
	4.3.8	Formation of hybrid DN hydrogels containing carbon nanomaterials	115
	4.3.9	Incorporation of the drug baclofen	116
	4.3.10	Photothermal profile of PAA/amino acid DN hydrogels	118
	4.3.11	Water and drug release from PAA/amino acid DN hydrogels	120
		Photothermal profile of agarose/amino acid DN hydrogels	
	4.3.13	Water and drug release of agarose/amino acid DN hydrogels	123
	4.4 C	onclusion	125
	4.5 R	eferences	126
C	HAPTER 5	. CONCLUSION AND PERSPECTIVES	130
	5.1 C	onclusion	130
	5.2 P	erspectives	132
C		EXPERIMENTAL SECTION	
		1aterials and Methods	
	6.1.1	Amino acids	
	6.1.2	Dipeptides	
	6.1.3	Carbon nanomaterials	
	6.1.4	Chemicals and solvents	
	6.1.5	Characterization methods and instruments	
	а	Sonication	
	b	. High performance liquid chromatography	134
	C.	UV-Vis-NIR spectroscopy	134
	d	. Transmission electron microscopy	134
	е	. Scanning electron microscopy	134
	f.	Circular dichroism	135
	g	. Rheological study	135
	h		135
	6.2 E	xperimental section	136
	6.2.1	Self-assembly	136
	6.2.2	Gelation	
	a		
	b		
	C.		
	d		
	e		
	C		

f. Gelation tests using phenylalanine derivatives for photo cross-linkir
procedures
6.2.3 Incorporation of carbon nanomaterials
a. Amino acid hydrogels13
b. Dipeptide hydrogels13
c. Double network hydrogels14
6.2.4 Drug loading14
a. Amino acid hydrogels14
b. Dipeptide hydrogels14
c. Double network hydrogels14
6.2.5 Cross-linking
a. Cross-linking of L-tyrosine with HRP followed by UV-Vis spectroscopy 14
b. Cross-linking of L-tyrosine and tyrosine derivatives with HRP followed by
fluorescence spectroscopy14
c. Cross-linking of L-tyrosine and Fmoc-tyrosine with HRP followed by HPLC 14
d. Cross-linking of L-tyrosine by Fenton and photo-Fenton reactions followed by
fluorescence spectroscopy14
e. Cross-linking of L-tyrosine by Fenton and photo-Fenton reactions followed by
HPLC14
f. Cross-linking of Fmoc-tyrosine by Fenton and photo-Fenton reaction
followed by fluorescence spectroscopy14
g. Cross-linking of Fmoc-tyrosine by Fenton and photo-Fenton reaction
followed HPLC
h. Cross-linking using Fremy's salt
i. Cross-linking using tyrosinase
j. Photo cross-linking using phenylalanine derivatives
6.2.6 Photothermal studies
a. Carbon nanomaterials
b. Hydrogels
6.2.7 Drug release
a. Amino acid hydrogels
b. Dipeptide hydrogels
c. Double network hydrogels
6.2.8 Stability studies in physiological conditions
6.2.9 Skin sensibilisation
6.3 References
LIST OF PUBLICATIONS AND COMMUNICATIONS

#### **ACRONYMS AND ABBREVIATIONS**

a.u. Arbitrary unit

APS Ammonium persulfate

Asp Aspartic acid

Boc *tert*-butoxycarbonyl

Bzl Benzyl

CD Circular dichroïsm

CNTs Carbon nanotubes

DFT Density functional theory

DMEM Dulbecco's Modified Eagle Medium

DMSO Dimethyl sulfoxide

DN Double network

DNA Deoxyribonucleic acid

Fmoc Fluorenyl-9-methoxycarbonyl

G' Real part, elastic (or storage) modulus

G" Imaginary part, viscous (or loss) modulus

GdL Glucono-δ-lactone

GO Graphene oxide

HEMA Poly(2-hydroxyethyl) methacrylate

HFIP Hexafluoro-2-propanol

HPLC High performance liquid chromatography

HRP Horseradish peroxidase

IPNs Interpenetrating polymer networks

LC-MS liquid chromatography mass spectroscopy

LMWGs Low molecular weight gelators

MD Molecular dynamics

MeOH Methanol

MWCNTs Multi-walled carbon nanotubes

Nap Naphthyl

NIR Near-infrared irradiation

NMR Nuclear magnetic resonance

PAA Polyacrylamide

PEG Poly(ethylene glycol)

PEO Poly(ethylene oxide)

PNIPAAm Poly(*N*-isopropylacrylamide)

PPO Poly(propylene oxide)

RPMI Roswell Park Memorial Institute

SBF Serum bovine fetal

SEM Scanning electron microscopy

SWCNTs Single-walled carbon nanotubes

*t*Bu *tert*-butyl

TEM Transmission electron microscopy

TEMED Tetramethylethylenediamine

UV-vis Ultraviolet-visible spectroscopy

wt% Percentage by weight

Z Carboxybenzyl

#### RESUME DE THESE

#### 1. Introduction

Les hydrogels sont définis comme des gels poreux capables de stocker une importante quantité d'eau ou de liquide biologique. Ils peuvent être classés en différentes catégories : les gels physiques ou chimiques ou les gels à base de polymères de synthèse ou naturels. La capacité de stocker des molécules d'eau dépend de la présence de fonctions hydrophiles (amide, amine, carboxyle, hydroxyle, etc.) au sein des molécules ou polymères et la quantité d'eau peut varier de 10% à des milliers de fois le poids du polymère sec. Les hydrogels ont suscité énormément d'intérêt dans de nombreux domaines et en particulier dans le domaine biomédical grâce à leur structure similaire à celle de la matrice extracellulaire ainsi qu'à leurs propriétés mécaniques ajustables et leur comportement modulable.<sup>2</sup>

En particulier, les hydrogels constitués d'auto-assemblage supramoléculaire d'acides aminés ou de petits peptides ont fait l'objet d'une grande attention pour l'administration de médicaments ou l'ingénierie tissulaire grâce à leur biocompatibilité.<sup>3</sup> Cependant, leurs faibles propriétés mécaniques dues à leur forte teneur en eau et aux interactions non covalentes constituent une limitation importante. De plus, leur sensibilité à la dégradation enzymatique à l'intérieur des cellules est un autre facteur limitant pour une application à long terme.

Face à ce constat, plusieurs stratégies peuvent être envisagées pour améliorer les propriétés physiques et mécaniques des hydrogels supramoléculaires naturels. L'utilisation de peptides composés entièrement de résidus bêta et gamma dérivés de l'homologation d'acides aminés protéinogènes natifs est une approche intéressante pour le développement d'hydrogels dotés d'une résistance à la dégradation enzymatique et offrant de meilleures propriétés mécaniques. 4-6 Une autre façon possible pour renforcer les hydrogels supramoléculaires est soit de créer chimiquement des liaisons covalentes au sein du gel supramoléculaire par « cross-linking » soit de combiner le réseau physique avec un second réseau polymère pour construire un double réseau. Ces dernières années, les hydrogels hybrides incorporant des nanomatériaux carbonés tels que les nanotubes de carbone (NTC) et le graphène, ont attiré une attention croissante en raison de leur biocompatibilité et de leur grande résistance

mécanique.<sup>7,8</sup> Ces hydrogels hybrides sont utiles pour la libération de médicaments déclenchée par irradiation, grâce à la capacité des nanomatériaux carbonés à générer de la chaleur lors d'une irradiation dans le proche infrarouge (NIR).<sup>9,10</sup>

Dans ce contexte, le but de ma thèse a été de développer des hydrogels à base d'acides aminés ou de dipeptides pour le relargage de médicament photo-induit via l'incorporation de nanomatériaux carbonés. Mon projet s'est centré autour de trois stratégies : (1) le développement d'hydrogels supramoléculaires à base d'acides aminés aromatiques, (2) le développement d'hydrogels supramoléculaires à base de Boc- $\alpha$ -diphenylalanine et Boc- $\alpha$ -dityrosine et leurs homologues  $\beta$  et  $\gamma$  ainsi que (3) la création de liaisons covalentes au sein des hydrogels supramoléculaires développés par procédés de « cross-linking » ou par ajout d'un second réseau de polymère (Figure 1). Nous avons ensuite réalisé une caractérisation des structures auto-assemblées dans l'eau et des gels développés. Nous avons étudié l'incorporation de nanomatériaux carbonés et de molécules médicaments modèles ainsi que leur relargage sous irradiation infrarouge.

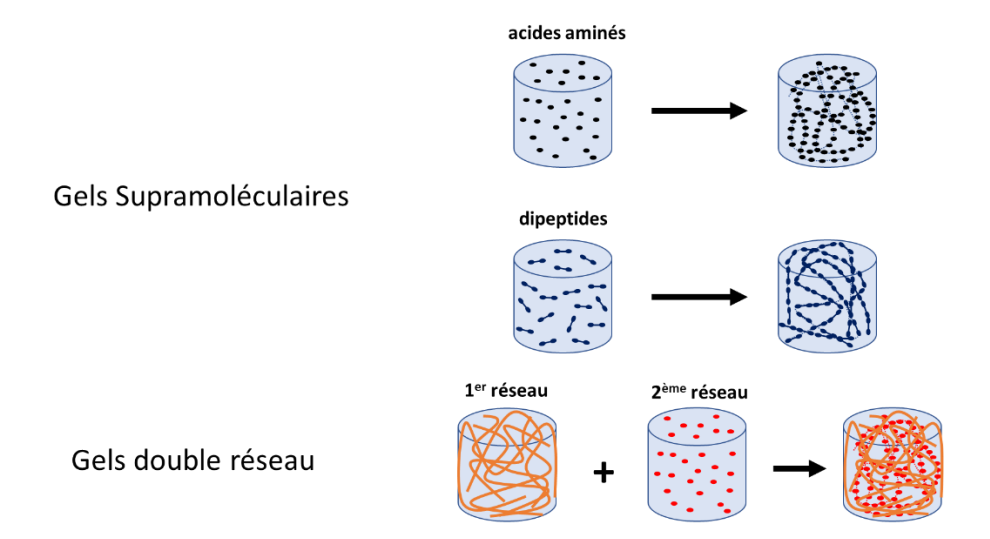


**Figure 1**. Schéma représentant la formation de gels supramoléculaires à bases d'acides aminés ou de dipeptides ou de gels à double réseau.

#### 2. Résultats et discussion

#### 2.1. Gels supramoléculaires

La capacité d'une série de mélanges binaires d'acides aminés aromatiques à former des hydrogels a tout d'abord été étudiée. Chaque acide aminé a été dissout dans du

diméthylsulfoxide (DMSO) (247 mM) et chaque mélange binaire a été réalisé en mélangeant deux solutions d'acides aminés (ratio 1:1) avant dilution dans l'eau jusqu'à une concentration finale de 4.9 mM (2.45 mM/2.45 mM) correspondant à une concentration de 2%DMSO/H<sub>2</sub>O (v/v). Parmi les hydrogels obtenus les mélanges Fmoc-Tyr-OH + Fmoc-Tyr(Bzl)-OH (gel 1) et Fmoc-Phe-OH + Fmoc-Tyr(Bzl)-OH (gel 2) ont formé les deux gels les plus stables. Des nanotubes de carbones oxydés ainsi que des feuillets d'oxyde de graphène ont été incorporés au sein de la matrice des deux hydrogels à une concentration maximale de 0.025 wt%. Les gels ont montré une structure fibrillaire que nous avons caractérisée par microscopie électronique et dichroïsme circulaire. Les propriétés mécaniques de gels 1 et 2 en présence et en absence des nanomatériaux carbonés ont été étudiées par rhéologie. Les gels 1 et 2 ont un module de rigidité similaire. L'incorporation des nanomatériaux de carbone dans le gel 1 n'a pas modifié sa rigidité ni la structure du réseau fibrillaire. Néanmoins, la cinétique de gélification a été affectée et s'est avérée fortement dépendante du type de nanomatériaux de carbone. Nous avons également effectué des simulations de dynamique moléculaire pour mettre en évidence les principales interactions qui conduisent à la formation des hydrogels. Pour les deux mélanges, les principales interactions  $\pi$ - $\pi$  sont entre le groupe aromatique de la tyrosine et le groupe protecteur Fmoc suivies par toutes les interactions où le groupe Fmoc est impliqué (Fmoc/Fmoc, Fmoc/Bzl et Fmoc/Phe) et les interactions Tyr/Tyr (Figure 2). En plus de ces attractions entre groupements aromatiques, les molécules interagissent également via des liaisons H.

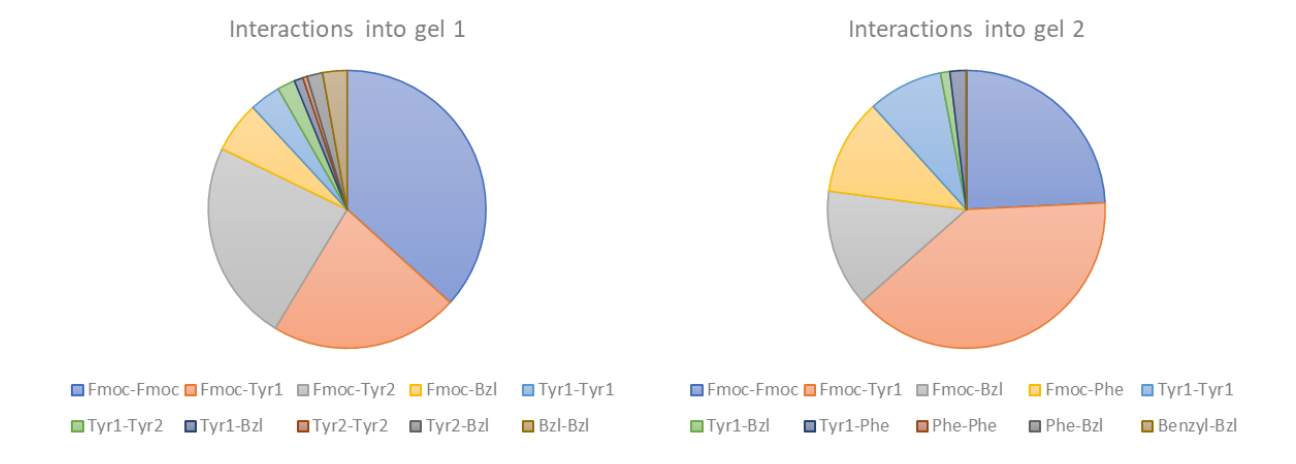


**Figure 2**. Graphique représentant la proportion d'interactions  $\pi$ - $\pi$  calculées en pourcentage pour les gels 1 et 2 par simulations de dynamique moléculaire.

L'incorporation et le relargage de plusieurs modèles médicaments (bleu de methylène, acide L-ascorbique) ou de molécules modèles (rhodamine B) ont été étudiés. Les meilleurs résultats ont été obtenus avec l'acide L-ascorbique incorporé dans les hydrogels à une concentration élevée (0.7 mg·mL<sup>-1</sup>), ce qui peut s'expliquer notamment par sa forte solubilité dans l'eau.

Nous avons étudié l'augmentation de température des gels natifs et hybrides au cours d'une irradiation NIR à 808 nm pendant 10 min à 2 W.cm<sup>-2</sup>. Pour les hydrogels hybrides composés de 0.025 wt% de nanotubes de carbone (ox-CNTs) ou de l'oxyde de graphène (GO) une forte augmentation de température a été mesurée entraînant la déstabilisation des interactions et la dégradation du gel. La libération d'eau et de médicament a été étudiée en irradiant les quatre gels hybrides contenant de la rhodamine B, du bleu de méthylène ou de l'acide L-ascorbique. Les meilleurs résultats ont été obtenus pour les gels contenant l'acide L-ascorbique. Le gel 2 + ox-CNTs s'est avéré être le système le plus efficace avec une libération maximale de médicament de 82% (Figure 3).

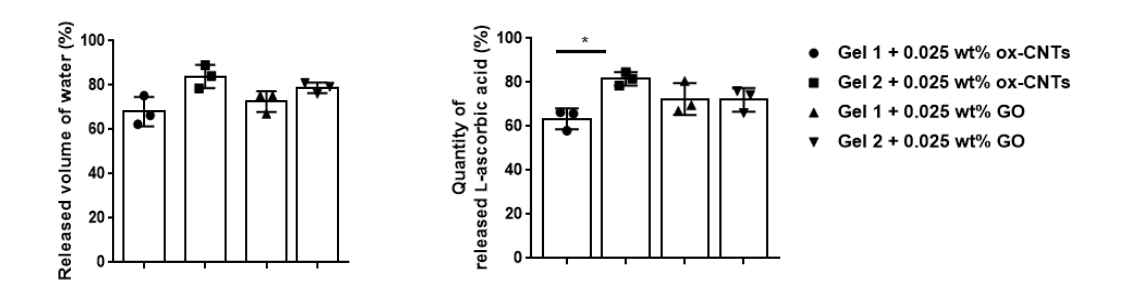


Figure 3. (gauche) Volume d'eau libérée après 10 min d'irradiation et (droite) quantité d'acide L-ascorbique libérée après 10 min d'irradiation.

En outre, nous avons effectué des expériences préliminaires de stabilité dans une solution saline physiologique (0.9% NaCl) et dans du RPMI ou du DMEM supplémenté avec 10% de sérum de veau fœtal. Ces expériences de stabilité ont montré que les gels hybrides 2 sont plus stables dans des conditions physiologiques. Ces résultats confirment le fait que le gel 2 est plus efficace que le gel 1 pour notre objectif de libération contrôlée de médicaments.

#### 2.2. Gels à base de dipeptides

Comme alternative aux acides aminés, nous avons étudié le développement d'hydrogels supramoléculaires à base de dérivés de diphénylalanine et dityrosine et de leurs homologues

β et γ protégés par un groupement Boc en position N-terminale. Nous avons développé un protocole de gélification afin d'obtenir la formation d'hydrogels pour les trois homologues Boc-α-Phe-α-Phe-OH, Boc-β-Phe-β-Phe-OH et Boc-γ-Phe-γ-Phe-OH (Figure 4).

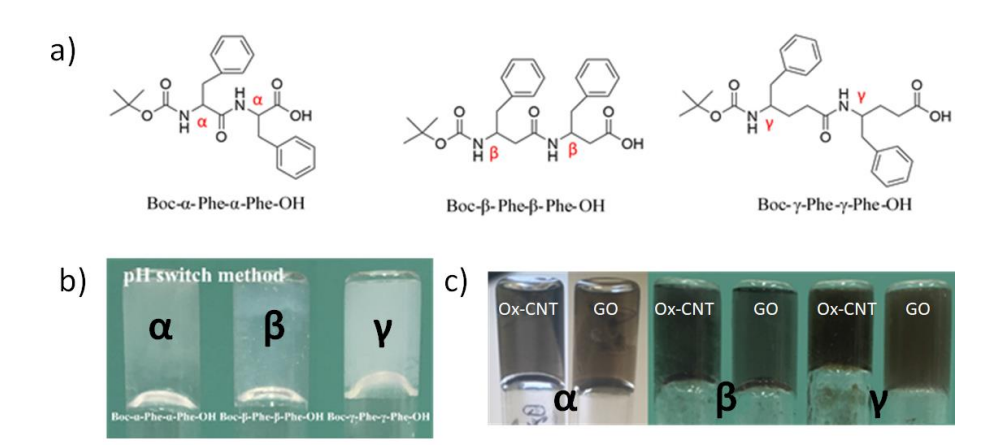


**Figure 4**. a) Structure des différents homologues de diphénylanine, b) photographies des gels obtenus à base des homologues de diphénylalanine et, c) photographies des gels après incorporation des GO et ox-CNTs.

Cette méthode de gélification consiste à dissoudre les dipeptides dans une solution basique et à déclencher la gélification par acidification. Ces gels ont l'avantage de ne pas contenir de DMSO et ainsi de favoriser leur biocompatibilité. Cependant, aucun gel n'a été obtenu à partir des homologues de Boc-dityrosine. Les trois gels ont montré une structure fibrillaire par microscopie électronique à transmission et à balayage. L'incorporation de nanotubes de carbone oxydés ou de l'oxyde de graphène a également été étudiée à la concentration de 0.025 wt% au sein des gels Boc-diphénylalanine. Des gels hybrides ont été obtenus avec les deux types de nanomatériaux carbonés pour les trois homologues (Figure 4). Les propriétés photothermiques des hydrogels ont été étudiées par mesure de l'augmentation de température sous irradiation infrarouge pendant 10 min à 2 W/cm<sup>2</sup>. Les plus grandes augmentations de température ont été obtenues pour les gels hybrides à base de Boc-α-Phe- $\alpha$ -Phe-OH et Boc- $\beta$ -Phe- $\beta$ -Phe-OH. Les gels hybrides à base de Boc- $\alpha$ -Phe- $\alpha$ -Phe-OH sont totalement déstructurés alors que les hybrides homologues beta et gamma se déstructurent partiellement avec l'apparition d'une phase liquide. De l'acide L-ascorbique a été incorporé à une concentration de 0.7 mg·mL<sup>-1</sup> dans les hydrogels hybrides hormis le gel Boc-γ-Phe-γ-Phe-OH + 0.025 wt% ox-CNTs qui se déstructure en présence du médicament modèle. L'hydrogel boc-γ-Phe-γ-Phe-OH + GO montre une plus grande quantité d'acide ι-ascorbique libérée par rapport aux différents gels hybrides Boc-β-Phe-β-Phe-OH. Le gel boc-γ-Phe-γ-Phe-OH + GO, avec sa stabilité et sa libération élevée de médicament sous irradiation infrarouge, est parmi nos gels de boc-dipeptide, le plus approprié pour les applications de libération contrôlée de médicaments.

En collaboration avec les biologistes de notre unité, nous avons étudié les propriétés sensibilisatrices et irritantes de nos gels sur peaux humaines. Un explant de peau humaine de 4 cm² de surface et de 800 μm d'épaisseur a été placé sur un filtre en nylon en RPMI à 37°C pendant 24 h en présence ou en l'absence de gel. Les échantillons de peau ont été analysés par immunofluorescence. Les marquages de la molécule d'adhésion intégrine-α6, spécifique à la lame basale, et de la filaggrine, spécifique à la couche cornée, n'ont pas révélé de différence entre l'épiderme de la peau en absence ou en présence des hydrogels de dipeptides. Nos gels à base de Boc-diphénylalanine ne semblent donc pas déclencher de réaction de sensibilisation sur la peau et ne sont pas irritants. Ils peuvent donc être envisagés pour des applications topiques.

#### 2.3. Gels à double réseaux

La faible stabilité mécanique des hydrogels supramoléculaires limite leur utilisation *in vivo*. Une solution pour améliorer les propriétés physiques et mécaniques des hydrogels physiques consiste à créer des liaisons covalentes au sein de la structure supramoléculaire. Des techniques de réticulation au sein des hydrogels supramoléculaires peuvent être réalisées en créant des liaisons entre les molécules du réseau. Un second réseau de polymères chimiques peut également être mélangé au premier réseau supramoléculaire pour former un double réseau. Afin d'envisager leur utilisation *in vivo*, nous avons étudié différentes procédures sur les gels 1 (Fmoc-Tyr-OH/Fmoc-Tyr(BzI)-OH) et 2 (Fmoc-Phe-OH/Fmoc-Tyr(BzI)-OH) préalablement développés.

Différentes techniques peuvent être utilisées pour provoquer la réticulation du réseau en fonction de la nature du monomère. En particulier, de nombreuses stratégies de « cross-linking » de résidus tyrosine ont été décrites dans la littérature. Sa réticulation peut se faire par condensation via la polymérisation des monomères par irradiation (« photo-cross-linking ») ou par polymérisation provoquée par des enzymes. La polymérisation de résidus

de tyrosine a en effet été démontrée par photo-réduction et réticulation du radical tyrosyl. 11 La réaction de réticulation est initiée par la formation du radical tyrosyl sous irradiation lumineuse qui peut ensuite se coupler avec d'autres résidus tyrosine. Le « cross-linking » des tyrosines peut également avoir lieu grâce à des catalyseurs tels que le cuivre (réactions de type Fenton) ou du ruthénium. 12,13 Des enzymes telles que la peroxydase du raifort ou la tyrosinase sont également connues pour catalyser des réactions de polymérisation oxydante de dérivés de tyrosine. 14,15 Cependant, des tests réalisés sur nos mélanges Fmoc-Tyr-OH/Fmoc-Tyr(Bzl)-OH en solution ou en gel n'ont pas permis de mettre en évidence la formation de dityrosine ou d'oligotyrosine. D'autres alternatives ont été testées comme l'incorporation de dérivés de tyrosine tels que la 4-azido-phénylalanine, la Fmoc-azidoPhe ou la Fmoc-Tyr(propargyl)-OH pour introduire de nouveaux groupements réactifs et ainsi permettre de créer de nouvelles liaisons covalentes. Ces approches n'ont également pas permis d'induire un « cross-linking » de nos gels.

Une autre approche pour former un hydrogel robuste consiste à introduire un polymère chimique dans le réseau supramoléculaire. Le polyacrylamide (PAA) est un polymère capable de former des hydrogels en absorbant une très grande quantité d'eau et est largement utilisé dans le domaine biomédical. <sup>16</sup> Une autre procédure pour développer les hydrogels DN consiste à incorporer un polymère préformé, tel que l'agarose, qui ne nécessite aucune étape de polymérisation. Les gels d'agarose sont facilement formés par un simple processus de chauffage et de refroidissement.

Différentes concentrations de PAA (0.1 % à 10 %) et d'agarose (0.1 % à 1 %) ont été testées pour améliorer les propriétés mécaniques des deux hydrogels supramoléculaires gel 1 et gel 2. En présence de PAA le gel 1 ne s'est pas formé alors que le mélange Fmoc-Phe-OH/Fmoc-Tyr(Bzl)-OH du gel 2 est stable avec du polyacrylamide dans les concentrations étudiées de 0,1 % à 10 %. alors que les gels à base de PAA uniquement se forment rapidement en moins d'une heure. Tandis que le gel 2 a une gélification rapide d'environ 2 h, la gélification du gel 2 en présence de 1 % à 10 % de PAA est plus longue (24 h). Les hydrogels DN contenant le gel 1 ou le gel 2 avec 0,1 % d'agarose se sont formés plus rapidement, en 1 h. Les hydrogels DN obtenus avec une concentration plus élevée d'agarose (0,5 % et 1 %) se sont formés en quelques secondes. Le mélange des deux réseaux permet l'obtention d'un gel non cassant,

contrairement aux gels de PAA et d'agarose purs, tout en augmentant la stabilité par rapport aux hydrogels supramoléculaires préalablement développés.

Dans le but d'étudier le relargage de médicaments, nous avons réalisé l'incorporation de baclofène au sein des différents gels à double réseau développés. Le baclofène aussi connu sous l'appellation Lioresal® est un myorelaxant agissant au niveau de la moelle épinière comme agoniste du récepteur GABA-B. 17,18 Il est prescrit contre la spasticité musculaire qui accompagne de nombreux troubles neurologiques lors d'accidents vasculaires cérébraux, de traumatismes crâniens, de lésions médullaires, de sclérose en plaques ou encore de paralysie cérébrale. Le baclofène administré par voie orale souffre d'un mauvais franchissement de la barrière hémato-méningée et d'une distribution non sélective au niveau du système nerveux central. L'obtention d'une réponse thérapeutique adéquate suppose donc des doses élevées de 30 à 80 mg par jour avec un risque d'effets secondaires importants. L'unique alternative actuelle pour réduire les doses administrées est un traitement via une pompe programmable positionnée chez le patient au niveau du rachis. La dose journalière pour un adulte est alors réduite à une concentration de 300 µg à 800 µg par jour en injection continue mais ce mode d'administration reste très invasif. Le développement d'hydrogel injectable à libération contrôlée en baclofène apparaît comme une nouvelle alternative prometteuse. (Figure 5).

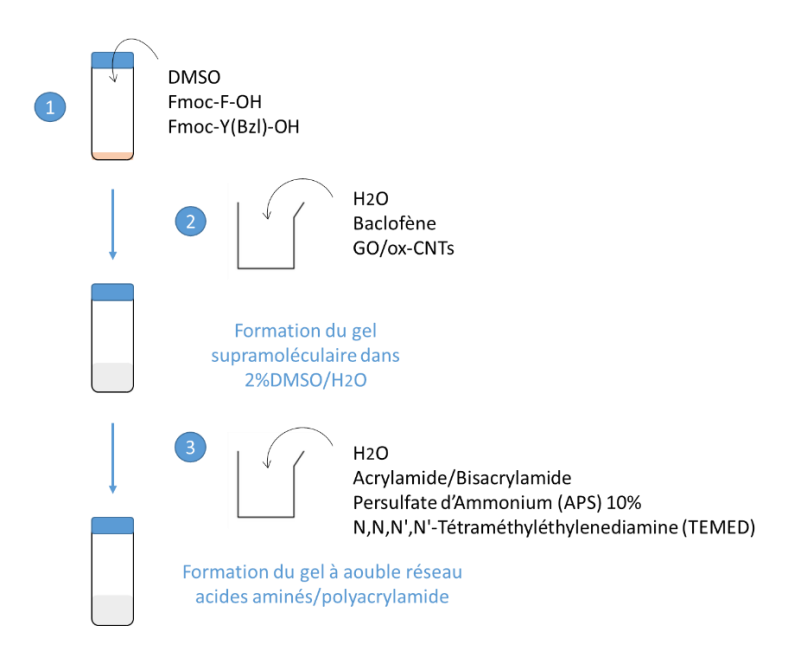


Figure 5. Schéma du protocole de synthèse des gels double réseau.

La présence du baclofène à une concentration de 1 mg·mL<sup>-1</sup> n'influence pas le temps de gélification et n'altère pas la structure stable et non cassante des différents gels développés.

Des nanotubes de carbone oxydés ainsi que des feuillets d'oxyde de graphène ont également été incorporés au sein du gel pour étudier le relargage du baclofène sous irradiation NIR. Pour cela, les nanomatériaux carbonés ont été dispersés dans l'eau en présence du baclofène avant d'être ajoutés au mélange d'acides aminés dans le DMSO suivi de l'ajout des réactifs pour la formation du PAA. Des gels hybrides stables ont ainsi été obtenus. Nous avons étudié l'augmentation de température des gels au cours d'une irradiation NIR à 808 nm de 10 min à 2 W.cm<sup>-2</sup> et mesuré la quantité d'eau et de médicament relargués.

#### 3. Conclusion

En conclusion, nous avons développé des gels supramoléculaires à base d'acides aminés aromatiques protégés par le groupement Fmoc et d'homologues de Boc-diphénylalanine. Nous avons étudié en détail la gélification des différents gels obtenus et leurs propriétés structurelles et physiques ont été évaluées à l'aide de diverses techniques microscopiques et de la rhéologie. Des gels à double réseau ont également été obtenus par introduction de PAA. Des nanotubes de carbone oxydés et de l'oxyde de graphène ont été incorporés dans ces hydrogels. La chaleur générée par les nanomatériaux de carbone lors de l'irradiation dans le proche infrarouge a induit la libération de médicaments à un taux élevé. Ces hydrogels à base d'auto-assemblage d'acides aminés offrent de nouvelles perspectives en particulier pour le développement de nouveaux biomatériaux pour le relargage de médicament.

#### 4. Références

- 1. Hoffman, A. S. Hydrogels for Biomedical Applications. Adv. Drug Delivery Rev. 2012, 64, 18–23.
- 2. Mahinroosta, M.; Jomeh Farsangi, Z.; Allahverdi, A.; Shakoori, Z. Hydrogels as Intelligent Materials: A Brief Review of Synthesis, Properties and Applications. Mater. Today Chem. 2018, 8, 42–55.
- 3. Lim, J. Y. C.; Lin, Q.; Xue, K.; Loh, X. J. Recent Advances in Supramolecular Hydrogels for Biomedical Applications. Materials Today Advances 2019, 3, 100021.
- 4. Hook, D. F.; Bindschädler, P.; Mahajan, Y. R.; Sebesta, R.; Kast, P.; Seebach, D. The Proteolytic Stability of "designed" Beta-Peptides Containing Alpha-Peptide-Bond Mimics

- and of Mixed Alpha, Beta-Peptides: Application to the Construction of MHC-Binding Peptides. Chem. Biodivers. 2005, 2 (5), 591–632.
- 5. Seebach, D.; Beck, A. K.; Bierbaum, D. J. The World of Beta- and Gamma-Peptides Comprised of Homologated Proteinogenic Amino Acids and Other Components. Chem. Biodivers. 2004, 1 (8), 1111–1239.
- β-Amino acid containing proteolitically stable dipeptide based hydrogels: encapsulation and sustained release of some important biomolecules at physiological pH and temperature. Soft Matter. 2012, 8, 3380-3386
- 7. Vashist, A.; Kaushik, A.; Vashist, A.; Sagar, V.; Ghosal, A.; Gupta, Y. K.; Ahmad, S.; Nair, M. Advances in Carbon Nanotubes—Hydrogel Hybrids in Nanomedicine for Therapeutics. Adv. Healthc Mater. 2018, 7 (9), 1701213.
- 8. Wang, P.; Huang, C.; Xing, Y.; Fang, W.; Ren, J.; Yu, H.; Wang, G. NIR-Light- and PH-Responsive Graphene Oxide Hybrid Cyclodextrin-Based Supramolecular Hydrogels. Langmuir 2019, 35 (4), 1021–1031.
- 9. Singh, R.; Torti, S. V. Carbon Nanotubes in Hyperthermia Therapy. Adv. Drug Delivery Rev. 2013, 65 (15), 2045–2060.
- 10. Marangon, I.; Ménard-Moyon, C.; Silva, A. K. A.; Bianco, A.; Luciani, N.; Gazeau, F. Synergic Mechanisms of Photothermal and Photodynamic Therapies Mediated by Photosensitizer/Carbon Nanotube Complexes. Carbon 2016, 97, 110–123.
- 11. Giulivi, C.; Traaseth, N. J.; Davies, K. J. A. Tyrosine Oxidation Products: Analysis and Biological Relevance. Amino Acids 2003, 25 (3–4), 227–232.
- 12. Choi, J.; McGill, M.; Raia, N. R.; Hasturk, O.; Kaplan, D. L. Silk Hydrogels Crosslinked by the Fenton Reaction. Adv. Healthc Mater. 2019, 8 (17), 1900644.
- 13. Ding, Y.; Li, Y.; Qin, M.; Cao, Y.; Wang, W. Photo-Cross-Linking Approach to Engineering Small Tyrosine-Containing Peptide Hydrogels with Enhanced Mechanical Stability. Langmuir 2013, 29 (43), 13299–13306.
- 14. Jin, R.; Lin, C.; Cao, A. Enzyme-Mediated Fast Injectable Hydrogels Based on Chitosan—Glycolic Acid/Tyrosine: Preparation, Characterization, and Chondrocyte Culture. Polym. Chem. 2013, 5 (2), 391–398.
- 15. Zhong, Q.-Z.; Richardson, J. J.; Li, S.; Zhang, W.; Ju, Y.; Li, J.; Pan, S.; Chen, J.; Caruso, F. Expanding the Toolbox of Metal—Phenolic Networks via Enzyme-Mediated Assembly. Angewandte Chemie International Edition 2020, 59 (4), 1711–1717.
- 16. Yang, T.-H. Recent Applications of Polyacrylamide as Biomaterials. Recent Patents on Materials Science 2008, 100, 29-40.
- 17. Pucks-Faes, E.; Dobesberger, J.; Hitzenberger, G.; Matzak, H.; Mayr, A.; Fava, E.; Genelin, E.; Saltuari, L. Intrathecal Baclofen in Hereditary Spastic Paraparesis. Front. Neurol. 2019, 10, 901-909.
- 18. Sammaraiee, Y.; Yardley, M.; Keenan, L.; Buchanan, K.; Stevenson, V.; Farrell, R. Intrathecal Baclofen for Multiple Sclerosis Related Spasticity: A Twenty Year Experience. Mult. Scler. and Relat. Disord. 2019, 27, 95–100.

#### Liste des présentations

- Guilbaud-Chéreau, C., Bianco, A., Ménard-Moyon. Amino acids based hydrogels in combination with carbon nanomaterials for controlled drug released, Colloque Francophone du Carbone, Obernai, 15-18 mai 2018, présentation orale
- Guilbaud-Chéreau, C., Bianco, A., Ménard-Moyon. Self-assembled amino acids- and peptides-based hydrogels in combination with carbon nanomaterials, Journée des doctorants de l'école doctorale des Sciences Chimiques, Strasbourg, 3 décembre 2019, présentation orale

#### <u>Liste des publications</u>

- Guilbaud-Chéreau, C.; Dinesh, B.; Schurhammer, R.; Collin, D.; Bianco, A.; Ménard-Moyon, C. Protected Amino Acid-Based Hydrogels Incorporating Carbon Nanomaterials for Near-Infrared Irradiation-Triggered Drug Release. ACS Appl. Mater. Interfaces 2019, 11 (14), 13147–13157.
- 2. Aloisi, A.; Christensen, N. J.; Sørensen, K. K.; Guilbaud-Chéreau, C.; Jensen, K. J.; Bianco, A. Synthesis and Characterization of Adamantane-Containing Heteropeptides with a Chirality Switch. European Journal of Organic Chemistry 2020, 2020 (7), 815–820.

#### **CHAPTER 1. INTRODUCTION**

#### 1.1 Hydrogels for drug delivery

Hydrogels are defined as porous systems able to retain a large amount of water or biological fluid under physiological conditions. The hydrophilicity, or capacity to capture water molecules into the gel structure, depends on the presence of hydrophilic groups such as -NH<sub>2</sub>, -COOH, -OH, -CONH<sub>2</sub>, -CONH- and SO<sub>3</sub>H, in the molecules or the polymers. The amount of water can vary from 10 % to thousands of times the weight of the dry polymer. The first hydrogel was synthesized in 1960 by Wichterle et al. from poly(2-hydroxyethyl) methacrylate (HEMA) and was used as a biomaterial for contact lenses.<sup>2</sup> Since then, many gels developed from synthetic or natural molecules have shown their potential in different fields such as food industry, cosmetics, pharmaceutical applications, environmental cleaning, etc.<sup>3</sup> Thanks to their structure similar to the extracellular matrix with a high water content, hydrogels are being applied to several biomedical applications such as drug delivery, diagnostics, tissue engineering and regenerative medicine. 4-8 Conventional drug delivery systems include oral, trans-mucosal (nasal, buccal, sublingual, vaginal or rectal) and intravenous or intramuscular routes of administration and face many limitations such as high dosage requirement, low effectiveness, toxicity and adverse side effects. To overcome these current limitations, hydrogels are being studied extensively to develop new drug delivery devices. 9-11 Their structure not only allows them to contain therapeutic molecules in their pores but it can also be modified by an external stimulus triggering drug release with spatial and temporal control through diffusion, degradation or deformation of the gel structure (Figure 1.1). With this strategy it is possible to maximize the effect of the therapeutic agent, reduce side effects and minimize drug dosage. Several hydrogels have received regulatory approval for healthcare applications such as cancer treatment (e.g., Vantas® or SpaceOAR®), aesthetic corrections (Radiesse®, Artefill®, Sculptra®, Teosyal® or Hylaform®) or spinal fusion (EUFLEXXA®, INFUSE® bone graft or osteogenic protein 1(OP-1)® implant). Some hydrogels are currently studied in clinical trials mainly for the development of soft contact lenses but also for tissue regeneration (Aquamid®'s polyacrylamide hydrogels, Gelstix®, Algisyl-LVR® device), cancer treatment (polyethylene glycol/SpaceOAR®,

polyethylene glycol/TracelT®) or incontinence (Bulkamid®'s polyacrylamide hydrogels) (Figure 1.2).

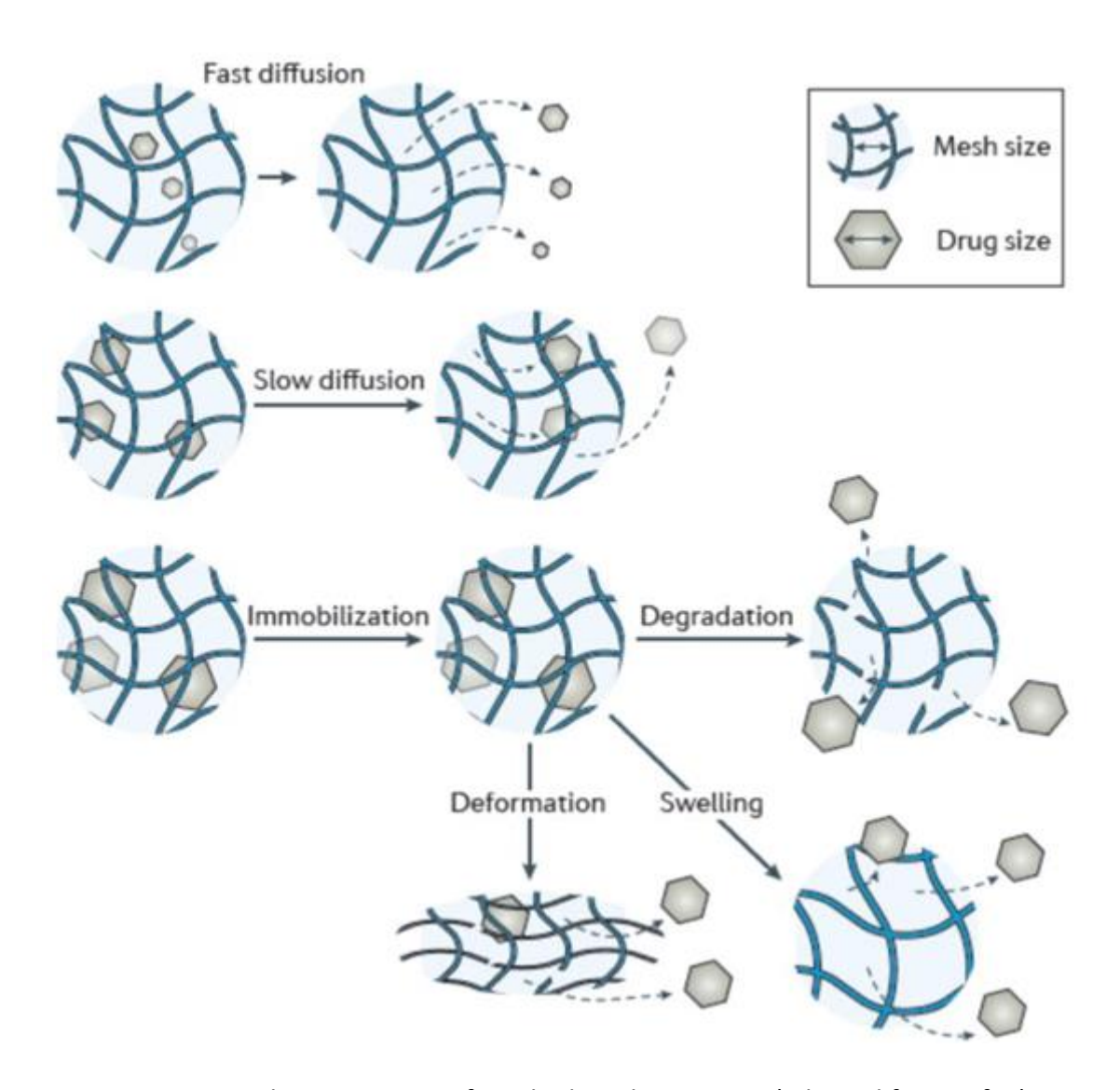


Figure 1.1. Drug release processes from hydrogel structures (adapted from ref. 9).

Although great advances have been made in this field, further progress is still needed to treat many diseases such as rheumatoid arthritis, diabetes, heart rhythm disorders or spasticity for which the drug must be able to be delivered in response to the metabolic fluctuations of patients. It is highly desirable that the drug can be administered in such a way that it precisely matches physiological needs at specific times, locations, and doses. Depending on their composition, hydrogels can have a wide range of mechanical properties that can be adapted to the different tissues and injection sites in the body. The development of research in supramolecular chemistry has made possible the design of new types of

hydrogels with tailor-made properties. In particular, gels formed from amino acids and small peptides are emerging as innovative materials and represent the future of biomedicine due to their low synthesis cost, ease of preparation, biocompatibility and biodegradation.

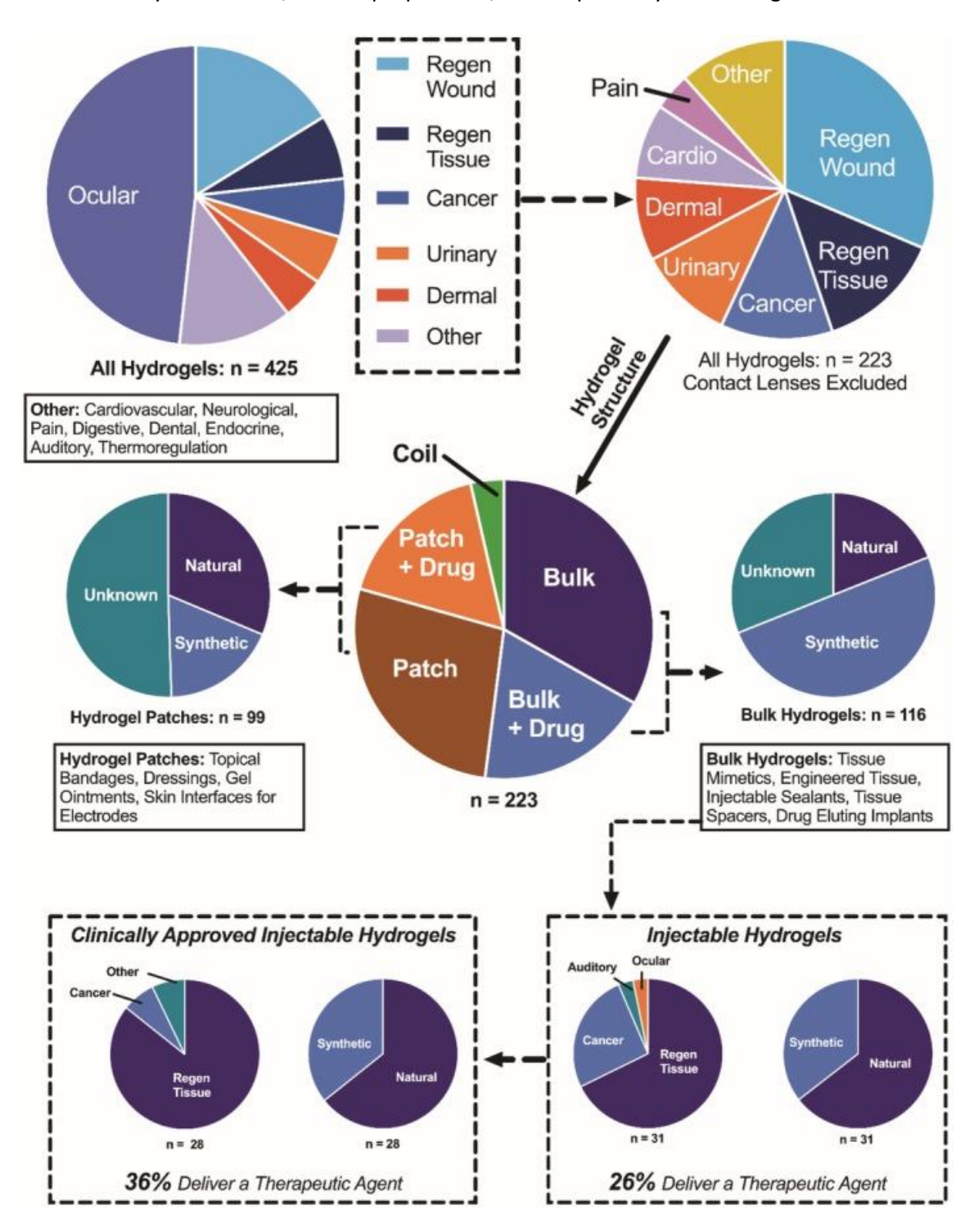


Figure 1.2. Statistical representation of hydrogels clinical applications (from ref. 12).

Hydrogels can be classified into different categories depending on several properties as represented in Figure 1.3. It is possible to divide hydrogels into groups by their structure, the type of molecules used, their ionic charge, their degradability, the method of preparation or their response to various external stimuli.<sup>8</sup> But, the most common way to classify hydrogels is probably by the type of cross-linking.

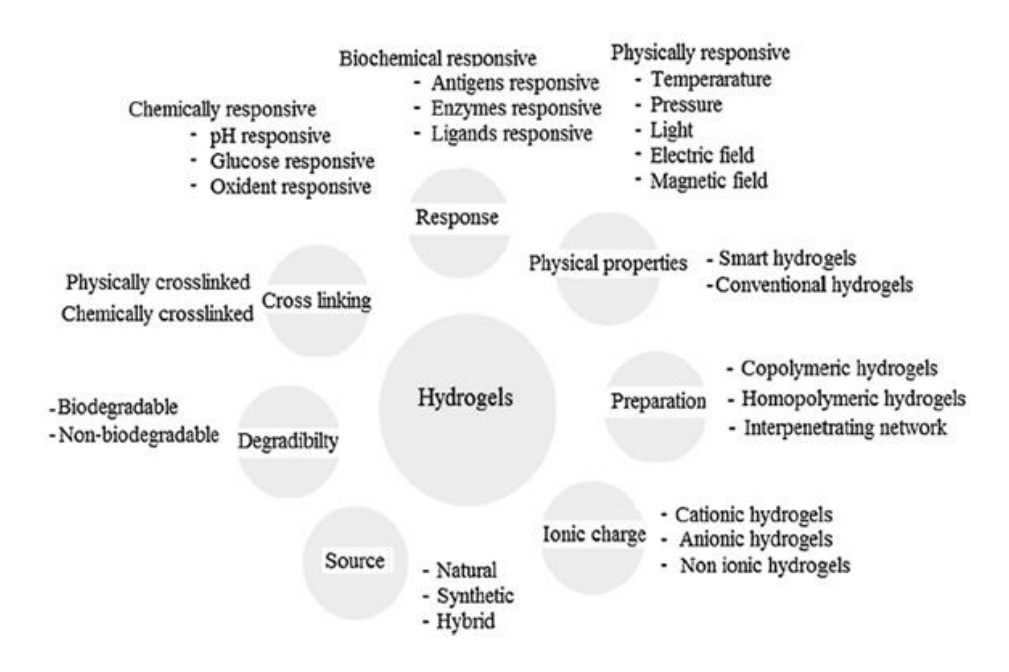


Figure 1.3. Classification of hydrogels based on the different properties (from ref. 8).

#### 1.1.1 Chemically cross-linked hydrogels

Hydrogels are called chemical gels when covalent bonds are formed between the polymer chains often resulting in high mechanical stability. Many methods have been explored for the development of chemical hydrogels. Covalent linkages between polymer chains can be established by the reaction of functional groups with complementary reactivity, such as an amine and a carboxylic acid to form an amide bond<sup>12</sup> or between an isocyanate and an amine or alcohol to form an urea or an urethane, respectively, or by a Schiff base formation between an amine and an aldehyde leading to the formation of an imine (Figure 1.4).<sup>13</sup> The formation of a hydrazone bond via the reaction of an aldehyde and a hydrazine also facilitates rapid cross-linking of gel precursors<sup>14</sup> and have the advantage of being cleavable in acidic media allowing a control of the release depending on the pH. This method has been used with hyaluronic acid cross-linked by hydrazone bonds to provide prolonged-duration local anesthesia and to control the release of drugs to the peritoneum.<sup>15</sup> Following the same

approach, hydrogels based on dextran,<sup>16</sup> poly(vinyl alcohol)<sup>17</sup> and poly(aldehyde guluronate)<sup>18</sup> have been designed as injectable systems for drug delivery to osteoblasts.

**Figure 1.4.** Example of cross-linking reactions between a) an aldehyde and an amine to form a Schiff base, b) an aldehyde and a hydrazide to form a hydrazone, c) a Michael reaction of an acrylate and either a primary amine or a thiol to from a secondary amine or a sulfide (from ref. 11).

The Michael addition between a nucleophile (*e.g.* primary amine or a thiol) and a vinyl group is also widely used for the development of cross-linked hydrogels due to its rapid reaction time, its flexibility in forming multiple types of bonds and the relative biological inertness of the polymeric precursors. The Michael addition has been used to cross-link vinyl sulfone-functionalized dextran with thiolated poly(ethylene glycol)<sup>19</sup> (PEG) or to cross-link PEG diacrylate with dithiolated PEG<sup>20</sup> or with thiolated natural polymers including hyaluronic acid, chondroitin sulfate and gelatin<sup>21</sup>. One of the most widely used method for the development of chemical cross-linked hydrogels is the radical polymerization in presence of a free radical initiator, a very efficient system that results in the rapid formation of the gels even in mild conditions. Other chemical hydrogels can be polymerized by high-energy radiation such as unsaturated compounds using gamma or electron beam radiations.<sup>22,23</sup>

Cross-linkers can also be used to produce *in situ* cross-linked hydrogels such as enzymes. Dextran-tyramine<sup>24</sup> and hyaluronic acid-tyramine<sup>25</sup> hydrogels have been prepared using horseradish peroxidase with rapid and controllable gelation time. Genipin<sup>26,27</sup> (Figure 1.5) or glutaraldehyde<sup>28</sup> that can react with amine groups have also been found to efficiently cross-link polymers into hydrogel. A disadvantage of methods using crosslinkers is the potential toxicity of unreacted compounds in the gel. For instance, glutaraldehyde is often used to form carbohydrate-based hydrogels, but it is also used as a tissue fixative.

**Figure 1.5.** Presumable reaction between genipin and chitosan derivatives leading to the formation of hydrogels (from ref. 26).

#### 1.1.2 Physically cross-linked hydrogels

Physical gels are formed from polymers interacting together by non-covalent bonds through hydrophobic interactions, hydrogen bonding, electrostatic interactions or  $\pi$ -stacking. These non-covalent interactions can be influenced by many environmental parameters such as pH or temperature. Among the different types of weak bonds at the origin of the formation of physical gels, hydrophobic interactions are occurring in most of the cases. Polymers with hydrophobic domains can expand and cross-link in aqueous medium via reverse thermal gelation also known as "sol-gel" gelation process (Figure 1.6). As the temperature is increased, hydrophobic domains aggregate to minimize the hydrophobic surface area in contact with the bulk water, thus reducing the amount of structured water surrounding the hydrophobic domains and minimizing solvent entropy. The temperature at which gelation occurs depends strongly on the polymer concentration as well as the size of the hydrophobic domains. This is the case for poly(ethylene oxide)-poly(propylene oxide)-poly(ethylene

oxide) (PEO-PPO-PEO) copolymers, the most commonly used polymer for the synthesis of heat-sensitive physical gels.<sup>8</sup>

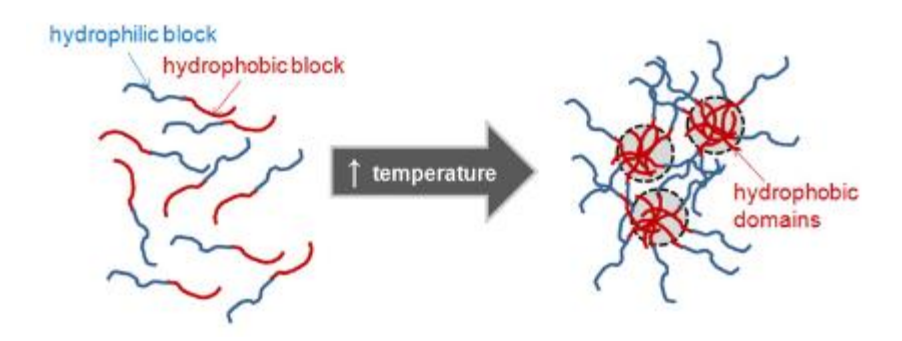
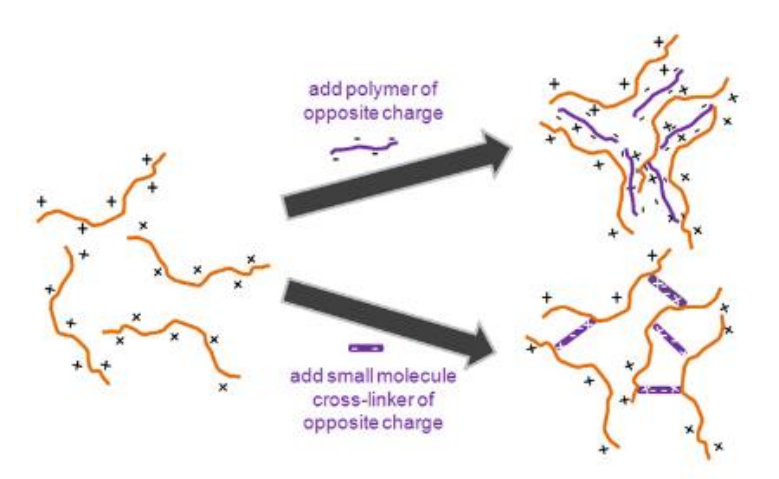


Figure 1.6. Mechanism of physical gelation driven by hydrophobic interactions (from ref. 8).

Hydrogen bonding is another type of interactions that can be used to synthesize hydrogels. Numerous natural polymers such as gelatin-agar,<sup>29</sup> starch-carboxymethyl cellulose<sup>30</sup>, and hyaluronic acid-methylcellulose<sup>31</sup> can form physical injectable gels.

Charge interactions also occur between polymers or molecules of opposite charges to form hydrogels (Figure 1.7). Recent studies have shown that hydrogels formed through electrostatic interactions are produced by various anionic and cationic polyelectrolytes, such as chitosan, cellulose, and alginate. Protonated chitosan is a linear cationic polysaccharide with primary aliphatic amines, which can electrostatically interact with anionic molecules to form gels.



**Figure 1.7.** Mechanism of physical gelation based on charge interactions with an opposite charged polymer or an oppositely charged small molecules (from ref. 8).

Carboxymethyl cellulose, a commercially available water soluble cellulose derivatives can form hydrogels through electrostatic interactions with cationic groups, such as polyethyleneimine, poly(vinyl amine) and chitosan.<sup>32-34</sup> Alginate linear polysaccharides with carboxyl groups can interact with polyelectrolytes such as chitosan, pectin, and ethyl cellulose to form hydrogels.<sup>35,36</sup> In all cases, electrostatic interactions depend on many factors such as the ratio between the opposite charges, the solvent, the pH and the temperature.

#### 1.1.3 Supramolecular hydrogels from low molecular weight hydrogelators

Within physical hydrogels, a new approach based on supramolecular chemistry has emerged in recent years for the formation of hydrogels with adjustable properties. <sup>37</sup> Supramolecular gels are physical gels composed of monomeric subunits capable of self-assembling into networks while trapping water molecules. Molecular self-assembly is a natural process used by amino acids, peptides, nucleic acids, and phospholipids to form ordered structures, for the organization of proteins into secondary and tertiary structures or nucleic acids into a double helix of DNA. This mechanism is driven by various non-covalent interactions including hydrophobic interactions, hydrogen bonding,  $\pi$ -stacking or electrostatic interactions (Figure 1.8).

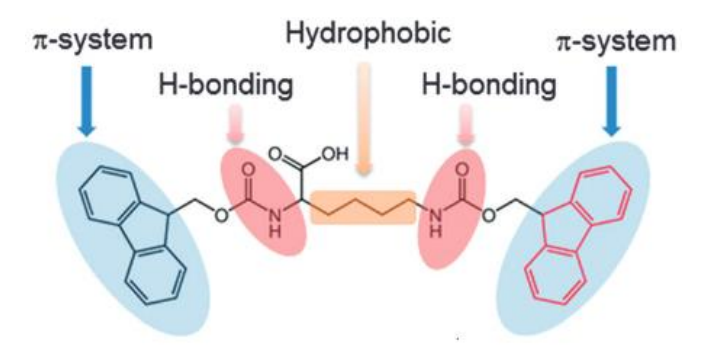


**Figure 1.8**. Representation of Fmoc-protected L-lysine showing the groups involved in self-assembly (from ref. 62).

Compared to synthetic or natural polymers, small molecules can be prepared in large quantities with a high degree of purity and a precise molecular structure. The knowledge of the structure of the molecules used allows a better understanding of the interactions leading to the gel formation. Interactions between different functional groups and solvent molecules

play an important role in the gelation mechanism but the knowledges of the mechanism of gel formation are still limited. Computational approaches using density functional theory<sup>38</sup> (DFT) or molecular dynamics (MD) simulations, <sup>38,39</sup> are increasingly explored to study the self-assembly of gelation agents, to determine the most favorable geometry of the gel state and to predict gelation. The formation of supramolecular hydrogels is usually induced by the entanglement of fibrillar structures providing a dense network that limits solvent flow. Although the self-assembly of the monomeric units of the fibrils is a prerequisite for hydrogelation, it is important to note that the self-assembly of monomers into fibrils does not necessarily leads to gelation.<sup>40</sup> Numerous studies have shown that it is possible to play on several criteria to obtain hydrogels that are assembled in aqueous medium and to modulate their mechanical properties. The formation of a supramolecular hydrogel originates from a balance between dissolution and precipitation of the hydrogelators in water. It requires adequate intermolecular interactions to form a molecular network, meanwhile the chains of the network must interact with a large amount of water molecules. Therefore, hydrogelators should possess both hydrophobic and hydrophilic moieties to achieve the essential balance for hydrogelation. Additionally, to produce supramolecular hydrogels, an appropriate perturbation of a physical or chemical state is necessary for triggering a phase transition from solution to hydrogel.

The change of temperature is the most common physical stimulus to trigger the formation of a supramolecular hydrogel.  $^{41-48}$  Many supramolecular hydrogels undergo a sol-gel transition in response to a decrease in temperature, which results in thermally reversible hydrogels by formation or breakage of the non-covalent interactions. Besides temperature, ultrasound is another type of physical stimulus for tuning supramolecular assembly in water.  $^{49-54}$  Ultrasound provides adequate energy for disrupting weak intermolecular interactions to favor the formation of molecular networks, thus resulting in enhanced hydrogelation rate. In addition, light-triggered hydrogelation was shown to be a very useful process as reported by Yamamoto *et al.* with the formation of photo-cross-linked hydrogels made of copoly(L-lysine) containing  $\epsilon$ -7-coumaryloxyacetyl-L-lysine residues.  $^{55}$ 

The most commonly used chemical process for making supramolecular hydrogels is the change of pH when a hydrogelator bears carboxylic acids or amino groups. This property likely promotes the use of amino acids for making supramolecular hydrogelators. A change

in the pH of an aqueous phase alters the degree of ionization of the amino acid groups thus controlling sol-gel or gel-sol transitions. Notably, Sutton et~al. have reported the use of the hydrolysis of glucono- $\delta$ -lactone (GdL) to gluconic acid for adjusting pH. <sup>56</sup> By applying the process to a range a naphtalene-dipeptide-based hydrogelators they formed highly reproducible hydrogels. Another important and increasingly explored chemical process is the ligand-receptor interaction for the formation of supramolecular gels. For example, supramolecular hydrogels based on the coordination of phenylalanine and Cu(II) or on the complexation between cyclodextrin and adamantane have been reported by Shen et~al. and Kogiso et~al. respectively. <sup>57,58</sup>

#### 1.2 Supramolecular hydrogels made of amino acids and peptides

Research on natural gels focuses on the use of biological molecules such as polysaccharides (e.g., chitosan, alginate, carrageenan, hyaluronic acid, heparin, cellulose or agarose), proteins (e.g., silk, keratin or collagen), other natural polymers such as lignin or natural small molecules such as nucleic acids and amino acids. In particular, amino acids or peptides are nowadays extremely studied for the development of biomedical supramolecular hydrogels thanks to their high biocompatibility.<sup>59</sup> From a biological point of view, amino acids play the role of hormones, precursors of enzymes and neurotransmitters and they are present in many metabolic processes. They can be classified according to their physical and chemical characteristics (isoelectric point, hydrophobicity, pKa, etc.) but also according to the position of the amino group in relation to the carboxyl group by distinguishing  $\alpha$ -amino,  $\beta$ -amino,  $\gamma$ amino and  $\delta$ -amino acids.  $\alpha$ -Amino acids play a crucial role in the structure, metabolism, and physiology of the cells of living beings as constituents of peptides and proteins. Peptides are composed of amino acids linked by a limited number of amide bonds (<15-20 amino acids) unlike polypeptides and proteins (>15-20 amino acids). Amino acids can self-assemble into different types of nanostructures according to their intrinsic properties through the formation of non-covalent bonds. Aromatic amino acids or short peptides have particularly attracted considerable attention for the design of novel biomaterials. Diphenylalanine, which is the core recognition of β-amyloid peptide found in Alzheimer's disease, was demonstrated to be the simplest building block leading to the formation of highly ordered nanostructures such as nanovesicles or nanotubes. 60-62 The team of Ehud Gazit has described the thermal and chemical stability of diphenylalanine nanotubes both in aqueous solution and under dry conditions.<sup>63</sup> They also demonstrated their semi-conductive or antibacterial activity<sup>64</sup> and confirmed that other dipeptides such as diphenylglycine could form ordered structures.<sup>63</sup> Stimuli responding gels have been developed such as leucine-phenylalanine dipeptide hydrogels capable of storing therapeutic molecules and releasing them under different types of stimuli such as change in temperature, pH or ionic strength.<sup>65,66</sup> Other stimuli have also been studied on peptide-based hydrogels such as light or enzymatic reactions. As another example, Zhang *et al.* used octapeptides and hexadecapeptides with hydrophobic amino acids to create highly hydrated gels for culture of nerve cells, endothelial cells, and chondrocytes.<sup>67</sup>

# 1.2.1 Influence of modification at both the N- and C-terminus

The use of protected non-natural amino acids can improve the self-assembly properties and it has been extensively exploited in the development of new hydrogels. The most widely used protective group is undeniably the fluorenyl-9-methoxycarbonyl (Fmoc) group in the N-terminus position. Widely used for the protection of amino acids it is also found in the protection of many dipeptides, tripeptides or longer peptides. This is the case for example of Fmoc-leucine-glycine,<sup>68</sup> Fmoc-phenylalanine,<sup>69</sup> and Fmoc-diphenylalanine,<sup>70</sup> or Fmoc-lysine derivatives.<sup>71</sup> In these systems, parallel and anti-parallel arrangements between Fmoc groups induced their self-assembly (Figure 1.9).

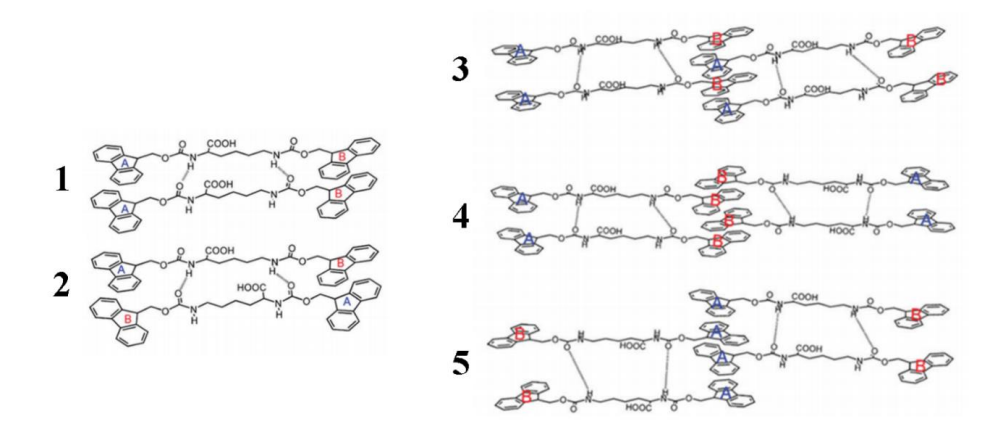


**Figure 1.9.** Structure of di-Fmoc-lysine (top) and possible molecular arrangements between Fmoc groups in a hydrogel state. The structures are stabilized by  $\pi$ -stacking between the aromatic groups in parallel (1 and 2) and anti-parallel (3-5) orientations and by hydrogen bonds (dotted lines) between the -CO-NH groups (from ref. 71).

These self-assembly processes become even more complex if additional aromatic groups are present. For instance, di-Fmoc-lysine with two Fmoc groups in the N $\alpha$  and N $\epsilon$  position undergo hydrogenation via  $\pi$ - $\pi$  interactions involving the Fmoc moiety compared to single N $\alpha$  Fmoc-protected lysine that was found to be non-gelator. Other aromatic groups such as carboxybenzyl (Z)<sup>72</sup>, naphthyl (Nap),<sup>73</sup> phenothazine,<sup>74</sup> pyrene<sup>,75,76</sup> spiropyran<sup>77</sup> or pyridine<sup>78</sup> have also been shown to be effective (Figure 1.10).

Aromatic moeity	Chemical structure		
Carboxybenzyl			
Naphthyl			
Phenothazine	C s s		
Pyrene			
Spiropyran	H <sub>3</sub> C CH <sub>3</sub>		
Pyridine			

**Figure 1.10.** Aromatic moieties use to develop hydrogelators.

Another method of improving the gelation properties is to attach a long alkyl chain to the N-terminus to form an amphiphilic molecule.<sup>79</sup> Functionalization of hydrophobic amino acids by hydrophilic chains is also used to increase the water solubility of peptides. Much less used, some hydrogelators are protected by the tert-butoxycarbonyl (Boc) group at the N-terminus.<sup>80,81</sup> The presence of the Boc group strongly reduces the solubility in water. Baral *et al.* have demonstrated the antibacterial properties of hydrogels developed from Boc-protected peptides (Figure 1.11).<sup>82</sup> In this context, research into the development of

hydrogels based on amino acids and peptides protected by a Boc group leaves a wide range of possibilities.

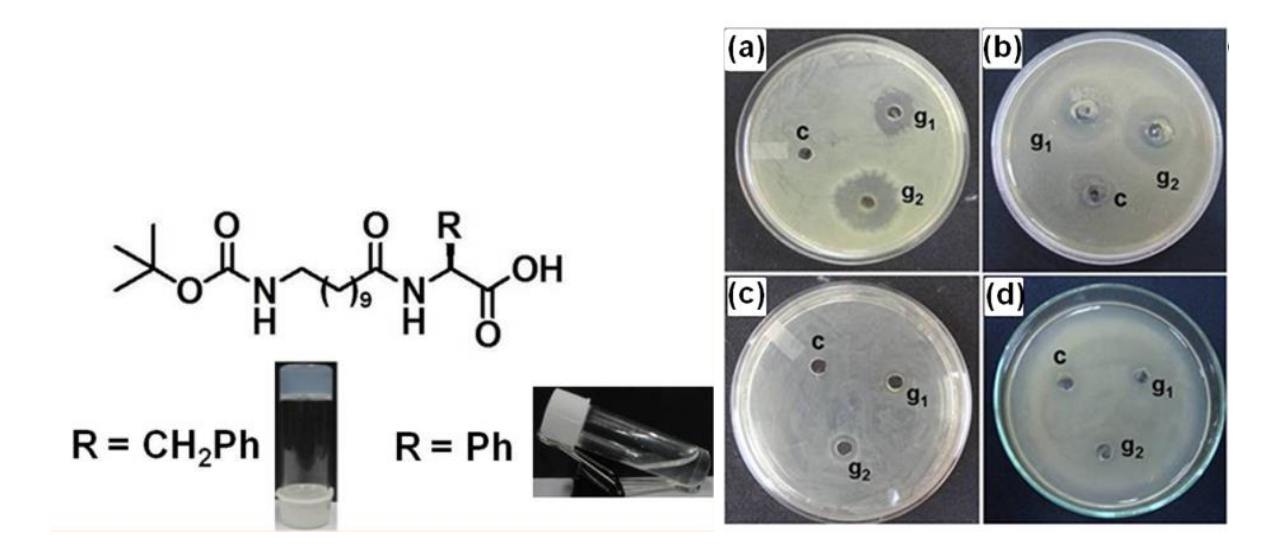


**Figure 1.11**. Left: Chemical structure of the peptides used for the development of hydrogels with antibacterial properties. Right: Determination of the effect of the hydrogel on Gramnegative and Gram-positive bacteria by agar-diffusion assay method. Various bacteria (a) *Escherichia coli*, (b) *Pseudomonas aeruginosa*, (c) *Staphylococcus aureus*, and (d) *Bacillus subtilis* were spread on an agar plate. In each case, two different amounts of 1% (w/v) hydrogel with  $R = CH_2Ph$  (g<sub>1</sub>: 10 μL/well) and g<sub>2</sub>: 20 μL/well) were added to the wells, where C represents the control (50 μL of phosphate buffer) (from ref. 79).

Only a few modifications of the C-terminal are used for the development of stable hydrogels. <sup>83</sup> In general, the conversion of the C-terminal carboxylic acid into an amide leads to a perturbation of the hydrophobicity and hydrogen bonding capacity of the C-terminal. It has been shown that C-terminal amide derivatives self-assemble much faster than the parent carboxylic acid, but they exhibit mechanical instability due to the lower solubility of the amide functionality. <sup>84</sup> The conversion of the C-terminal carboxylic acid to C-terminal methyl or ethyl ester generally fail to form hydrogels due to the higher hydrophobicity of these derivatives, but they may lead to the formation of stable organogels. Other C-terminus modification can be cited such as the derivatization with pyridinium moieties <sup>85</sup>, cysteamine <sup>86</sup>, polyethylene or tetraethylene glycol <sup>87</sup> and glucoside <sup>88</sup>.

# 1.2.2 Influence of the amino acid sequence or side chain modification

Another way to improve hydrogelation properties consists in introducing an organic linker in the amino acid structure. Long alkyl chains incorporated inside the backbone tend to favor hydrogelation.<sup>89</sup> Unsaturated hydrocarbon chains were also used like diacethylene moieties providing the possibility of cross-linking upon ultraviolet (UV) irradiation. 90 The intrinsic hydrophobicity of the hydrogelators as well as the presence of electron-withdrawing groups influence the ability of the molecules to form hydrogels. The incorporation of halogenated substituents can drastically influence the gelation properties of monomers due to high electronegativity and steric effects. For example, halogenated Fmoc-Phe derivatives can selfassemble efficiently in water when non-halogenated Fmoc-Phe does not. The type of halogen used and its position on the aromatic side chain influence the kinetic of selfassembly and the morphology of the fibrillar structure (Figure 1.12). It has been shown that Fmoc-F5-Phe formed hydrogels in an aqueous solution at an accelerated rate compared to Fmoc-Tyr and that no gelation occurred using Fmoc-Phe in the same conditions.91 In addition, the use of Fmoc-F5-Phe resulted in hydrogels with higher stiffness compared to Fmoc-Tyr gels. The hydrophobicity of the amino acids increased in the order of Fmoc-Tyr < Fmoc-Phe < Fmoc-F5-Phe. Therefore, the difference in hydrophobicity alone cannot explain the difference in self-assembly and hydrogelation behavior of these molecules. The presence of OH or F electron-withdrawing groups can disrupt the electronic structure of the benzyl side chains of Fmoc-Tyr and Fmoc-F5-Phe compared to Fmoc-Phe, with Fmoc-F5-Phe having the most dramatically electron-deficient side chain.<sup>91</sup>

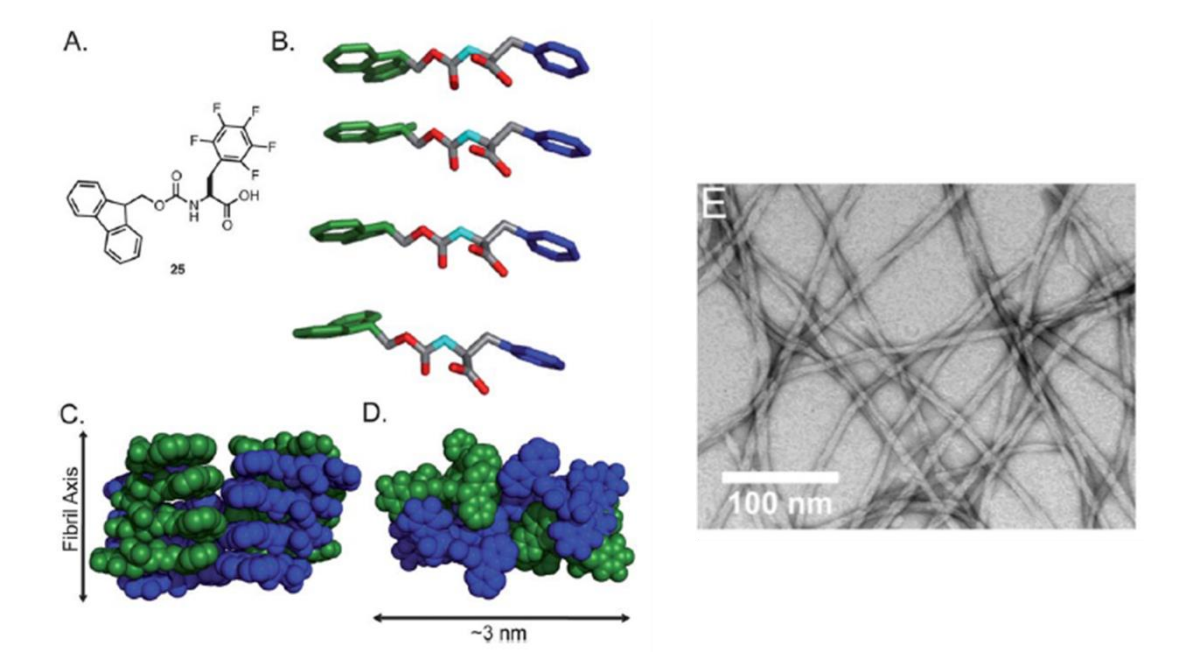


Figure 1.12. (A) Chemical structure of Fmoc-F5-Phe. (B) Proposed packing model of Fmoc-F5-Phe (from ref. 92). Hydrogens are omitted for clarity, Fmoc (green), Phe side chain (blue). (C) Proposed mode of lamination of fibrils leading to fibers, green and blue indicate individual fibrils. (D) Proposed mode of fiber formation, green and blue indicate individual fibrils. (E) Transmission electron microscopy (TEM) image of fibrils in the Fmoc-F5-Phe hydrogel 1 h after mixing (from ref. 91).

#### 1.2.3 Homologated amino acids

The rapid proteolysis of natural amino acids and peptides can be an advantage because of high biocompatibility but also a limitation concerning the mechanical stability of the hydrogel structures *in vivo*. Whereas peptides composed of  $\alpha$  amino acids are easily degraded *in vivo* and *in vitro* by peptidases, studies have shown that peptides containing homologated  $\beta$ - and  $\gamma$ -amino acids exhibited a superior stability.<sup>93</sup> The  $\beta$ -peptides displayed no or very weak cytotoxicity, immunogenic or inflammatory properties.  $\beta$ - and  $\gamma$ -amino acids differ from natural  $\alpha$ -amino acids by the presence of additional carbon atom(s) in the amino acid backbone (Figure 1.13). The homologated  $\alpha$ -amino acids are produced through the insertion of CH<sub>2</sub> groups, the side chain remaining unaltered. The location of the side chain on the  $\beta$ - or on the  $\gamma$ - amino acids are identified as  $\beta^2$ ,  $\beta^3$ ,  $\gamma^2$ ,  $\gamma^3$ , and  $\gamma^4$ .

$$β$$
-Peptides
$$β$$
-Peptides
$$β$$
-Peptides
$$β$$
-Poptides
$$β$$

**Figure 1.13.** Structure and nomenclature for the abbreviation used for β- and γ-peptides derived from the natural proteinogenic α-amino acids (from ref. 93).

The proteolytic stability can be due to the changes of the electronic environment of the peptide bonds upon homologation of the  $\alpha$  amino acids or to a lack of substrate recognition by the peptidases. In a recent work Misra *et al.* demonstrated that  $\beta$ - and  $\gamma$ -diphenylalanine were able to form stimuli-responsive, injectable, and biocompatible hydrogels in conditions where no hydrogels were obtained with  $\alpha$ -diphenylalanine. The use of homologated amino acids thus provides opportunities for the development of new supramolecular hydrogels with better mechanical properties and higher proteolytic stability.

#### 1.3 Characteristics of smart hydrogels for drug delivery applications

Smart hydrogels are bioresponsive materials able to undergo structural modifications under external or internal stimuli such as temperature, pH, enzymes, and light. Chemical or physical gels based on polymers and peptides have been widely studied for drug delivery applications. In particular, self-assembled peptides appear as the ideal candidates for the development of smart drug delivery systems thanks to their high biocompatibility, ease of production and dynamic interactions.

#### 1.3.1 Thermo-sensitive hydrogels

Temperature-sensitive hydrogels are probably the most studied and used to date. Many polymers exhibit temperature-dependent phase transitions (sol-gel). The common characteristic of temperature-sensitive polymers is the presence of hydrophobic groups such as methyl, ethyl and propyl. Among the temperature-sensitive polymers, poly(*N*-isopropylacrylamide) (PNIPAAm) is probably the most widely used as well as poly(*N*,*N*-diethylacrylamide) having a phase transition temperature close to the human body temperature (Figure 1.14). Block copolymers based on poly(ethylene oxide) and poly(phenylene oxide) have also been extensively studied for the synthesis of drug delivery systems. Many poly(ethylene oxide) (PEO) and poly(propylene oxide) (PPO) block copolymers are commercially available under the Pluronics® and Tetronics® brand names. However, clinical applications of PNIPAAm-based hydrogels and its derivatives have certain limitations. The polymer is not biodegradable and the monomers and crosslinkers used in the hydrogel synthesis can be toxic, carcinogenic and teratogenic. Peptide-based hydrogels sensitive to temperature have also been developed by Pochan *et al.* Or Hartgerink and coworkers Playing with the incorporation of hydrophobic amino acid residues.

Figure 1.14. Structure of temperature sensitive polymers (from ref. 96).

# 1.3.2 pH-sensitive hydrogels

pH-sensitive peptides and polymers usually contain acidic or basic groups including carboxylic acids, sulfonic acids, and ammonium salts. Polymers containing a large number of ionizable groups are known as electrolytes such as polyacrylic acid or poly(*N-N*-diethylamide-amidoethyl methacrylate).<sup>99</sup> The pH-sensitivity of hydrogels can be adjusted using neutral comonomers such as 2-hydroxyethyl methacrylate or maleic anhydride. Much research has been done on the development of pH-sensitive and biodegradable hydrogels based on polypeptides,<sup>100</sup> proteins and/or polysaccharides.<sup>101</sup> Recently, Ghosh *et al.*<sup>102</sup> synthesized a

biocompatible supramolecular hydrogel based on an octapeptide that showed pH-responsivity due to the presence of aspartic acid and lysine residues. Zhu and coworkers<sup>100</sup> developed a series of pH-sensitive hydrogels by incorporation of peptide-based bis-acrylate as a cross-linker into hydrogels containing glycine and lysine residues.

### 1.3.3 Light sensitive hydrogels

Many light sensitive hydrogels use UV light to induce an isomerization or chemical reaction that can induce drug release. For example, Rastogi *et al.* have developed a UV-photoresponsive hydrogel prepared containing azobenzene for drug delivery application. Azobenzene undergoes a reversible transformation from hydrophobic trans form to hydrophilic cis form, upon irradiation by UV light (340–380 nm) and the cis form can revert to trans form either thermally or by irradiation by visible light (420-490 nm). Mamada *et al.* have synthesized UV-sensitive hydrogels by incorporating bis(4-(dimethylamino)phenyl)(4-vinylphenyl)methyl leucocyanide into a polymer network. The UV light induced the gel swelling due to the dissociation of the triphenylmethane leuco derivative, which is normally neutral but is dissociated into ions pairs under UV irradiation (Figure 1.15). However, UV irradiation is not suitable for clinical applications due to the low tissue transparency in the UV region, which can induce DNA and tissues damage.

**Figure 1.15.** Structure of bis(4-(dimethylamino)phenyl)(4-vinylphenyl)methyl leucocyanide sensitive to UV light (from ref. 104).

Visible and near-infrared light (NIR) eliminates the negative side effect of UV irradiation. Visible light, which can be applied instantly, can be used to control the release of molecules incorporated into hydrogels containing chromophores that absorb light and dissipate it locally as heat by non-radiative transition such as cardiogreen, methylene blue or riboflavin. The increase of temperature changes the structure of heat-sensitive polymers.

However, if the chromophore is not covalently bound to the polymer it may be released during the process and may induce some toxicity. Near-infrared light can also be used to induce a hydrogel response in absence of a chromophore but in presence of other photothermal agents such as gold nanoparticles, indocyanine green, metallic sulfides/oxides or carbon nanomaterials.

#### 1.3.4 Electrical sensitive hydrogels

Alternatively, an electric current can be used as an external stimulus. Hydrogels that are sensitive to electric fields are usually composed of polyelectrolytes like pH-sensitive hydrogels.<sup>106</sup> For instance, hydrogels based on poly(2-acrylamido-2-methyl-1propanesulfonic acid) have been shown to release hydrocortisone and edrophonium chloride (anticholinesterase drug) in a pulsatile manner using an electric current. On-off control was achieved by varying the intensity of electrical stimulation. Volume variations of a poly(dimethylaminopropyl acrylamide) hydrogel under an electric field were also used to release insulin. 107 The main advantage of electric field-responsive systems is that the rate of release can be controlled by simply modulating the intensity of the applied field. However, few electric field-sensitive devices have yet been developed. In addition to the difficulties common to all hydrogels, they require the use of an electrical source. Most of the systems developed operate in environments without electrolytes, which makes it difficult to use them in physiological conditions.

# 1.4 Strategies for the rigidification of supramolecular amino acid- and small peptidebased hydrogels

The non-covalent nature of supramolecular hydrogels allows the gels to rapidly respond to a multitude of external stimuli. However, most of the existing amino acid- or peptide-based hydrogels have low mechanical properties leading to instability during injection or *in vivo*. Self-assembled Fmoc-dipeptide hydrogels have been used for 3D cell cultures such as Fmoc-Phe-Phe<sup>108</sup> or a mixture of Fmoc-Gly-Gly and Fmoc-Phe-Phe<sup>109</sup>. But in 2012, Nilsson and his team, pioneers in the development of non-covalent hydrogels based on amino acid derivatives and small peptides, concluded that none of the amino acid- and small peptide supramolecular hydrogels developed so far meet universally the criteria required for ideal cell culture medium (must be stable in common cell culture media and support cell viability,

adhesion differentiation, proliferation and migration). <sup>110</sup> For drug delivery, despite promising *in vitro* results of drug release, amino acid and small peptide supramolecular hydrogels failed to show their potential *in vivo* because of low mechanical properties.

# 1.4.1 Chemical cross linking of amino acids

One method of improving the mechanical properties of supramolecular gels is to selectively create covalent bonds within the matrix by chemical cross-linking. The difficulty of supramolecular gel stiffening process is to improve the mechanical properties while preserving the advantages of the supramolecular structure (i.e., the presence of noncovalent interactions allowing controlled drug release and not impacting biocompatibility). While the  $\alpha$ -carbonyl and the  $\alpha$ -amino groups are used to form peptide bonds, a number of amino acids have reactive functional groups in their side chains that can be enzymatically or chemically modified. For example, cysteine represents one of the most targeted amino acids for cross-linking reaction. The side chain thiol group can easily react in oxidative conditions to form dimers by disulfide bonds. Tyrosine is another interesting amino acid since several cross-linking methods can be used by exploiting the reactivity of the side chain phenol. Cross-linked dityrosine has been identified in many structural proteins such as collagen, elastin, resilin and silk fibroin. The tyrosine cross-linking reaction is initiated by the formation of a tyrosyl radical, which can couple with another nucleophilic sites on the other tyrosine residue. Several strategies have been proposed in literature using enzymes like horseradish peroxidase (HRP), or through a photo oxidation process using a metallic catalyst or by addition of a natural or chemical cross-linker (i.e. genipin, glutaraldehyde) to covalently link tyrosine or phenol derivatives that can be applied to supramolecular hydrogel synthesis. 111-

#### 1.4.2 Formation of robust hydrogels

For the fabrication of robust hydrogels several other strategies can be proposed (Figure 1.16) such as the creation of dissipating energy materials comprising a second network able to dissipate the energy during the gel destructuration or the development of combined systems with addition or nanomaterials. <sup>114</sup> In their review, Fuchs *et al.* described the behavior of hydrogels during destructuration. When a crack forms, the material failure occurs when the tip of the crack begins to propagate (Figure 1.17). During the crack

propagation the polymer chain undergoes a large deformation both in the crack tips and in the surrounding area called the process zone. The crack would continue to propagate into the whole system only if the energy released is sufficient to rupture polymer chains along the crack path.

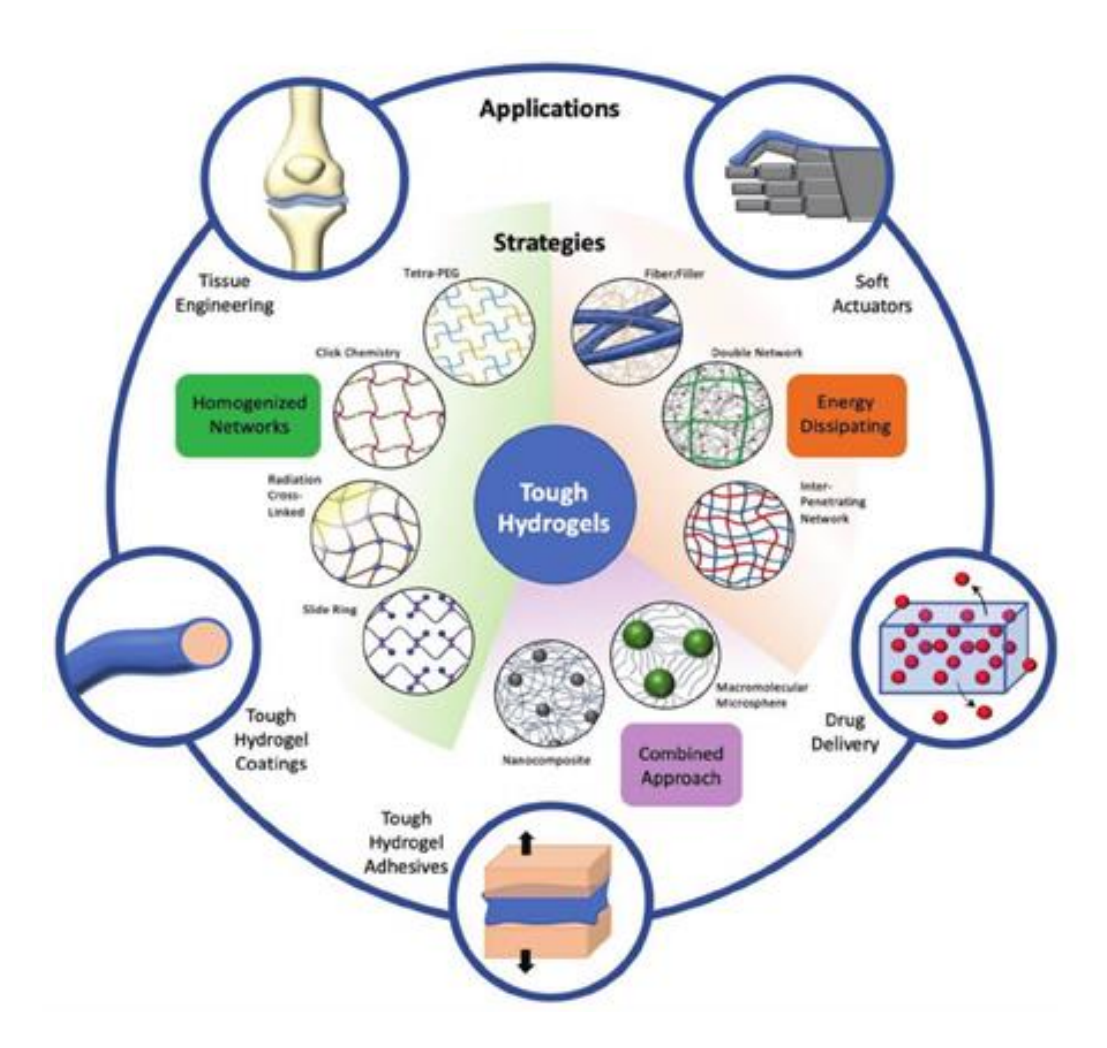


**Figure 1.16.** Overview of different strategies to develop tough hydrogels and their biomedical applications (from ref. 114).

The incorporation of an energy dissipation system can limit the crack propagation by diffusing the energy. Such energy dissipation occurs for example when mixing physical and covalent bonds into a network. Interpenetrating polymer networks (IPNs) are such dissipating energy hydrogels with two or more cross-linked polymers interconnected through non-covalent interactions. These networks can be synthetized simultaneously by free radical or condensation polymerization, or sequentially where after forming the first polymer, the system is mixed in a second monomer solution for a second polymerization. <sup>115</sup>-

<sup>117</sup> Double network (DN) hydrogels are specific IPNs and consist of a first rigid but brittle network and a second ductile network. DN hydrogels are characterized by a large fracture toughness.

Okumura, Brown and Tanaka have proposed theories explaining this behavior stipulating that the crack propagation in DN hydrogels was prevented by i) a first dissipation of energy through the formation of multiple microcracks in the first brittle network, and ii) a viscous dissipation in the ductile network. 118

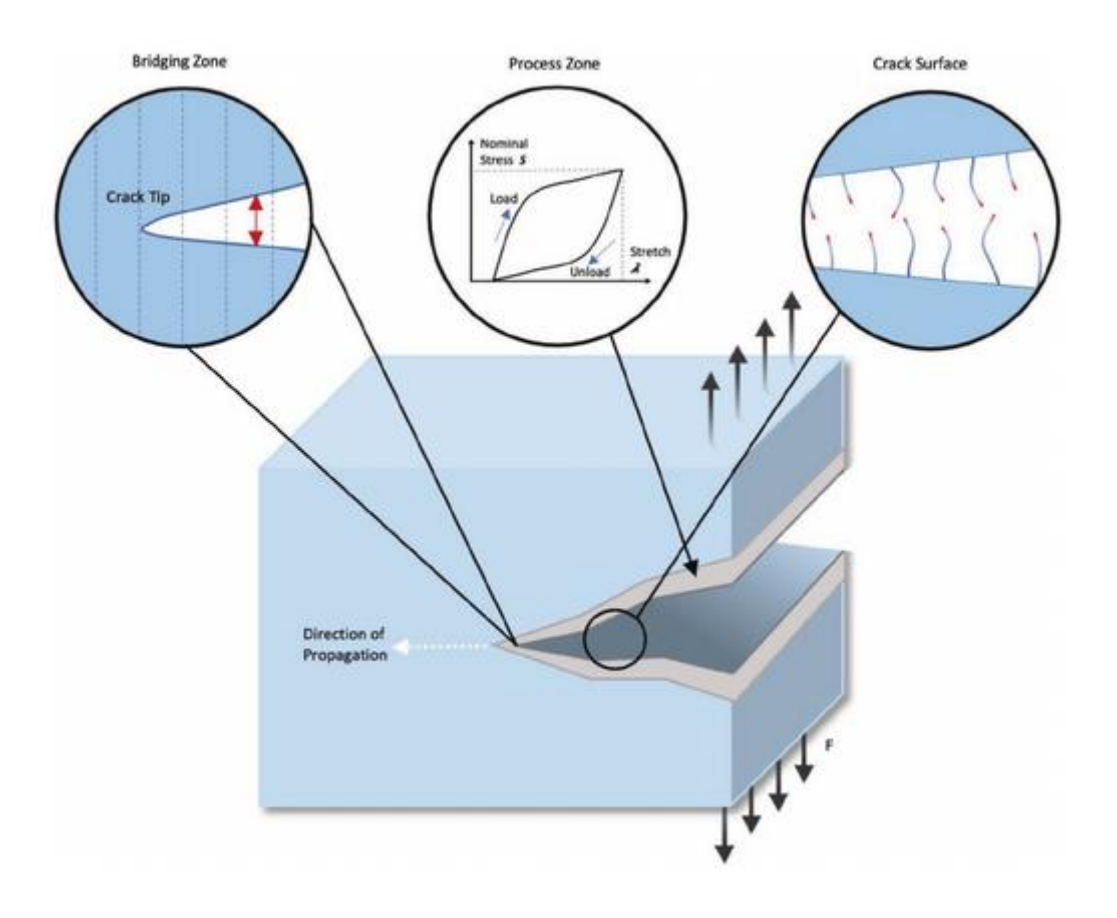


**Figure 1.17.** Schematic representation of crack propagation in a hydrogel network (from ref. 114).

Micro or nanocomposite hydrogels are polymer networks containing micro or nanomaterials that exhibit new properties compared to the native hydrogels (devoid of micro- and nanomaterials). The micro/nanomaterials can be cross-linked or physically entrapped into the gel network. The formation of additional cross-links with the polymer network contributes to enhance the mechanical strength of the gels. It has also been shown that reversible breaking of physical bonds between the micro/nanomaterials and the hydrogels

dissipate energy to prevent crack propagation. Tough nanocomposite hydrogels have been developed from various types of nanomaterials such as clay nanoparticles, polymeric nanoparticles, inorganic/ceramic nanoparticles, metal/metal-oxide nanoparticles or carbon-based nanomaterials (e.g., carbon nanotubes, graphene, and nanodiamonds) with applications in the biomedical field. 119-121

# 1.5 Hybrid hydrogels containing carbon nanomaterials for biomedical applications

# 1.5.1 Hybrid hydrogels containing carbon nanomaterials

The development of hybrid hydrogels containing carbon nanomaterials is a promising alternative to mechanically strengthen hydrogels and endow them with new properties and responsivity to external stimuli. Carbon nanotubes or graphene are the most widely used carbon nanomaterials for the development of hybrid hydrogels. The synthesis can be obtained through covalent or non-covalent functionalization of the carbon nanostructures with the monomer or polymer matrix. For tissue regeneration the incorporation of carbon nanotubes has been largely studied with both synthetic and biological tissue scaffold to improve their mechanical properties or electrical conductance. The electrical conductivity of carbon nanotubes could be a useful tool for directing cell growth as shown with neural cells or osteoblasts proliferation. Graphene incorporated into chitosan-lactic acid matrix also demonstrated excellent biocompatibility with high fibroblast adhesion and growth on the gel surface. In addition, carbon nanotubes and graphene have the capacity to generate heat upon NIR light irradiation. This property can be used for on-demand drug release with NIR as an external stimulus to control the liberation of active molecules preloaded in the hybrid hydrogels due to enhanced local temperature, with high spatial and temporal precision.

#### 1.5.2 Property of carbon nanomaterials for biomedical applications

Graphene is a two-dimensional single layer sheet of sp<sup>2</sup> hybridized carbon atoms organized in a hexagonal arrangement (Figure 1.16). Carbon nanotubes (CNTs) are cylindrical structures composed of rolled graphene sheets. The structure of carbon nanotubes is composed of one layer, single-walled carbon nanotubes (SWCNTs), or more, multi-walled carbon nanotubes (MWCNTs). They are terminated by hemispherical arrangements of carbon atoms corresponding to half-fullerenes (Figure 1.18). The diameter ranges from 2.5 to ~100 nm, while the diameter of a SWCNT ranges from 0.6 to 2.4 nm.

Graphene and carbon nanotubes have attracted tremendous attention with its unique features such as high electron mobility, thermal conductivity comparable to that of metals, as well as high optical absorption and mechanical strength. 124 The increased mechanical strength is due to the carbon-carbon double bonds formed by the sp<sup>2</sup> orbitals, which leads to the formation of a network of conjugated  $\pi$  bonds. This  $\pi$  conjugation causes electron delocalization, giving CNTs and graphene excellent thermal and electrical conductivity properties. CNTs and graphene family nanomaterials offer many advantages as photothermal agents. As with CNTs, graphene absorbs near-infrared irradiation, leading to heat generation used to treat tumor or to destroy pathogens such as bacteria. Several studies have focused on the use of both carbon nanotubes and graphene in biological systems: for protein crystallization<sup>125</sup>, as biological probes<sup>126</sup> or as substrates for the growth of embryonic neurons in rats<sup>127</sup>. They can also be used as delivery systems for directing therapeutic molecules to a target organ and overcoming some of the limitations associated to drugs such as low aqueous solubility, rapid inactivation, unfavorable pharmacokinetic profile and limited biodistribution. Their near one-dimensional size makes them ideal for drug delivery. The covalent grafting or adsorption of molecules with a high loading is possible thanks to their large specific surface area. Graphene oxide (GO), the oxidized form of graphene, has also generated great interest in the biomedical field for the development of biosensors, in drug delivery, or for the preparation of implants for tissue engineering. 128-131

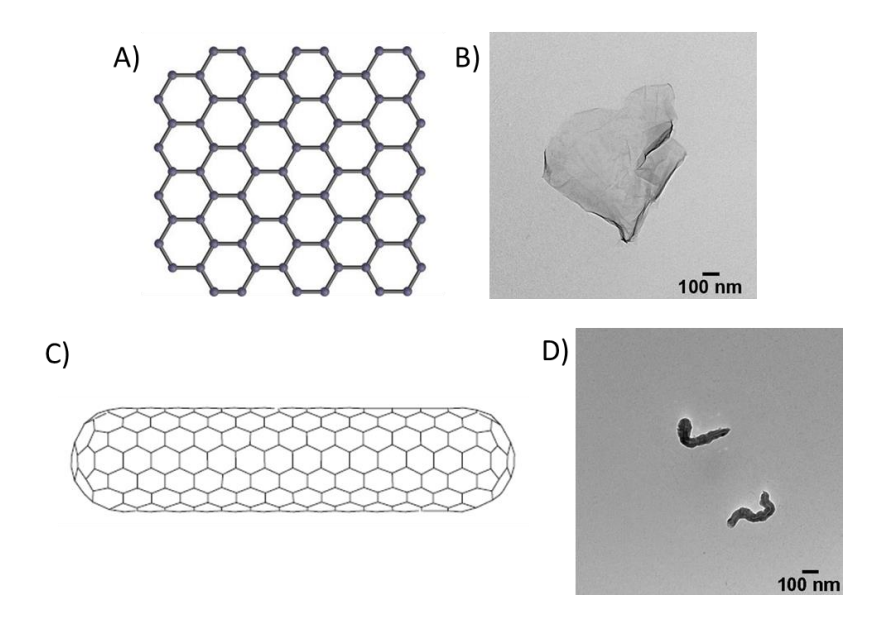


**Figure 1.18.** A) Molecular structure of graphene, B) TEM image of graphene, C) molecular structure of a single-walled carbon nanotube and D) TEM image of carbon nanotubes.

#### 1.5.3 Biocompatibility of carbon nanomaterials

In order to use carbon nanomaterials in medical devices it is important to know their biocompatibility as well as their biodistribution within the human body. The biocompatibility can be defined as the capacity of a material to be tolerated inside the body without causing immunogenic responses, deleterious interaction (*e.g.*, apoptosis, cells detachment, tissue necrosis) or modification and without long term accumulation in the body. The study of the biocompatibility of CNTs and graphene is a complex topic as many variables have to be considered such as the purity, the dose, the surface functionalization, the surface area, the number of layers and the dimension. These parameters are highly dependent on the method of synthesis.

#### 1.5.3.1 Biocompatibility of carbon nanotubes

Pristine carbon nanotubes are not soluble in aqueous solution and tend to aggregate because of their highly hydrophobic surface. Chemical functionalization of carbon nanotubes plays a very important role to increase their dispersibility, improve their integration into physiological environments and their interactions with cells, tissues, and organs. One method to enhance the dispersibility of CNTs in water is the oxidation using strong acids such as HNO<sub>3</sub>. During the process, carboxyl groups are formed at the extremities and at the defects on the sidewall of the carbon nanotubes. CNTs can also be functionalized by other methods such as 1,3-dipolar cycloaddition, nitrene cycloaddition or arylation using diazonium salts allowing the grafting of different types of functional groups. 132 Our team showed that SWCNTs and MWSNTs functionalized by 1,3-dipolar cycloaddition with amino groups were eliminated very rapidly by renal excretion, 133,134 with limited accumulation in the lungs, liver and spleen. In contrast, non-functionalized single- or multi-walled carbon nanotubes tend to accumulate in the liver and spleen. 135 According to these results, the type of functionalization and the number of functional groups on the nanotube surface play a key role in their biodistribution. In addition, it has also been shown that the risk of accumulation of CNTs can be reduced if the length of the tubes is decreased to promote their removal from the body by cells such as macrophages. 136

Non-biodegradable nanomaterials can accumulate into the body causing harmful side effects. Therefore, their biodegradation represents an important and challenging objective.

Several studies have reported that strong oxidative enzymes such as horseradish peroxidase and human peroxidases (e.g., myeloperoxidase) are able to degrade functionalized carbon nanotubes in the presence of  $H_2O_2$ . In the same conditions pristine carbon nanotubes were not observed to degraded showing the crucial role of chemical functionalization. <sup>137,138</sup>

# 1.5.3.2 Biocompatibility of graphene-based materials

Graphene-based materials are currently among the most studied materials in the field of nanomedicine. As with carbon nanotubes, appropriate functionalization, control of the size and shape can improve the biocompatibility of graphene. There are conflicting results on the biocompatibility and biosafety of graphene family nanomaterials. This is partially due to large variations in physicochemical properties of different graphene derivatives. There is a clear impact of the functionalization, although results are mitigated for GO and it is difficult to generalize about GO toxicity. The route of administration is an important parameter affecting the biodistribution. When GO was administered intravenously at low dose, no impact on the kidney, liver, spleen, and lungs was observed. After pulmonary administration GO permeated through the air-blood barrier into the blood and to other organs before being eliminated in the urine. However, GO was still localized in the lungs after 3 months leading to persistent lung injury. Graphene and GO can also be enzymatically degraded. Well-dispersed GO has been degraded by horseradish peroxidase and myeloperoxidase in presence of H<sub>2</sub>O<sub>2</sub>. In vivo the degradation of carboxylated graphene and GO have also been demonstrated in lungs 146 and in the brain. After pulmonary 147

# 1.6 Objectives of the Thesis

The aim of this thesis is to develop new supramolecular hydrogels based on amino acids and small peptides containing carbon nanomaterials for drug delivery applications. We aim to improve the knowledge about the self-assembly of amino acids and small peptides. This is of primary importance to predict hydrogelation and adapt the hydrogel properties in function of their application.

#### 1.7 References

- 1. Singh, B.; Pal, L. Development of Sterculia Gum Based Wound Dressings for Use in Drug Delivery. Eur. Polym. J. 2008, 44, 3222–3230.
- 2. Wichterle, O.; Lím, D. Hydrophilic Gels for Biological Use. Nature 1960, 185 (4706), 117–118.
- 3. Samchenko, Y.; Ulberg, Z.; Korotych, O. Multipurpose Smart Hydrogel Systems. Adv Colloid Interface Sci 2011, 168 (1–2), 247–262.
- 4. Suzuki, M. Amphoteric Polyvinyl Alcohol Hydrogel and Electrohydrodynamic Control Method for Artificial Muscles. In Polymer Gels: Fundamentals and Biomedical Applications; DeRossi, D., Kajiwara, K., Osada, Y., Yamauchi, A., Eds.; Springer US: Boston, MA, 1991; pp 221–236.
- 5. Osada, Y.; Hasebe, M. Electrically Activated Mechanochemical Devices Using Polyelectrolyte Gels. Chem. Lett. 1985, 14 (9), 1285–1288.
- 6. Shiroya, T.; Tamura, N.; Yasui, M.; Fujimoto, K.; Kawaguchi, H. Enzyme Immobilization on Thermosensitive Hydrogel Microspheres. Colloids Surf., B 1995, 4 (5), 267–274.
- 7. Park, T. G.; Hoffman, A. S. Immobilization and Characterization of Beta-Galactosidase in Thermally Reversible Hydrogel Beads. J. Biomed. Mater. Res. 1990, 24 (1), 21–38.
- 8. Ullah, F.; Othman, M. B. H.; Javed, F.; Ahmad, Z.; Akil, H. Md. Classification, Processing and Application of Hydrogels: A Review Mater. Sci. Eng., 57, 414–433.
- 9. Li, J.; Mooney, D. J. Designing Hydrogels for Controlled Drug Delivery. Nat. Rev. Mater. 2016, 1 (12), 1–17.
- 10. Zhang, Y. S.; Khademhosseini, A. Advances in Engineering Hydrogels. Science 2017, 356 (6337).
- 11. Hoare, T.; Kohane, D. Hoare TR, Kohane DS. Hydrogels in Drug Delivery: Progress and Challenges. Polymer 49: 1993-2007. Polymer 2008, 49, 1993–2007.
- 12. Mandal, A.; Clegg, J. R.; Anselmo, A. C.; Mitragotri, S. Hydrogels in the Clinic. Bioeng. Transl. Med. 2020, 5 (2).
- 13. Yoshimura, T. Alginate-Based Superabsorbent Hydrogels Composed of Carboxylic Acid-Amine Interaction. E-Polymers 2009.
- 14. Xu, J.; Liu, Y.; Hsu, S. Hydrogels Based on Schiff Base Linkages for Biomedical Applications. Molecules 2019, 24 (16).
- 15. Bulpitt, P.; Aeschlimann, D. New Strategy for Chemical Modification of Hyaluronic Acid: Preparation of Functionalized Derivatives and Their Use in the Formation of Novel Biocompatible Hydrogels. J. Biomed. Mater. Res. 1999, 47 (2), 152–169.
- 16. Lin, Y.; Sun, J.; Jiang, G.; Zan, J.; Ding, F. In Vitro Evaluation of Lysozyme-Loaded Microspheres in Thermosensitive Methylcellulose-Based Hydrogel. Chin. J. Chem. Eng. 2007, 15 (4), 566–572.
- 17. Ito, T.; Yeo, Y.; Highley, C. B.; Bellas, E.; Kohane, D. S. Dextran-Based in Situ Cross-Linked Injectable Hydrogels to Prevent Peritoneal Adhesions. Biomaterials 2007, 28 (23), 3418–3426.
- 18. Ossipov, D. A.; Brännvall, K.; Forsberg-Nilsson, K.; Hilborn, J. Formation of the First Injectable Poly(Vinyl Alcohol) Hydrogel by Mixing of Functional PVA Precursors. J. Appl. Polym. Sci. 2007, 106 (1), 60–70.
- 19. Lee, K. Y.; Alsberg, E.; Mooney, D. J. Degradable and Injectable Poly(Aldehyde Guluronate) Hydrogels for Bone Tissue Engineering. J. Biomed. Mater. Res. 2001, 56 (2), 228–233.

- 20. Hiemstra, C.; van der Aa, L. J.; Zhong, Z.; Dijkstra, P. J.; Feijen, J. Novel in Situ Forming, Degradable Dextran Hydrogels by Michael Addition Chemistry: Synthesis, Rheology, and Degradation. Macromolecules 2007, 40 (4), 1165–1173.
- 21. Elbert, D. L.; Pratt, A. B.; Lutolf, M. P.; Halstenberg, S.; Hubbell, J. A. Protein Delivery from Materials Formed by Self-Selective Conjugate Addition Reactions. J Control Release 2001, 76 (1–2), 11–25.
- 22. Shu, X. Z.; Ahmad, S.; Liu, Y.; Prestwich, G. D. Synthesis and Evaluation of Injectable, in Situ Crosslinkable Synthetic Extracellular Matrices for Tissue Engineering. J Biomed Mater Res A 2006, 79 (4), 902–912.
- 23. Zhao, L.; Mitomo, H.; Zhai, M.; Yoshii, F.; Nagasawa, N.; Kume, T. Synthesis of Antibacterial PVA/CM-Chitosan Blend Hydrogels with Electron Beam Irradiation. Carbohydr. Polym. 2003, 4 (53), 439–446.
- 24. Maolin, Z.; Yoshii, F.; Kume, T.; Hashim, K. Syntheses of PVA/Starch Grafted Hydrogels by Irradiation. Carbohydr. Polym. 2002, 50, 295–303.
- 25. Jin, R.; Hiemstra, C.; Zhong, Z.; Feijen, J. Enzyme-Mediated Fast in Situ Formation of Hydrogels from Dextran-Tyramine Conjugates. Biomaterials 2007, 28 (18), 2791–2800.
- 26. Kurisawa, M.; Chung, J. E.; Yang, Y. Y.; Gao, S. J.; Uyama, H. Injectable Biodegradable Hydrogels Composed of Hyaluronic Acid-Tyramine Conjugates for Drug Delivery and Tissue Engineering. Chem. Commun. (Camb.) 2005, 34, 4312–4314.
- 27. Chen, S.-C.; Wu, Y.-C.; Mi, F.-L.; Lin, Y.-H.; Yu, L.-C.; Sung, H.-W. A Novel PH-Sensitive Hydrogel Composed of N,O-Carboxymethyl Chitosan and Alginate Cross-Linked by Genipin for Protein Drug Delivery. J. Controlled Release 2004, 96 (2), 285–300.
- 28. Butler, M.; Ng, Y.; Pudney, P. Mechanism and Kinetics of Crosslinking Reaction between Biopolymers Containing Primary Amine Groups and Genipin. Journal of Polymer Science Part A: Polymer Chemistry 2003, 41, 3941–3953.
- 29. Beena, M. S.; Chandy, T.; Sharma, C. P. Heparin Immobilized Chitosan Poly Ethylene Glycol Interpenetrating Network: Antithrombogenicity. Artif. Cells, Blood Substitutes, Biotechnol. 1995, 23 (2), 175–192.
- 30. Liu, J.; Lin, S.; Li, L.; Liu, E. Release of Theophylline from Polymer Blend Hydrogels. Int. J. Pharm. 2005, 298 (1), 117–125.
- 31. Bajpai, A. K.; Shrivastava, J. In Vitro Enzymatic Degradation Kinetics of Polymeric Blends of Crosslinked Starch and Carboxymethyl Cellulose. Polymer International 2005, 54 (11), 1524–1536.
- 32. Gupta, D.; Tator, C. H.; Shoichet, M. S. Fast-Gelling Injectable Blend of Hyaluronan and Methylcellulose for Intrathecal, Localized Delivery to the Injured Spinal Cord. Biomaterials 2006, 27 (11), 2370–2379.
- 33. Wu, Y.; Wang, L.; Qing, Y.; Yan, N.; Tian, C.; Huang, Y. A Green Route to Prepare Fluorescent and Absorbent Nano-Hybrid Hydrogel for Water Detection. Sci Rep 2017, 7 (1), 4380.
- 34. Wang, W.; Zhang, X.; Teng, A.; Liu, A. Mechanical Reinforcement of Gelatin Hydrogel with Nanofiber Cellulose as a Function of Percolation Concentration. Int. J. Biol. Macromol. 2017, 103, 226–233.
- 35. Dolan, G. K.; Yakubov, G. E.; Bonilla, M. R.; Lopez-Sanchez, P.; Stokes, J. R. Friction, Lubrication, and in Situ Mechanics of Poroelastic Cellulose Hydrogels. Soft Matter 2017, 13 (19), 3592–3601.

- 36. Wei, Z.; Zhao, J.; Chen, Y. M.; Zhang, P.; Zhang, Q. Self-Healing Polysaccharide-Based Hydrogels as Injectable Carriers for Neural Stem Cells. Sci Rep 2016, 6, 37841.
- 37. Lym, J. S.; Nguyen, Q. V.; Ahn, D. W.; Huynh, C. T.; Jae, H. J.; Kim, Y. I.; Lee, D. S. Sulfamethazine-Based PH-Sensitive Hydrogels with Potential Application for Transcatheter Arterial Chemoembolization Therapy. Acta Biomaterialia 2016, 41, 253–263.
- 38. Du, X.; Zhou, J.; Shi, J.; Xu, B. Supramolecular Hydrogelators and Hydrogels: From Soft Matter to Molecular Biomaterials. Chem Rev 2015, 115 (24), 13165–13307.
- 39. Cao, H.; Yuan, Q.; Zhu, X.; Zhao, Y.-P.; Liu, M. Hierarchical Self-Assembly of Achiral Amino Acid Derivatives into Dendritic Chiral Nanotwists. Langmuir 2012, 28 (43), 15410–15417.
- 40. Frederix, P. W. J. M.; Ulijn, R. V.; Hunt, N. T.; Tuttle, T. Virtual Screening for Dipeptide Aggregation: Toward Predictive Tools for Peptide Self-Assembly. J Phys Chem Lett 2011, 2 (19), 2380–2384.
- 41. Bairi, P.; Roy, B.; Nandi, A. K. Bicomponent Hydrogels of Lumichrome and Melamine: Photoluminescence Property and Its Dependency on PH and Temperature. J Phys Chem B 2010, 114 (35), 11454–11461.
- 42. Basit, H.; Pal, A.; Sen, S.; Bhattacharya, S. Two-Component Hydrogels Comprising Fatty Acids and Amines: Structure, Properties, and Application as a Template for the Synthesis of Metal Nanoparticles. Chem. Eur. J. 2008, 14 (21), 6534–6545.
- 43. Zhang, Y.; Gu, H.; Yang, Z.; Xu, B. Supramolecular Hydrogels Respond to Ligand-Receptor Interaction. J. Am. Chem. Soc. 2003, 125 (45), 13680–13681.
- 44. Bhattacharjee, S.; Datta, S.; Bhattacharya, S. Remarkable Regioisomer Control in the Hydrogel Formation from a Two-Component Mixture of Pyridine-End Oligo(p-Phenylenevinylene)s and N-Decanoyl-L-Alanine. Chem. Eur. J. 2013, 19 (49), 16672—16681.
- 45. Dastidar, P.; Okabe, S.; Nakano, K.; Iida, K.; Miyata, M.; Tohnai, N.; Shibayama, M. Facile Syntheses of a Class of Supramolecular Gelator Following a Combinatorial Library Approach: Dynamic Light Scattering and Small-Angle Neutron Scattering Studies. Chem. Mater. 2005, 17 (4), 741–748.
- 46. Kawano, S.; Kobayashi, D.; Taguchi, S.; Kunitake, M.; Nishimi, T. Construction of Continuous Porous Organogels, Hydrogels, and Bicontinuous Organo/Hydro Hybrid Gels from Bicontinuous Microemulsions. Macromolecules 2010, 43 (1), 473–479.
- 47. Shankar, B. V.; Patnaik, A. A New PH and Thermo-Responsive Chiral Hydrogel for Stimulated Release. J. Phys. Chem. B 2007, 111 (31), 9294–9300.
- 48. Wu, J.; Tang, L.; Chen, K.; Yan, L.; Li, F.; Wang, Y. Formation of Supramolecular Hydrogels with Controlled Microstructures and Stability via Molecular Assembling in a Two-Component System. J. Colloid Interface Sci. 2007, 307 (1), 280–287.
- 49. Naota, T.; Koori, H. Molecules That Assemble by Sound: An Application to the Instant Gelation of Stable Organic Fluids. J. Am. Chem. Soc. 2005, 127 (26), 9324–9325.
- 50. Isozaki, K.; Takaya, H.; Naota, T. Ultrasound-Induced Gelation of Organic Fluids with Metalated Peptides. Angew. Chem., Int. Ed. 2007, 46 (16), 2855–2857.
- 51. Bardelang, D.; Camerel, F.; Margeson, J. C.; Leek, D. M.; Schmutz, M.; Zaman, Md. B.; Yu, K.; Soldatov, D. V.; Ziessel, R.; Ratcliffe, C. I.; Ripmeester, J. A. Unusual Sculpting of Dipeptide Particles by Ultrasound Induces Gelation. J. Am. Chem. Soc. 2008, 130 (11), 3313–3315.

- 52. Garvin, K. A.; VanderBurgh, J.; Hocking, D. C.; Dalecki, D. Controlling Collagen Fiber Microstructure in Three-Dimensional Hydrogels Using Ultrasound. J Acoust Soc Am 2013, 134 (2), 1491–1502.
- 53. Xie, Z.; Zhang, A.; Ye, L.; Z. Organo and Hydrogels Derived from Cyclo(L-Tyr-L-Lys) and Its ε-Amino Derivatives. Soft Matter 2009, 5.
- 54. Pan, S.; Luo, S.; Li, S.; Lai, Y.; Geng, Y.; He, B.; Gu, Z. Ultrasound Accelerated Gelation of Novel L-Lysine Based Hydrogelators. Chem. Commun. 2013, 49 (73), 8045–8047.
- 55. Yamamoto, H.; Kitsuki, T.; Nishida, A.; Asada, K.; Ohkawa, K. Photoresponsive Peptide and Polypeptide Systems. 13. Photoinduced Cross-Linked Gel and Biodegradation Properties of Copoly(I-Lysine) Containing  $\epsilon$ -7-Coumaryloxyacetyl-I-Lysine Residues. Macromolecules 1999, 32 (4), 1055–1061.
- 56. Sutton, S.; Campbell, N. L.; Cooper, A. I.; Kirkland, M.; Frith, W. J.; Adams, D. J. Controlled Release from Modified Amino Acid Hydrogels Governed by Molecular Size or Network Dynamics. Langmuir 2009, 25 (17), 10285–10291.
- 57. Shen, J.-S.; Mao, G.-J.; Zhou, Y.-H.; Jiang, Y.-B.; Zhang, H.-W. A Ligand-Chirality Controlled Supramolecular Hydrogel. Dalton Trans. 2010, 39 (30), 7054–7058.
- 58. Kogiso, M.; Okada, Y.; Yase, K.; Shimizu, T. Metal-Complexed Nanofiber Formation in Water from Dicarboxylic Valylvaline Bolaamphiphiles. J. Colloid Interface Sci. 2004, 273 (2), 394–399.
- 59. Dou, X.-Q.; Feng, C.-L. Amino Acids and Peptide-Based Supramolecular Hydrogels for Three-Dimensional Cell Culture. Adv. Mater. 2017, 29 (16), 1604062.
- 60. Guo, C.; Luo, Y.; Zhou, R.; Wei, G. Probing the Self-Assembly Mechanism of Diphenylalanine-Based Peptide Nanovesicles and Nanotubes. ACS Nano 2012, 6 (5), 3907–3918.
- 61. Mason, T. O.; Chirgadze, D. Y.; Levin, A.; Adler-Abramovich, L.; Gazit, E.; Knowles, T. P. J.; Buell, A. K. Expanding the Solvent Chemical Space for Self-Assembly of Dipeptide Nanostructures. ACS Nano 2014, 8 (2), 1243–1253.
- 62. Reches, M.; Gazit, E. Formation of Closed-Cage Nanostructures by Self-Assembly of Aromatic Dipeptides. Nano Lett. 2004, 4 (4), 581–585.
- 63. Adler-Abramovich, L.; Reches, M.; Sedman, V. L.; Allen, S.; Tendler, S. J. B.; Gazit, E. Thermal and Chemical Stability of Diphenylalanine Peptide Nanotubes: Implications for Nanotechnological Applications. Langmuir 2006, 22 (3), 1313–1320.
- 64. Schnaider, L.; Brahmachari, S.; Schmidt, N. W.; Mensa, B.; Shaham-Niv, S.; Bychenko, D.; Adler-Abramovich, L.; Shimon, L. J. W.; Kolusheva, S.; DeGrado, W. F.; Gazit, E. Self-Assembling Dipeptide Antibacterial Nanostructures with Membrane Disrupting Activity. Nat. Commun. 2017, 8 (1), 1365.
- 65. Yadav, N.; Chauhan, M. K.; Chauhan, V. S. Short to Ultrashort Peptide-Based Hydrogels as a Platform for Biomedical Applications. Biomater. Sci. 2019, 8 (1), 84–100.
- 66. Thota, C. K.; Yadav, N.; Chauhan, V. S. "A Novel Highly Stable and Injectable Hydrogel Based on a Conformationally Restricted Ultrashort Peptide." Sci Rep 2016, 6 (1), 31167.
- 67. Zhang, S. Fabrication of Novel Biomaterials through Molecular Self-Assembly. Nat. Biotechnol. 2003, 21 (10), 1171–1178.
- 68. Tang, C.; Ulijn, R. V.; Saiani, A. Self-Assembly and Gelation Properties of Glycine/Leucine Fmoc-Dipeptides. Eur. Phys. J. E 2013, 36 (10), 111.

- 69. Ryan, D. M.; Doran, T. M.; Nilsson, B. L. Complementary  $\pi$ – $\pi$  Interactions Induce Multicomponent Coassembly into Functional Fibrils. Langmuir 2011, 27 (17), 11145–11156.
- 70. Raeburn, J.; Pont, G.; Chen, L.; Cesbron, Y.; Lévy, R.; Adams, D. J. Fmoc-Diphenylalanine Hydrogels: Understanding the Variability in Reported Mechanical Properties. Soft Matter 2012, 8 (4), 1168–1174.
- 71. Reddy, S. M. M.; Shanmugam, G.; Duraipandy, N.; Kiran, M. S.; Mandal, A. B. An Additional Fluorenylmethoxycarbonyl (Fmoc) Moiety in Di-Fmoc-Functionalized L-Lysine Induces PH-Controlled Ambidextrous Gelation with Significant Advantages. Soft Matter 2015, 11 (41), 8126–8140.
- 72. Shi, J.; Gao, Y.; Yang, Z.; Xu, B. Exceptionally Small Supramolecular Hydrogelators Based on Aromatic–Aromatic Interactions. Beilstein J. Org. Chem. 2011, 7 (1), 167–172.
- 73. Yang, Z.; Liang, G.; Ma, M.; Gao, Y.; Xu, B. Conjugates of Naphthalene and Dipeptides Produce Molecular Hydrogelators with High Efficiency of Hydrogelation and Superhelical Nanofibers. J. Mater. Chem. 2007, 17 (9), 850–854.
- 74. Ou, C.; Zhang, J.; Zhang, X.; Yang, Z.; Chen, M. Phenothiazine as an Aromatic Capping Group to Construct a Short Peptide-Based 'Super Gelator.' Chem. Commun. 2013, 49 (18), 1853–1855.
- 75. Ma, M.; Kuang, Y.; Gao, Y.; Zhang, Y.; Gao, P.; Xu, B. Aromatic–Aromatic Interactions Induce the Self-Assembly of Pentapeptidic Derivatives in Water To Form Nanofibers and Supramolecular Hydrogels. J. Am. Chem. Soc. 2010, 132 (8), 2719–2728.
- 76. Nanda, J.; Biswas, A.; Banerjee, A. Single Amino Acid Based Thixotropic Hydrogel Formation and PH-Dependent Morphological Change of Gel Nanofibers. Soft Matter 2013, 9 (16), 4198–4208.
- 77. Qiu, Z.; Yu, H.; Li, J.; Wang, Y.; Zhang, Y. Spiropyran-Linked Dipeptide Forms Supramolecular Hydrogel with Dual Responses to Light and to Ligand–Receptor Interaction. Chem. Commun. 2009, 23, 3342–3344.
- 78. Nebot, V. J.; Armengol, J.; Smets, J.; Prieto, S. F.; Escuder, B.; Miravet, J. F. Molecular Hydrogels from Bolaform Amino Acid Derivatives: A Structure—Properties Study Based on the Thermodynamics of Gel Solubilization. Chem. Eur. J. 2012, 18 (13), 4063–4072.
- 79. Shroff, K.; Rexeisen, E. L.; Arunagirinathan, M. A.; Kokkoli, E. Fibronectin-Mimetic Peptide-Amphiphile Nanofiber Gels Support Increased Cell Adhesion and Promote ECM Production. Soft Matter 2010, 6 (20), 5064–5072.
- 80. Das, A.; Bose, P.; Drew, M.; Banerjee, A. The Role of Protecting Groups in the Formation of Organogels Through a Nano-Fibrillar Network Formed by Self-Assembling Terminally Protected Tripeptides. Tetrahedron 2007, 63, 7432–7442.
- 81. Banerjee, A.; Palui, G.; Banerjee, A. Pentapeptide Based Organogels: The Role of Adjacently Located Phenylalanine Residues in Gel Formation. Soft Matter 2008, 4 (7), 1430–1437.
- 82. Baral, A.; Roy, S.; Ghosh, S.; Hermida-Merino, D.; Hamley, I. W.; Banerjee, A. A Peptide-Based Mechano-Sensitive, Proteolytically Stable Hydrogel with Remarkable Antibacterial Properties. Langmuir 2016, 32 (7), 1836–1845.
- 83. Loic, S. Amino Acids Modification to Improve and Fine-Tune Peptide- Based Hydrogels. Amino Acid: New Insights Roles Plant Anim. 2017.

- 84. Ryan, D. M.; Doran, T. M.; Anderson, S. B.; Nilsson, B. L. Effect of C-Terminal Modification on the Self-Assembly and Hydrogelation of Fluorinated Fmoc-Phe Derivatives. Langmuir 2011, 27 (7), 4029–4039.
- 85. Debnath, S.; Shome, A.; Das, D.; Das, P. K. Hydrogelation Through Self-Assembly of Fmoc-Peptide Functionalized Cationic Amphiphiles: Potent Antibacterial Agent. J. Phys. Chem. B 2010, 114 (13), 4407–4415.
- 86. Ren, C.; Song, Z.; Zheng, W.; Chen, X.; Wang, L.; Kong, D.; Yang, Z. Disulfide Bond as a Cleavable Linker for Molecular Self-Assembly and Hydrogelation. Chem. Commun. 2011, 47 (5), 1619–1621.
- 87. Tzokova, N.; Fernyhough, C. M.; Topham, P. D.; Sandon, N.; Adams, D. J.; Butler, M. F.; Armes, S. P.; Ryan, A. J. Soft Hydrogels from Nanotubes of Poly(Ethylene Oxide)-Tetraphenylalanine Conjugates Prepared by Click Chemistry. Langmuir 2009, 25 (4), 2479–2485.
- 88. Li, X.; Yi Kuang; Shi, J.; Gao, Y.; Lin, H.-C.; Xu, B. Multifunctional, Biocompatible Supramolecular Hydrogelators Consist Only of Nucleobase, Amino Acid, and Glycoside. J. Am. Chem. Soc. 2011, 133 (43), 17513–17518.
- 89. Kogiso, M.; Hanada, T.; Yase, K.; Shimizu, T. Intralayer Hydrogen-Bond-Directed Self-Assembly of Nano-Fibers from Dicarboxylic Valylvaline Bolaamphiphiles. Chem. Commun. 1998, 17, 1791–1792.
- 90. Diegelmann, S. R.; Hartman, N.; Markovic, N.; Tovar, J. D. Synthesis and Alignment of Discrete Polydiacetylene-Peptide Nanostructures. J. Am. Chem. Soc. 2012, 134 (4), 2028–2031.
- 91. Ryan, D. M.; Anderson, S. B.; Senguen, F. T.; Youngman, R. E.; Nilsson, B. L. Self-Assembly and Hydrogelation Promoted by F5-Phenylalanine. Soft Matter 2010, 6 (3), 475–479.
- 92. Ryan, D. M.; Nilsson, B. L. Self-Assembled Amino Acids and Dipeptides as Noncovalent Hydrogels for Tissue Engineering. Polym. Chem. 2011, 3 (1), 18–33.
- 93. Seebach, D.; Beck, A. K.; Bierbaum, D. J. The World of  $\beta$  and  $\gamma$ -Peptides Comprised of Homologated Proteinogenic Amino Acids and Other Components. Chem. Biodiversity 2004, 1 (8), 1111–1239.
- 94. Misra, R.; Sharma, A.; Shiras, A.; Gopi, H. N. Backbone Engineered γ-Peptide Amphitropic Gels for Immobilization of Semiconductor Quantum Dots and 2D Cell Culture. Langmuir 2017, 33 (31), 7762–7768.
- 95. Ron, E; Bromberg, L. Temperature-Responsive Gels and Thermogelling Polymer Matrices for Protein and Peptide Delivery. Adv. Drug Deliv. Rev. 1998, 31 (3), 197–221.
- 96. Qiu, Y.; Park, K. Environment-Sensitive Hydrogels for Drug Delivery. Adv. Drug Deliv. Rev. 2001, 53 (3), 321–339.
- 97. Pochan, D. J.; Schneider, J. P.; Kretsinger, J.; Ozbas, B.; Rajagopal, K.; Haines, L. Thermally Reversible Hydrogels via Intramolecular Folding and Consequent Self-Assembly of a de Novo Designed Peptide. J. Am. Chem. Soc. 2003, 125 (39), 11802–11803.
- 98. O'Leary, L. E. R.; Fallas, J. A.; Bakota, E. L.; Kang, M. K.; Hartgerink, J. D. Multi-Hierarchical Self-Assembly of a Collagen Mimetic Peptide from Triple Helix to Nanofibre and Hydrogel. Nat. Chem. 2011, 3 (10), 821–828.
- 99. Rizwan, M.; Yahya, R.; Hassan, A.; Yar, M.; Azzahari, A. D.; Selvanathan, V.; Sonsudin, F.; Abouloula, C. N. PH Sensitive Hydrogels in Drug Delivery: Brief History, Properties,

- Swelling, and Release Mechanism, Material Selection and Applications. Polymers 2017, 9 (4), 137.
- 100. Zhu, J.; Han, H.; Ye, T.-T.; Li, F.-X.; Wang, X.-L.; Yu, J.-Y.; Wu, D.-Q. Biodegradable and PH Sensitive Peptide Based Hydrogel as Controlled Release System for Antibacterial Wound Dressing Application. Molecules 2018, 23 (12).
- 101. Gholamali, I. Stimuli-Responsive Polysaccharide Hydrogels for Biomedical Applications: A Review. Regen. Eng. Transl. Med. 2019.
- 102. Ghosh, G.; Barman, R.; Sarkar, J.; Ghosh, S. PH-Responsive Biocompatible Supramolecular Peptide Hydrogel. J. Phys. Chem. B 2019, 123 (27), 5909–5915.
- 103. Rastogi, S. K.; Anderson, H. E.; Lamas, J.; Barret, S.; Cantu, T.; Zauscher, S.; Brittain, W. J.; Betancourt, T. Enhanced Release of Molecules upon Ultraviolet (UV) Light Irradiation from Photoresponsive Hydrogels Prepared from Bifunctional Azobenzene and Four-Arm Poly(Ethylene Glycol). ACS Appl. Mater. Interfaces 2018, 10 (36), 30071–30080.
- 104. Mamada, A.; Tanaka, T.; Kungwatchakun, D.; Irie, M. Photoinduced Phase Transition of Gels. Macromolecules 1990, 23 (5), 1517–1519.
- 105. Linsley, C. S.; Quach, V. Y.; Agrawal, G.; Hartnett, E.; Wu, B. M. Visible Light and Near-Infrared-Responsive Chromophores for Drug Delivery-on-Demand Applications. Drug Deliv Transl Res 2015, 5 (6), 611–624.
- 106. Kwon, I. C.; Bae, Y. H.; Okano, T.; Kim, S. W. Drug Release from Electric Current Sensitive Polymers. J. Controlled Release 1991, 17 (2), 149-153,156.
- 107. Sawahata, K.; Hara, M.; Yasunaga, H.; Osada, Y. Electrically Controlled Drug Delivery System Using Polyelectrolyte Gels. J. Controlled Release 1990, 14 (3), 253–262.
- 108. Liebmann, T.; Rydholm, S.; Akpe, V.; Brismar, H. Self-Assembling Fmoc Dipeptide Hydrogel for in Situ 3D Cell Culturing. BMC Biotechnology 2007, 7 (1), 88.
- 109. Jayawarna, V.; Ali, M.; Jowitt, T. A.; Miller, A. F.; Saiani, A.; Gough, J. E.; Ulijn, R. V. Nanostructured Hydrogels for Three-Dimensional Cell Culture Through Self-Assembly of Fluorenylmethoxycarbonyl–Dipeptides. Adv. Mater. 2006, 18 (5), 611–614.
- 110. Ryan, D. M.; Nilsson, B. L. Self-Assembled Amino Acids and Dipeptides as Noncovalent Hydrogels for Tissue Engineering. Polym. Chem. 2011, 3 (1), 18–33.
- 111. Fukuoka, T.; Tachibana, Y.; Tonami, H.; Uyama, H.; Kobayashi, S. Enzymatic Polymerization of Tyrosine Derivatives. Peroxidase- and Protease-Catalyzed Synthesis of Poly(Tyrosine)s with Different Structures. Biomacromolecules 2002, 3 (4), 768–774.
- 112. Rosu, C.; Cueto, R.; Russo, P. S. Poly(Colloid)s: "Polymerization" of Poly(I-Tyrosine)-Silica Composite Particles through the Photoinduced Cross-Linking of Unmodified Proteins Method. Langmuir 2016, 32 (33), 8392–8402.
- 113. Ding, Y.; Li, Y.; Qin, M.; Cao, Y.; Wang, W. Photo-Cross-Linking Approach to Engineering Small Tyrosine-Containing Peptide Hydrogels with Enhanced Mechanical Stability. Langmuir 2013, 29 (43), 13299–13306.
- 114. Fuchs, S.; Shariati, K.; Ma, M. Specialty Tough Hydrogels and Their Biomedical Applications. Adv. Healthcare Mater. 2020, 9 (2), 1901396.
- 115. Sperling, L. H. Interpenetrating Polymer Networks: An Overview. In Interpenetrating Polymer Networks Advances in Chemistry; American Chemical Society, 1994; Vol. 239, pp 3–38.

- 116. Myung, D.; Waters, D.; Wiseman, M.; Duhamel, P.-E.; Noolandi, J.; Ta, C. N.; Frank, C. W. Progress in the Development of Interpenetrating Polymer Network Hydrogels. Polym Adv Technol 2008, 19 (6), 647–657.
- 117. Dragan, E. S. Design and Applications of Interpenetrating Polymer Network Hydrogels. A Review. Chem. Eng. J. 2014, 243, 572–590.
- 118. Xin, H.; Saricilar, S. Z.; Brown, H. R.; Whitten, P. G.; Spinks, G. M. Effect of First Network Topology on the Toughness of Double Network Hydrogels. Macromolecules 2013, 46 (16), 6613–6620.
- 119. Song, F.; Li, X.; Wang, Q.; Liao, L.; Zhang, C. Nanocomposite Hydrogels and Their Applications in Drug Delivery and Tissue Engineering. J. Biomed. Nanotechnol. 2015, 11.
- 120. Gaharwar, A. K.; Peppas, N. A.; Khademhosseini, A. Nanocomposite Hydrogels for Biomedical Applications. Biotechnol. Bioeng. 2014, 111 (3), 441–453.
- 121. Carrow, J. K.; Gaharwar, A. K. Bioinspired Polymeric Nanocomposites for Regenerative Medicine. Macromol. Chem. Phys. 2015, 216 (3), 248–264.
- 122. Ahadian, S.; Ramón-Azcón, J.; Estili, M.; Liang, X.; Ostrovidov, S.; Shiku, H.; Ramalingam, M.; Nakajima, K.; Sakka, Y.; Bae, H.; Matsue, T.; Khademhosseini, A. Hybrid Hydrogels Containing Vertically Aligned Carbon Nanotubes with Anisotropic Electrical Conductivity for Muscle Myofiber Fabrication. Sci rep. 2014, 4 (1), 4271.
- 123. Sayyar, S.; Murray, E.; Thompson, B. C.; Chung, J.; Officer, D. L.; Gambhir, S.; Spinks, G. M.; Wallace, G. G. Processable Conducting Graphene/Chitosan Hydrogels for Tissue Engineering. J. Mater. Chem. B 2014, 3 (3), 481–490.
- 124. Weiss, N. O.; Zhou, H.; Liao, L.; Liu, Y.; Jiang, S.; Huang, Y.; Duan, X. Graphene: An Emerging Electronic Material (Adv. Mater. 43/2012). Adv. Mater. 2012, 24 (43), 5776–5776.
- 125. Balavoine, F.; Schultz, P.; Richard, C.; Mallouh, V.; Ebbesen, T. W.; Mioskowski, C. Helical Crystallization of Proteins on Carbon Nanotubes: A First Step towards the Development of New Biosensors. Angew. Chem., Int. Ed. 1999, 38 (13–14), 1912–1915.
- 126. Guo, Z.; Sadler, P. J.; Tsang, S. C. Immobilization and Visualization of DNA and Proteins on Carbon Nanotubes. Adv. Mater. 1998, 10 (9), 701–703.
- 127. Mattson, M. P.; Haddon, R. C.; Rao, A. M. Molecular Functionalization of Carbon Nanotubes and Use as Substrates for Neuronal Growth. J Mol Neurosci 2000, 14 (3), 175–182.
- Lu, C.-H.; Yang, H.-H.; Zhu, C.-L.; Chen, X.; Chen, G.-N. A Graphene Platform for Sensing Biomolecules. Angew. Chem. Int. Ed. Engl. 2009, 48 (26), 4785–4787.
- 129. (H, W.; Q, Z.; X, C.; T, C.; J, G.; R, Y. Graphene Oxide-Peptide Conjugate as an Intracellular Protease Sensor for Caspase-3 Activation Imaging in Live Cells. Angew Chem Int Ed Engl 2011, 50 (31), 7065–7069.
- 130. Feng, L.; Chen, Y.; Ren, J.; Qu, X. A Graphene Functionalized Electrochemical Aptasensor for Selective Label-Free Detection of Cancer Cells. Biomaterials 2011, 32 (11), 2930–2937.
- 131. Feng, L.; Zhang, S.; Liu, Z. Graphene Based Gene Transfection. Nanoscale 2011, 3 (3), 1252–1257.
- 132. Zhang, Y.; Bai, Y.; Yan, B. Functionalized Carbon Nanotubes for Potential Medicinal Applications. Drug Discov Today 2010, 15 (11–12), 428–435.

- 133. Singh, R.; Pantarotto, D.; Lacerda, L.; Pastorin, G.; Klumpp, C.; Prato, M.; Bianco, A.; Kostarelos, K. Tissue Biodistribution and Blood Clearance Rates of Intravenously Administered Carbon Nanotube Radiotracers. PNAS 2006, 103 (9), 3357–3362.
- 134. Lacerda, L.; Herrero, M. A.; Venner, K.; Bianco, A.; Prato, M.; Kostarelos, K. Carbon-Nanotube Shape and Individualization Critical for Renal Excretion. Small 2008, 4 (8), 1130–1132.
- 135. Lacerda, L.; Ali-Boucetta, H.; Herrero, M. A.; Pastorin, G.; Bianco, A.; Prato, M.; Kostarelos, K. Tissue Histology and Physiology Following Intravenous Administration of Different Types of Functionalized Multiwalled Carbon Nanotubes. Nanomedicine 2008, 3 (2), 149–161.
- 136. Mohanta, D.; Patnaik, S.; Sood, S.; Das, N. Carbon Nanotubes: Evaluation of Toxicity at Biointerfaces. J. Pharm. Anal. 2019, 9 (5), 293–300.
- 137. Allen, B. L.; Kichambare, P. D.; Gou, P.; Vlasova, I. I.; Kapralov, A. A.; Konduru, N.; Kagan, V. E.; Star, A. Biodegradation of Single-Walled Carbon Nanotubes through Enzymatic Catalysis. Nano Lett. 2008, 8 (11), 3899–3903.
- 138. Allen, B. L.; Kotchey, G. P.; Chen, Y.; Yanamala, N. V. K.; Klein-Seetharaman, J.; Kagan, V. E.; Star, A. Mechanistic Investigations of Horseradish Peroxidase-Catalyzed Degradation of Single-Walled Carbon Nanotubes. J. Am. Chem. Soc. 2009, 131 (47), 17194–17205.
- 139. Orecchioni, M.; Ménard-Moyon, C.; Delogu, L. G.; Bianco, A. Graphene and the Immune System: Challenges and Potentiality. Adv. Drug Deliv. Rev. 2016, 105 (Pt B), 163–175.
- 140. Sasidharan, A.; Panchakarla, L. S.; Sadanandan, A. R.; Ashokan, A.; Chandran, P.; Girish, C. M.; Menon, D.; Nair, S. V.; Rao, C. N. R.; Koyakutty, M. Hemocompatibility and Macrophage Response of Pristine and Functionalized Graphene. Small 2012, 8 (8), 1251–1263?
- 141. Lalwani, G.; D'Agati, M.; Khan, A. M.; Sitharaman, B. Toxicology of Graphene-Based Nanomaterials. Adv. Drug Deliv. Rev. 2016, 105 (Pt B), 109–144.
- 142. Yang, K.; Gong, H.; Shi, X.; Wan, J.; Zhang, Y.; Liu, Z. In Vivo Biodistribution and Toxicology of Functionalized Nano-Graphene Oxide in Mice after Oral and Intraperitoneal Administration. Biomaterials 2013, 34 (11), 2787–2795.
- 143. Mao, L.; Hu, M.; Pan, B.; Xie, Y.; Petersen, E. J. Biodistribution and Toxicity of Radio-Labeled Few Layer Graphene in Mice after Intratracheal Instillation. Part Fibre Toxicol 2016, 13.
- 144. Zhang, D.; Zhang, Z.; Liu, Y.; Chu, M.; Yang, C.; Li, W.; Shao, Y.; Yue, Y.; Xu, R. The Short- and Long-Term Effects of Orally Administered High-Dose Reduced Graphene Oxide Nanosheets on Mouse Behaviors. Biomaterials 2015, 68, 100–113.
- 145. Kurapati R, Russier J, Squillaci MA, *et al.* Dispersibility-Dependent Biodegradation of Graphene Oxide by Myeloperoxidase. Small 2015;11(32):3985–94.
- 146. Girish, C. M.; Sasidharan, A.; Gowd, G. S.; Nair, S.; Koyakutty, M. Confocal Raman Imaging Study Showing Macrophage Mediated Biodegradation of Graphene in Vivo. Adv Healthc Mater 2013, 2 (11), 1489–1500.
- 147. Newman, L.; Rodrigues, A. F.; Jasim, D. A.; Vacchi, I. A.; Ménard-Moyon, C.; Bianco, A.; Bussy, C.; Kostarelos, K. Nose-to-Brain Translocation and Cerebral Biodegradation of Thin Graphene Oxide Nanosheets. Cell Rep Phys Sci. 2020, 100176.

# CHAPTER 2. AMINO ACID-BASED SUPRAMOLECULAR HYDROGELS IN COMBINAISON WITH CARBON NANOMATERIALS

#### 2.1 Introduction

Supramolecular gels formed by the self-assembly of low molecular weight gelators (LMWGs) are receiving significant attention thanks to their potential in the biological field, for instance in drug delivery.<sup>2</sup> LMWG-based gels possess advantages such as easy preparation and multiple responsiveness, compared to polymer gels, where the monomers are covalently bonded. Indeed, they can be responsive to different stimuli including pH and temperature, as they are held together through non-covalent bonds.<sup>3</sup> Molecular selfassembly is a natural process used by amino acids, peptides, nucleic acids and phospholipids to form ordered structures.<sup>4</sup> This mechanism is driven by various non-covalent interactions including hydrophobic interactions, hydrogen bonds,  $\pi$ -stacking between aromatic rings and/or electrostatic interactions. Some amino acids having the capacity to self-assemble into fibrils have been exploited as LMWGs.5-8 These types of hydrogels have shown potential applications in drug delivery, 9,10 tissue engineering, 11 and regenerative medicine. 12 Hybrid hydrogels incorporating carbon-based nanomaterials such as carbon nanotubes (CNTs) and graphene, have recently attracted increasing attention due to their high electrical conductivity and high mechanical strength. 13-17 In addition, these hybrid hydrogels are useful for near-infrared (NIR) irradiation-triggered drug release, thanks to the capacity of carbon nanomaterials to generate heat upon NIR light irradiation. 18-22 This feature is advantageous for an on-demand drug release because light can be used as an external stimulus to control the liberation of active molecules preloaded in the hybrid hydrogels due to enhanced local temperature, with high spatial and temporal precision. In addition, NIR light is more favorable than visible light for in vivo applications due to its higher tissue penetration, low energy absorption, and minimum side effects for human tissue and organs. Both graphene oxide (GO) and functionalized CNTs have been extensively used for biomedical applications. <sup>23,24</sup> We and other groups have previously demonstrated the absence of toxicity of well-purified and functionalized CNTs<sup>25-27</sup> and GO<sup>28,29</sup> in vitro and in vivo.

#### 2.2 Objectives

With this study, we have screened a variety of aromatic amino acid derivatives for their capacity to self-assemble and to form hydrogels. Oxidized CNTs (ox-CNTs) or GO were incorporated into the most stable hydrogels, to study their photothermal properties and to control the release of different drug models. The hybrid hydrogels were characterized by different techniques including electron microscopy, circular dichroism (CD), and rheology. Molecular dynamics (MD) simulations were performed to understand the main interactions leading to the formation of the hydrogels. Finally, rhodamine B, methylene blue and Lascorbic acid were incorporated in the hybrid hydrogels as model drugs. A comparative study of the quantity of water and drug released during NIR irradiation was performed.

The purpose of this study was to develop stable hybrid supramolecular hydrogels containing carbon nanomaterials for high performance drug release and to provide new elements of understanding concerning the self-assembly of amino acids into hydrogels.

#### 2.3 Results and discussion

#### 2.3.1 Self-assembly of aromatic amino acids

In 2015 our team investigated the capacity of tyrosine to form well-ordered nanostructures under different experimental conditions. It was observed that Tyr can self-assemble into different supramolecular architectures including nanoribbons, branched structures and fern-like arrangement influenced by the concentration, the aging of the solution and the type of solvent used. <sup>30</sup> In this context and following these previous results, we studied the self-assembly properties of tyrosine, phenylalanine and several derivatives of these two amino acids with protected amine, carboxylic acid and/or hydroxyl functions. The influence of the solvent on the self-assembly was studied by comparing the structures obtained in MilliQ® water and in methanol (MeOH). The amino acids were dissolved in the solvent and let under ambient condition for 1 h. The supernatant of the amino acid solution was then withdrawn and deposited onto a TEM grid. Figure 1 shows the transmission electron microscopy images of the self-assembly of L and D-tyrosine. At the concentration studied (0.5 mg·mL-¹) L- or D-tyrosine in water formed nanoribbons, which are relatively flexible with visible twists (see arrows in Figure 2.1a). These structures are several hundred micrometers long and form a more or less dense network. In methanol, L-Tyr is organized in rods, while D-Tyr forms

shorter fibers with the appearance of small spherical particles. Previous results obtained in the laboratory have shown that the effect of the concentration in the self-assembly of tyrosine could induce such structural differences.<sup>30</sup> These differences observed in methanol are thus probably due to the lower solubility of tyrosine in this solvent, which does not guarantee the same amino acid concentration in the supernatant.

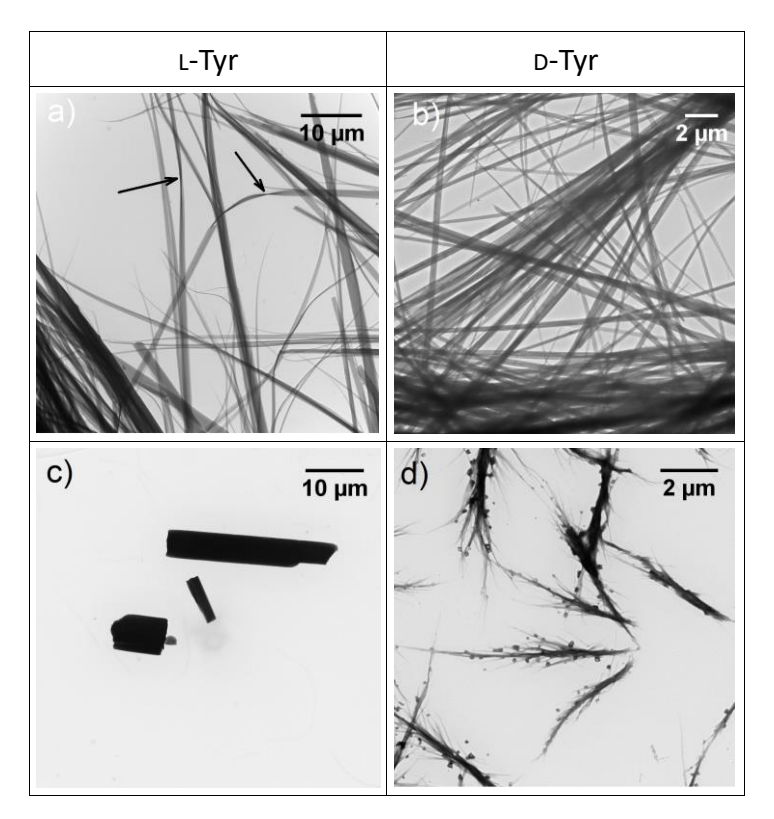


**Figure 2.1.** TEM images of L-Tyr and D-Tyr samples at a concentration of 0.5 mg·mL<sup>-1</sup> in water (a and b) and methanol (c and d).

When the carboxylic acid is protected as a methyl ester and the amine with a carboxybenzyl (Z-Tyr-OMe), shorter rod structures are formed in water (Figure 2.2). In methanol it forms instead spherical structures with a large diameter distribution ranging from 0.2 to 10.7 µm (n=60). For L-Tyr with the carboxylic acid protected as a benzyl ester (H-Tyr-OBzl), structures similar to those observed for the self-assembly of Z-Tyr-OMe are found. However, when the amine and hydroxyl are protected with a carboxybenzyl (Z) and benzyl group, respectively (Z-Tyr(Bzl)-OH), tyrosine gives fibrillar structures in methanol with a network of very fine fibers having a length of a few micrometers, linked with agglomerates. The self-assembly of tyrosine derivatives protected by a Fmoc group (Fmoc-Tyr-OH, Fmoc-Tyr(tBu)-OH and Fmoc-Tyr(Bzl)-OH) was also studied. In water these amino acid derivatives were self-organized into

single rods (Fmoc-Tyr(tBu)-OH) or rods linked together by a dense network of fine fibers (Fmoc-Tyr-OH) or in a needle structure capable of aggregation (Fmoc-Tyr(BzI)-OH) (Figure 2.3).

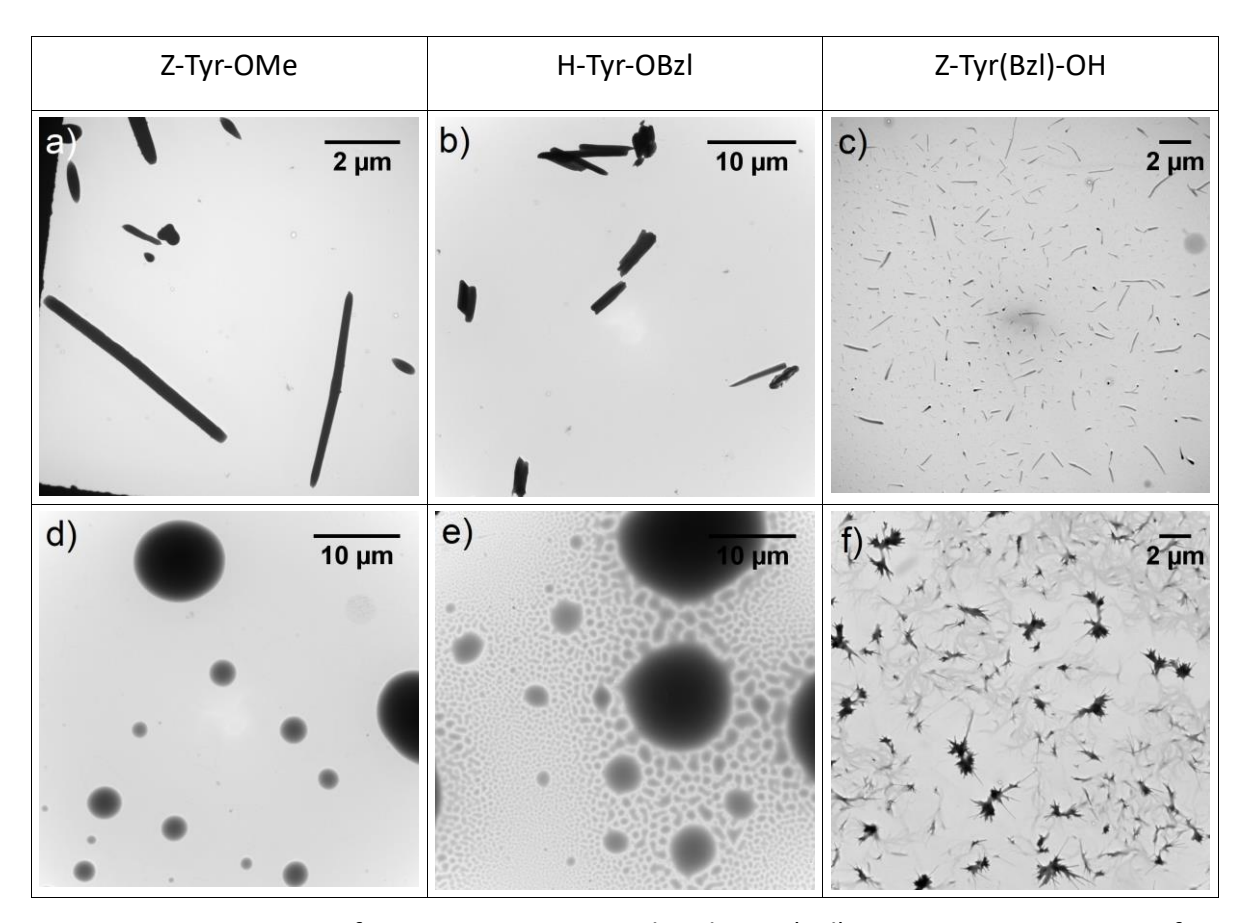


**Figure 2.2.** TEM images of Z-Tyr-OMe H-Tyr-OBzl and Z-Tyr(Bzl)-OH at a concentration of 0.5 mg·mL<sup>-1</sup> in water (a, b and c) and methanol (d, e and f).

For the three amino acids solubilized in methanol, the appearance of spherical particles with dendritic structures was observed in the case of the Fmoc-Tyr(Bzl)-OH. Tyrosine has different interaction sites such as the aromatic ring, as well as the amine, the carboxylic acid, and the hydroxyl groups, which may be involved in hydrogen bonds. The presence of aromatic protecting groups promotes aggregation probably by increasing hydrophobic interactions and  $\pi$ -stacking. Our results showed that tyrosine gives shorter condensed structures (rods/aggregates) with protecting aromatic groups. The particles formed from the self-assembly of Fmoc-Tyr(tBu)-OH in methanol were also studied by scanning electron microscopy (Figure 2.4). Rounded structures with wide disparity in size were observed. Some structures appear to be completely spherical while others appear to be partially flattened, which is probably due to the interface with the substrate.

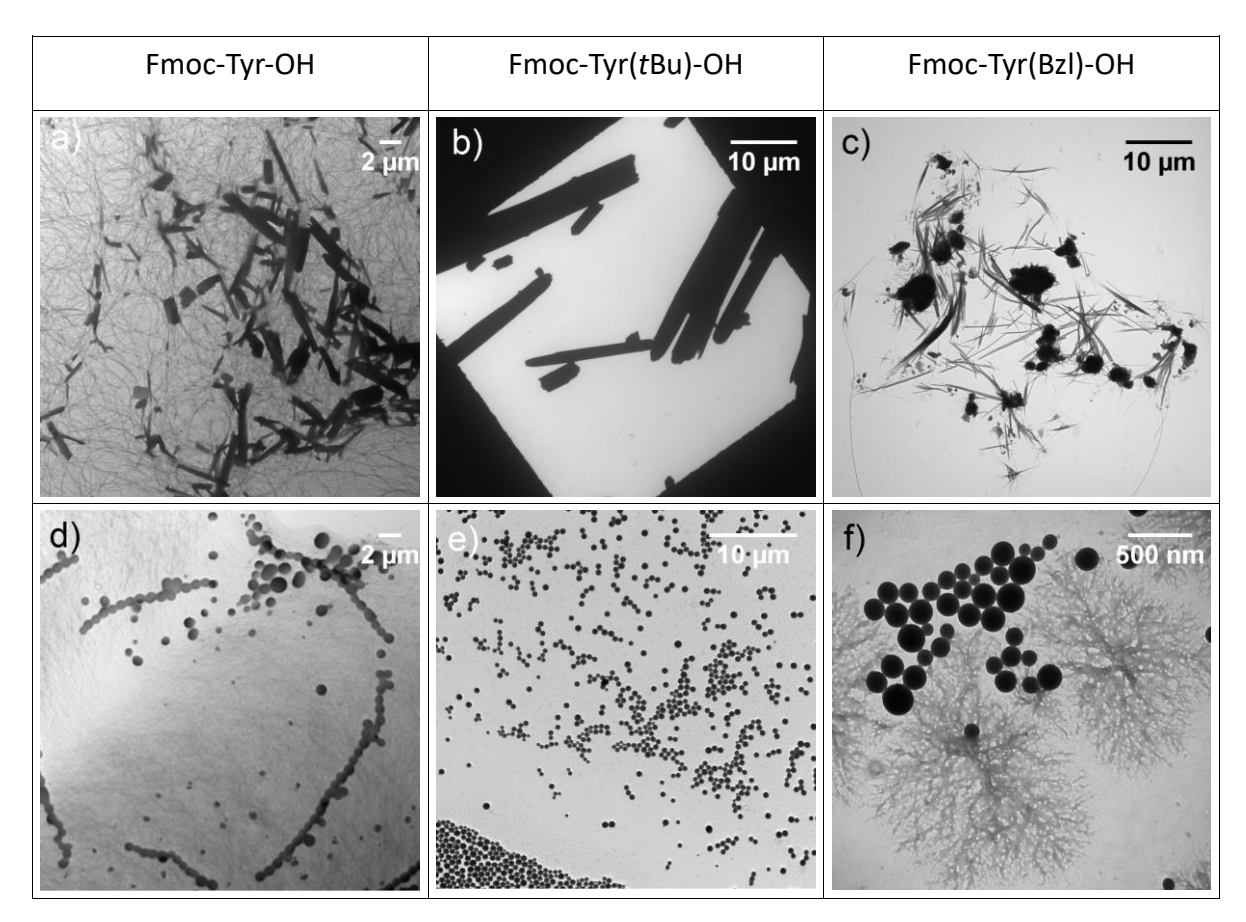


**Figure 2.3.** TEM images of Fmoc-Tyr-OH, Fmoc-Tyr(tBu)-OH and Fmoc-Tyr(Bzl)-OH at a concentration of 0.5 mg·mL<sup>-1</sup> in water (a, b and c) and methanol (d, e and f).

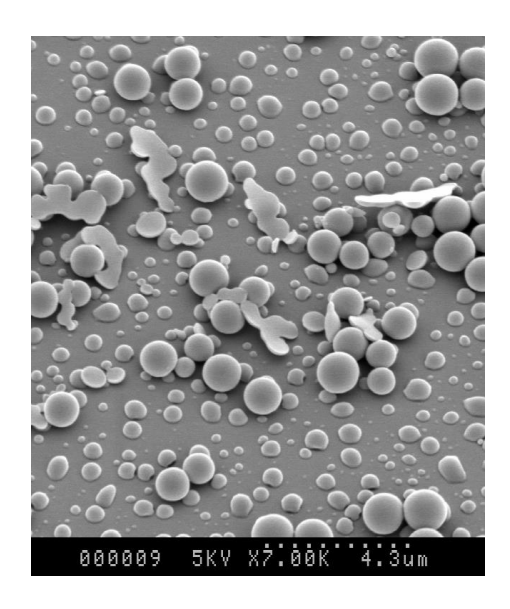


**Figure 2.4.** SEM image of Fmoc-Tyr(*t*Bu)-OH sample at a concentration of 0.5 mg·mL<sup>-1</sup> in methanol.

Like Fmoc-Tyr-OH, Fmoc-Phe-OH formed rod-like structures in water. It organizes itself into fibrous tree-like structures in methanol, which were numerous and homogeneously

distributed on the TEM grid. Our results indicated that L-Phe and Fmoc-Phe-OH are capable of self-assembling into fibrillar structures in aqueous and organic solvents (Figure 2.5).

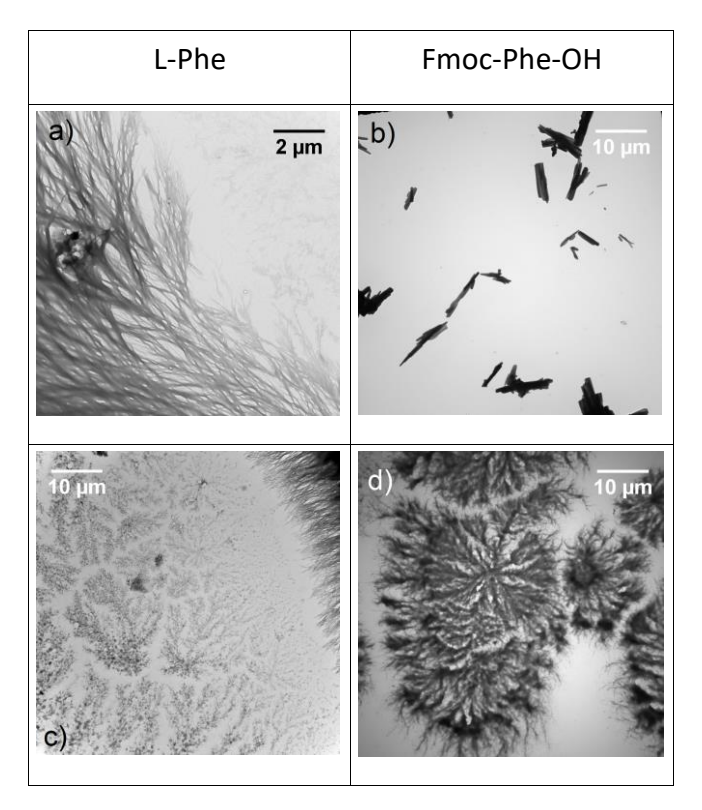


**Figure 2.5.** TEM images of L-Phe and Fmoc-Phe-OH samples at a concentration of 0.5 mg·mL<sup>-1</sup> in water (a and b) and methanol (c and d).

# 2.3.2 Hydrogel formation

Different single and binary mixtures of protected and non-protected aromatic amino acids were initially studied for hydrogelation (Figure 2.6). The samples were prepared using the solvent-triggered approach, where the gelators are first dissolved in dimethyl sulfoxide (DMSO) by using sonication followed by addition of water to reach 2 % DMSO/H<sub>2</sub>O (v/v).<sup>31</sup> At such low concentration DMSO can be used in biological experiments as it shows no cytotoxicity.<sup>32,33</sup> We observed that binary systems composed of non-protected amino acids were highly soluble leading to optically transparent solutions, whereas co-assemblies of protected amino acids resulted in the formation of precipitates in biphasic systems made of gel and liquid, or led to gel-like structures (Table 2.1). The gelation of the samples was confirmed by the vial inversion

Figure 2.6. Aromatic amino acids and their protected derivatives used for the hydrogel formation study.

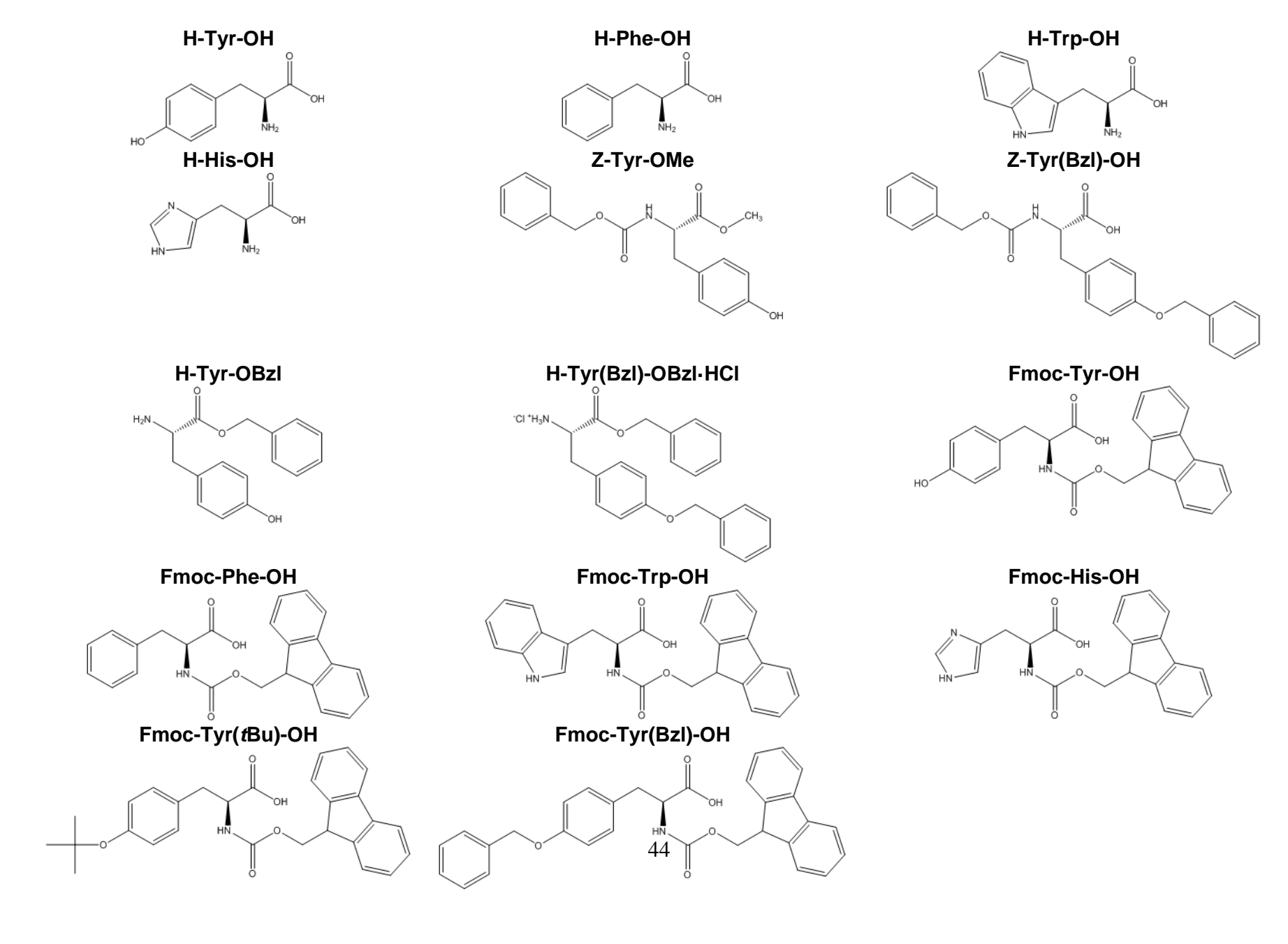
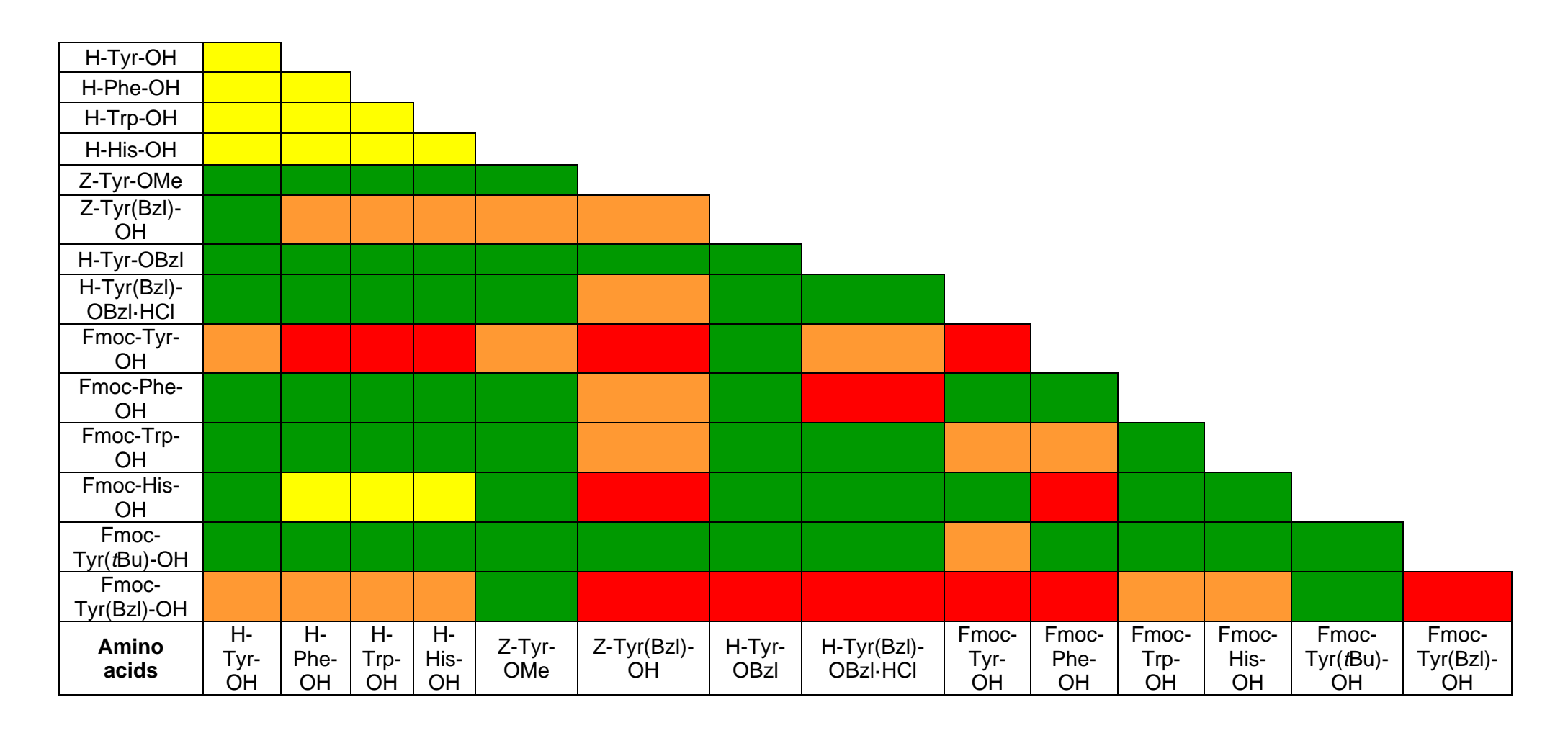


**Table 2.1.** Co-assembly of amino acid derivatives in 2% DMSO/H<sub>2</sub>O (v/v). Yellow color = transparent liquid, green = liquid + suspensions/precipitates, orange = liquid + gel, red = gel.



test and we observed that 14 mixtures formed hydrogels. In all cases at least one of the components was a Fmoc-protected amino acid derivative. Our results confirm that the presence of the aromatic fluorenyl ring helps in the gelation process. Most hydrogels were obtained from a binary mixture containing Fmoc-Tyr-OH or Fmoc-Tyr(Bzl)-OH. For this reason, we decided to focus our comparative work on two stable hydrogels corresponding to the binary systems Fmoc-Tyr-OH/Fmoc-Tyr(Bzl)-OH (named gel 1) and Fmoc-Phe-OH/Fmoc-Tyr(Bzl)-OH (named gel 2) (Figure 2.7). We noticed that a sequential addition of DMSO and water was very important as the dissolution of the gelators directly in a mixture of 2 % DMSO in water did not result in gel formation.

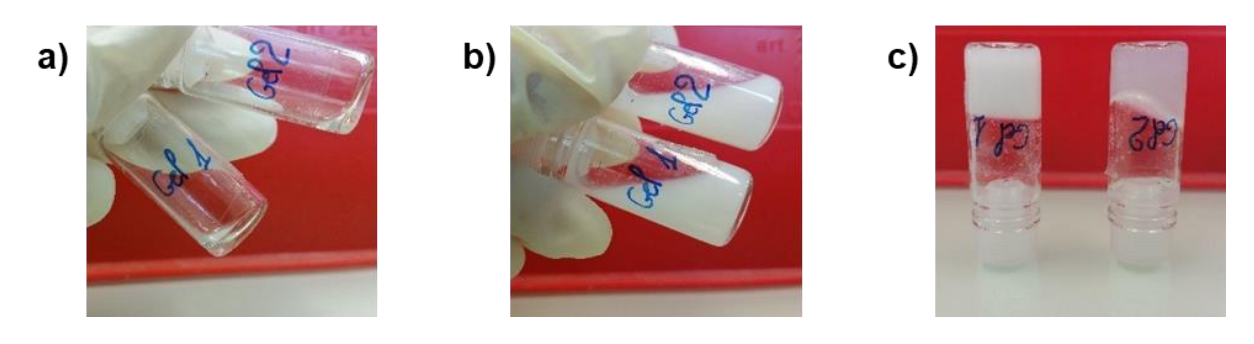


**Figure 2.7.** Photographs of the formation of gel 1 and gel 2: a) solution of the amino acids in DMSO, b) immediately after the addition of water, and c) after 2 h.

# 2.3.3 Formation of hybrid hydrogels containing carbon nanomaterials

Since carbon nanomaterials have excellent photothermal properties under NIR light irradiation, hybrid hydrogels containing CNTs or graphene offer a great potential for NIR irradiation-triggered drug release applications. We first studied the incorporation of pristine CNTs and ox-CNTs at three different concentrations (0.025 wt%, 0.1 wt% and 0.5 wt%) into gel 1. For this purpose, aqueous suspensions of pristine CNTs or ox-CNTs were prepared by sonication and immediately added to the solution of gelators in DMSO. The gelation time was not affected by the presence of the pristine CNTs. However, due to their low water dispersibility, the pristine CNTs were non-homogenously dispersed in the gel at all concentrations obtaining heterogeneous gels (Figure 2.8a-c).

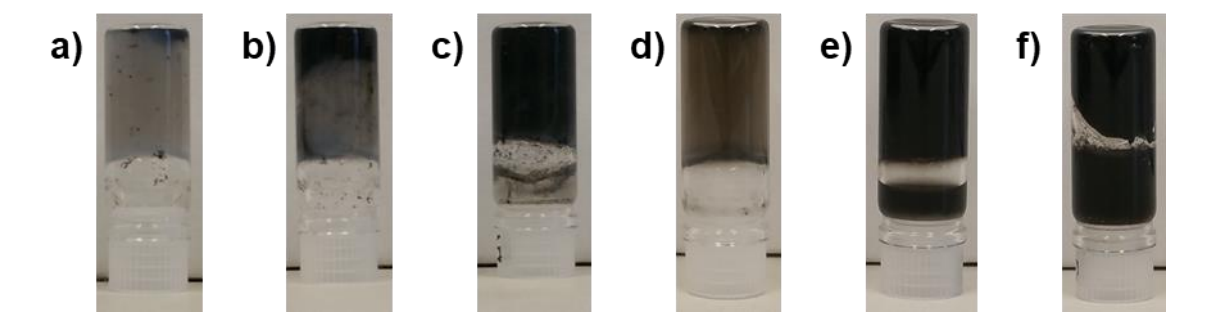


**Figure 2.8.** Photographs of a) gel 1 + 0.025 wt% pristine CNTs, b) gel 1 + 0.1 wt% pristine CNTs, c) gel 1 + 0.5 wt% pristine CNTs, d) gel 1 + 0.025 wt% ox-CNTs, e) gel 1 + 0.1 wt% ox-CNTs, and f) gel 1 + 0.5 wt% ox-CNTs, after 2 h gelation.

The dispersion was drastically improved by using ox-CNTs and we observed that the maximum concentration of ox-CNTs that can be incorporated into gel 1 to obtain a homogeneous hybrid gel was 0.025 wt% (Figure 2.8d). Increasing the concentration of nanomaterials disturbed the gelation process as we observed the appearance of a liquid phase (Figure 2.8e-f). Therefore, 0.025 wt% was chosen as the optimal concentration of ox-CNTs. The same experiments were performed using 0.025 wt% of GO to compare the gelation behavior of GO did not prevent the gel formation (Figure 2.9). We noticed that the gel color was more homogeneous for gel 2 compared to gel 1, whatever ox-CNTs or GO had been incorporated into the gel. This difference indicates that gel 2 seems to be more homogeneous compared to gel 1.

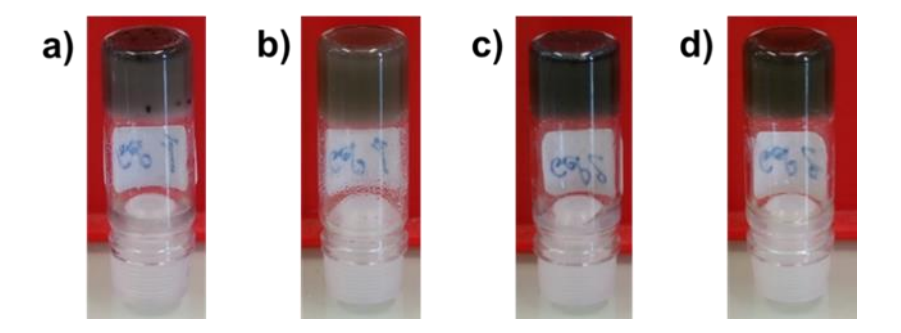


**Figure 2.9.** Photographs of a) gel 1 + 0.025 wt% ox-CNTs, b) gel 1 + 0.025 wt% GO, c) gel 2 + 0.025 wt% ox-CNTs, and d) gel 2 + 0.025 wt% GO, after 2 h gelation.

#### 2.3.4 Structural characterization

The morphology of native and hybrid gel 1 and gel 2 was studied by SEM and TEM. The SEM images of the native gels show the presence of long fibrils organized into highly

interconnected networks (Figure 2.10a-b). The TEM analysis revealed that the majority of the fibrils in gel 1 (Figure 2.10c) has a width of 10-50 nm with a few larger fibrils (50-80 nm) (Figure 2.11a). In the case of gel 2 (Figure 2.10d), although the majority has a width of 20-50 nm similar to gel 1, the fibrils are more variable in size having a diameter in the range of 20-100 nm (Figure 2.11b). This difference suggests that the presence of the hydroxyl group of tyrosine can influence the fibril width probably due to the formation of additional hydrogen bonding. The presence of ox-CNTs does not disturb the self-assembly of the amino acid derivatives into fibrils of similar size and morphology (Figure 2.10e-f, Figure 2.11c-d), but we observed a higher diameter distribution for both gels containing GO from 10 to 200 nm (Figure 2.10g-h, Figure 2.11e-f).

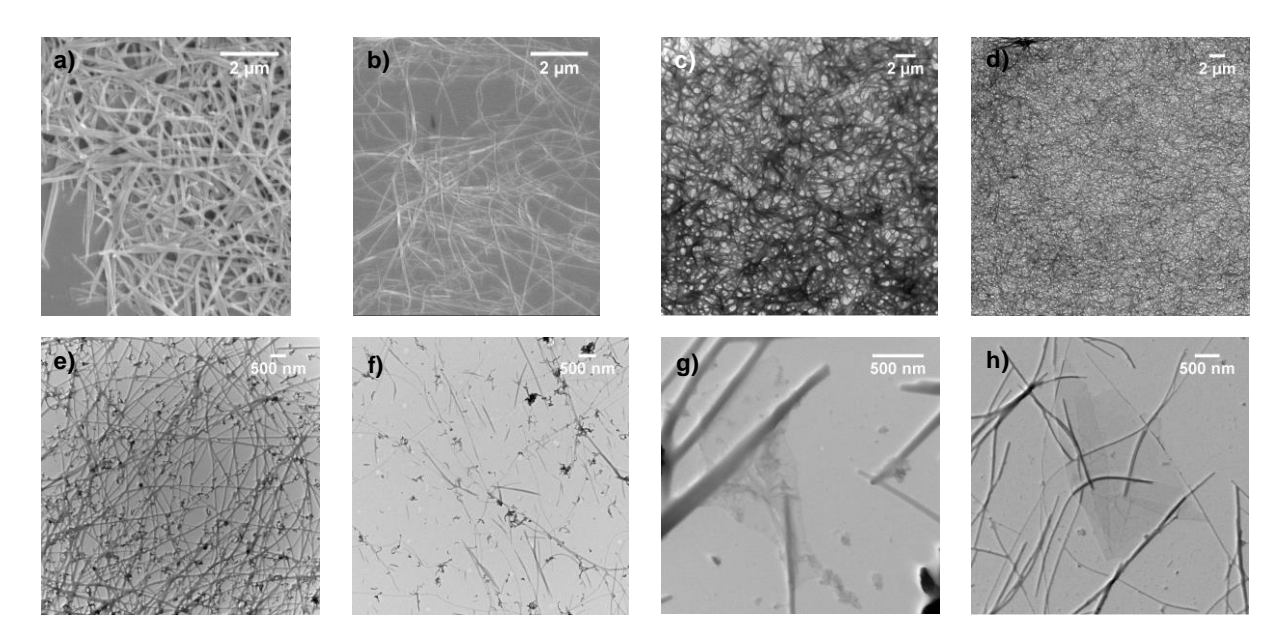


**Figure 2.10.** SEM images of a) gel 1 and b) gel 2. TEM images of c) gel 1, d) gel 2, e) gel 1 + 0.025 wt% ox-CNTs, f) gel 2 + 0.025 wt% ox-CNTs, g) gel 1 + 0.025 wt% GO, and h) gel 2 + 0.025 wt% GO.

The TEM images also show that the ox-CNTs and GO are in contact with the fibrils certainly due to  $\pi$ - $\pi$  interactions with the aromatic moieties of the gelators (Figure 2.10e-h). Especially, the ox-CNTs are in close interactions with the surface of the fibrils, which may be facilitated by their tubular shape. In Figure 2.10f-h, we selected images showing a lower fibril density in order to be able to visualize the carbon nanomaterials and their interactions with the fibrils. This is the reason why the fibrils look less aggregated.

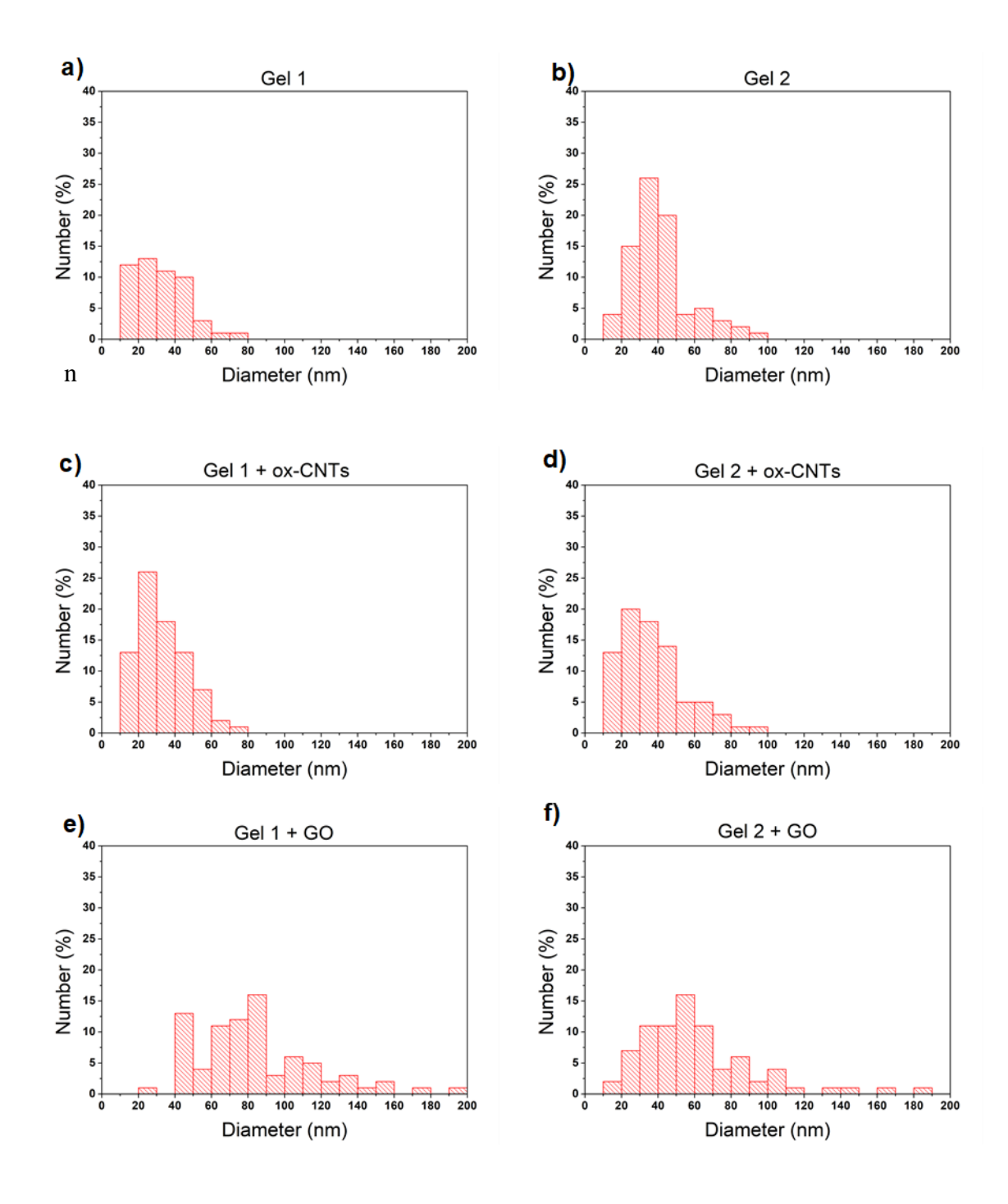


Figure 2.11. Diameter distribution of the amino acid fibrils in a) gel 1 (n=80), b) gel 2 (n=80), c) gel 1 + 0.025 wt% ox-CNTs (n=80), d) gel 2 + 0.025 wt% of ox-CNTs (n=80), e) gel 1 + 0.025 wt% GO (n=80), and f) gel 2 + 0.025 wt% GO (n=80).

#### 2.3.5 Circular dichroism

The native gel 1 and gel 2 and the hybrid gels containing the nanomaterials were characterized by CD. Previous studies have shown that fibrils derived from Fmoc aromatic amino acids are supported by  $\pi-\pi$  interactions between the aromatic moieties with characteristic CD signatures at 270-310 nm attributed to the  $\pi-\pi^*$  Fmoc-Fmoc excitation and at 200-230 nm corresponding to the  $\pi-\pi^*$  phenyl side chain excitation and a hydrogen bond network involving the carbamate functionality.<sup>38</sup>

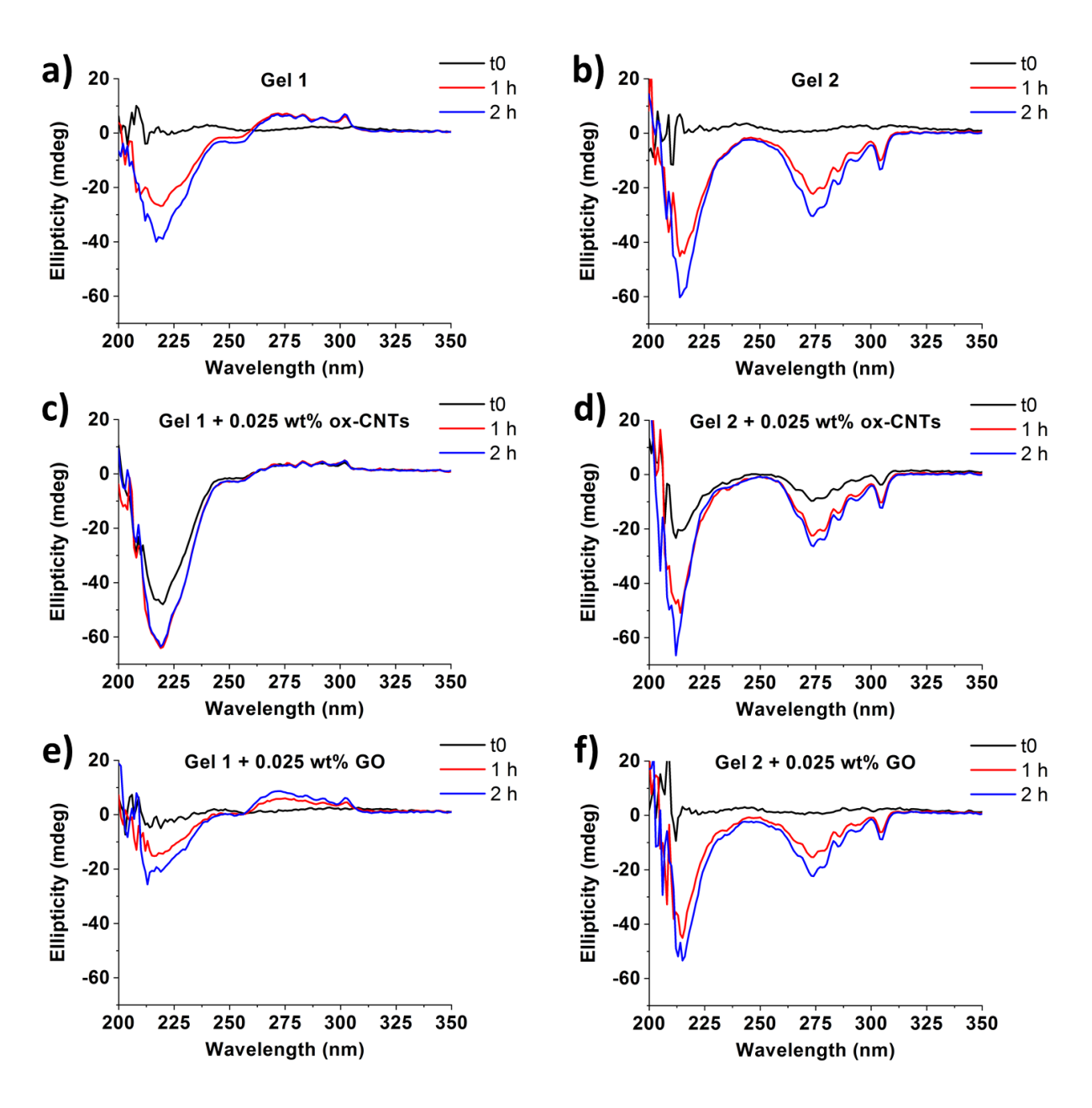


Figure 2.12. CD spectra of a) gel 1, b) gel 2, c) gel 1 + 0.025 wt% ox-CNTs, d) gel 2 + 0.025 wt% ox-CNTs, e) gel 1 + 0.025 wt% GO, and f) gel 2 + 0.025 wt% GO, at different time points.

For all samples, the gel solutions were sonicated for 10 s before being transferred into a cylindrical 0.1 mm quartz cuvette. The kinetics of the hydrogelation process was studied by monitoring the CD signal as a function of time. The CD spectrum of gel 1 does not show any signal at t0 (Figure 2.12a). After 1 h the hydrogelation was characterized by the appearance of a negative band centered at ~220 nm and a broad positive band between 270 and 310 nm. These two bands are derived from the  $\pi$ - $\pi$  amino acid side chain-side-chain and Fmoc-Fmoc interactions.<sup>39</sup> An increase of the signal was observed between 1 h and 2 h showing that the co-assembly can be described as a two-step mechanism, a first step of fibril organization into chiral structures and a second step of evolution of the final fibrils towards a state of equilibrium. The CD analysis was performed for longer time (> 2 h), but no significant differences were observed compared to the spectrum at 2 h indicating that the three-dimensional network reached a stable state. Similarly, the CD spectrum of gel 2 showed no signal at t0 with the appearance of characteristic bands after 1 h of gelation (Figure 2.12b). Indeed, a negative band was also observed at ~220 nm, as well as another negative band between 270 and 310 nm, which looks like a sort of mirror image of the band obtained for gel 1 in this region. We observed instead a difference in the hydrogelation kinetics for the hybrid CNT-based gels. For both gel 1 and gel 2 the hydrogelation was more rapid, showing CD signals already at tO (Figure 2.12c-d). The presence of the ox-CNTs in the hydrogel matrix had no impact on the structural organization of the fibrils as similar bands appeared in both cases. For the gels containing GO we also observed similar bands and kinetics in comparison with the native gels (Figure 2.12e-f). As control we analyzed an aqueous suspension of ox-CNTs or GO at similar concentrations and no CD signals were observed (Figure 2.13), allowing to conclude that ox-CNTs and GO do not interfere with the CD measurements.

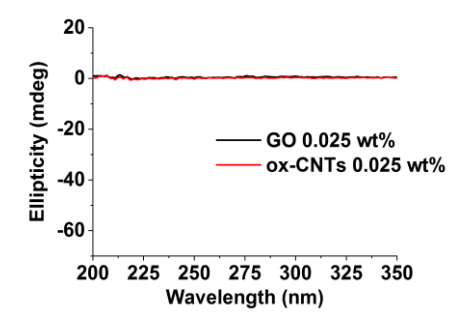
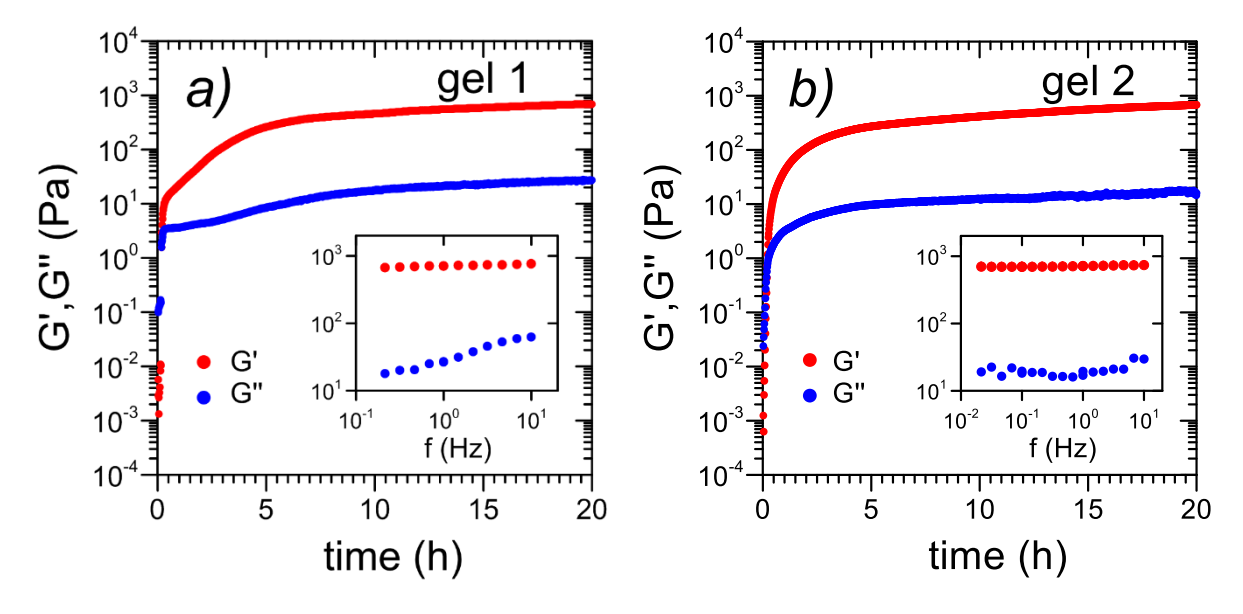


Figure 2.13. Circular dichroism spectra of 0.025 wt% GO and ox-CNTs suspensions in water.

Compared to the two-dimensional shape of the GO sheets, the quasi-one-dimensional tubular shape of the ox-CNTs, probably facilitated the interactions with the gel fibrils, which accelerated the gelation process.

# 2.3.6 Mechanical properties

Both hydrogels were characterized by rheology (oscillatory time and frequency sweep) to assess the time of gelation and their viscoelastic properties in collaboration with Dr. Dominique Collin at the Institut Charles Sadron (ICS, Strasbourg). Time sweeps were first performed by monitoring the evolution of the real part G' and imaginary part G" of the complex shear modulus as a function of time for native gel 1 (Figure 2.14a) and gel 2 (Figure 2.14b).



**Figure 2.14.** Evolution of the real part G' and imaginary part G" of the shear modulus for a) gel 1 and b) gel 2. The frequency was 1 Hz and the temperature was 20°C. The inset figures correspond to the variation of G' and G" as a function of frequency, measured 20 h after the gel formation.

A gradual change in behavior from a liquid (G' < G'') to a solid state (G' > G'') was observed for both gels in approximatively 10 min after adding water to the solution of the amino acids in DMSO (Figure 2.15). A second growth regime was noticed approximatively 5 h after the gelation, showing a much slower change in the hydrogel rheological response over time. This regime was associated with an aging phenomenon, which is also usually found in polymer gels<sup>40,41</sup> and organogels,<sup>42,43</sup> corresponding to the progressive strengthening of the elastic

network. In this regime, the evolution of the complex shear modulus with frequency (Figure 2.14, insets) revealed a behavior, which is similar to many organogels<sup>43,44</sup> and physical gels.<sup>45,46</sup> Indeed, a low frequency behavior characterized by a plateau was observed for G' and G". Both gel 1 and gel 2 displayed similar G' values, indicating that these two systems have almost the same modulus of rigidity. Regarding the G" values, the hydrodynamic regime was reached in a slightly lower frequency range for gel 1 compared to gel 2. This small difference could be due to the presence of larger heterogeneities in size and number for gel 1 compared to gel 2, which was confirmed by the photographs of the hybrid gels in Figure 2.9. These heterogeneities could also explain the slight successive slope failures observed for gel 1 in the first part of the gel formation kinetics curve.

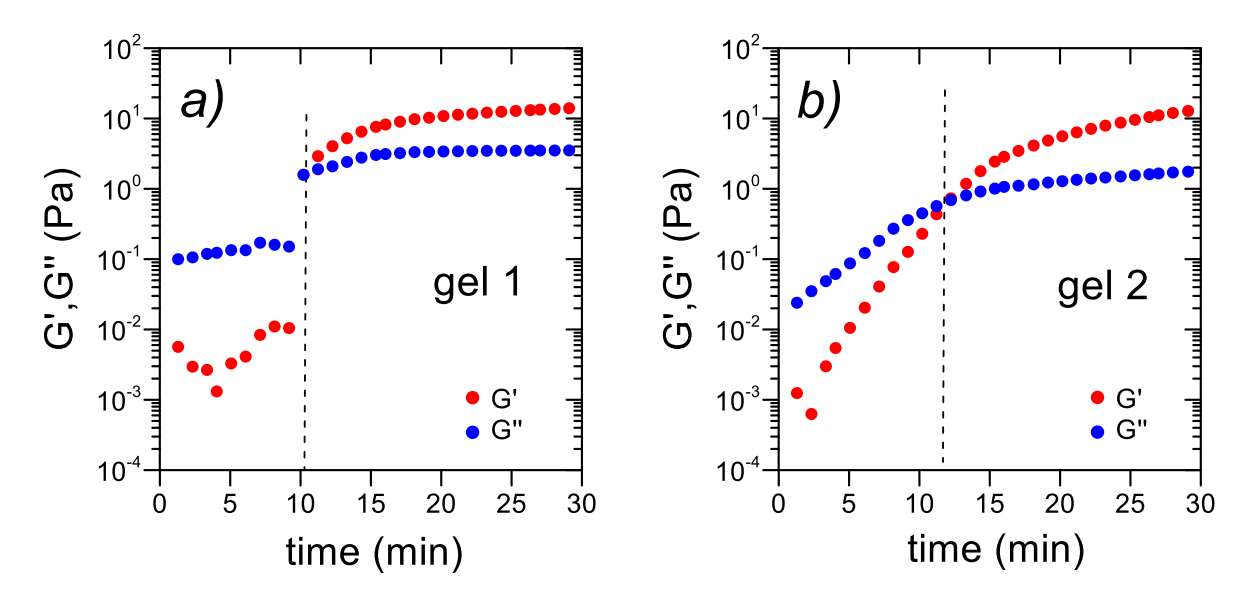


**Figure 2.15.** Evolution of G' and G" for a) gel 1 and b) gel 2. The frequency was 1 Hz and the temperature was 20°C. The time of gelation, given by the crossover of G' and G", is quite similar for both gels.

The rheological studies were then extended to the hybrid gels. The experiments were performed on gel 1 containing ox-CNTs or GO at a concentration of 0.025 wt% and the incorporation of the carbon nanomaterials did not change its rigidity, which remained quite similar to that of the native gel (Figure 2.16). Likewise, the response in frequency of both hybrid gels was not affected by the presence of GO or ox-CNTs, suggesting that the structure of the fibrillar network was not altered by the presence of GO and ox-CNTs, as we also showed by TEM (Figure 2.10e-h). Generally, carbon nanomaterials are used as reinforcing agents into hydrogels due to the mechanical strength of CNTs and graphene-based

nanomaterials (using higher concentrations in comparison to our study), which can be exploited for tissue engineering. <sup>19,47</sup> But, in our case similar rheological properties were expected between the native gels and hybrid gels due to the very low concentration of carbon nanomaterials, which is however sufficient to induce a photothermal effect (*vide infra*). Nevertheless, the kinetics of gelation was affected and was found to be strongly dependent on the shape of the carbon nanomaterials. Indeed, the gelation time was slightly reduced for GO-loaded gel 1, whereas it was so lowered when ox-CNTs were incorporated into the gel, that it could not be measured during our experiments (Figure 2.17a-b). In the latter case the faster gelation time could be explained by the tubular shape of the CNTs, which favors tight interactions with the amino acid fibrils compared to the two-dimensional shape of the GO sheets, as previously observed by TEM (Figure 2.10e-h). These results are also in good agreement with CD showing a faster gelation time for CNT-loaded gels (Figure 2.12c-d). The altered gelation time, which is linked to the shape of the carbon nanomaterials, suggests that the gelation mechanism is driven by a nucleation growth process, in which the CNTs promote the nucleation of the fibrils.

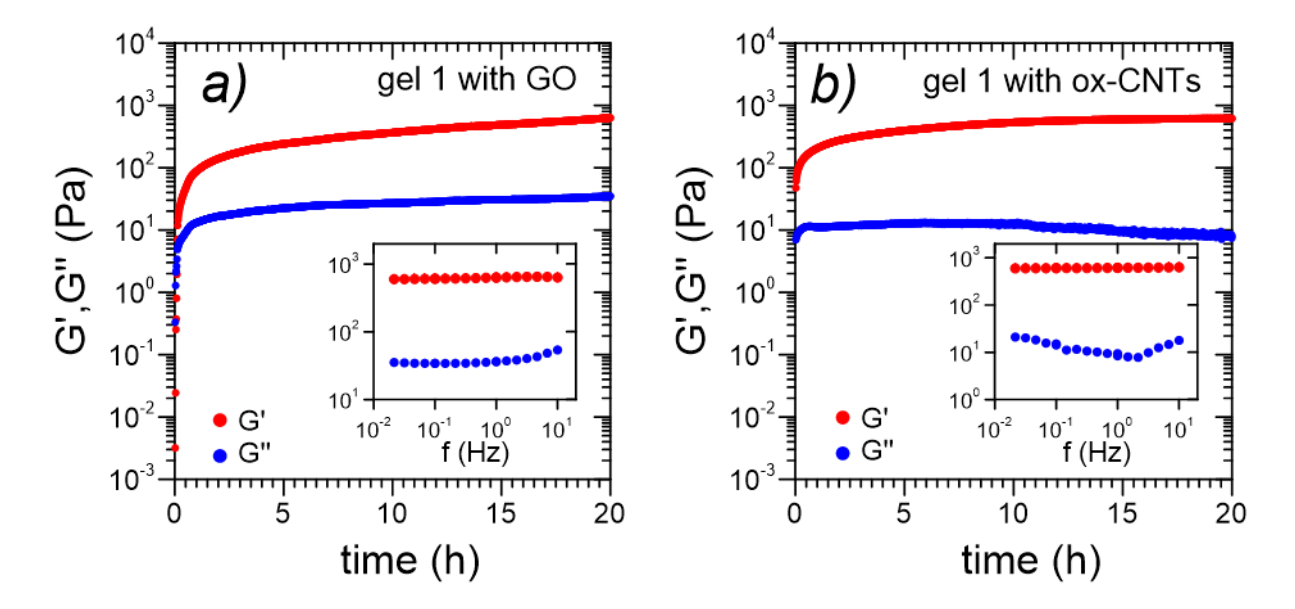


**Figure 2.16.** Evolution of G' and G" for gel 1 loaded with a) GO and b) ox-CNTs. The frequency was 1 Hz and the temperature was 20°C. The inset figures correspond to the variation of G' and G" as a function of frequency, measured 20 h after the gel formation.

To support this hypothesis, shear measurements were performed on gel 1 loaded with ox-CNTs at a concentration 10 times lower (0.0025 wt%). The gelation time found for this concentration was  $^4$  min (Figure 2.17c), a value intermediate between the time for the gel at the concentration of 0.025 wt% (< 1 min) and that of the native gel (10 min). This result shows that the gelation time can be fully monitored by the amount of ox-CNTs loaded in the gel.

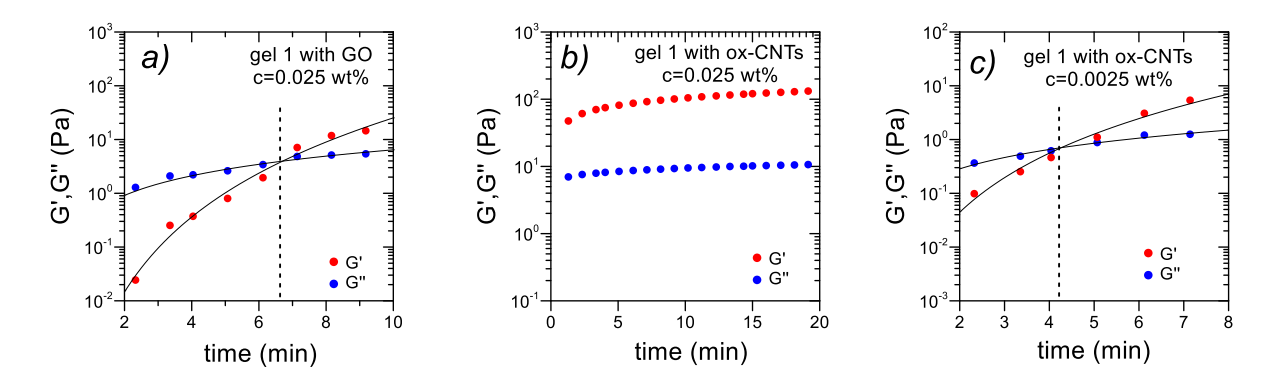


Figure 2.17. Evolution of G' and G" near the sol-gel transition for a) gel 1 loaded with GO and b) with ox-CNTs at a concentration of 0.025 wt% and c) at 0.0025 wt%. The frequency was 1 Hz and the temperature was 20°C. The time of gelation (indicated by the dashed line) is given by the crossover of G' and G". b) For gel 1 with the highest concentration of ox-CNTs, the gelation time could not be assessed as the gelation was too fast to be detected in our experimental conditions.

#### 2.3.7 Computational analysis

We decided to perform MD simulations to highlight the main interactions that lead to the hydrogel formation in collaboration with Dr. Rachel Schurhammer from the University of Strasbourg. Both gel 1 and gel 2 were simulated at different concentrations of protected amino acids either in 2 % DMSO/H<sub>2</sub>O (v/v) solution or in pure DMSO (see Table 2.2 for the composition of the simulated systems). Each solution was simulated for at least 50 ns. Final snapshots are given in Figure 2.18 and Figure 2.19. Both mixtures show the same behavior in aqueous solution with the formation of aggregates during the dynamics, independently of the initial concentration. The conclusions are quite different in pure DMSO where the protected amino acids stay well-dispersed in the box. These results can explain why the gelation process needs a two-step procedure with a first dilution in DMSO, allowing to solubilize the amino acids, followed by the dilution in water where the nano-arrangement occurs. More specifically, as illustrated in Figure 2.18, the aggregation of the protected

amino acids is induced in DMSO/ $H_2O$  by specific  $\pi$ - $\pi$  and CH- $\pi$  interactions. Table 2.3 gives the average number of these interactions among the dynamics.

**Table 2.2.** Description of the simulated systems: mol1 designs either Fmoc-Phe-OH or Fmoc-Tyr-OH and mol2 refers to Fmoc-Tyr(Bzl)-OH.

Number of	Box size (in ų)	Type of box	Number of	Number of	Simulated	
mol1+			$H_2O$	DMSO	time (ns)	
mol2			molecules	molecules		
10 + 10	96.8 <sup>3</sup>	Cubic box	28 800	1 600	100	
30 + 30	93.6 <sup>3</sup>	Cubic box	25 200	1 400	100	
30 + 30	69.5x69.5x169.	Rectangular	25 200	1 400	50	
	3	box				
30 + 30	100.83	Cubic box	-	8 500	100	
60 + 60	85.8 <sup>3</sup>	Cubic box	18 000	1 000	300	

For all the simulated systems, the principal  $\pi$ - $\pi$  interactions are between the aromatic group of tyrosine and the Fmoc protecting group (Figure 2.18), followed by all the interactions where the Fmoc group is involved (Fmoc/Fmoc, Fmoc/Bzl and Fmoc/Phe) and the Tyr/Tyr interactions. These simulations support the results observed by CD. The number of amino acids considered are represented as (mol1 + mol2) with mol1 designing either Fmoc-Phe-OH or Fmoc-Tyr-OH and mol2 referring to Fmoc-Tyr(Bzl)-OH. At low (10+10) and high (60+60) concentration of amino acids, the number of  $\pi$ - $\pi$  interactions is quite similar in the two gels (7.4 vs 6.0 at 10+10 and 36.7 vs 38.7 at 60+60). At medium concentration, the Fmoc-Tyr-OH/Fmoc-Tyr(Bzl)-OH mixture forms twice as much interactions than Fmoc-Phe-OH/Fmoc-Tyr(Bzl)-OH (26.1 vs 13.1). This difference is due to a larger amount of interactions between the Fmoc and Tyr moieties leading to a more compact aggregate. Jointly to these aromatic attractions, the molecules also interact via H-bonds between the amino acid groups. The amount of H-bonds as a function of the concentration follows the same order than the aromatic interactions with similar number of H-bonds at low (10+10) and high (60+60) concentration of amino acids (2.0 vs 3.2 at 10+10 and 15.3 vs 10.8 at 60+60). At medium

concentration (30+30) Fmoc-Tyr-OH/Fmoc-Tyr(Bzl)-OH mixture also forms twice as much H-bonds than Fmoc-Phe-OH/Fmoc-Tyr(Bzl)-OH does (3.7 *vs* 6.3). These additional aromatic interactions and hydrogen bonding induced by the presence of the hydroxyl group of tyrosine may explain the difference in fibril diameters between both systems observed by microscopy.

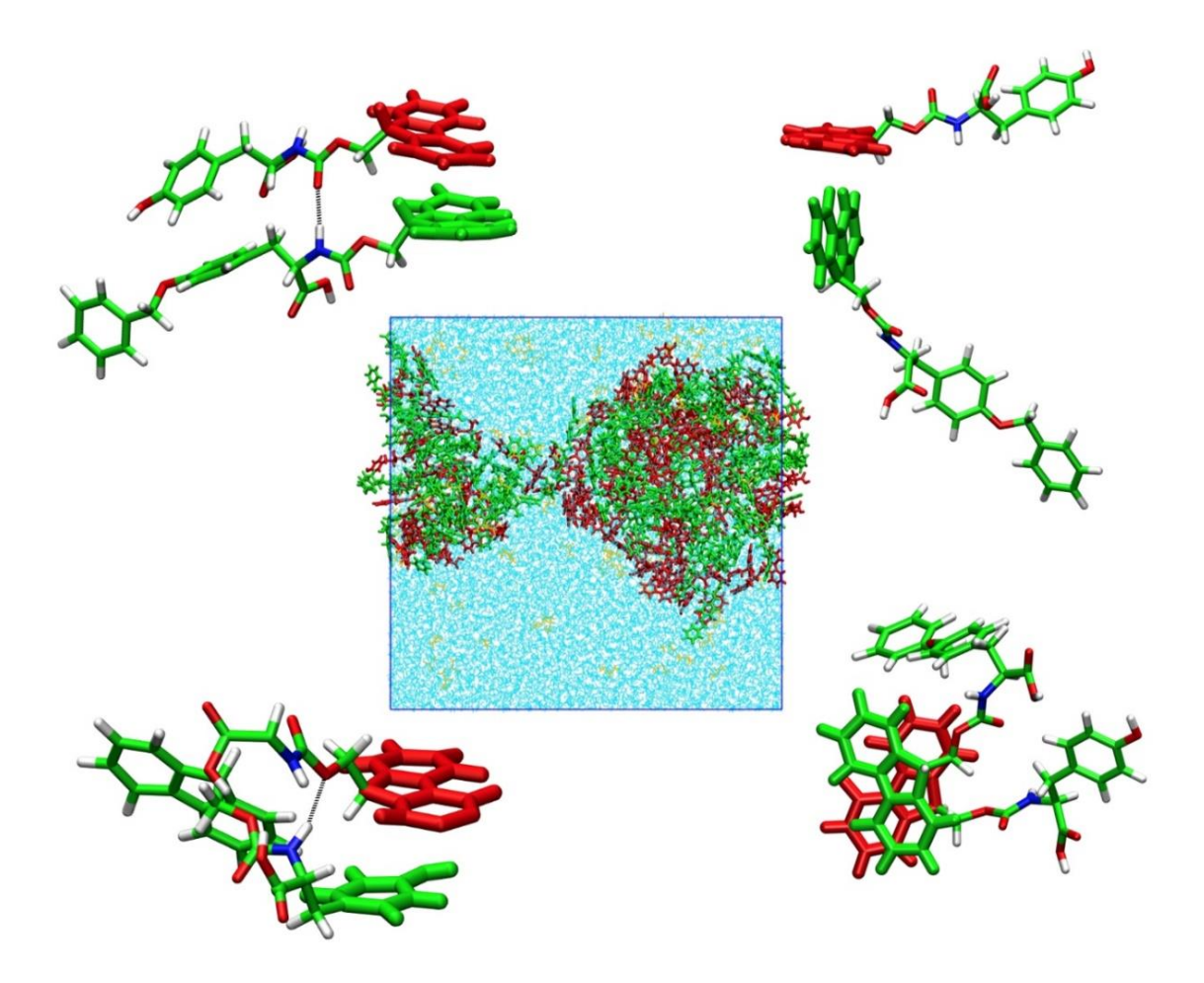


**Figure 2.18.** Final snapshots of the 60 Fmoc-Tyr-OH + 60 Fmoc-Tyr(Bzl)-OH system simulated in 2 % DMSO/H<sub>2</sub>O (v/v) showing typical  $\pi$ - $\pi$  and CH- $\pi$  arrangements between the two components. In the box Fmoc-Tyr-OH molecules are represented in red and Fmoc-Tyr(Bzl)-OH in green.

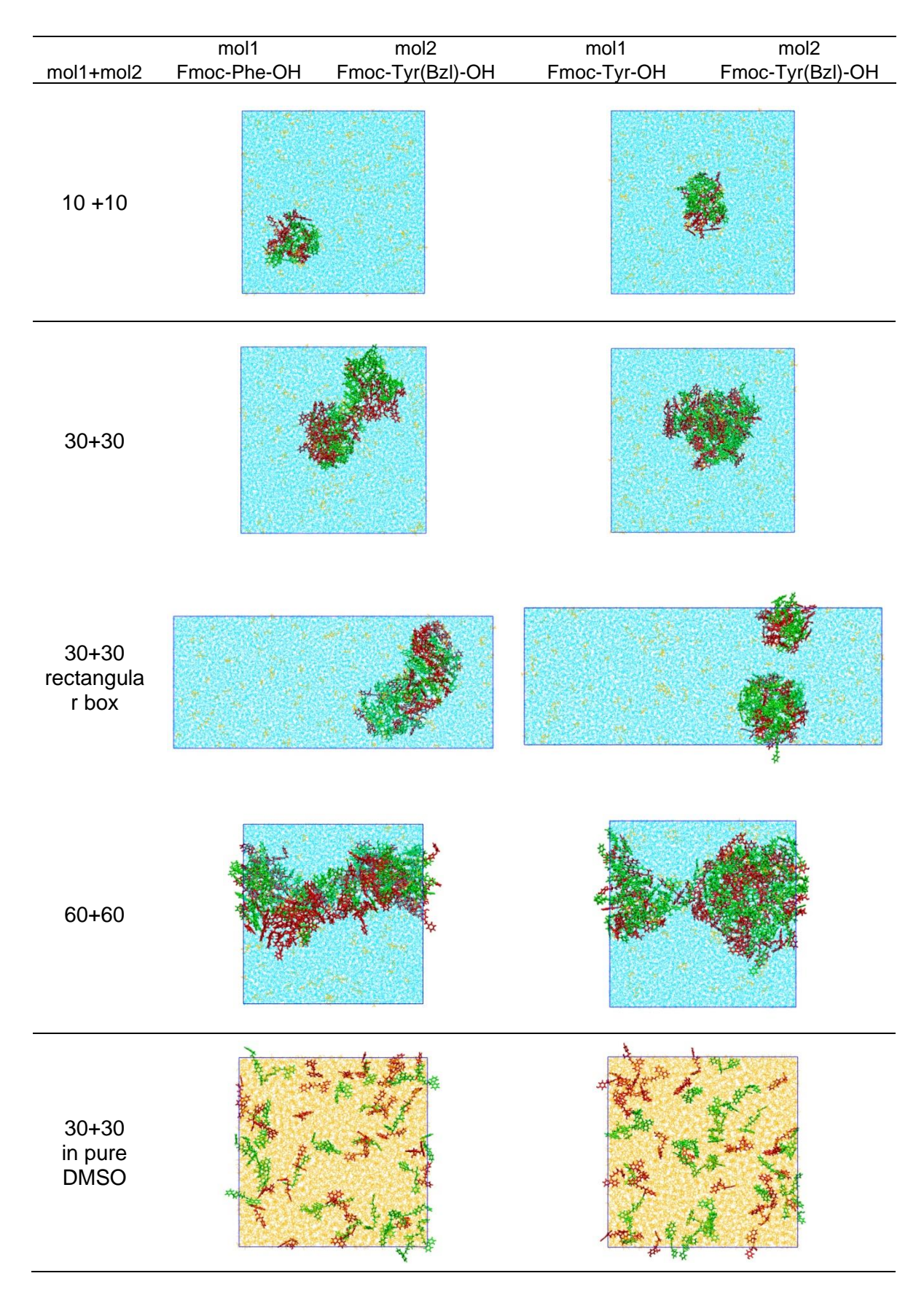


**Figure 2.19.** Final snapshots of the mixed systems simulated in 2% DMSO/H<sub>2</sub>O (v/v) and in pure DMSO (bottom) solutions (mol1 in red and mol2 in green).

**Table 2.3**.  $\pi-\pi$  interactions in the simulated systems. Number of  $\pi-\pi$  interactions between two specific parts of the simulated molecules (averaged values during the last 5 ns of dynamics, fluctuations are around 0.2). Average number of C=O···H-N hydrogen bonds (distance < 2.2 Å) between the different components of the system (averaged values during the last 5 ns of dynamics, fluctuations are around 0

		$\pi - \pi$ interactions								H- bonds			
		Fmoc/Fmoc	Fmoc/Tyr	Fmoc/Bzl	Fmoc /Phe	Tyr/Tyr	Tyr/Bzl	Tyr/Phe	Phe/Phe	Phe/Bzl	Bzl/Bzl	Sum	
	10+10	2.0	2.7	0.9	1.5	0.0	0.3	0.0	0.0	0.0	0.0	7.4	2.0
<u>‡</u> 후	30+30	5.6	3.5	1.2	0.5	1.6	0.4	0.0	0.0	0.3	0.0	13.1	3.7
9-0H BZI)-C	60+60	8.9	14.4	5.0	4.1	3.2	0.4	0.7	0.0	0.0	0.0	36.7	15.3
Fmoc-Phe-OH + Fmoc-Tyr(Bzl)-OH	30+30 rectangular box	5.9	4.3	0.9	0.5	1.6	0.1	0.7	0.0	0.0	0.0	14.0	7.6
	30+30 in pure DMSO	0.8	0.3	0.0	0.0	0.0	0.0	0.0	0.0	0.0	0.0	1.1	0.0
_	10+10	0.0	5.9	0.1	-	0.0	0.0	-	ı	-	0.0	6.0	3.2
<u>+</u>	30+30	9.8	11.6	1.8	-	2.2	0.9	-	-	-	0.0	26.3	6.3
r-Ol	60+60	14.2	17.6	2.3	-	2.4	1.1	-	-	-	1.1	38.7	10.8
Fmoc-Tyr-OH + Fmoc-Tyr(Bzl)-OH	30+30 rectangular box	7.3	12.1	1.0	-	2.6	1.3	-		-	0.0	23.8	5.5
	30+30 in pure DMSO	0.4	0.0	0.0	-	0.0	0.0	-	-	-	0.0	0.4	0.0

#### 2.3.8 Photothermal properties

After thoroughly analyzing the structure and the mechanical properties of the native and hybrid gels, we investigated their photothermal properties. For this purpose, the photothermal conversion of different concentrations of suspensions of ox-CNTs and GO alone in water was first examined by monitoring the temperature increase during exposure to NIR light irradiation (at 808 nm, under 2 W/cm² for 10 min). At each concentration a similar dose-dependent photothermal behavior was observed for both ox-CNTs and GO (Figure 2.20). The temperature increase was 20 °C, 28 °C, and 47 °C in 10 min for a concentration of 0.005 wt%, 0.01 wt%, and 0.025 wt%, respectively. The native and hybrid gels were also studied in similar conditions. The change in temperature for both gel 1 and gel 2 was very low with an increase of less than 5 °C after 10 min of irradiation as expected and the gels remained totally intact (Figure 2.21).

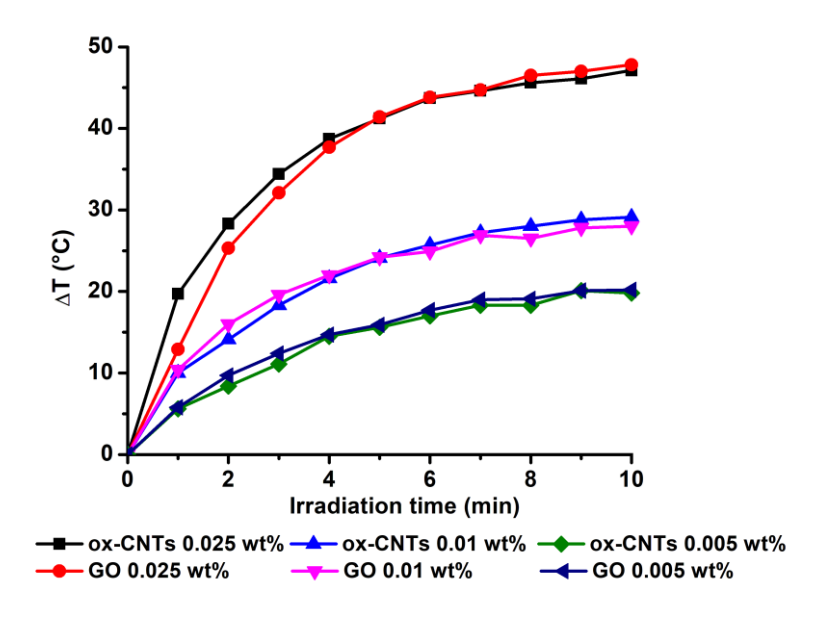


**Figure 2.20.** Temperature increase for different concentrations of suspensions of ox-CNTs or GO in water when exposed to a NIR laser (808 nm) at a power of 2 W/cm<sup>2</sup> as a function of the laser irradiation time.

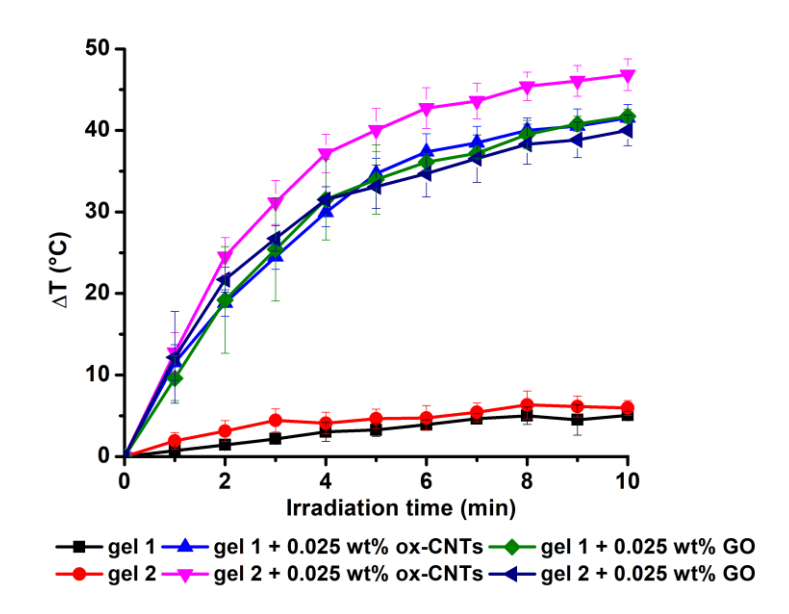


**Figure 2.21.** Temperature increase of the native gels in comparison to the hybrid gels when exposed to a NIR laser (at 808 nm, under 2 W/cm²) as a function of the laser irradiation time.

The hybrid gel 1 showed a similar temperature increase whatever it contained ox-CNTs or GO, which was not the case for gel 2. Indeed, after 10 min of irradiation the temperature difference was 40-41 °C for gel 1 + ox-CNTs or GO, and gel 2 + GO, whereas the temperature increase was 47 °C for gel 2 + ox-CNTs. The presence of ox-CNTs, which accelerates the hydrogelation process for both gels, also improves the increase of temperature during NIR irradiation in the case of gel 2. In addition, the gel structure slightly reduces the heating capacity of the carbon nanomaterials compared to their suspensions in water except for gel 2 + ox-CNTs reaching 47°C. Interestingly, we observed that in presence of ox-CNTs or GO the hybrid gel 1 was destructured, while the hybrid gel 2 shrank and formed a compact block (Figure 2.22).

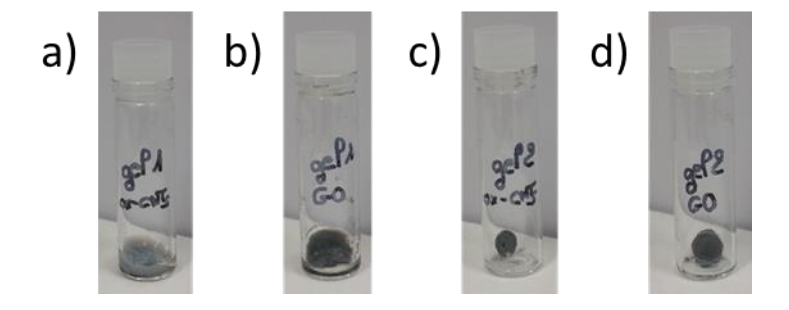


Figure 2.22. Photographs of a) gel 1 + 0.025 wt% ox-CNTs, b) gel 1 + 0.025 wt% GO, c) gel 2 + 0.025 wt% ox-CNTs, and d) gel 2 + 0.025 wt% GO remaining after the removal of water released after 10 min NIR light irradiation.

This result is concordant with a more homogeneous three-dimensional fibrous network in gel 2. It seems that the presence of the hydroxyl group of tyrosine not only influences the fibril diameter, but it can also decrease the structural stability of the gel in presence of the carbon nanomaterials.

## 2.3.9 Drug loading properties

To prove that our hydrogels have potential therapeutic applications, we decided to study the loading and the release of different drug models encapsulated into the gels, triggered by irradiation in the NIR region. A comparative loading study of three drug models was performed using two hydrophobic dyes, rhodamine B and methylene blue and one hydrophilic therapeutic molecule, vitamin C. To prepare the drug-loaded hydrogels, the drugs were first dissolved in water before the addition of the solution of Fmoc-Tyr-OH/Fmoc-Tyr(BzI)-OH (leading to gel 1) or Fmoc-Phe-OH/Fmoc-Tyr(BzI)-OH (leading to gel 2) in DMSO. The gelation was monitored using the vial inversion test.

## 2.3.9.1 Incorporation of hydrophobic drug models: rhodamine B or methylene blue

Dyes are ideal drug models for monitoring release visually and by spectroscopic measurement at very low concentrations thanks to their high absorbance in the UV-Vis region. Rhodamine B is a fluorescent dye often used in biological studies and in biotechnological applications such as fluorescence microscopy, flow cytometry, fluorescence correlation spectroscopy and ELISA.<sup>48,49</sup> The incorporation of different amounts of rhodamine B (concentration from 0.03 mg·mL<sup>-1</sup> to 3.0 mg·mL<sup>-1</sup>) was studied and we observed that a concentration of 0.1 mg·mL<sup>-1</sup> was the maximum that can be incorporated into native or hybrid gel 1 and gel 2. The incorporation of rhodamine B did not impact the gelation process up to the maximum concentration with a gelation time of 2 h, as observed previously. No gels were obtained above 0.1 mg·mL<sup>-1</sup> of rhodamine B into the samples. This relative low capacity of drug loading is probably due to the large and aromatic structure of the dye which can alter the non-covalent interactions between the amino acid derivatives at the origin of the gelation process.

As alternative hydrophobic dye, we decided to introduce methylene blue which also possesses therapeutic characteristics.<sup>50</sup> Similarly to rhodamine B, the incorporation of methylene blue into the native and hybrid gels was studied from 0.03 to 3.0 mg·mL<sup>-1</sup> and the

maximum concentration that could be loaded into the gel was the same as rhodamine B (0.1 mg·mL<sup>-1</sup>) as shown in figure 2.23.

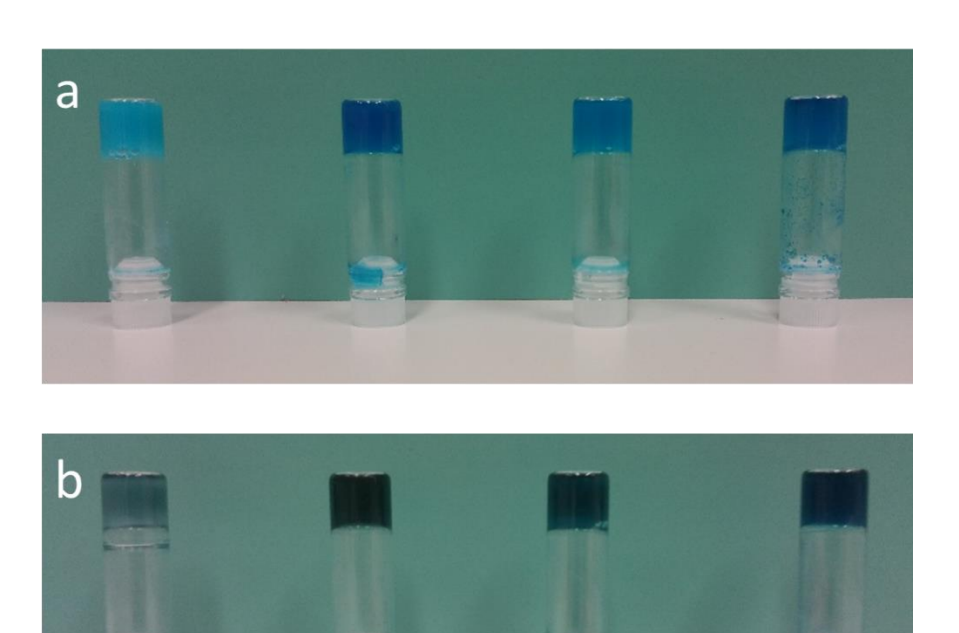


**Figure 2.23**. Photographs of gels 1 containing Methylene Blue (0.03, 0.05, 0.075, 0.1mg·mL<sup>-1</sup>) a) without carbon nanomaterials and b) with ox-CNTs 0.025 wt%.

## 2.3.9.2 Incorporation of hydrophilic drug model: L-ascorbic acid

L-ascorbic acid commonly known as vitamin C, has a wide range of clinical applications and it was selected as hydrophilic drug model. It promotes collagen biosynthesis, has antiscorbutic properties and protects against photoaging, UV-induced immunosuppression, and photocarcinogenesis. A range of L-ascorbic acid concentration (0.2-1.5 mg·mL<sup>-1</sup>) was studied and we observed that a concentration of 0.7 mg·mL<sup>-1</sup> (4 mM) of L-ascorbic acid was the maximum concentration that can be incorporated into the hydrogels. After approximately 2 h both L-ascorbic acid-loaded gel 1 and gel 2 formed a stable hydrogel. We observed a higher stability of L-ascorbic acid loaded in the gels over time (Figure 2.24). A range of drug concentration (0.2-1.5 mg·mL<sup>-1</sup>) was studied and we observed that a concentration of 0.7 mg·mL<sup>-1</sup> (4 mM) of L-ascorbic acid was the maximum concentration that can be incorporated into the hydrogels. Above 0.7 mg·mL<sup>-1</sup> the gelation process was disturbed with the appearance of a liquid phase. Due to its hydrophilic properties, ascorbic

acid could thus be incorporated in higher quantity to form stable hydrogels than the two hydrophobic drug models rhodamine B and methylene blue. The mass concentration is in the range of loadings of insulin and doxorubicin previously reported for some hydrogels containing carbon nanomaterials (0.08 to 2 mg·mL<sup>-1</sup>). $^{53-55}$  But, if we consider molar concentration, our loading value is higher compared to these studies (4 mM vs. 14  $\mu$ M to 3.7 mM of drug). To prepare the drug-loaded hybrid gels, the ox-CNTs or GO were dispersed at a concentration of 0.025 wt% into a 0.7 mg·mL<sup>-1</sup> solution of L-ascorbic acid before addition to the solution of the amino acids in DMSO.

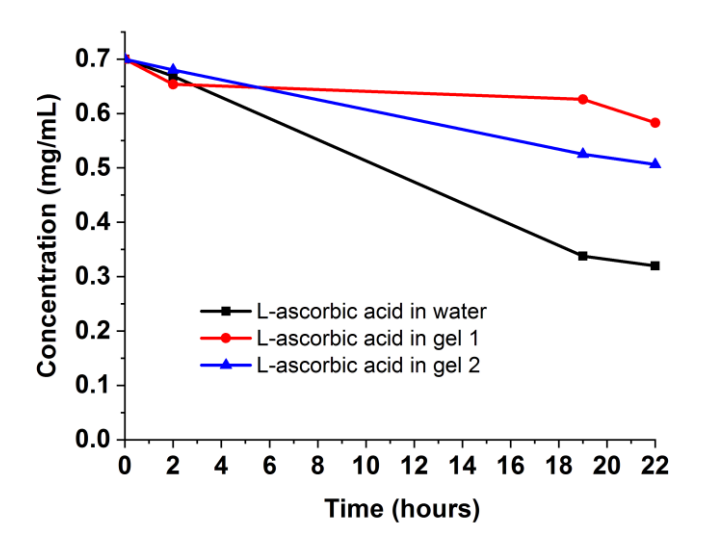


**Figure 2.24.** Degradation of L-ascorbic acid over time in solution in water and in the native gels 1 and 2.

## 2.3.10 Drug release

The drug release was investigated by irradiating the four hybrid gels containing rhodamine B, methylene blue or L-ascorbic acid. The volume of water released from the gels was measured after 10 min of NIR irradiation and the concentration of the released drug was determined by UV-Vis spectroscopy for the dyes and high-performance liquid chromatography (HPLC) for vitamin C.

## 2.3.10.1 Release of hydrophobic drug models: rhodamine B and methylene blue

The hybrid gels containing rhodamine B or methylene blue showed similar behavior during irradiation (Figures 2.25 and 2.26). Interestingly, whereas in absence of the dyes the gel 1 +

ox-CNTs or GO is destructured under NIR irradiation, in presence of the dyes only the gel 1 + GO is destructured and the gel 1 + ox-CNTs has the same shrinking behavior than the hybrid gels 2 (Figures 2.27 and 2.28). This result can be due to an increase of the structural stability of the gel 1 + ox-CNTs with the dyes. In the presence of both dyes we can observe a high amount of water released (60-80 %), but it contains only a very low amount of drug. The maximum amount of drug released after the irradiation was only 1.5 % of rhodamine B from gel 2 + GO and 13 % of methylene blue from gel 1 + GO. The maximum amount of water is released in both cases with the gel 2 + ox-CNTs probably due to the destructuration behavior. During the water release and gel shrinking the dyes remain trapped within the matrix. The entrapping of the dyes into the remaining gels can be explained by potential interactions between the aromatic moieties of the dyes and the carbon nanomaterials and amino acids.

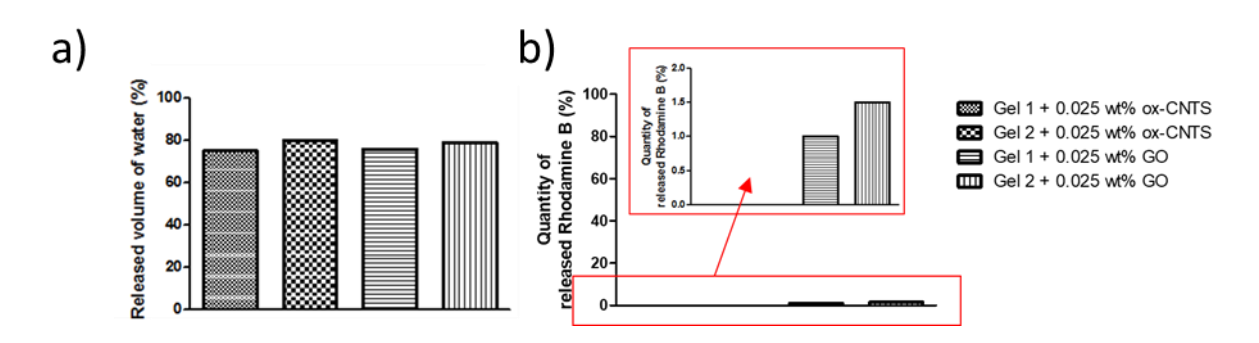


**Figure 2.25.** Release of a) water and b) Rhodamine B from the hybrid gels under NIR light irradiation.

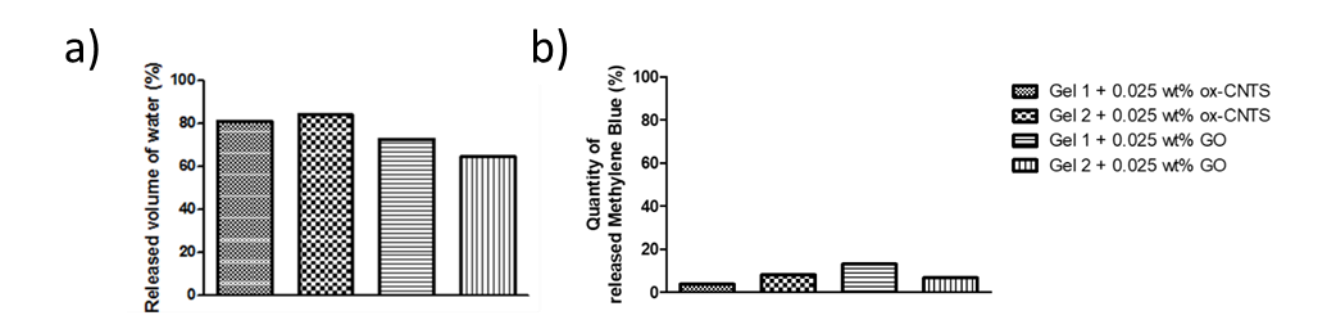


**Figure 2.26.** Release of a) water and b) Methylene Blue from the hybrid gels under NIR light irradiation.

We studied the potential physisorption of rhodamine B on the surface of ox-CNTs and GO by measuring the absorbance of a 0.1 mg·mL<sup>-1</sup> solution compared to the absorbance in the

presence of the carbon nanomaterials for 24 h. The results showed similar absorbance indicated no physical adsorption of rhodamine B on both ox-CNTs and GO, thus supporting the hypothesis that the dye seems to interact strongly with the amino acids which prevents its release during irradiation.

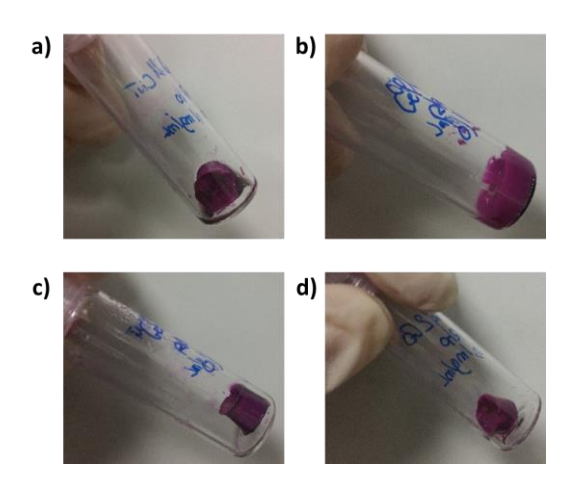
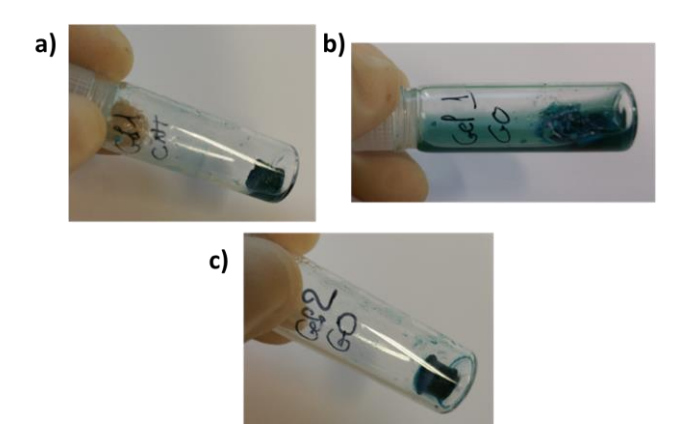


Figure 2.27. Photographs of the gels containing carbon nanomaterials and rhodamine B (0.1  $\text{mg}\cdot\text{mL}^{-1}$ ) after 10 min of NIR irradiation and removal of the water released: a) gel 1 + ox-CNTs, b) gel 1 + GO, c) gel 2 + ox-CNTs and d) gel 2 + GO.



**Figure 2.28.** Photographs of the gels containing carbon nanomaterials and methylene blue  $(0.1 \text{ mg} \cdot \text{mL}^{-1})$  after 10 min of NIR irradiation and removal of the water released: a) gel 1 + ox-CNTs, b) gel 1 + GO and c) gel 2 + GO.

## 2.3.10.2 Release of a hydrophilic drug model: L-ascorbic acid

The use of a hydrophilic molecule has permitted to enhance the quantity of drug loaded into the gels and released after NIR irradiation. In the presence of  $\iota$ -ascorbic acid and ox-CNTs or GO, gel 1 released 68 % and 73 % of water, respectively, whereas gel 2 released a higher

amount of water (84 % and 79 %, respectively) upon NIR irradiation (Figure 2.29a). The hybrid gel 1 loaded with L-ascorbic acid showed a structural destructuration of the gel matrix upon NIR light irradiation whatever it contains ox-CNTs or GO, while the hybrid gel 2 shrank leading to the formation of a compact block. Therefore, the lower volume of water released from the hybrid gel 1 containing ox-CNTs or GO is probably due to the destabilization of the gel structure during the irradiation. The higher water release capacity of gel 2 + ox-CNTs reveals a better photothermal behavior compared to the other hybrid gels, as observed in Figure 2.29. The temperature of the hydrogels was monitored during the irradiation starting at room temperature (Figure 2.30). This remarkable feature is probably linked to the higher homogeneity of the three-dimensional fibrous network in gel 2, as previously mentioned. The drug concentration was assessed by HPLC and the four hybrid gels showed a drug release comprised between 63 % and 82% after 10 min irradiation (Figure 2.29b). The gel 2 + ox-CNTs was found to be the most efficient system with a maximum drug release of 82 %. The amount of L-ascorbic acid release can be correlated to the water release capacity of the hydrogels. The higher water release capacity of gel 2 + ox-CNTs is in accordance with the better photothermal behavior compared to the other hybrid gels, as observed in Figure 2.21.

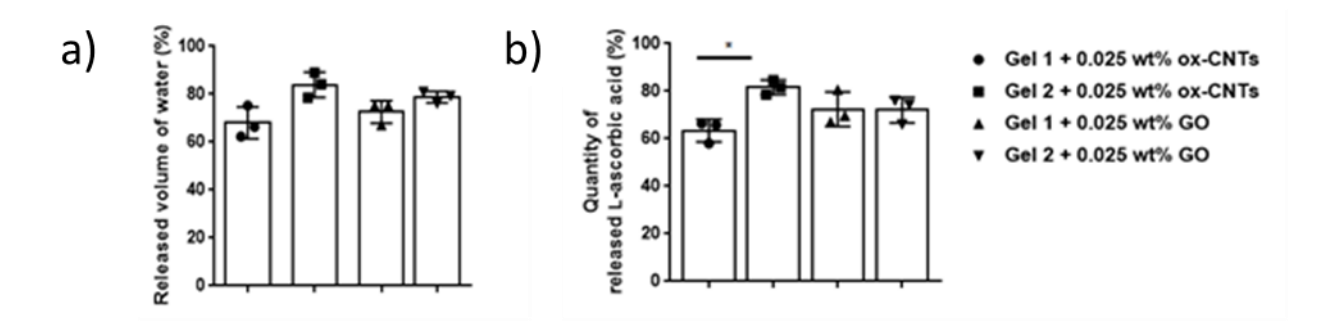


**Figure 2.29.** Release of a) water (n=3) and b) ι-ascorbic acid (n=3) from the hybrid gels under NIR light irradiation. Statistical analysis was performed by one-way ANOVA (including Bonferroni's multiple comparison test).

Overall, these results show that the drug release is triggered by the heat generation from the ox-CNTs or GO upon NIR light irradiation. We have investigated the drug release over time for the 4 different gels and observed that a plateau was reached after 8 to 10 min (Figure 2.31). The amount of drug released from the gels is primarily influenced by the nature of the amino acids constituting the hydrogel and the type of carbon nanomaterials has also some influence. We found that gel 2 loaded with the ox-CNTs was the most efficient

gel and this was correlated with the highest water release and best photothermal capacity observed for ox-CNT-loaded gel 2. This was probably due to a higher homogeneity of the 3D fibrous network in gel 2 and well-distributed ox-CNTs in the gel.

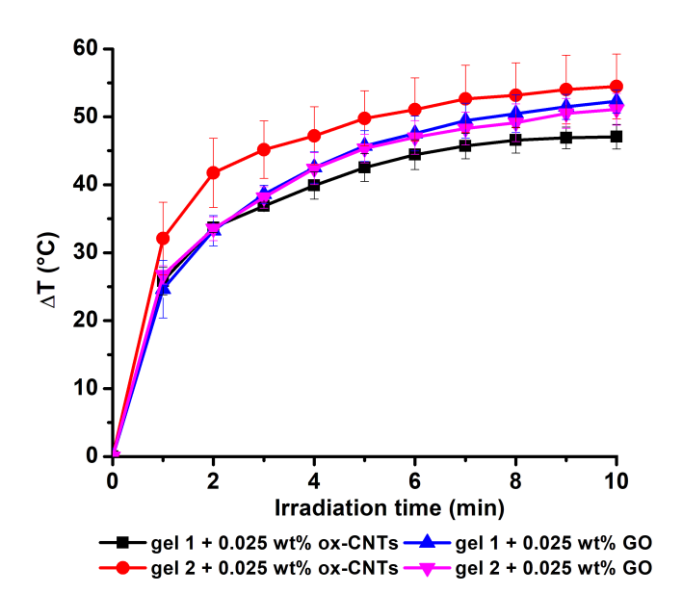


**Figure 2.30.** Temperature increase of the hybrid gels 1 and 2 containing 0.7 mg·mL<sup>-1</sup> of L-ascorbic acid when exposed to a NIR laser (808 nm) at a power of 2 W/cm<sup>2</sup> as a function of the laser irradiation time.

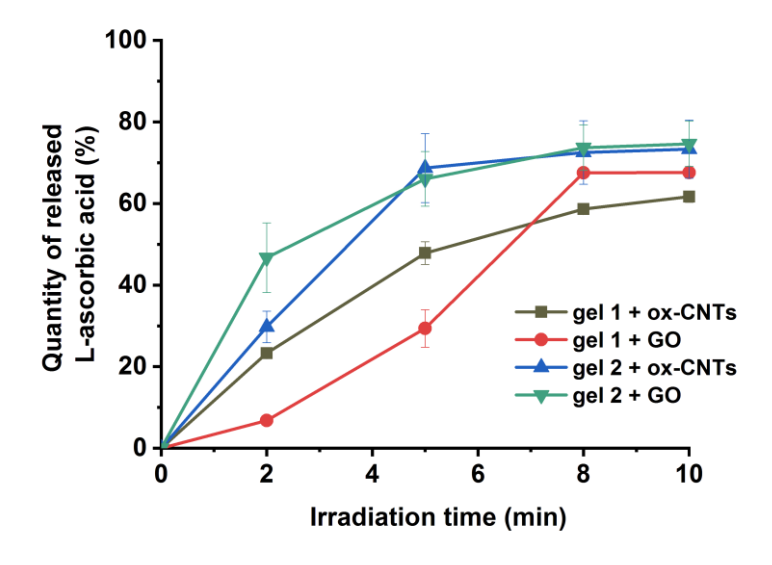


**Figure 2.31.** L-ascorbic acid release kinetics for the hybrid gel 1 (n=2) and gel 2 (n=3) when exposed to a NIR laser (at 808 nm, under 2 W/cm²) as a function of the laser irradiation time.

The high liberation of  $\iota$ -ascorbic acid reached in our study is similar or higher than NIR irradiation-induced drug release rates reported for other types of carbon

nanomaterial-containing hydrogels, 53,56 Control experiments were performed on the gels devoid of carbon nanomaterials containing L-ascorbic acid. We verified that L-ascorbic acid remains stable in these conditions. As expected, the control gels did not show any release of water and drug after 10 min irradiation Therefore, the gels are more appropriate for drug loading and release of hydrophilic drugs. The presence of aromatic moieties in the drug seems to prevent an efficient drug release due to interactions with the amino acids.

In addition, we performed preliminary stability experiments in physiological saline solution (0.9% NaCl) and in RPMI or DMEM supplemented with 10 % fetal bovine serum. For this purpose, a volume of 100  $\mu$ L of physiological saline solution or 10 % fetal bovine serum in culture medium was added on top of each hydrogel (400  $\mu$ L). After 15 h the solution was withdrawn and the amount of L-ascorbic acid was determined by HPLC. We observed that the hydrogels were not degraded when exposed to physiological saline solution (0.9 % NaCl). We noticed that a small amount of water was released only from the hybrid gels 2 (Figure 2.32a). We estimated that 15 to 21 % of L-ascorbic acid was liberated from the four hydrogels by diffusion. In 10 % fetal bovine serum in culture medium we found that the hybrid gels 1 were less stable and released a significant volume of water, which was not the case for the hybrid gels 2 (Figure 2.32b-c). This result was correlated with a higher amount of L-ascorbic acid released from the hybrid gels 1 (12-51 %), whereas only 8 to 12 % of drug were liberated from the hybrid gels 2. These stability experiments show that the hybrid gels 2 are more stable in physiological conditions and this is probably related to the higher homogeneity of the 3D fibrous network in gel 2.

These results support the fact that gel 2 is more efficient compared to gel 1 for our purpose of controlled drug release. Overall, our hydrogels present many advantages such as i) simple preparation as they are constituted of commercial amino acids, ii) low content of carbon nanomaterials, iii) high drug loading and release capacity, and iv) stability in physiological conditions (in particular for gel 2).

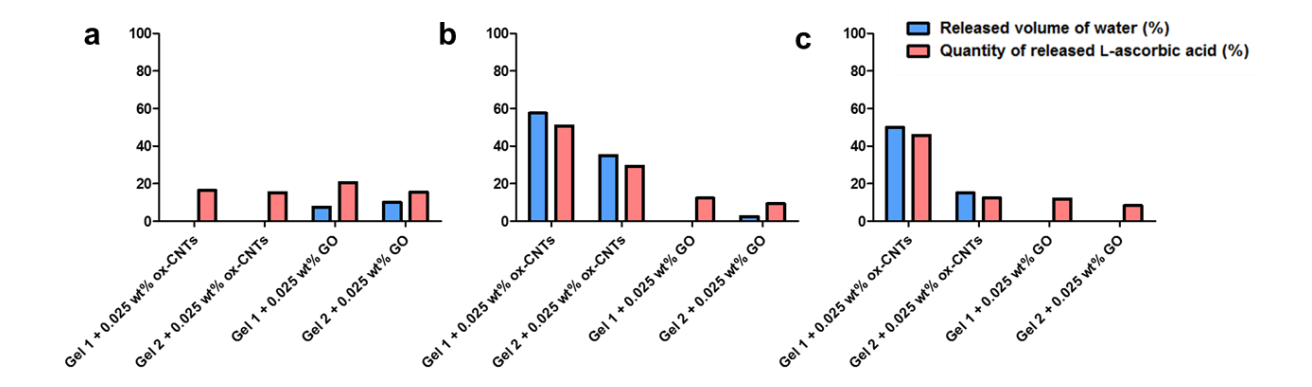


**Figure 2.32.** Released volume of water and quantity of released L-ascorbic acid from the hybrid gels in presence of a) physiological serum b) 10 % Fetal Bovine Serum (FBS) in RPMI and c) 10% FBS in DMEM after 15 h (overnight)

#### 2.4 Conclusion

We have demonstrated the spontaneous self-assembly of different commercially available Fmoc-protected amino acids into three-dimensional fibrous network leading to the formation of hydrogels. We have investigated more in detail the gelation of a binary mixture composed of Fmoc-Tyr-OH/Fmoc-Tyr(BzI)-OH or Fmoc-Phe-OH/Fmoc-Tyr(BzI)-OH. The structural and physical properties of these gels were assessed using various microscopic techniques and rheology. The hydrogel formation was mainly driven by aromatic interactions, as supported by CD and MD simulations. Oxidized CNTs and GO were incorporated in these hydrogels and they showed good interfacing with the fibrils, in particular the nanotubes. Different drug models were loaded in the hybrid hydrogels and L-ascorbic acid was released at high concentration in few minutes thanks to the heat generated by the carbon nanomaterials upon NIR light irradiation. These novel self-assembled hydrogels open up the possibilities of various applications and they will be explored further for drug delivery.

#### 2.5 References

- 1. Vigier-Carrière, C.; Boulmedais, F.; Schaaf, P.; Jierry, L. Surface-Assisted Self-Assembly Strategies Leading to Supramolecular Hydrogels. Angew. Chem. Int. Ed. Engl. 2018, 57, 1448–1456.
- 2. Tian, R.; Chen, J.; Niu, R. The Development of Low-Molecular Weight Hydrogels for Applications in Cancer Therapy. Nanoscale 2014, 6, 3474–3482.

- 3. Tao, N.; Li, G.; Liu, M.; Gao, W.; Wu, H. Preparation of Dual Responsive Low-Molecular-Weight Hydrogel for Long-Lasting Drug Delivery. Tetrahedron 2017, 73, 3173–3180.
- 4. Zhang, Z.; Ma, R.; Shi, L. Cooperative macromolecular Self-assembly toward polymeric assemblies with multiple and bioactive functions. Acc. Chem. Res. 2014, 47, 1426-1437
- 5. Rajbhandary, A.; Raymond, D. M.; Nilsson, B. L. Self-Assembly, Hydrogelation, and Nanotube Formation by Cation-Modified Phenylalanine Derivatives. Langmuir 2017, 33, 5803–5813.
- 6. Dasgupta, A.; Mondal, J. H.; Das, D. Peptide Hydrogels. RSC Adv. 2013, 3, 9117–9149.
- 7. Iglesias, D.; Melle-Franco, M.; Kurbasic, M.; Melchionna, M.; Abrami, M.; Grassi, M.; Prato, M.; Marchesan, S. Oxidized Nanocarbons-Tripeptide Supramolecular Hydrogels: Shape Matters! ACS Nano 2018, 12, 5530–5538.
- 8. Aggeli, A.; Boden, N.; Carrick, L. M.; Mcleish, T. C. B.; Nyrkova, I. A.; Semenov, A. N. Self-Assembling Peptide Gels. In Molecular Gels: Materials with Self-Assembled Fibrillar Networks; Weiss, R. G., Terech, P., Eds.; Springer Netherlands: Dordrecht, 2006; pp 99–130.
- 9. Sutton, S.; Campbell, N. L.; Cooper, A. I.; Kirkland, M.; Frith, W. J.; Adams, D. J. Controlled Release from Modified Amino Acid Hydrogels Governed by Molecular Size or Network Dynamics. Langmuir 2009, 25, 10285–10291.
- 10. Eskandari, S.; Guerin, T.; Toth, I.; Stephenson, R. J. Recent Advances in Self-Assembled Peptides: Implications for Targeted Drug Delivery and Vaccine Engineering. Adv. Drug Deliv. Rev. 2017, 110–111, 169–187.
- 11. Kumar, D.; Workman, V. L.; O'Brien, M.; McLaren, J.; White, L.; Ragunath, K.; Rose, F.; Saiani, A.; Gough, J. E. Peptide Hydrogels-A Tissue Engineering Strategy for the Prevention of Oesophageal Strictures. Adv. Funct. Mater. 2017, 27, 1702424.
- 12. Koutsopoulos, S. Self-Assembling Peptide Nanofiber Hydrogels in Tissue Engineering and Regenerative Medicine: Progress, Design Guidelines, and Applications. J. Biomed. Mater. Res. A 2016, 104, 1002–1016.
- 13. Bhattacharya, S.; Samanta, S. K. Soft-Nanocomposites of Nanoparticles and Nanocarbons with Supramolecular and Polymer Gels and Their Applications. Chem. Rev. 2016, 116, 11967–12028.
- 14. Servant, A.; Bussy, C.; Al-Jamal, K.; Kostarelos, K. Design, Engineering and Structural Integrity of Electro-responsive Carbon Nanotube-based Hydrogels for Pulsatile Drug Release. J. Mater. Chem. B 2013, 1, 4593–4600.
- 15. Adhikari, B.; Banerjee, A. Short Peptide Based Hydrogels: Incorporation of Graphene into the Hydrogel. Soft Matter 2011, 7, 9259–9266.
- 16. Mba, M.; Jiménez, A. I.; Moretto, A. Templating the Self-Assembly of Pristine Carbon Nanostructures in Water. Chem. Eur. J. 2014, 20, 3888–3893.
- 17. Roy, S.; Banerjee, A. Functionalized Single Walled Carbon Nanotube Containing Amino Acid Based Hydrogel: a Hybrid Nanomaterial. RSC Adv. 2012, 2, 2105–2111.

- 18. Wang, H.; Chen, Q.; Zhou, S. Carbon-based Hybrid Nanogels: A Synergistic Nanoplatform for Combined Biosensing, Bioimaging, and Responsive Drug Delivery. Chem. Soc. Rev. 2018, 47, 4198–4232.
- 19. Vashist, A.; Kaushik, A.; Vashist, A.; Sagar, V.; Ghosal, A.; Gupta, Y. K.; Ahmad, S.; Nair, M. Advances in Carbon Nanotubes-hydrogel Hybrids in Nanomedicine for Therapeutics. Adv. Healthc. Mater. 2018, 7, e1701213.
- 20. Ha, W.; Zhao, X.-B.; Jiang, K.; Kang, Y.; Chen, J.; Li, B.-J.; Shi, Y.-P. A Three-Dimensional Graphene Oxide Supramolecular Hydrogel for Infrared Light-responsive Cascade Release of Two Anticancer Drugs. Chem. Commun. 2016, 52, 14384–14387.
- 21. Merino, S.; Martín, C.; Kostarelos, K.; Prato, M.; Vázquez, E. Nanocomposite Hydrogels: 3D Polymer-nanoparticle Synergies for On-demand Drug Delivery. ACS Nano 2015, 9, 4686–4697.
- 22. Dong, X.; Wei, C.; Liang, J.; Liu, T.; Kong, D.; Lv, F. Thermosensitive Hydrogel Loaded with Chitosan-Carbon Nanotubes for Near Infrared Light Triggered Drug Delivery. Coll. Surf. B 2017, 154, 253–262.
- 23. Kumar, S.; Rani, R.; Dilbaghi, N.; Tankeshwar, K.; Kim, K.-H. Carbon Nanotubes: a Novel Material for Multifaceted Applications in Human Healthcare. Chem. Soc. Rev. 2017, 46, 158–196.
- 24. Reina, G.; González-Domínguez, J. M.; Criado, A.; Vázquez, E.; Bianco, A.; Prato, M. Promises, Facts and Challenges for Graphene in Biomedical Applications. Chem. Soc. Rev. 2017, 46, 4400–4416.
- 25. Delogu, L. G.; Venturelli, E.; Manetti, R.; Pinna, G. A.; Carru, C.; Madeddu, R.; Murgia, L.; Sgarrella, F.; Dumortier, H.; Bianco, A. Ex Vivo Impact of Functionalized Carbon Nanotubes on Human Immune Cells. Nanomedicine (Lond.) 2012, 7, 231–243.
- 26. Marangon, I.; Ménard-Moyon, C.; Kolosnjaj-Tabi, J.; Béoutis, M. L.; Lartigue, L.; Alloyeau, D.; Pach, E.; Ballesteros, B.; Autret, G.; Ninjbadgar, T.; Brougham, D. F.; Bianco, A.; Gazeau, F. Covalent Functionalization of Multi-walled Carbon Nanotubes with a Gadolinium Chelate for Efficient T<sub>1</sub>-Weighted Magnetic Resonance Imaging. Adv. Funct. Mater. 2014, 24, 7173–7186.
- 27. Jain, S.; Thakare, V. S.; Das, M.; Godugu, C.; Jain, A. K.; Mathur, R.; Chuttani, K.; Mishra, A. K. Toxicity of Multiwalled Carbon Nanotubes with End Defects Critically Depends on Their Functionalization Density. Chem. Res. Toxicol. 2011, 24, 2028–2039.
- 28. Jasim, D. A.; Murphy, S.; Newman, L.; Mironov, A.; Prestat, E.; McCaffrey, J.; Ménard-Moyon, C.; Rodrigues, A. F.; Bianco, A.; Haigh, S.; Lennon, R.; Kostarelos, K. The Effects of Extensive Glomerular Filtration of Thin Graphene Oxide Sheets on Kidney Physiology. ACS Nano 2016, 10, 10753–10767.
- 29. Ali-Boucetta, H.; Bitounis, D.; Raveendran-Nair, R.; Servant, A.; Van den Bossche, J.; Kostarelos, K. Purified Graphene Oxide Dispersions Lack In Vitro Cytotoxicity and In Vivo Pathogenicity. Adv. Healthc. Mater. 2013, 2, 433–441.

- 30. Ménard-Moyon, C.; Venkatesh, V.; Krishna, K. V.; Bonachera, F.; Verma, S.; Bianco, A. Self-Assembly of Tyrosine into Controlled Supramolecular Nanostructures. Chem. Eur. J. 2015, 21 (33), 11681–11686.
- 31. Ryan, D. M.; Doran, T. M.; Nilsson, B. L. Complementary  $\pi$ - $\pi$  Interactions Induce Multicomponent Coassembly into Functional Fibrils. Langmuir 2011, 27, 11145–11156.
- 32. Galvao, J.; Davis, B.; Tilley, M.; Normando, E.; Duchen, M.R.; Cordeiro, M.F. Unexpected Low-dose Toxicity of the Universal Solvent DMSO. FASEB J. 2014, 28, 1317–1330.
- 33. Lee, H.; Park, J. B. Evaluation of the Effects of Dimethylsulphoxide on Morphology, Cellular Viability, mRNA, and Protein Expression of Stem Cells Culture in Growth Media. Biomed. Rep. 2017, 7, 291–296.
- 34. Ryan, D. M.; Nilsson, B. L. Self-Assembled Amino Acids and Dipeptides as Noncovalent Hydrogels for Tissue Engineering. Polym. Chem. 2011, 3, 18–33.
- 35. Draper, E. R.; Morris, K. L.; Little, M. A.; Raeburn, J.; Colquhoun, C.; Cross, E. R.; McDonald, T. O.; Serpell, L. C.; Adams, D. J. Hydrogels Formed from Fmoc Amino Acids. CrystEngComm 2015, 17, 8047–8057.
- 36. Jayawarna, V.; Smith, A.; Gough, J. E.; Ulijn, R. V. Three-Dimensional Cell Culture of Chondrocytes on Modified Di-phenylalanine Scaffolds. Biochem. Soc. Trans. 2007, 35, 535–537.
- 37. Mahler, A.; Reches, M.; Rechter, M.; Cohen, S.; Gazit, E. Rigid, Self-Assembled Hydrogel Composed of a Modified Aromatic Dipeptide. Adv. Mater. 2006, 18, 1365–1370.
- 38. Ryan, D. M.; Anderson, S. B.; Nilsson, B. L. The Influence of Side-chain Halogenation on the Self-Assembly and Hydrogelation of Fmoc-phenylalanine Derivatives. Soft Matter 2010, 6, 3220–3231.
- 39. Smith, A. M.; Williams, R. J.; Tang, C.; Coppo, P.; Collins, R. F.; Turner, M. L.; Saiani, A.; Ulijn, R. V. Fmoc-diphenylalanine Self Assembles to a Hydrogel via a Novel Architecture Based on  $\pi$ – $\pi$  Interlocked  $\beta$ -sheets. Adv. Mater. 2008, 20, 37–41.
- 40. Ferry, J. D. Mechanical Properties of Substances of High Molecular Weight; Rigidities of Gelatin Gels; Dependence on Concentration, Temperature and Molecular Weight. J. Am. Chem. Soc. 1948, 70, 2244–2249.
- 41. te Nijenhuis, K.; Dijkstra, H. Investigation of the Aging Process of a Polyvinyl Chloride Gel by the Measurement of its Dynamic Moduli. Rheol Acta 1975, 14, 71–84.
- 42. Huang, X.; Terech, P.; Raghavan, S. R.; Weiss, R. G. Kinetics of 5α-Cholestan-3β-yl N-(2-Naphthyl)carbamate/n-Alkane Organogel Formation and its Influence on the Fibrillar Networks. J. Am. Chem. Soc. 2005, 127, 4336–4344.
- 43. Collin, D.; Covis, R.; Allix, F.; Jamart-Grégoire, B.; Martinoty, P. Jamming Transition in Solutions Containing Organogelator Molecules of Amino-Acid Type: Rheological and Calorimetry Experiments. Soft Matter 2013, 9, 2947–2958.
- 44. Terech, P.; Friol, S. Rheometry of an Androstanol Steroid Derivative Paramagnetic Organogel. Methodology for a Comparison with a Fatty Acid Organogel. Tetrahedron 2007, 63, 7366–7374.

- 45. Nijenhuis, K. te. Thermoreversible Networks: Viscoelastic Properties and Structure of Gels; Adv. Polym. Sci.; Springer-Verlag, Berlin Heidelberg, Germany, 1997.
- 46. Djabourov, M.; Nishinari, K.; Ross-Murphy, S. B. Physical Gels from Biological and Synthetic Polymers; Cambridge University Press, UK, 2013.
- 47. Mandal, S. K.; Kar, T.; Das, P. K. Pristine Carbon-nanotube-included Supramolecular Hydrogels with Tunable Viscoelastic Properties. Chem. Eur. J. 2013, 19, 12486–12496.
- 48. Zhu, J.; Li, J.-J.; Zhao, J.-W. Spectral Characters of Rhodamine B as a Multi-Information Fluorescence Probe for Bovine Serum Albumins. Sens. Actuators, B 2009, 138 (1), 9–13.
- 49. Reungpatthanaphong, P.; Dechsupa, S.; Meesungnoen, J.; Loetchutinat, C.; Mankhetkorn, S. Rhodamine B as a Mitochondrial Probe for Measurement and Monitoring of Mitochondrial Membrane Potential in Drug-Sensitive and -Resistant Cells. J. Biochem. Biophys. Methods 2003, 57 (1), 1–16.
- 50. Ginimuge, P. R.; Jyothi, S. D. Methylene Blue: Revisited. J Anaesthesiol Clin Pharmacol 2010, 26 (4), 517–520.
- 51. Al-Niaimi, F.; Chiang, N. Y. Z. Topical Vitamin C and the Skin: Mechanisms of Action and Clinical Applications. J. Clin. Aesthet. Dermatol. 2017, 10, 14–17.
- 52. Du, J.; Cullen, J. J.; Buettner, G. R. Ascorbic Acid: Chemistry, Biology and the Treatment of Cancer. Biochim. Biophys. Acta 2012, 1826, 443–457.
- 53. Teodorescu, F.; Oz, Y.; Quéniat, G.; Abderrahmani, A.; Foulon, C.; Lecoeur, M.; Sanyal, R.; Sanyal, A.; Boukherroub, R.; Szunerits, S. Photothermally Triggered On-demand Insulin Release from Reduced Graphene Oxide Modified Hydrogels. J. Control. Release 2017, 246, 164–173.
- 54. Wu, J.; Chen, A.; Qin, M.; Huang, R.; Zhang, G.; Xue, B.; Wei, J.; Li, Y.; Cao, Y.; Wang, W. Hierarchical Construction of a Mechanically Stable Peptide-graphene Oxide Hybrid Hydrogel for Drug Delivery and Pulsatile Triggered Release in vivo. Nanoscale 2015, 7, 1655–1660.
- 55. Li, B.; Zhang, L.; Zhang, Z.; Gao, R.; Li, H.; Dong, Z.; Wang, Q.; Zhou, Q.; Wang, Y. Physiologically Stable F127-GO Supramolecular Hydrogel with Sustained Drug Release Characteristic for Chemotherapy and Photothermal Therapy. RSC Adv. 2018, 8, 1693–1699.
- 56. Liu, W.; Zhang, X.; Zhou, L.; Shang, L.; Su, Z. Reduced Graphene Oxide (rGO) Hybridized Hydrogel as a Near-infrared (NIR)/pH Dual-responsive Platform for Combined Chemophotothermal Therapy. J. Coll. Interf. Sci. 2019, 536, 160–170.

# CHAPTER 3. PREPARATION OF HYDROGELS BASED ON DIPEPTIDES

#### 3.1 Introduction

Short peptide-based hydrogels have drawn tremendous interest in biomaterials research. This type of hydrogels has been extensively explored in recent years for tissue engineering<sup>1</sup>, as scaffolds for would healing<sup>2</sup> and for drug release.<sup>3,4</sup> Similarly to amino acids, the selfassembly of peptides in aqueous solution to form hydrogels is controlled by a perfect balance between hydrophobicity and hydrophilicity. Self-assembly of short peptides through  $\pi$ - $\pi$  stacking have been described by Reches and Gazit, who observed that aromatic dipeptides could self-assemble into nanotubes<sup>5</sup> or hollow spherical<sup>6</sup> structures with nanometer dimensions. Zhang and co-workers were the first to report that certain Fmocprotected dipeptides spontaneously formed fibrous networks.<sup>7</sup> Aromatic interactions between the peptides have been shown to play a key role into the gelation process<sup>8,9</sup> and aromatic group protection at the N-terminus such as Fmoc, naphthyl, and purenyl favors the formation of hydrogels under appropriate conditions. Several groups have studied the assembly and gelation properties of short peptides. 10-13 Adam and coworkers have studied hydrogelation of Fmoc/naphthyl conjugated dipeptides using glucono-d-lactone (GdL) whose hydrolysis actually controls the pH of the aqueous solution to induce gelation. 14 However, the majority of developed peptide-based hydrogels are composed of natural  $\alpha$ -amino acid residues leading to several disadvantages as these hydrogelator molecules are rapidly degraded in vitro and in vivo by proteolytic enzymes. Therefore, there is an important need for the discovery and development of proteolytically stable hydrogels. The incorporation of extra methylene groups into the peptide backbone and the modification of the terminal amino acid position can play a role on the stability against peptidases. 15,16 A first study performed in our team concerning the self-assembly of Boc-diphenylalanine backbone homologues with functionalized carbon nanotubes demonstrated that  $\beta$  and  $\gamma$  homologues self-assemble in water to generate fibers of different dimensions and shapes.<sup>17</sup> The generated fibers showed pH sensitivity with morphological modification at acidic pH. This behavior could provide the basis for developing novel pH-sensitive β and γ peptide-based materials including drug delivery systems.

#### 3.2 Objectives

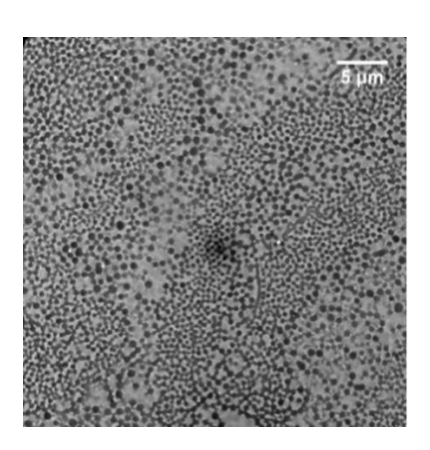
In this chapter, we have studied the gelation properties of the self-assembled nanostructures obtained with Boc-diphenylalanine compounds, namely Boc- $\alpha$ -Phe- $\alpha$ -Phe-OH, Boc- $\beta$ -Phe- $\beta$ -Phe-OH and Boc- $\gamma$ -Phe- $\gamma$ -Phe-OH. A comparative work was also performed using Boc-dityrosine homologues. The nanostructures obtained through self-assembly of the different dipeptides were characterized by microscopy. Several hydrogel formation protocols have been tested and the different hydrogels obtained were characterized by circular dichroism. Then, carbon nanomaterials such as GO or ox-CNTs and L-ascorbic acid was incorporated into the gel structures to compare their behavior under near-infrared irradiation for drug delivery applications. Finally, preliminary tests concerning the toxicity of the dipeptide hydrogels developed on human skin samples have been performed by topical application.

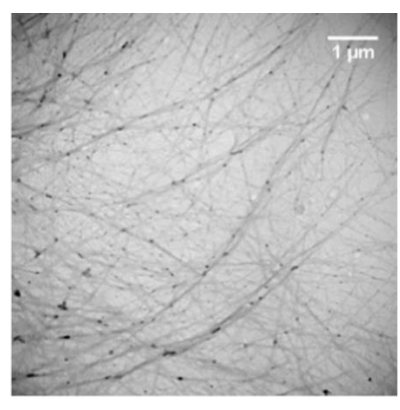
#### 3.3 Results and discussion

## 3.3.1 Self-assembly

The Boc-protected  $\alpha$ -diphenylalanine peptide has been widely studied by other groups. <sup>18,19</sup> It was found to form spherical assemblies in ethanol and tubular structures in water from a stock solution in hexafluoro-2-propanol (HFIP). Fibers formed mainly by  $\pi$ -stacking between the aryl side chain of phenylalanine can drive the gel formation. In our team, Dinesh et al. 17 previously studied the self-assembly of the two homologues Boc-β-Phe-β-Phe-OH and Boc-γ-Phe-y-Phe-OH from a stock solution of the di-peptide in HFIP and diluted in 1:1 proportion ethanol/water solution. At low concentration (25 μg·mL<sup>-1</sup>) they observed that the dipeptides were able to form well-defined and highly oriented nanofibers, whereas at higher concentration (from 0.1 to 1.0 mg·mL<sup>-1</sup>) both β and γ dipeptides were found to form extensive aggregated nanofibers. They also evaluated the role of water observing the selfassembly of the three dipeptides in water at 1.0 mg·mL<sup>-1</sup>. The morphology remained fibrillar for Boc-β-Phe-β-Phe-OH and Boc-γ-Phe-γ-Phe-OH but, as previously reported in literature, <sup>19</sup> the nanostructures changed from spherical to tubular structures upon changing the solvent from ethanol to water for Boc- $\alpha$ -Phe- $\alpha$ -Phe-OH. To further study the self-assembly properties of the dipeptides homologues we decided to characterize the nature of the assemblies directly dissolved in water without dilution from a stock solution in organic

solvents. The dipeptides were dissolved at a concentration of 0.5 mg·mL<sup>-1</sup> and rested for 1 h before deposition on a TEM grid. In pure water Boc- $\alpha$ -Phe- $\alpha$ -Phe-OH self-assembled into spheres connected by small elongated structures whereas Boc- $\beta$ -Phe- $\beta$ -Phe-OH and Boc- $\gamma$ -Phe- $\gamma$ -Phe-OH self-assembled into fibers (Figure 3.1).





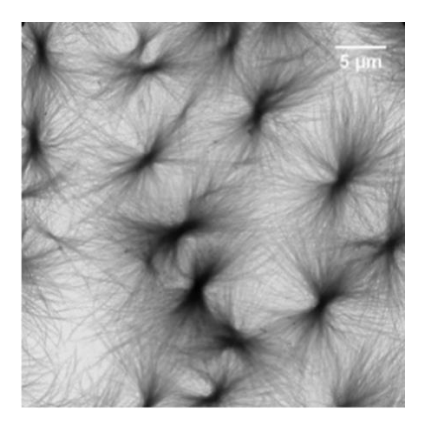


**Figure 3.1.** Self-assembly of Boc-diphenylalanine at 0.5 mg·mL<sup>-1</sup> in pure water from left to right: Boc-α-Phe-α-Phe-OH, Boc-β-Phe-β-Phe-OH and Boc-γ-Phe-γ-Phe-OH.

The nanospheres obtained with Boc- $\alpha$ -Phe- $\alpha$ -Phe-OH are variable in size with a diameter between 200 nm and 700 nm. Boc- $\beta$ -Phe- $\beta$ -Phe-OH in water self-assembled in highly oriented fibers whereas Boc- $\gamma$ -Phe- $\gamma$ -Phe-OH revealed a dense network of fibers growing from a central nucleation point. In the same conditions we studied the self-assembly process of Boc-dityrosine homologues. A previous work done in our team showed that L-tyrosine was able to form well-ordered assemblies depending on concentration, aging and solvent. Different morphologies were observed such as nanoribbons, fibers or branched structures. In chapter 2 we showed that the protection of tyrosine with aromatic group had a significant influence on the self-assembly nanostructures formed with a majority of fibers in water. Regarding the dipeptides, the Boc- $\alpha$ -Tyr- $\alpha$ Tyr-OH, Boc- $\beta$ -Tyr- $\beta$ -Tyr-OH and Boc- $\gamma$ -Tyr- $\gamma$ -Tyr-OH were dissolved at a concentration of 0.5 mg·mL-1 and rested for 1 h before deposition on a TEM grid. For the three homologues, the dityrosine derivatives did not assembled into organized nanostructures and only the presence of aggregates could be seen (Figure 3.2).

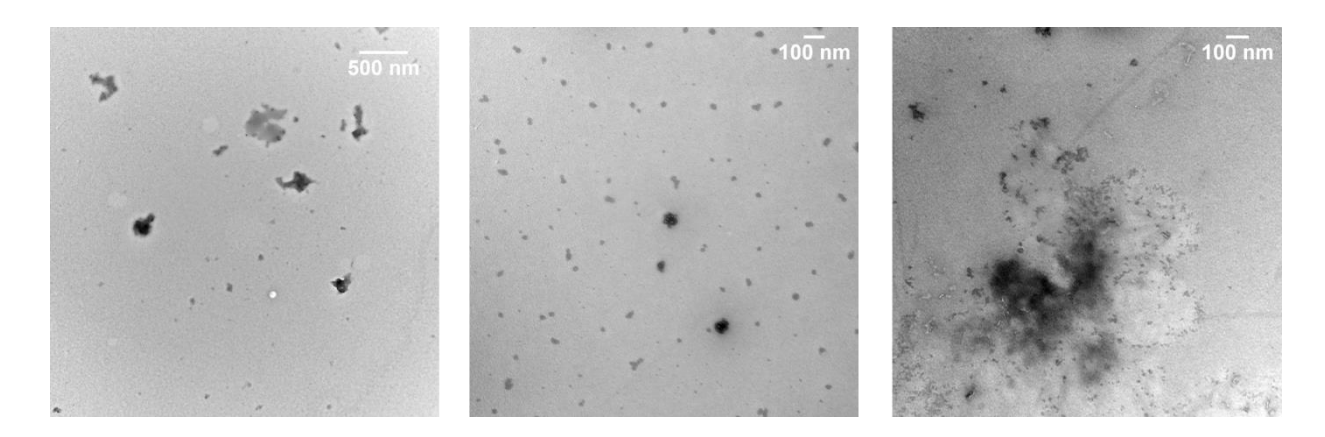


**Figure 3.2.** Self-assembly of Boc-dityrosine at 0.5 mg·mL<sup>-1</sup> in pure water from left to right: Boc- $\alpha$ -Tyr- $\alpha$ -Tyr-OH, Boc- $\beta$ -Tyr- $\beta$ -Tyr-OH and Boc- $\gamma$ -Tyr- $\gamma$ -Tyr-OH.

## 3.3.2 Hydrogels synthesis

The preliminary studies for hydrogel formation were initiated by Laurène Wagner during her third-year internship from engineering school within our team and presented in Table 3.1. The dipeptides used were synthesized by Dr. B. Dinesh postdoctoral researcher and Dr. O. Chaloin, research engineer in our team. The hydrogel formation of diphenylalanine homologues was first tested using the same method used with gel 1 and gel 2 from chapter 2. The dipeptides were dissolved in DMSO at a concentration of 247 mM and diluted in water to reach a final concentration of 4.9 mM in 2% DMSO in water. A homogeneous gel was obtained with Boc-γ-Phe-γ-Phe-OH while heterogeneous gel containing aggregates and a viscous solution were observed with the Boc- $\beta$ -Phe- $\beta$ -Phe-OH and the Boc- $\alpha$ -Phe- $\alpha$ -Phe-OH dipeptides, respectively. Different parameters were modified to try to optimize the protocol such as the temperature, the pH of added water, the dipeptide concentration, the nature of the organic solvent, the volume of organic solvent and the presence of monovalent or divalent salts. Modification of the temperature from room temperature to 4 °C or 37 °C did not give any improvement on the gel formation apart for  $Boc-\alpha$ -Phe- $\alpha$ -Phe-OH forming a stable homogeneous gel at 37 °C. Regarding the influence of the pH, we observed that no stable gel was formed with the addition of a basic aqueous solution (pH 11) to DMSO, whereas gels were formed using acidic one (pH 4) (Figure 3.3). These results can be explained by the morphological modifications previously observed of the dipeptides at acidic pH and confirm the pH sensitivity of the three systems.



**Figure 3.3.** Hydrogel tests formation with 2 % DMSO/H<sub>2</sub>O at different pH using 4.9 mM of Boc-γ-Phe-γ-Phe-OH.

The nature of the organic solvent used in the protocol also seems to play an important role. Changing DMSO with HFIP or MeOH did not give positive results with no gel obtained in the case of HFIP and only the formation of a heterogeneous gel with MeOH and Boc- $\beta$ -Phe- $\beta$ -Phe-OH (Figure 3.4). The three samples were viscous using 2 % HFIP/H<sub>2</sub>O. Observing that the  $\beta$ -dipeptides were poorly soluble in 2 % DMSO in water, we increased the percentage of DMSO to 5 % and 10 %. A stable gel was obtained for the Boc- $\beta$ -Phe- $\beta$ -Phe-OH with 10 % DMSO in water after 5 min of gelation and some water loss (Figure 3.5). Nevertheless, this method was not chosen for further study as 10 % DMSO is too high leading to cell toxicity.

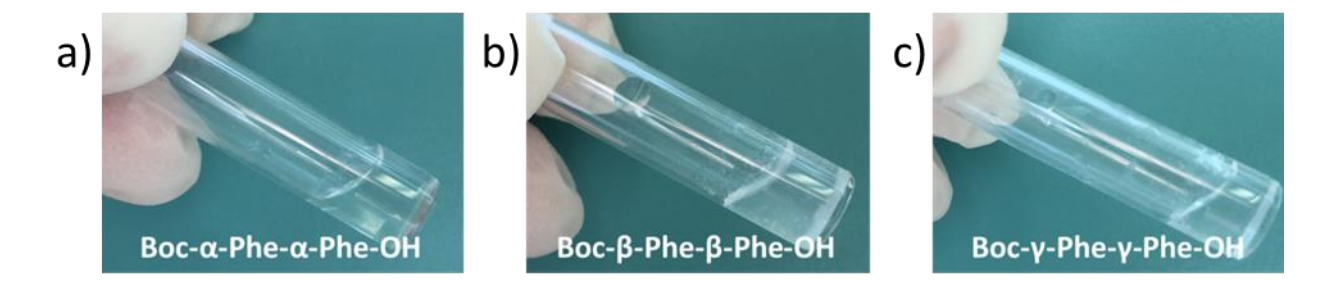


**Figure 3.4.** Hydrogel tests formation with 2 % HFIP/H<sub>2</sub>O using 4.9 mM of a) Boc-α-Phe-α-Phe-OH, b) Boc-β-Phe-β-Phe-OH and c) Boc-γ-Phe-γ-Phe-OH.

It has been shown by Yuran *et al.* that NaCl accelerates the formation of supramolecular linked nanostructures of highly concentrated Boc- $\alpha$ -Phe- $\alpha$ -Phe-OH.<sup>13</sup> Therefore, we tried to incorporate NaCl or CaCl<sub>2</sub> at different concentrations to induce the gelation. The tests performed were also not conclusive with the appearance of aggregates (Figure 3.6).

The influence of the di-peptide quantity was characterized by using two times less or double concentration in 2 % DMSO/H<sub>2</sub>O. When the dipeptide concentration was two times less (2.45 mM), a gel was obtained for Boc- $\alpha$ -Phe- $\alpha$ -Phe-OH, but it was not stable over time. On the contrary, when the concentration was doubled (9.8 mM), Boc- $\beta$ -Phe- $\beta$ -Phe-OH and Boc- $\gamma$ -Phe- $\gamma$ -Phe-OH formed heterogeneous and homogeneous gels, respectively. With these results, we were not able to design a unique protocol using the solvent triggered method giving homogeneous and stable gels for the three dipeptides.



**Figure 3.5.** Hydrogel test formation of 4.9 mM Boc- $\beta$ -Phe- $\beta$ -Phe-OH with 10 % DMSO/H<sub>2</sub>O at t0 and after 5 min.

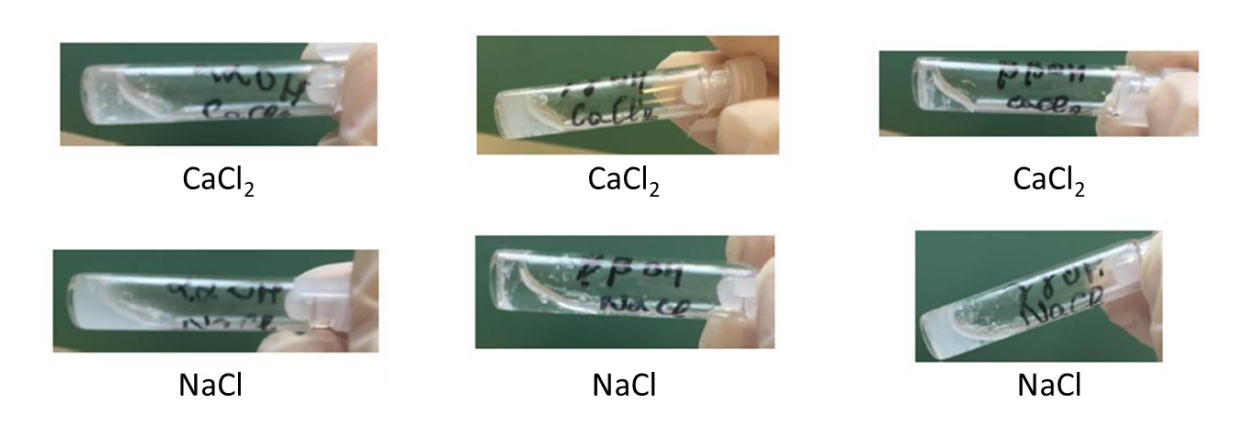


**Figure 3.6.** Hydrogel test formation of 4.9 mM di-phenylalanine and 2 % DMSO/H<sub>2</sub>O in presence of CaCl<sub>2</sub> or NaCl at 25 mM (from left to right Boc- $\alpha$ -Phe- $\alpha$ -Phe-OH, Boc- $\beta$ -Phe-OH and Boc- $\gamma$ -Phe- $\gamma$ -Phe-OH).

As the dipeptides are sensitive to pH modification, another method was tested based on pH changes that is called the "pH-switch protocol". This method consists in dissolving the

dipeptides in a basic solution and triggering the gel formation by acidification. The dipeptides were therefore dissolved in basic sodium hydroxide (NaOH) solution 10 mM, with the help of sonication, and acidic hydrochloric acid solution 0.5 M was added dropwise. Gelation was observed for the three Boc-diphenylalanine homologues (Figure 3.7) with color modification from transparent to opaque after the addition of an appropriate volume of hydrochloric acid (1 % (v/v) for Boc- $\alpha$ -Phe- $\alpha$ -Phe-OH and Boc- $\gamma$ -Phe- $\gamma$ -Phe-OH and 7% (v/v) for Boc- $\beta$ -Phe- $\beta$ -Phe-OH). The protocol was optimized to keep a final concentration of dipeptides of 4.9 mM for the three systems. Boc- $\beta$ -Phe- $\beta$ -Phe-OH and Boc- $\gamma$ -Phe- $\gamma$ -Phe-OH hydrogels were formed instantaneously and in approximatively 1 h, respectively. Boc- $\alpha$ -Phe- $\alpha$ -Phe-OH hydrogel formed a gel in approximatively 7 h and was less stable over time compared to the two other hydrogels with a structural degradation and some water leakage observed after 1 day.



**Figure 3.7.** Hydrogel formation of Boc- $\alpha$ -Phe- $\alpha$ -Phe-OH, Boc- $\beta$ -Phe-OH and Boc- $\gamma$ -Phe-OH using the pH switch method.

As numerous gels were obtained containing Fmoc-tyrosine derivatives in chapter 2, we aimed to compare the gelation properties of Boc-diphenylalanine homologues with Boc-dityrosine ones. The same gelation method was tested with Boc- $\alpha$ -Tyr- $\alpha$ -Tyr-OH, Boc- $\beta$ -Tyr- $\beta$ -Tyr-OH, and Boc- $\gamma$ -Tyr- $\gamma$ -Tyr-OH products but none of the test was conclusive. The formation of fibers in water is generally essential to obtain hydrogels by allowing the creation of a network encapsulating water molecules. The three Boc-dityrosine homologues did not self-assemble and formed amorphous structures whereas the three Boc-diphenylalanine derivatives self-assembled into fibers. This result indicates that the hydroxyl group present in the tyrosine side chain has a key role in inhibiting the self-assembly into nanofibers and thus gelation.

**Table 3.1** Summary of the hydrogelation tests performed for Boc- $\alpha$ -Phe-OH, Boc- $\beta$ -Phe- $\beta$ -Phe-OH, and Boc- $\gamma$ -Phe- $\gamma$ -Phe-OH.

	Boc-α-Ph	e-α-Phe-O	Н	Boc-β-Phe	e-β-Phe-Ol	1	Boc-γ-Phe-γ-Phe-OH			
	Aspect	Gelation duration	Stability in time	Aspect	Gelation duration	Stability in time	Aspect	Gelation duration	Stability in time	
T=4°C	V. 1	,	,			yes				
Ambient	Viscous liquid	/	/	Heterogenous gel	13 h		Homogenous	<5 min	yes	
T=37°C	Homogenous gel	15 h	no	neterogenous ger		no	gel			
pH = 4		2 h Heterogeneous gel		24 h	yes	Homogenous <5 min				
pH = 7	Heterogenous gel	15 h	no	Ustanasaasaa	/	/	gel	<5 min	yes	
pH = 11		15 h		Heterogenous viscous liquid	/	/	Viscous liquid	/	/	
2.45 mM	Homogenous gel	21 h	no	Heterogenous liquid	/	/	Heterogenous liquid	/	/	
9.8 mM	Heterogenous gel	15 h	no	Heterogeneous gel	1 h	yes	Homogenous gel	<5 min	yes	
2% HFIP	Heterogenous liquid	/	/	Heterogenous liquid	/	/	Heterogenous liquid	/	/	
2% MeOH	Heterogenous liquid	/	/	Heterogenous gel	24 h	yes	Heterogenous liquid	/	/	
5% DMSO	/	/	/	Heterogenous gel	1 h	no	/	/	/	
10% DMSO	/	/	/	Heterogenous gel	5 min	yes	/	/	/	
NaCl	Heterogenous	/	/	Heterogenous	/	/	Heterogenous	/	/	
CaCl <sub>2</sub>	liquid	/	/	liquid	/	/	liquid	/		
pH switch	Homogenous gel	7h	1 day	Homogenous gel	<1 min	yes	Homogenous gel	<1h	yes	

## 3.3.3 Formation of hybrid hydrogels containing carbon nanomaterials

Considering the excellent photothermal properties of carbon nanomaterials under NIR light irradiation we developed hybrid hydrogels containing ox-CNTs or GO for NIR irradiation-triggered drug release applications. Sonicated suspensions of ox-CNTs and GO at the optimal concentration of 0.025 wt% were firstly prepared in the basic dipeptide solutions before the addition of HCI. Gelation process was not impacted by the incorporation of the carbon nanomaterials and the gelation time stayed the same. We managed to form all hybrid homogeneous hydrogels for both carbon nanomaterials (ox-CNTs and GO) and for the three types of diphenylalanine hydrogels (Figure 3.8). GO and ox-CNTs were found aggregated in Boc- $\alpha$ -Phe- $\alpha$ -Phe-OH and Boc- $\beta$ -Phe- $\beta$ -Phe-OH gel whereas they were both better dispersed in Boc- $\gamma$ -Phe- $\gamma$ -Phe-OH hydrogel. The instability of the Boc- $\alpha$ -Phe- $\alpha$ -Phe-OH hydrogels and the very quick gelation of the Boc- $\beta$ -Phe- $\beta$ -Phe-OH can be responsible for the aggregation of the nanomaterials in these samples.

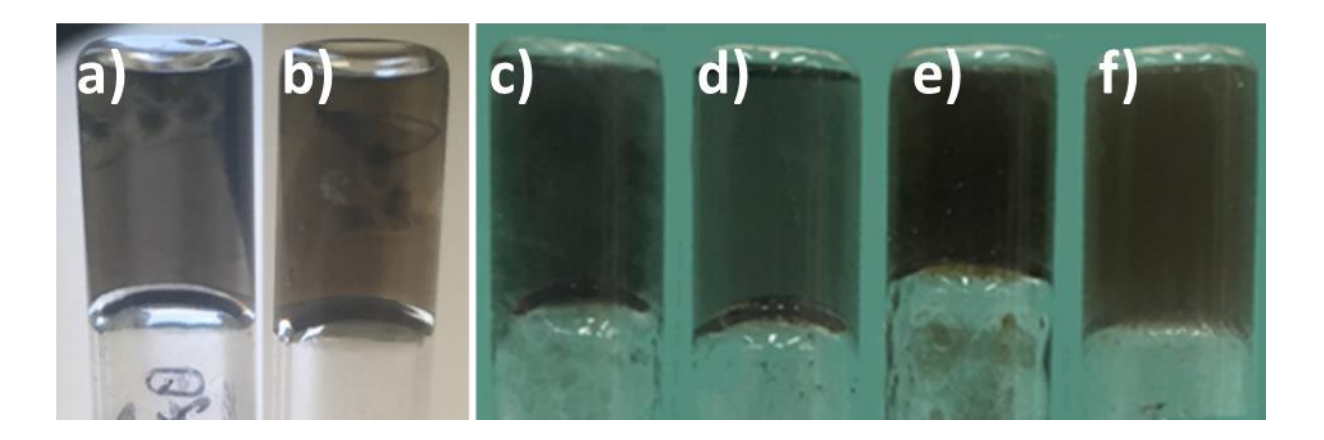


**Figure 3.8.** Photographs of hydrogels made with the pH switch method a) Boc- $\alpha$ -Phe- $\alpha$ -Phe-OH + 0.025 wt% ox-CNTs, b) Boc- $\alpha$ -Phe- $\alpha$ -Phe-OH + 0.025 wt% GO, c) Boc- $\beta$ -Phe- $\beta$ -Phe-OH + 0.025 wt% ox-CNTs, d) Boc- $\beta$ -Phe- $\beta$ -Phe-OH + 0.025 wt% GO, e) Boc- $\gamma$ -Phe- $\gamma$ -Phe-OH + 0.025 wt% ox-CNTs, and f) Boc- $\gamma$ -Phe- $\gamma$ -Phe-OH + 0.025 wt% ox-CNTs.

#### 3.3.4 Structural characterization

The morphological characterization of the hydrogels formed using pH switch method was studied by TEM (Figure 3.9). Whereas Boc- $\alpha$ -Phe- $\alpha$ -Phe-OH self-assembled in spheres in water, we instead observed fibers in the gel state. The TEM analysis revealed that most of the fibrils in the gel Boc- $\alpha$ -Phe- $\alpha$ -Phe-OH has a width of 10-30 nm (Figure 3.10). The structural change from spheres to fibers has already been observed in Boc-diphenylalanine supramolecular self-assembly in function of the concentration and aging. 13 The presence of ox-CNTs or GO into the gel structure did not have any impact on the Boc- $\alpha$ -Phe- $\alpha$ -Phe-OH fiber size with similar diameter measured. The two other gels made of Boc-β-Phe-β-Phe-OH and Boc-y-Phe-y-Phe-OH showed also long fibers interconnected with a higher variability in diameter. Boc-β-Phe-β-Phe-OH fibers have a diameter in the range of 30-90 nm with few larger (100-120 nm). Boc-y-Phe-y-Phe-OH fibers have similar diameter in the range of 20-90 nm with also few larger (100-120 nm). Similar to the supramolecular hydrogels 1 and 2 previously studied, the TEM images also showed that the ox-CNTs and GO are in contact with the fibrils, certainly due to  $\pi$ - $\pi$  interactions with the aromatic moieties of the gelators (Figure 3.9). The presence of both ox-CNTs and GO did not disturb the self-assembly of the three dipeptides into fibrils with similar size and morphology (Figures 3.9 and 3.10).

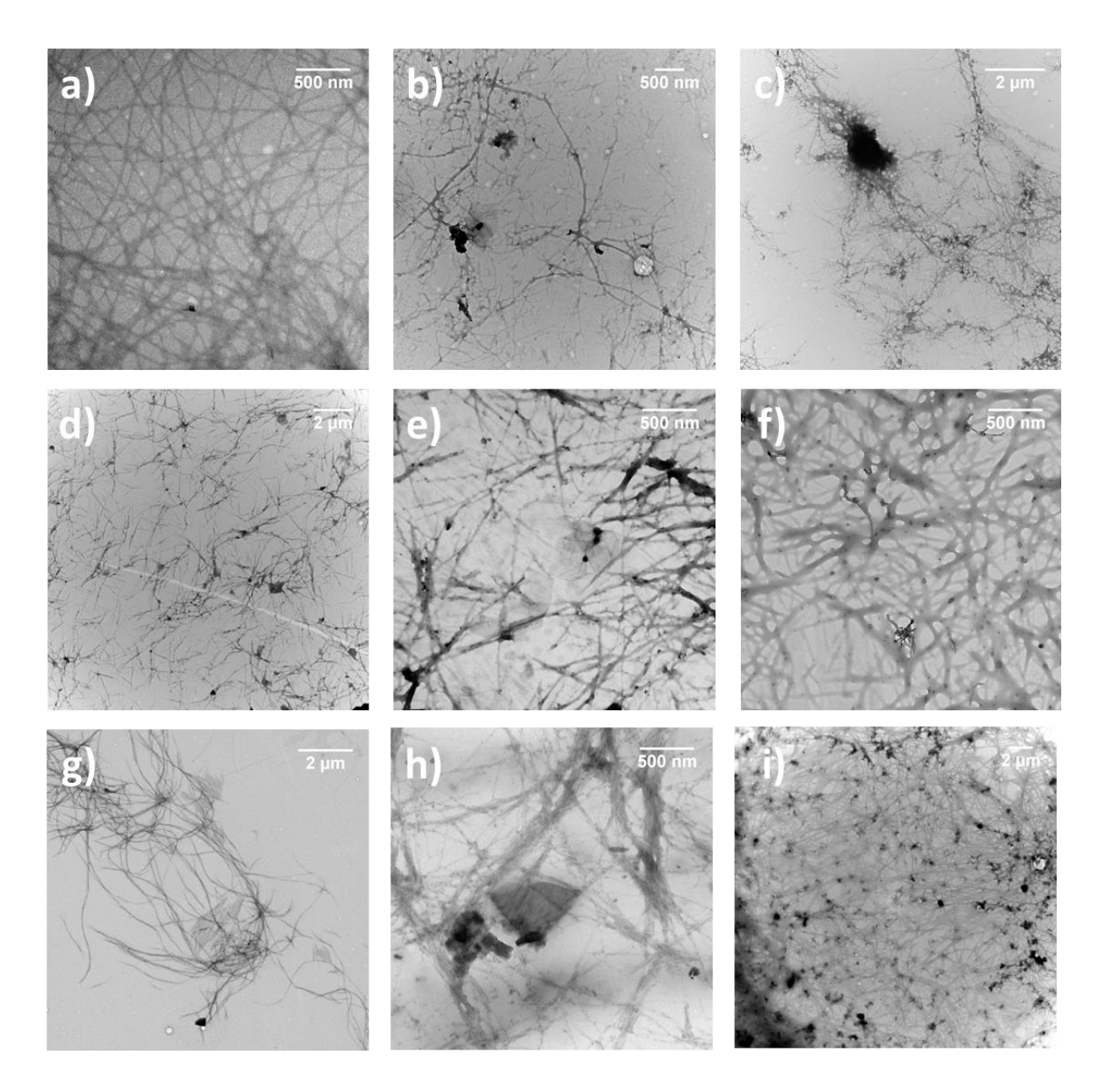


**Figure 3.9.** TEM images of a) Boc- $\alpha$ -Phe- $\alpha$ -Phe-OH, b) Boc- $\alpha$ -Phe-OH + 0.025 wt% ox-CNTs, c) Boc- $\alpha$ -Phe- $\alpha$ -Phe-OH + 0.025 wt% GO, d) Boc- $\beta$ -Phe- $\beta$ -Phe-OH, e) Boc- $\beta$ -Phe- $\beta$ -Phe-OH + 0.025 wt% ox-CNTs, f) Boc- $\beta$ -Phe- $\beta$ -Phe-OH + 0.025 wt% GO, g) Boc- $\gamma$ -Phe- $\gamma$ -Phe-OH + 0.025 wt% ox-CNTs and i) Boc- $\gamma$ -Phe- $\gamma$ -Phe-OH + 0.025 wt%

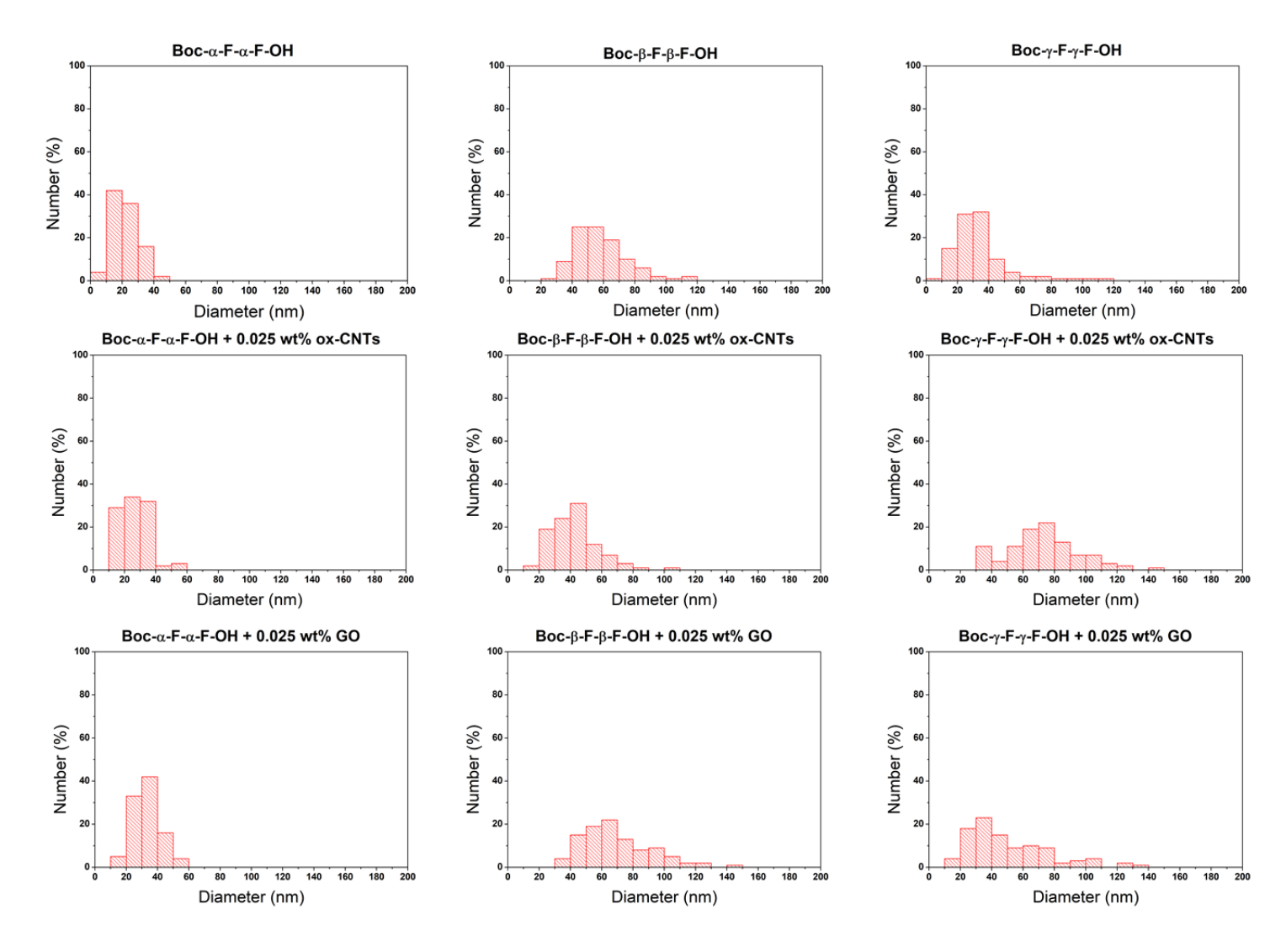
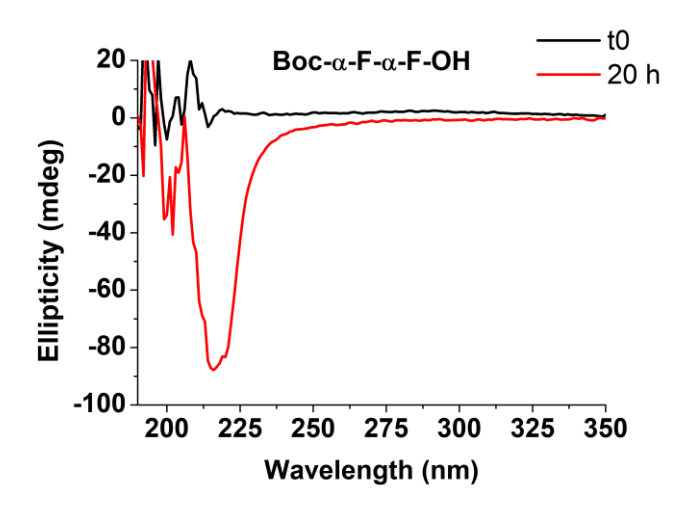


Figure 3.10. Diameter distribution of the fibrils of the native and hybrid hydrogels (n=100).

#### 3.3.5 Circular dichroism

The Boc-diphenylalanine hydrogels developed were characterized by circular dichroism (Figures 3.11 and 3.12). The gels were prepared in a vial and directly added to the cylindrical 0.1 mm quartz cuvette after the addition of HCl. During the synthesis it was observed that Boc- $\alpha$ -Phe- $\alpha$ -Phe-OH hydrogels were not formed before approximatively 7 h. The CD spectrum of Boc- $\alpha$ -Phe- $\alpha$ -Phe-OH did not show any signal at t0 but a negative peak appeared already after 1 h of gelation at 219 nm. The signal observed at 219 nm is similar to the one observed in the supramolecular gel 1 and gel 2, presented in Chapter 2, and can be attributed to the  $\pi$ - $\pi$ \* phenyl side chain excitation and a hydrogen bond network involving the carbamate functionality. The intensity of the signal increased over time until 20 h (limit of the time measurement). However, the instability of the Boc- $\alpha$ -Phe-OH gel did not allow the analysis of Boc- $\alpha$ -Phe- $\alpha$ -Phe-OH hydrid gels with 0.025 wt% ox-CNTs or GO.



**Figure 3.11.** CD spectrum of gel Boc- $\alpha$ -Phe- $\alpha$ -Phe-OH directly after the addition of HCl (t0) and 20 h after gelation into the cuvette.

The Boc- $\beta$ -Phe- $\beta$ -Phe-OH hydrogel showed a signal already at t0 when the gel was directly inserted into the cuvette. The signals were totally identical from t0 to 30 min of measurement. This result confirmed the instantaneous gelation and the stability of the Boc- $\beta$ -Phe- $\beta$ -Phe-OH hydrogel after the addition of HCl. We observed the same signal and hydrogelation kinetics in presence of ox-CNTs and GO with a minimum around ~200-220 nm and a maximum at 190 nm. The signal observed with two negative peaks at 200 nm and 220

nm and an intense maximum peak at 190 nm were indicative a non-identified folded structures.

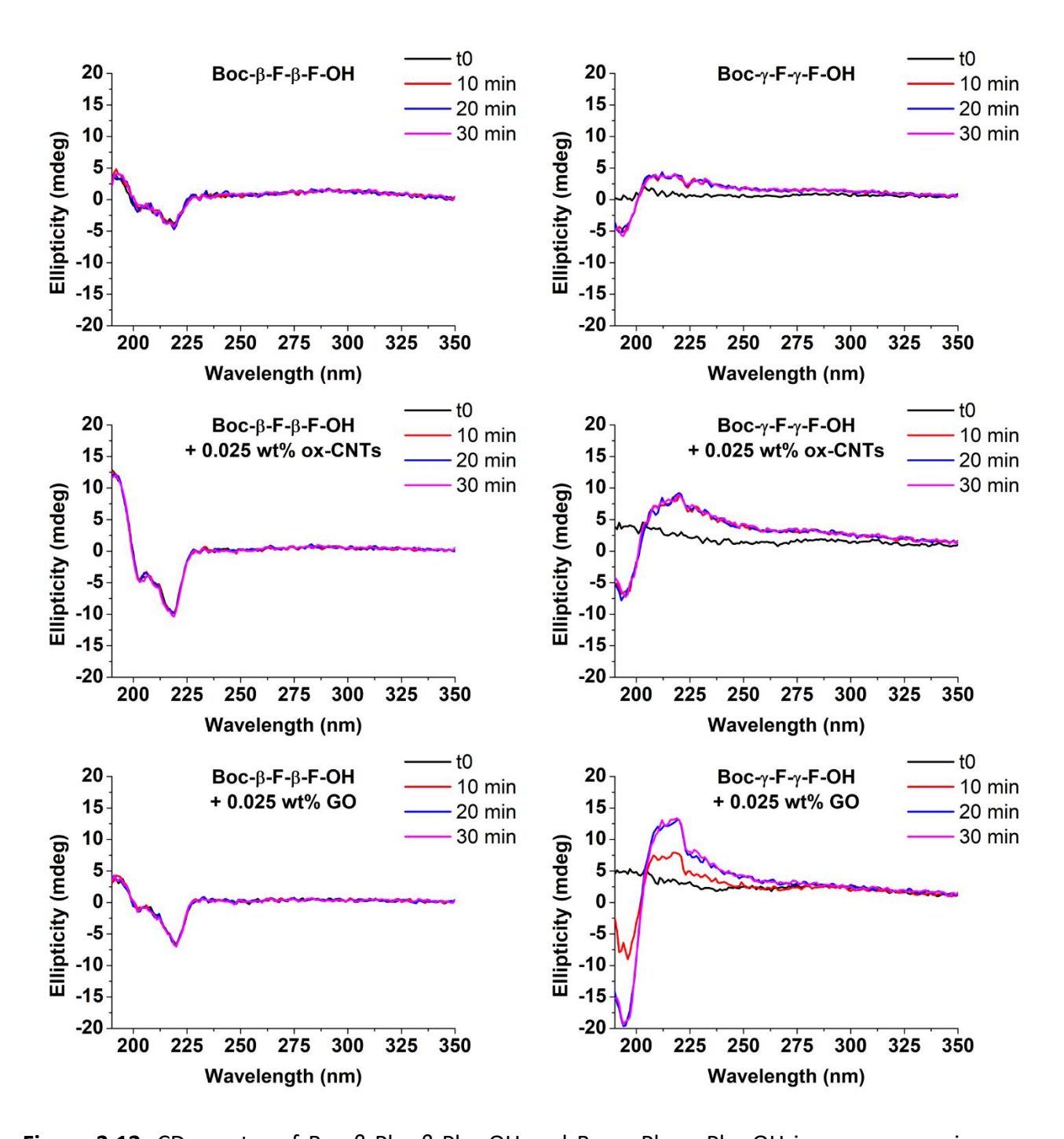


**Figure 3.12.** CD spectra of Boc- $\beta$ -Phe- $\beta$ -Phe-OH and Boc- $\gamma$ -Phe-OH in presence or in absence of carbon nanomaterials.

The Boc-γ-Phe-γ-Phe-OH did not show any signal before 10 min. However, the signals observed were totally different compared to the two other peptides. Indeed, the CD spectra

was more characteristic of random coils with a maximum between 205-240 nm and a minimum at 193 nm.<sup>22</sup> The kinetics were similar in presence and in absence of ox-CNTs. In contrast, in presence of GO we observed an increase of the signal between t0 and 20 min followed by a stabilization.

#### 3.3.6 Photothermal properties

We studied the photothermal properties of the dipeptide hydrogels under NIR irradiation (Figure 3.13). The change in temperature for the three native gels was very low with an increase of 6°C, 6.5°C and 5.4°C after 10 min of irradiation for Boc- $\alpha$ -Phe- $\alpha$ -Phe-OH, Boc- $\beta$ -Phe- $\beta$ -Phe-OH and Boc- $\gamma$ -Phe- $\gamma$ -Phe-OH, respectively. The three gels remained totally intact after irradiation. In all cases, the hybrid gels were destructured under irradiation. In the case of hybrid gel Boc- $\alpha$ -Phe- $\alpha$ -Phe-OH, it was completely liquefied whereas the irradiation of the hybrid gels Boc- $\beta$ -Phe- $\beta$ -Phe-OH and Boc- $\gamma$ -Phe- $\gamma$ -Phe-OH induced the appearance of a liquid phase. The highest increase of temperature (50°C-60°C) was obtained for the hybrid gels Boc- $\alpha$ -Phe-OH and its beta homologues. The lowest temperature increase was obtained for the hybrid gels Boc- $\gamma$ -Phe- $\gamma$ -Phe-OH with a temperature increase slightly below 50°C.

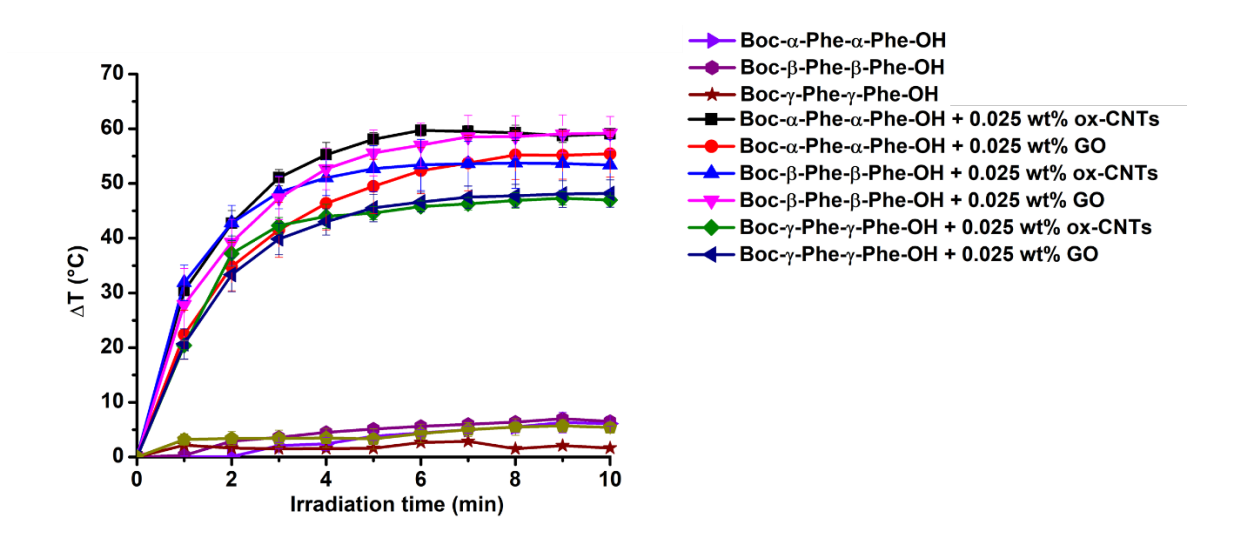


**Figure 3.13.** Temperature increase of the native gels in comparison to the hybrid gels when exposed to a NIR laser (at 808 nm, under 2 W/cm²) as a function of the laser irradiation time.

### 3.3.7 Drug loading

To perform a comparative study with the supramolecular hydrogels made of Fmoc-Y-OH/Fmoc-Y(Bzl)-OH and Fmoc-F-OH/Fmoc-Y(Bzl)-OH, we studied the incorporation of L-ascorbic acid into the Boc-diphenylalanine hybrid hydrogels at a concentration of 0.7 mg·mL<sup>-1</sup>. L-ascorbic acid was diluted into NaOH solution before the dissolution of the dipeptides. After sonication and heating, HCl drops were added into the NaOH solution containing L-ascorbic acid and dipeptides until observing a gelation (Figure 3.14). Without carbon nanomaterials the three Boc-diphenylalanine hydrogels were stable in presence of 0.7 mg·mL<sup>-1</sup> of L-ascorbic acid. The carbon nanomaterials were dissolved into the basic solution containing the drug before the addition of HCl. Only the gel Boc-γ-Phe-γ-Phe-OH in presence of L-ascorbic acid and ox-CNTs was destabilized, all the other systems gave gels. The gelation did not occur and aggregates of ox-CNTs appeared.

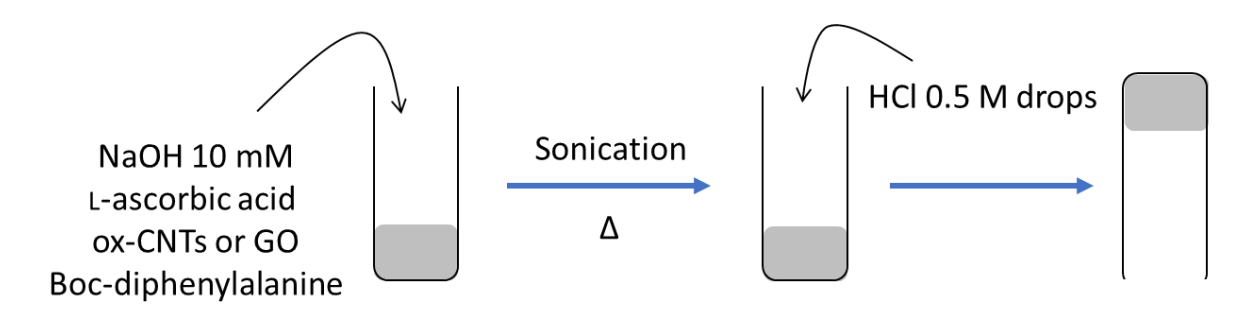


**Figure 3.14.** Scheme of the incorporation of L-ascorbic acid into the Boc-diphenylalanine hydrogels.

# 3.3.8 Drug release

The quantity of water and drug release was measured during the irradiation (Figure 3.15). The Boc- $\alpha$ -Phe- $\alpha$ -Phe-OH hybrid gels were fully destructured after 10 min of irradiation with 100% of the water released. The Boc- $\gamma$ -Phe- $\gamma$ -Phe-OH + GO with the highest increase of temperature also showed a high volume of water released (76 %). Both hybrid gels made of Boc- $\beta$ -Phe- $\beta$ -Phe-OH released a low volume of water of 28.7 % and 39.4 % in presence of GO and ox-CNTs, respectively. The amount of drug released was determined by HPLC and was consistent with the amount of water released. The Boc- $\gamma$ -Phe- $\gamma$ -Phe-OH + GO hydrogel showed a higher amount of L-ascorbic acid released (49.2 %) compared to the Boc- $\beta$ -Phe- $\beta$ -Phe-OH hybrid gels (21.6% and 29.7% in presence of GO and ox-CNTs, respectively). The gel

Boc-β-Phe-β-Phe-OH + GO showed the highest thermal increase with a relatively small amount of drug and water released compared to the other hydrogels studied. It appears to be the most stable gel among the samples developed during our study. The lower water and drug released obtained for the beta and gamma homologue hybrid hydrogels is due to a higher stability compared to the alpha hydrogels. The gel Boc-γ-Phe-γ-Phe-OH + GO showed similar percentage of water and drug release than the supramolecular hydrogels 1 and 2. With its homogeneity, its stability over time and high release under NIR irradiation, Boc-γ-Phe-γ-Phe-OH is the most suitable Boc-diphenylalanine hydrogel for controlled drug release applications.

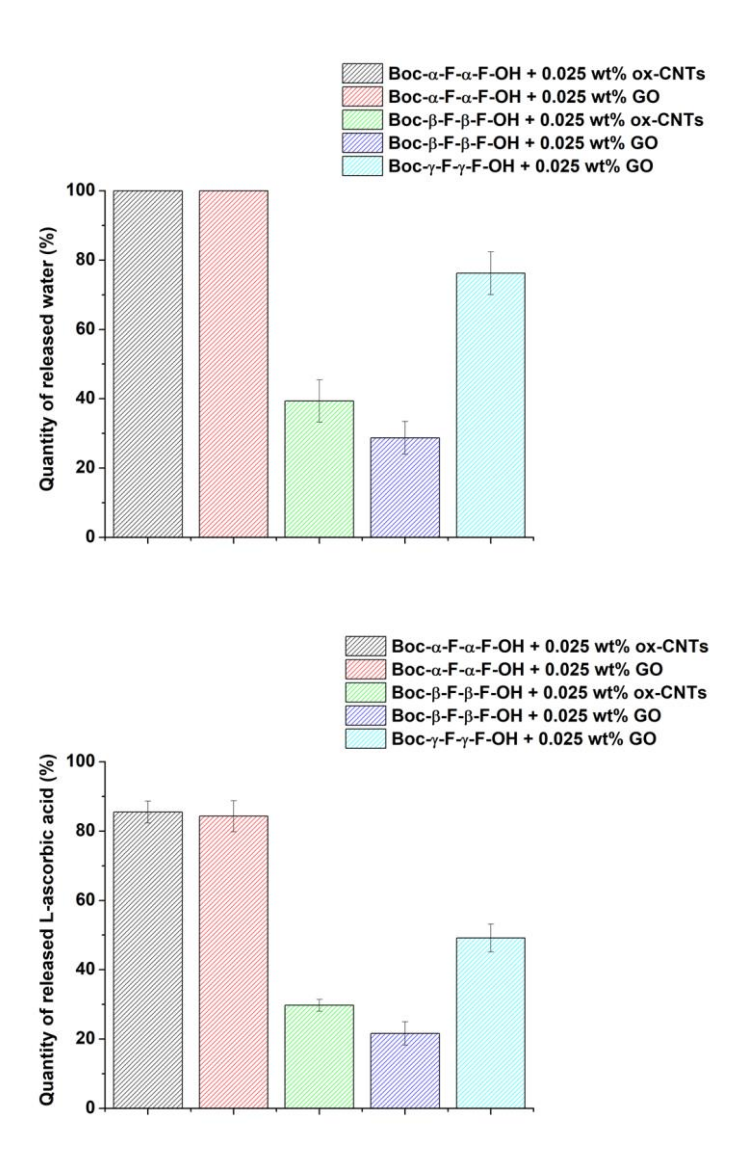


**Figure 3.15.** Release of a) water (n=3) and b) ι-ascorbic acid (n=3) from the hybrid gels under NIR light irradiation.

### 3.3.9 Skin sensibility for topical application

Skin represents 16 % of the body weight in average with a surface between 1.2 and 2 m<sup>2</sup> for an adult. The skin protects against ultraviolet light (between 100 and 400 nm) and forms a physical barrier between the inside and the outside of the body and helps to maintain the body temperature and homeostasis. The epidermis is the most external layer of the skin responsible for impermeability. It is composed of five cellular layers. The stratum corneum is the most external one and can be characterized by the presence of filaggrin, a protein whose role is to aggregate the intermediate filaments of keratins during the formation of the corneal envelope. The basal layer is the deepest layer of epidermis, attached to the dermis by basal membrane, via the integrins α6 and β4. To consider skin application of our system as topical drug release system we tested the inflammation and sensibilization of the skin with a preliminary study of the epidermis integrity after depositing our gels on the top of human skin. This study was performed in collaboration with the team of Dr. Christopher Mueller in our research unit. An explant of human skin of 4 cm<sup>2</sup> surface area and 800 μm thickness was placed on a nylon filter in RPMI at 37°C for 24 hours in presence or absence of gel samples. After immunostaining of integrin  $\alpha$ 6, filaggrin and nucleus the skin samples were analyzed by immunofluorescence. The nuclei were characterized using DAPI, a nuclear counterstain which emits in blue after binding to adenine (A) and thymine (T) residues of DNA. Immunofluorescence images showed that cells were positive to all markers (Figure 3.16).

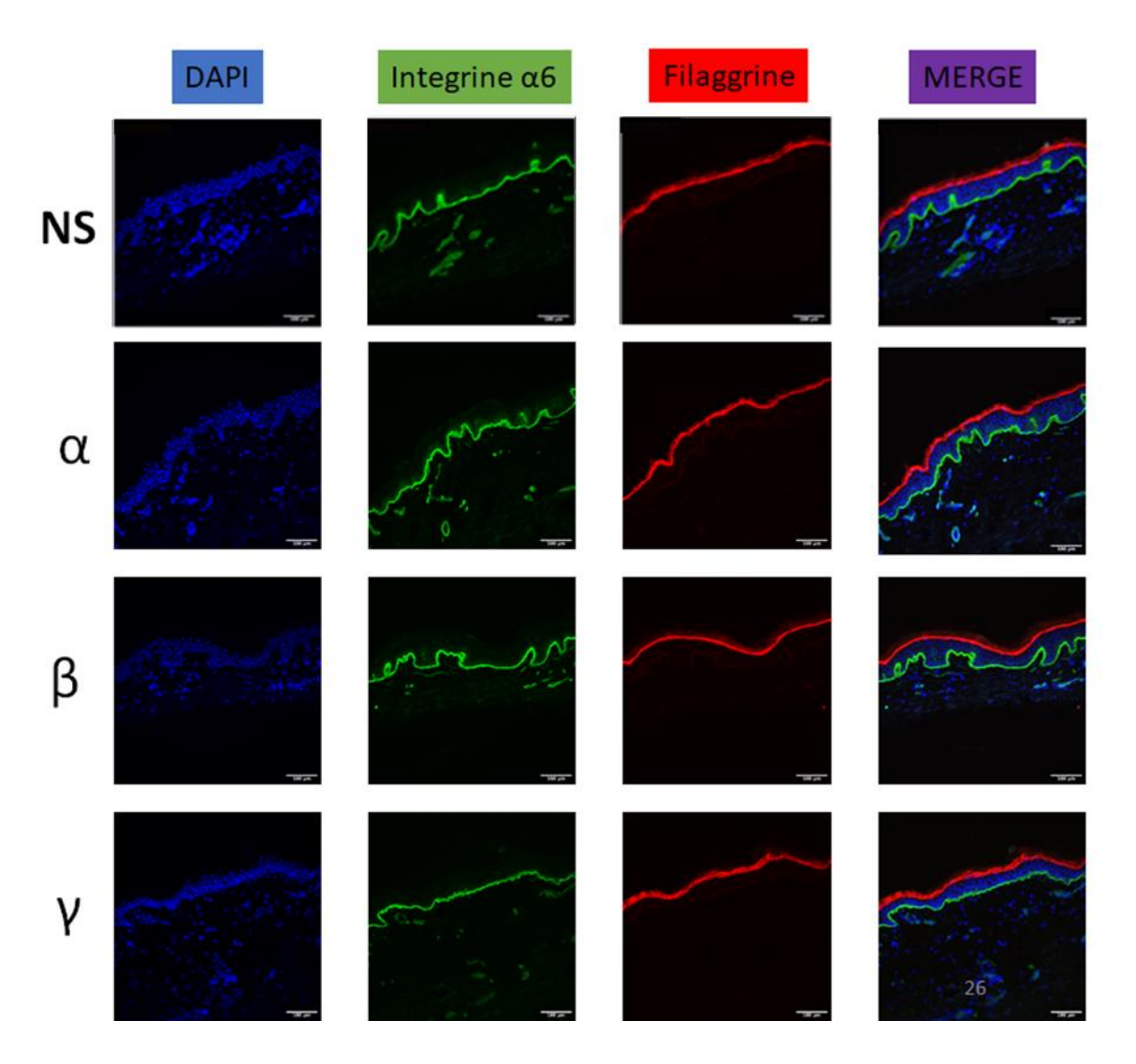


Figure 3.16. Immunofluorescence of cross-sections of human skins without dipeptides deposition (non-stimulated = NS) or with dipeptide deposits. The epidermis of the skin samples with DAPI staining (first column) was compared according to the expression of integrin- $\alpha$ 6 (second column), specific to the basal lamina, and filaggrin (third column), specific to the stratum corneum. The merge images are presented in the fourth column.

The staining of the adhesion molecule integrin- $\alpha$ 6, specific to the basal lamina, and filaggrin, specific to the stratum corneum, did not reveal any difference between the epidermis of the skin in absence of gels (non-stimulated = NS) and the epidermis of the skin in presence of the dipeptide hydrogels. This experiment has been carried out only one time and needs to be repeated to confirm our observations and conclusions.

#### 3.4 Conclusion

In this chapter we have investigated the self-assembly behavior of Boc-diphenylalanine and Boc-dityrosine and their  $\beta$  and  $\gamma$  homologues in water by electron microscopy. The results indicated that the Boc-diphenylalanine holomogues were able to self-organize in nanospheres (Boc- $\alpha$ -Phe- $\alpha$ -Phe-OH) or nanofibers (Boc- $\beta$ -Phe- $\beta$ -Phe-OH and Boc- $\gamma$ -Phe- $\gamma$ -Phe-OH) at the concentration studied, whereas Boc-dityrosine homologues showed aggregates with no defined morphology. These observations illustrate the influence of the hydroxyl group in the self-assembly process. We have applied several distinct protocols to obtain hydrogels with the different dipeptides. Even if some methods showed the possibility to form at least one Boc-diphenylalanine hydrogel, only pH switch method allowed the formation of hydrogels for the three Boc-diphenylalanine derivatives. In contrast, Bocdityrosine did not form hydrogels following the pH switch procedure. Oxidized CNTs and GO were incorporated into the hydrogels without impacting the gelation process. L-ascorbic acid was also loaded into the gels. Only one gel (Boc-y-Phe-y-Phe-OH) was destabilized in presence of the drug while the other gels were stable in presence of the carbon nanomaterials and the drug. Upon NIR light irradiation L-ascorbic acid was released at high concentration due to the destabilization of the gel structure caused by the photothermal effect of the carbon nanomaterials. Our preliminary test concerning the toxicity of the dipeptide hydrogels on human skin showed positive results with no apparent inflammation or sensibilization of the skin. Other experiments are currently in progress to quantify the sensitizing or irritating potential of our gels by measuring the presence or absence of TNF- $\alpha$ released in the culture medium. The study of enzymatic degradation should also be tested to confirm the resistance of the  $\beta$  and  $\gamma$  homologues.

#### 3.5 References

- 1. Zhou, M.; Smith, A. M.; Das, A. K.; Hodson, N. W.; Collins, R. F.; Ulijn, R. V.; Gough, J. E. Self-Assembled Peptide-Based Hydrogels as Scaffolds for Anchorage-Dependent Cells. Biomaterials 2009, 30 (13), 2523–2530.
- 2. Yang, Z.; Liang, G.; Ma, M.; Abbah, A. S.; Lu, W. W.; Xu, B. D-Glucosamine-Based Supramolecular Hydrogels to Improve Wound Healing. Chem. Commun. 2007, 8, 843–845
- 3. Huang, R.; Qi, W.; Feng, L.; Su, R.; He, Z. Self-Assembling Peptide—Polysaccharide Hybrid Hydrogel as a Potential Carrier for Drug Delivery. Soft Matter 2011, 7 (13), 6222–6230.

- 4. Naskar, J.; Palui, G.; Banerjee, A. Tetrapeptide-Based Hydrogels: For Encapsulation and Slow Release of an Anticancer Drug at Physiological PH. J. Phys. Chem. B 2009, 113 (35), 11787–11792.
- 5. Reches, M.; Gazit, E. Casting Metal Nanowires Within Discrete Self-Assembled Peptide Nanotubes. Science 2003, 300 (5619), 625–627.
- 6. Reches, M.; Gazit, E. Formation of Closed-Cage Nanostructures by Self-Assembly of Aromatic Dipeptides. Nano Lett. 2004, 4 (4), 581–585.
- 7. Zhang, Y.; Gu, H.; Yang, Z.; Xu, B. Supramolecular Hydrogels Respond to Ligand–Receptor Interaction. J. Am. Chem. Soc. 2003, 125 (45), 13680–13681.
- 8. Banerjee, A.; Palui, G.; Banerjee, A. Pentapeptide Based Organogels: The Role of Adjacently Located Phenylalanine Residues in Gel Formation. Soft Matter 2008, 4 (7), 1430–1437.
- 9. Ma, M.; Kuang, Y.; Gao, Y.; Zhang, Y.; Gao, P.; Xu, B. Aromatic–Aromatic Interactions Induce the Self-Assembly of Pentapeptidic Derivatives in Water To Form Nanofibers and Supramolecular Hydrogels. J. Am. Chem. Soc. 2010, 132 (8), 2719–2728.
- 10. Doran, T. M.; Ryan, D. M.; Nilsson, B. L. Reversible Photocontrol of Self-Assembled Peptide Hydrogel Viscoelasticity. Polym. Chem. 2013, 5 (1), 241–248.
- 11. Marchesan, S.; Waddington, L.; Easton, C. D.; Winkler, D. A.; Goodall, L.; Forsythe, J.; Hartley, P. G. Unzipping the Role of Chirality in Nanoscale Self-Assembly of Tripeptide Hydrogels. Nanoscale 2012, 4 (21), 6752–6760.
- 12. Orbach, R.; Mironi-Harpaz, I.; Adler-Abramovich, L.; Mossou, E.; Mitchell, E. P.; Forsyth, V. T.; Gazit, E.; Seliktar, D. The Rheological and Structural Properties of Fmoc-Peptide-Based Hydrogels: The Effect of Aromatic Molecular Architecture on Self-Assembly and Physical Characteristics. Langmuir 2012, 28 (4), 2015–2022.
- 13. Orbach, R.; Adler-Abramovich, L.; Zigerson, S.; Mironi-Harpaz, I.; Seliktar, D.; Gazit, E. Self-Assembled Fmoc-Peptides as a Platform for the Formation of Nanostructures and Hydrogels. Biomacromolecules 2009, 10 (9), 2646–2651.
- 14. Adams, D. J.; Topham, P. D. Peptide Conjugate Hydrogelators. Soft Matter 2010, 6 (16), 3707–3721.
- 15. Seebach, D.; Overhand, M.; Kühnle, F. N. M.; Martinoni, B.; Oberer, L.; Hommel, U.; Widmer, H. β-Peptides: Synthesis by Arndt-Eistert Homologation with Concomitant Peptide Coupling. Structure Determination by NMR and CD Spectroscopy and by X-Ray Crystallography. Helical Secondary Structure of a β-Hexapeptide in Solution and Its Stability towards Pepsin. Helv. Chim. Acta 1996, 79 (4), 913–941.
- 16. Nanda, J.; Banerjee, A. β-Amino Acid Containing Proteolitically Stable Dipeptide Based Hydrogels: Encapsulation and Sustained Release of Some Important Biomolecules at Physiological PH and Temperature. Soft Matter 2012, 8 (12), 3380–3386..
- 17. Dinesh, B.; Squillaci, M. A.; Ménard-Moyon, C.; Samorì, P.; Bianco, A. Self-Assembly of Diphenylalanine Backbone Homologues and Their Combination with Functionalized Carbon Nanotubes. Nanoscale 2015, 7 (38), 15873–15879.
- 18. Adler-Abramovich, L.; Kol, N.; Yanai, I.; Barlam, D.; Shneck, R. Z.; Gazit, E.; Rousso, I. Self-Assembled Organic Nanostructures with Metallic-Like Stiffness. Angew. Chem., Int. Ed. 2010, 49 (51), 9939–9942.
- 19. Yuran, S.; Razvag, Y.; Reches, M. Coassembly of Aromatic Dipeptides into Biomolecular Necklaces. ACS Nano 2012, 6 (11), 9559–9566.

- 20. Ménard-Moyon, C.; Venkatesh, V.; Krishna, K. V.; Bonachera, F.; Verma, S.; Bianco, A. Self-Assembly of Tyrosine into Controlled Supramolecular Nanostructures. Chem. Eur. J. 2015, 21 (33), 11681–11686.
- 21. Ryan, D. M.; Anderson, S. B.; Nilsson, B. L. The Influence of Side-chain Halogenation on the Self-Assembly and Hydrogelation of Fmoc-phenylalanine Derivatives. Soft Matter 2010, 6, 3220–3231.
- 22. Correcirc, D. H. A.; a; Ramos, C. H. I. The Use of Circular Dichroism Spectroscopy to Study Protein Folding, Form and Function. AJBR 2009, 3 (5), 164–173.

# CHAPTER 4. STRATEGIES FOR HYDROGEL RIGIDIFICATION: TYROSINE CROSS-LINKING AND DOUBLE NETWORK HYDROGELS

#### 4.1 Introduction

The supramolecular hydrogels developed in chapter 2 and 3 from amino acids and diphenylalanine suffer from a low mechanical strength due to the non-covalent interactions which severely limit their practical applications. One solution for improving the physical and mechanical properties of physical hydrogels is to create covalent bonds within the supramolecular structure. Different techniques can be used to cross-link the network depending on the nature of the monomer. In particular, many strategies for cross-linking tyrosine residues have been described in the literature. The polymerization of tyrosine has been largely demonstrated by the use of enzymes<sup>2</sup> or by cross-linking of the tyrosyl radical.<sup>3,4</sup> Coordination bonds with metallic ions are also particularly attractive due to their high stability depending on the metal-ligand combination.<sup>5-7</sup> Another possible way of reinforcing supramolecular hydrogels is to combine the physical network with a second polymeric one to construct a double network (DN) hydrogel.<sup>8-10</sup> Double networks are interpenetrating polymer with extraordinary mechanical properties that are generally composed of one rigid but brittle network where the polymer is tightly covalently crosslinked and a second ductile and flexible loosely cross-linked network. The mechanical properties can be modulated according to the ratio between the two networks as well as their cross-linking proportion. In most of the cases, two chemically cross-linked networks are mixed, and fractures can cause irreversible damage to the gel structure. To overcome these limitations, the incorporation of a physically cross-linked network by supramolecular selfassembly within a chemically cross-linked network would provide better mechanical properties and also crack resistance by reversible rupture of the non-covalent physical bonds.8 Several methods for the synthesis of double network hydrogels have been used since several years, such as two-step radical polymerization processes, 11 molecular stent methods (a medical device that dilates stuffed blood vessels), 12 "one-pot" synthesis methods combining the formation of both networks simultaneously in one step, 13 or 3D printing. 14 To enable medical applications and further improve the mechanical properties of the gels, new processing techniques have been used such as the development of biopolymer-based DN,<sup>15</sup>

nanomaterial-reinforced gels,<sup>16,17</sup> liquid crystal DN gels leading to the formation of highly extensible anisotropic hydrogels,<sup>18</sup> or ultrafine DN gels with very high toughness under micro-scale thickness.<sup>19</sup> However, low mechanical strength (elastic modulus, deformation) and high fatigue remains an essential limitation of hydrogels after incorporation of a supramolecular network. Further research is needed to design a new protocol to develop DN gels with robust mechanical properties and high stability.

### 4.2 Objectives

The aim of this chapter is to explore the possibility to enhance the rigidity of the supramolecular gel 1 and gel 2 to increase their stability. Our first approach consisted on the formation of covalent bonds by crosslinking procedures. We performed preliminary tests with different strategies of cross-linking: i) formed through enzymatic polymerization of tyrosine, ii) using metallic ions or iii) using amino acid derivatives bearing photo-crosslinkable groups. As a second approach to increase the mechanical stability we developed new DN hydrogels to enhance the mechanical properties and injectability of the supramolecular hydrogels. For this purpose, we have tested the incorporation of two different chemical networks into the pre-formed supramolecular structure. The first strategy was to combine supramolecular network with a polyacrylamide synthetic polymer formed in situ by polymerization of the polymeric acrylamide monomers. The second combination was with agarose, a natural polymeric saccharide network with high mechanical properties and biocompatibility. We tried different agarose and polyacrylamide concentrations to obtain DN hydrogels with ideal characteristics for injection and drug delivery application. Similarly, to the previous chapter, we also studied the incorporation of carbon nanomaterials into the gel structure. Finally, the drug baclofen was incorporated in the hybrid hydrogels. An in-depth study of the new photothermal properties, incorporation and release of the drug molecule was also performed.

#### 4.3 Results and discussion

# 4.3.1 Cross-linking using horseradish peroxidase

In order to stabilize the self-assembled structures, we wanted to enhance their stability by cross-linking. The enzyme horseradish peroxidase (HRP) is known to catalyze oxidative polymerization reactions of many phenol derivatives including tyrosine.<sup>2</sup> A model study of

tyrosine and tyrosine derivatives polymerization using HRP as an enzyme catalyst in water was performed in order to extend this protocol to the gel 1 and gel 2 if we obtained successful results. In the presence of hydrogen peroxide, HRP generates the formation of a free radical on the aromatic ring. This process induces a polymerization of tyrosine residues by condensation.<sup>20</sup> Enzymatic polymerization was monitored by UV-Vis spectroscopy, fluorescence spectroscopy and HPLC. A previous work of Sarma *et al.*<sup>21</sup> has shown the appearance of a shoulder at 320-360 nm in the UV-Vis spectra of cross-linked decyl esters of L-tyrosine. In more details, they proposed that the extended absorption into the visible region was characteristic of the extended polymer chain conjugation resulting from the enzymatic polymerization. In their study, <sup>1</sup>H nuclear magnetic resonance (NMR) also indicated that polymers were formed by equal substitution at both ortho or meta position of the benzene ring. In our case with L-tyrosine, a similar shoulder appeared at 300-360 nm by UV-Vis absorption (Figure 4.1).

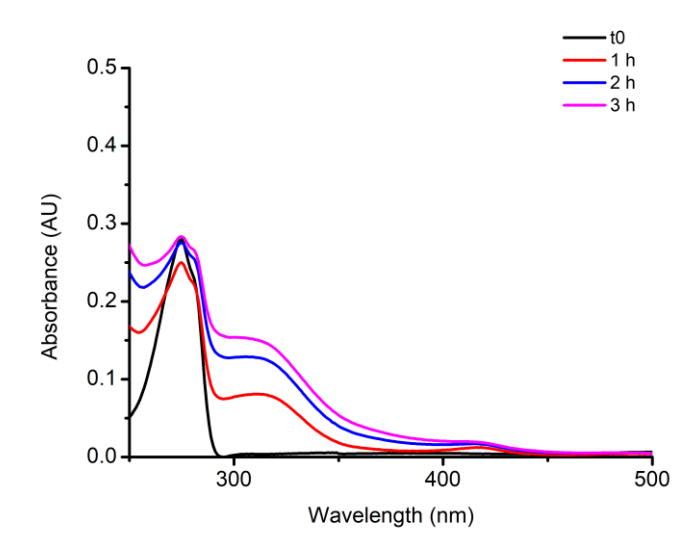


**Figure 4.1.** UV-Vis absorbance spectrum of L-tyrosine in presence of HRP and  $H_2O_2$  at different time point.

Fluorescence spectra were collected with excitation wavelength of 260 nm to explore tyrosine and dityrosine signals. Fluorescence spectra were also collected using excitation wavelength of 325 nm to focus on dityrosine signals.<sup>22</sup> After the addition of  $H_2O_2$  the tyrosine fluorescence emission at 300 nm appeared to decrease with simultaneous appearance of a new increasing emission around 410 nm typical of the dityrosine fluorophore (Figure 4.2). The emission spectra recorded with an excitation of 325 nm

showed the increasing of the dityrosine signal. However, by monitoring the reaction by HPLC we observed that the tyrosine peak was not decreased and no cross-linking by-products (e.g., dityrosine, trityrosine etc.) were observed (Figure 4.3)

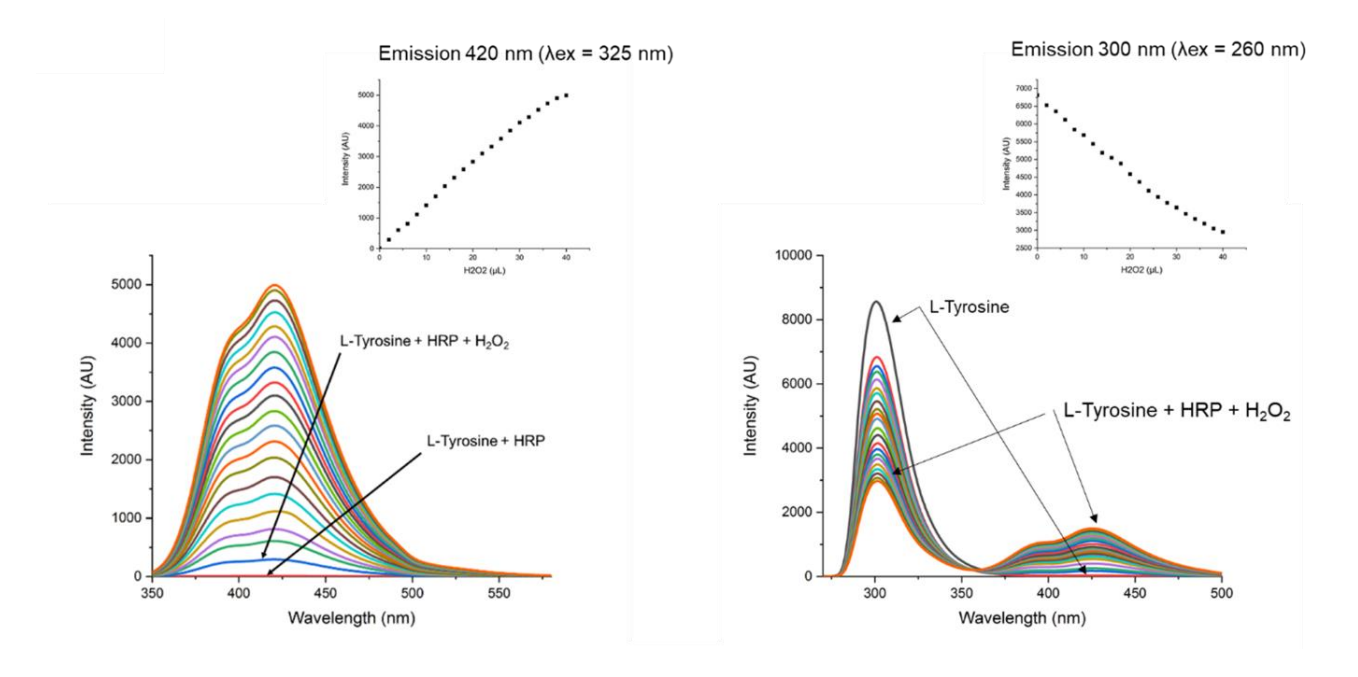


**Figure 4.2.** Fluorescence emission of L-tyrosine with  $\lambda_{ex}$  = 260 nm and  $\lambda_{em}$  = [270-500] nm (left) and with  $\lambda_{ex}$  =325 nm and  $\lambda_{em}$  = [350-580] nm.

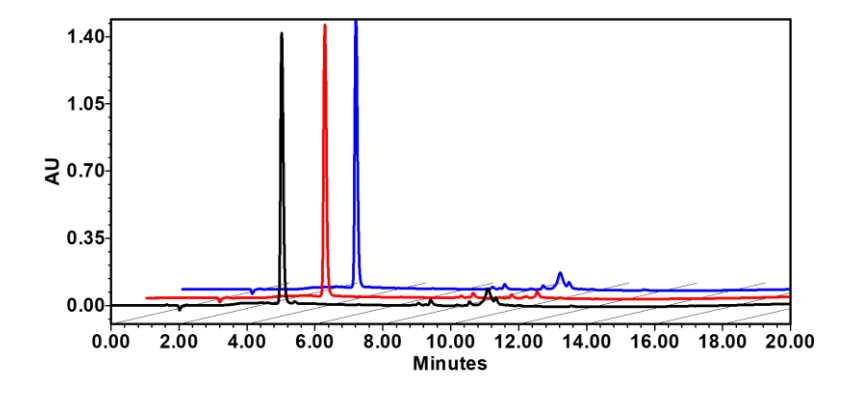
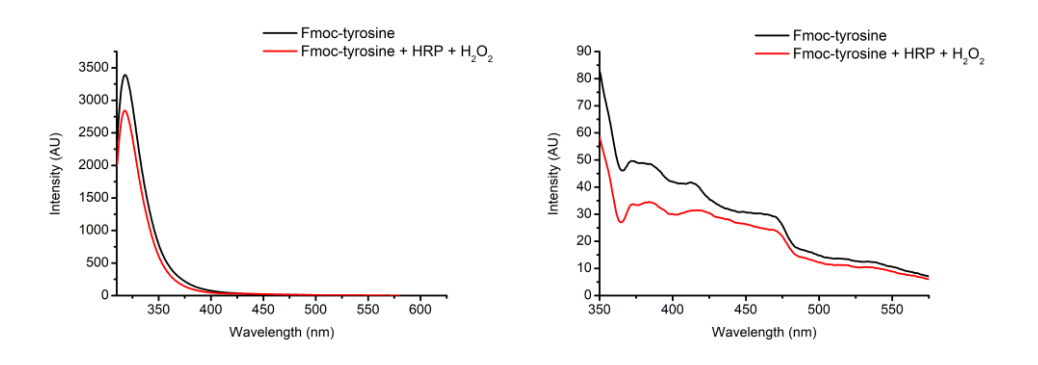


Figure 4.3. HPLC chromatogram of L-tyrosine (red), L-tyrosine + HRP (blue) and L-tyrosine + HRP and  $H_2O_2$  (black) at an absorbance of 220 nm.

Further characterization methods should be done to investigate the results of this cross-linking procedure such as liquid chromatography mass spectroscopy (LC-MS) measurements and NMR. In the supramolecular gel 1 and gel 2 tyrosine derivatives are protected by a Fmoc moiety. We studied the influence of the presence of a protecting group in the cross-linking reaction with HRP and  $H_2O_2$ . A comparative work was carried out on different tyrosine

derivatives protected by various groups such as Fmoc-tyrosine, *O-tert*-butyl-L-tyrosine and *N*-acetyl-L-tyrosine under the same conditions. With the presence of the protecting groups, the reaction rates were drastically decreased. The fluorescence emission of the tyrosine derivatives after an excitation at 300 nm remained intense in the presence of HRP and  $H_2O_2$  and we observed a much lower emission intensities between 350 and 500 nm with  $\lambda_{ex}$  =325 nm than for L-tyrosine (Figures 4.4 and 4.5).



**Figure 4.4.** Fluorescence emission of Fmoc-tyrosine with  $\lambda_{ex}$  = 300 nm and  $\lambda_{em}$  = [310-580] nm (left) and with  $\lambda_{ex}$  =325 nm and  $\lambda_{em}$  = [350-580] nm.

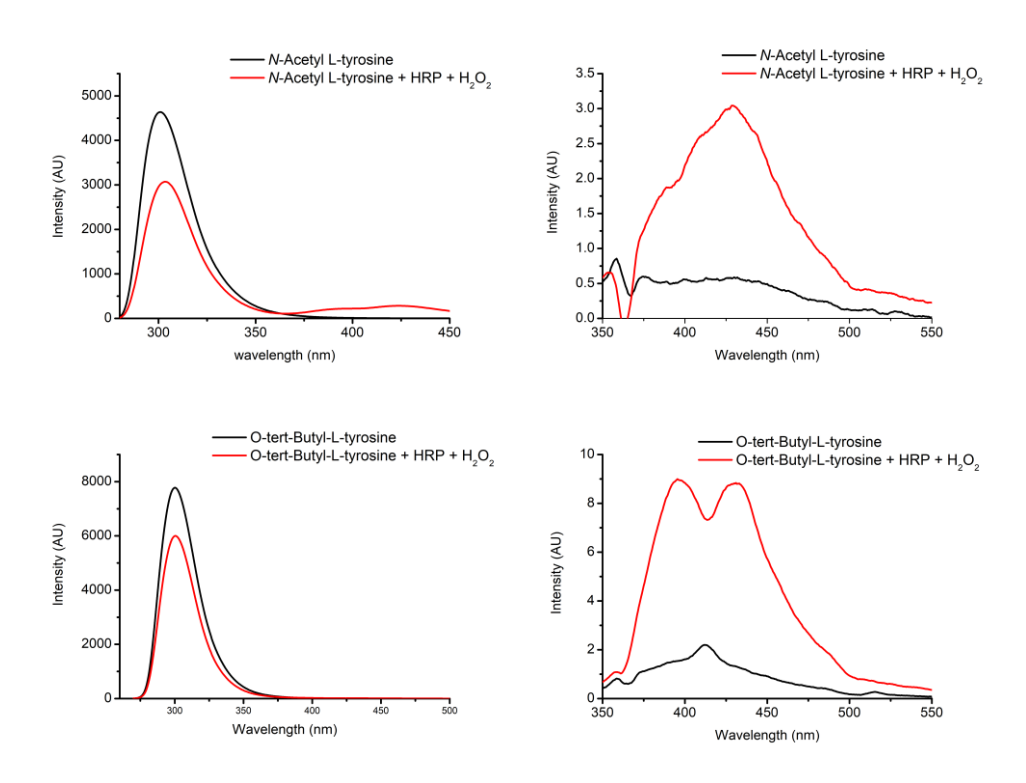


**Figure 4.5.** Fluorescence emission of *N*-acetyl-L-tyrosine and *O-tert*-butyl-L-tyrosine + HRP + H2O2 with  $\lambda_{ex}$  = 260 nm and  $\lambda_{em}$  = [270-500] nm (left) and with  $\lambda_{ex}$  =325 nm and  $\lambda_{em}$  = [350-580] nm.

The reaction with Fmoc-tyrosine was also analyzed by HPLC and no by-products were observed (Figure 4.6).

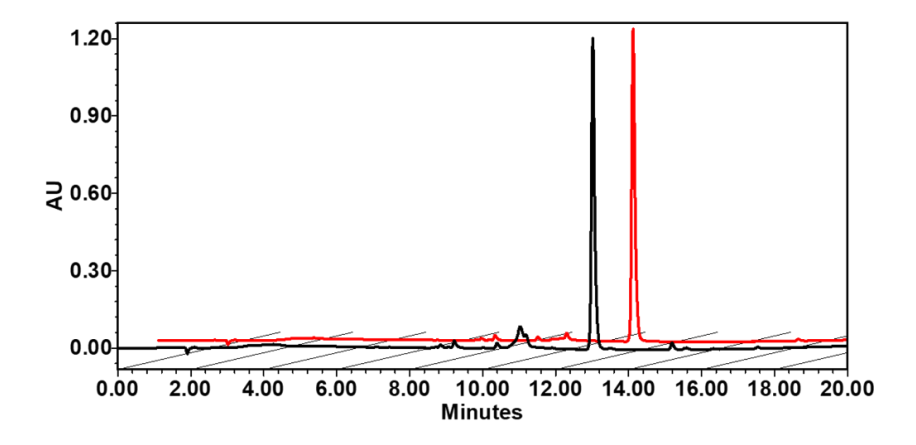


**Figure 4.6.** HPLC chromatogram of Fmoc-tyrosine (red) and Fmoc-tyrosine + HRP +  $H_2O_2$  (black) at an absorbance of 220 nm.

Fukuoaka *et al.* investigated the enzymatic polymerization of tyrosine derivatives such as L-tyrosine ethyl ester, L- and D-tyrosine methyl ester, L-tyrosine ethyl ester hydrochloride or *N*-acetyl L-tyrosine.<sup>23</sup> They show that the polymer yield strongly depends on the monomer concentration with 17% yield for 40 mM of tyrosine derivatives to 82% with 320 mM. These observations can indicate that our concentration of 2.45 mM of tyrosine derivatives is clearly too low to observe any polymerization or that the presence of a protecting group such as the Fmoc moiety prevents enzymatic or chemical cross-linking reactions.

#### 4.3.2 Cross-linking using Fenton, Fenton-like and photo-Fenton reactions

Similarly to HRP, other enzymes or HRP mimetics have shown great potential in tyrosine polymerization such as papain.<sup>23</sup> Other alternatives have been reported in the literature for the oxidative polymerization of phenols involving hematin<sup>24,25</sup>, which is an iron containing porphyrin with a Fe(III) compound structure similar to the prosthetic iron protoporphyrin IX found in HRP or Fe-salen<sup>26</sup> complexes. The oxidation of tyrosine can also be induced by Fenton reaction where Fe(II) ions react with H<sub>2</sub>O<sub>2</sub> generating Fe(III) ions and hydroxyl radicals.<sup>22</sup> The team of Kaplan used Fenton reaction to prepare silk hydrogels through oxidation of tyrosine residues leading to dityrosine cross-linking.<sup>27</sup> Photo-Fenton process is also a powerful source of hydroxyl radicals generated by hydrogen peroxide in the presence of iron cations using UV irradiation that reduces Fe(III) to Fe(II). Photo-Fenton reaction has

been widely used for photochemical wastewater treatment, and comparative studies have proved that the presence of UV irradiation can enhance the efficiency of the Fenton process. Atwood *et al.* showed that A $\beta$ , the amyloid peptides involved in Alzeihmer's disease, is tyrosine cross-linked by Cu at concentrations lower than those detected in the senile plaque *in vivo*. We therefore hypothesized that tyrosine derivates and in particular Fmoc-tyrosine could be cross-linked using Fenton, Fenton-like and photo-Fenton reaction using FeSO<sub>4</sub> or CuCl<sub>2</sub> in the presence of H<sub>2</sub>O<sub>2</sub>. The reactions were monitored by fluorescence spectroscopy and HPLC. Different concentrations of FeSO<sub>4</sub> and CuCl<sub>2</sub> in the presence of H<sub>2</sub>O<sub>2</sub> were tested on both L-tyrosine and Fmoc-tyrosine. Irradiation at 254 nm or 365 nm were used to induce the photo-Fenton reaction. We observed a decrease of the fluorescence emission with an excitation at 260 nm and 300 nm for both L-tyrosine and Fmoc-tyrosine, respectively, in the presence of FeSO<sub>4</sub> and CuCl<sub>2</sub> and H<sub>2</sub>O<sub>2</sub> with or without irradiation (Figure 4.7).

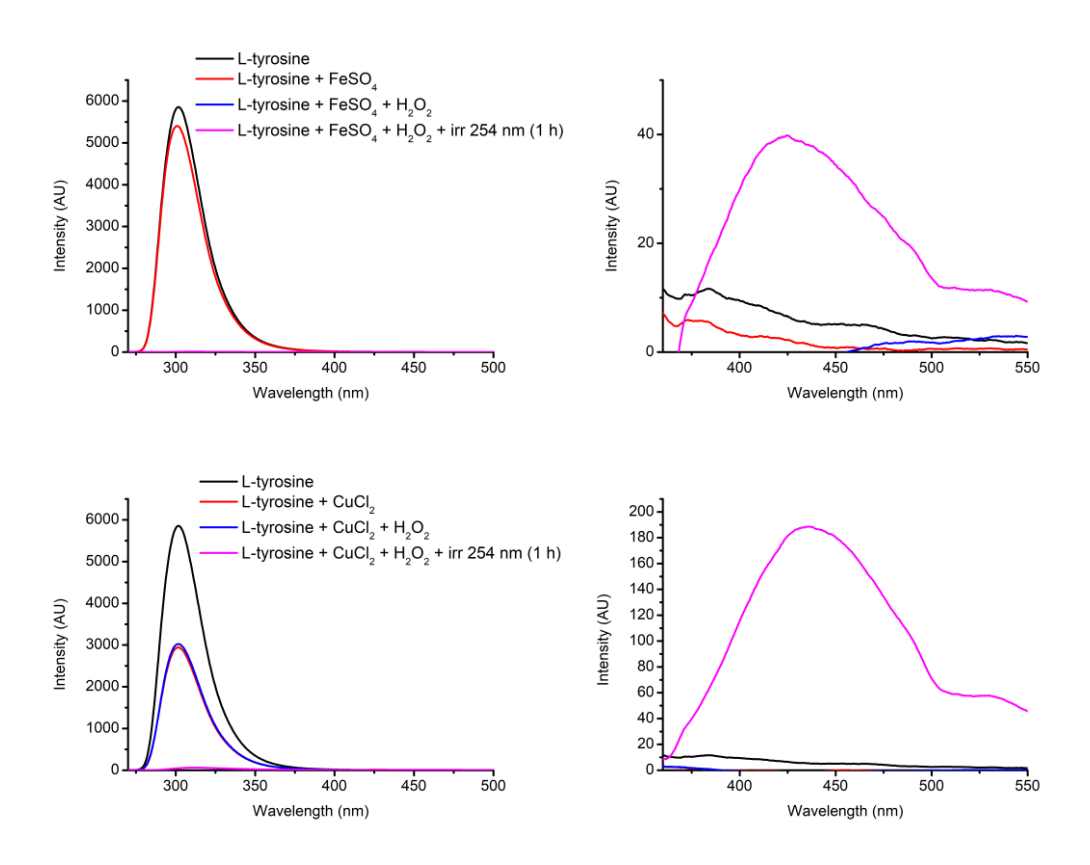


**Figure 4.7.** Fluorescence emission of L-tyrosine with FeSO<sub>4</sub> or CuCl<sub>2</sub> + H<sub>2</sub>O<sub>2</sub> with  $\lambda_{ex}$  = 260 nm and  $\lambda_{em}$  = [270-500] nm (left) and with  $\lambda_{ex}$  =325 nm and  $\lambda_{em}$  = [350-580] nm.

In the case of L-tyrosine in the presence of  $CuCl_2$  and  $H_2O_2$  under 1 h of irradiation at 254 nm, HPLC analysis showed a second peak at 4.2 min that could be attributed to dityrosine (Figure 4.8). However, LC-MS or  $^1H$  NMR measurements should be performed to confirm this hypothesis. In these conditions the fluorescence emission at 300 nm showed a slight decrease after the addition of  $CuCl_2$  and  $H_2O_2$  probably due to the oxidation and the total disappearance of the emission peak after 1 h irradiation (Figure 4.7). However, the fluorescence emission at 350-550 nm characteristic of dityrosine remained too low to conclude that dityrosine was obtained.

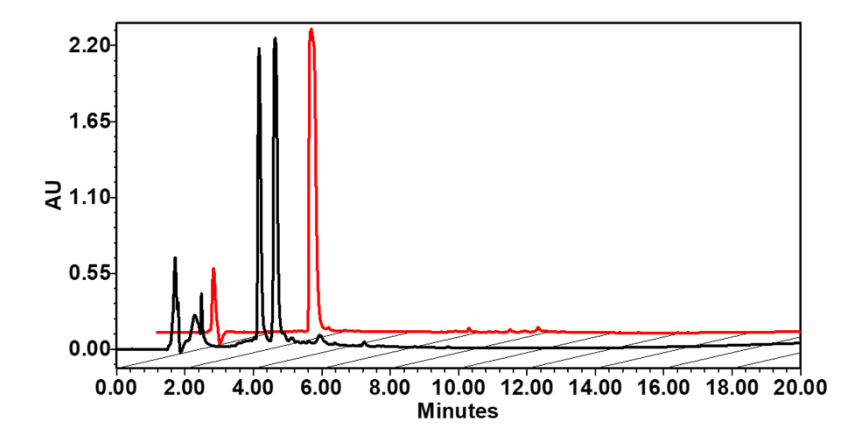


**Figure 4.8.** HPLC chromatogram of L-tyrosine (red) and L-tyrosine +  $CuCl_2$  +  $H_2O_2$  (black) under 1 h irradiation at 254 nm at an absorbance of 220 nm.

With Fmoc-tyrosine, the fluorescence emission peak at 320 nm ( $\lambda_{ex}$  = 300 nm) was reduced after the addition of FeSO<sub>4</sub> and H<sub>2</sub>O<sub>2</sub> and we did not observe any significant differences with 254 nm or 365 nm irradiation (Figure 4.9). The addition of Fe(III) to the Fmoc-tyrosine solution induced a precipitation and therefore decreased the solubility which can explain the reduced Fmoc-tyrosine fluorescence emission. In the presence of CuCl<sub>2</sub> and H<sub>2</sub>O<sub>2</sub>, the emission peak at 310 nm ( $\lambda_{ex}$  = 300 nm) was significantly reduced after 1 h of irradiation at 254 nm (Figure 4.9). However, the absorbance of Fmoc-tyrosine with both FeSO<sub>4</sub> and CuCl<sub>2</sub> with or without irradiation were not decreased in HPLC and we did not observe the appearance of new products (Figures 4.10 and 4.11).

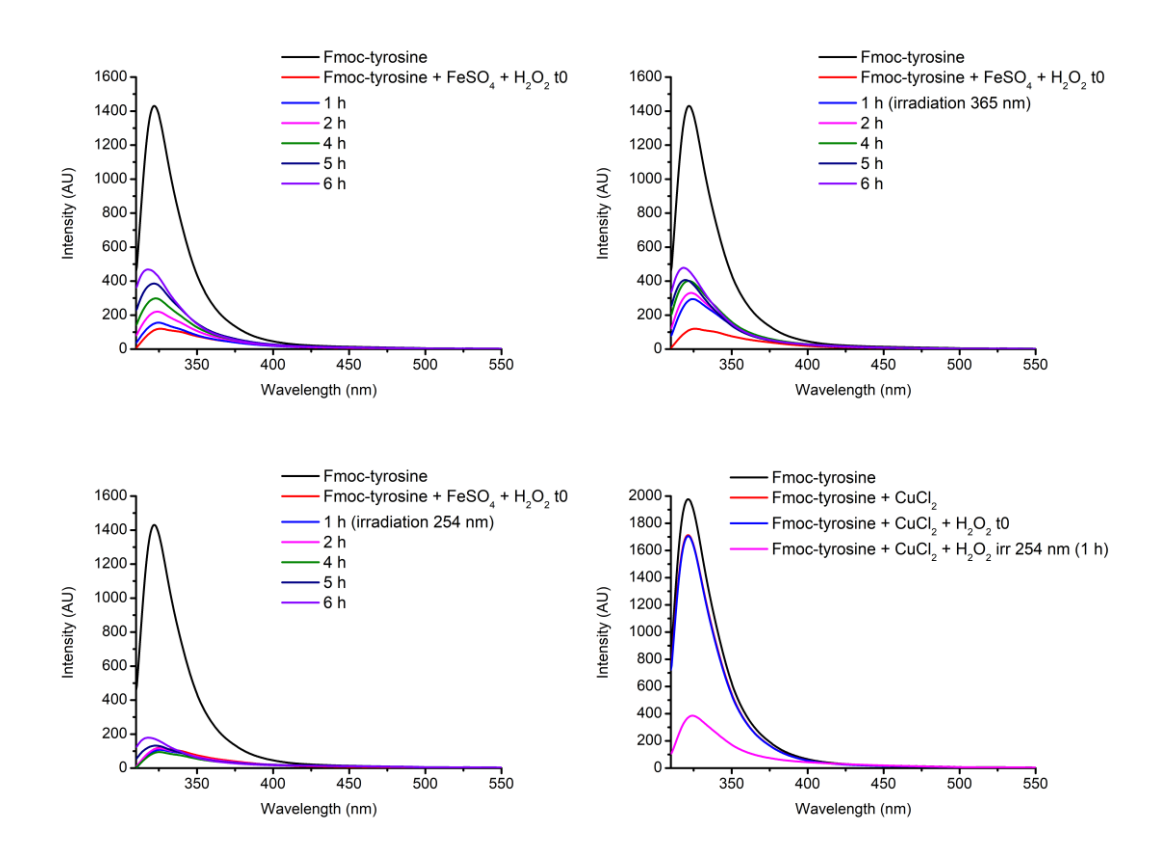


**Figure 4.9**. Fluorescence emission of Fmoc-tyrosine with FeSO<sub>4</sub> or CuCl<sub>2</sub> + H<sub>2</sub>O<sub>2</sub> with or without irradiation (254 nm/365 nm) with  $\lambda_{ex}$  = 300 nm and  $\lambda_{em}$  = [310-580] nm.

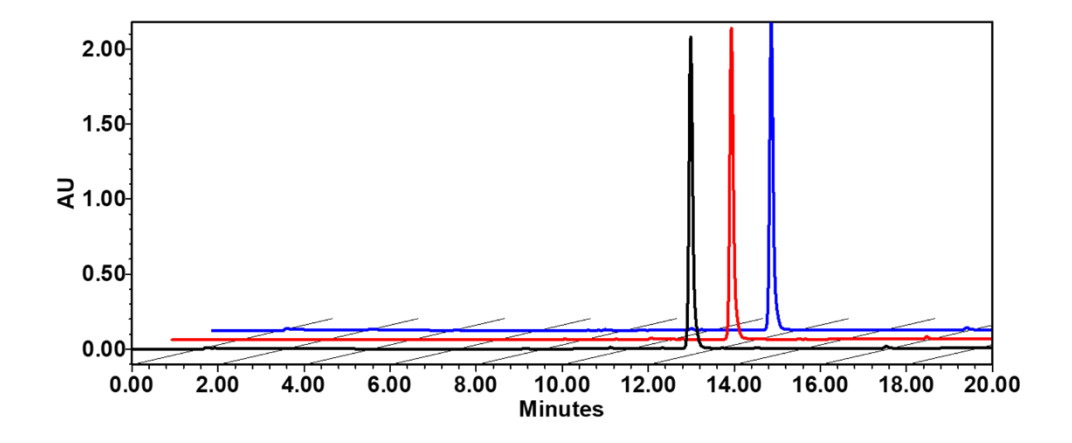


**Figure 4.10.** HPLC chromatogram of Fmoc-tyrosine (red), Fmoc-tyrosine + FeSO<sub>4</sub> (blue) and Fmoc-tyrosine + FeSO<sub>4</sub> +  $H_2O_2$  (black) at an absorbance of 220 nm.

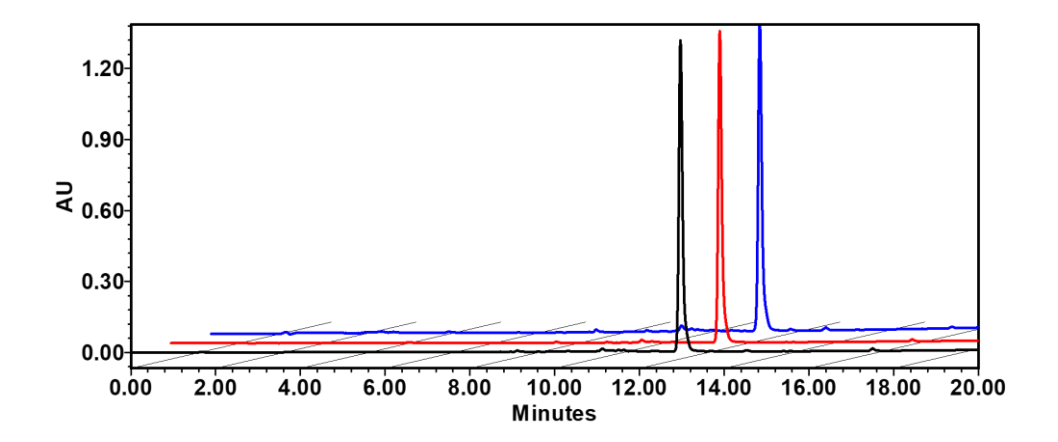


**Figure 4.11.** HPLC chromatogram of Fmoc-tyrosine (red), Fmoc-tyrosine + FeSO<sub>4</sub> +  $H_2O_2$  under 3 h irradiation at 254 nm (blue) and Fmoc-Tyrosine +  $CuCl_2$  +  $H_2O_2$  under 3 h irradiation at 254 nm (black) at an absorbance of 220 nm.

Similarly to the results obtained with the use of HRP, our observations did not allow to confirm the formation of cross-linking products. Further analysis should be done to confirm the formation of dityrosine from L-tyrosine and  $CuCl_2$  under UV irradiation. The presence of the Fmoc-moiety seems again to prevent cross-linked reactions using FeSO<sub>4</sub> or  $CuCl_2$  in the presence of  $H_2O_2$  and other cross-linking methods should be envisaged.

### 4.3.3 Cross-linking using Fremy's salt

Fremy's salt (K<sub>2</sub>NO(SO<sub>3</sub>)<sub>2</sub>) is also used for oxidative cross-linking procedures.<sup>29</sup> Fremy's salt permits chemical conversion of protein containing tyrosine residues to DOPA-o-quinones, which consequently induces polymerization and cross-linking. Fremy's salt was dissolved in MilliQ water and mixed with Fmoc-Tyr-OH (2.45 mM) or with both amino acids of gel 1 Fmoc-Tyr-OH and Fmoc-Tyr(Bzl)-OH (2.45 mM/2.45 mM) in 2% DMSO/H<sub>2</sub>O with a final ratio of 1:3 (Fmoc-Tyr-OH/Fremy's Salt) for sample 1 and 1:3 (Fmoc-Tyr-OH/Fmoc-Tyr(Bzl)-OH) / Fremy's Salt for sample 2 (Figure 4.12). In both cases precipitation occurs after 5 min and we did not observe the formation of any new products by HPLC (Figure 4.13).

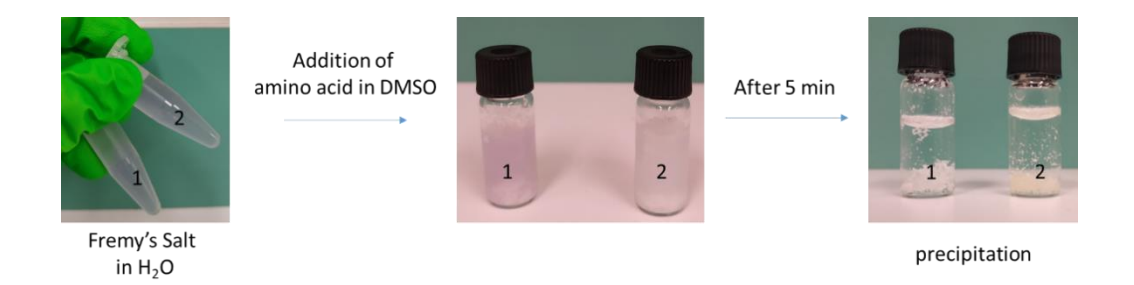


**Figure 4.12.** Photographs of 1:3 Fmoc-Tyr-OH/Fremy's Salt (sample 1) and 1:3 (Fmoc-Tyr-OH/Fmoc-Tyr(Bzl)-OH) / Fremy's Salt (sample 2) before and after precipitation.

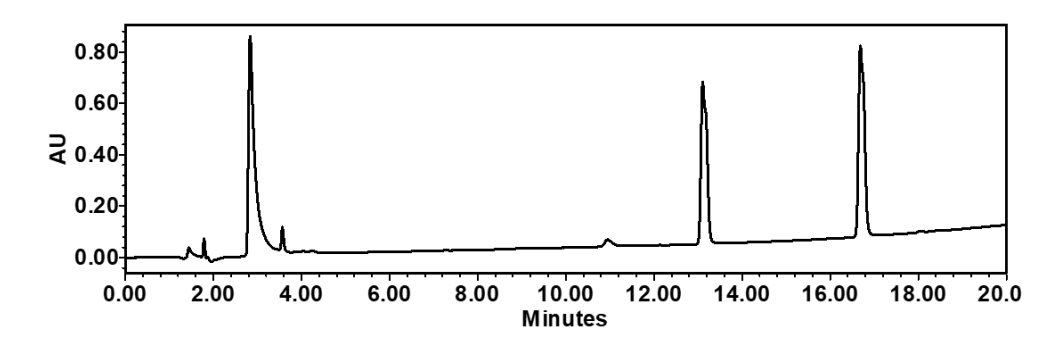


**Figure 4.13.** HPLC chromatogram of 1:3 (Fmoc-Tyr-OH/Fmoc-Tyr(Bzl)-OH) / Fremy's Salt (sample 2) after precipitation with Fmoc-Tyr-OH peak at 13.25 min and Fmoc-Tyr(Bzl)-OH at 16.8 min.

### 4.3.4 Cross-linking using tyrosinase

Finally, we tried a cross-linking procedure using tyrosinase following the recent work of Zhong *et al.*<sup>30</sup> Tyrosinase catalyzes the oxidation of various phenol compounds to their corresponding quinones. In their work, the authors conceived a two-step cross-linking strategy where the phenol group of tyrosine and other studied molecules including phenol, hydroquinone, 4-chlorophenol,4-bromophenol and tyramine was first converted into catechol moiety followed by a cross-linking through covalent and coordination bonding with iron ions. The authors speculated that tyrosine was first hydroxylated by tyrosinase into 3,4-dihydroxyphenylalanine (DOPA) which can be further oxidized into DOPA-quinone, DOPA-chrome a cyclization product with an indole moiety, or DOPA-polymer with a color change from white to orange. Then, FeCl<sub>2</sub> was added to create coordination bonds with the catechol moiety. This reaction was characterized by a black-green solution and followed by UV-Vis spectroscopy with the appearance of a peak at 650 nm, which was attributed to ligand-to-metal charge transfer (LMCT) band of catechol moiety interacting with iron ions. We were

able to reproduce the results using L-tyrosine with the appropriate color changes from white to pink and orange in 1 h, turning black after the addition of  $FeCl_2$  with an LMCT peak at 650 nm (Figures 4.14 and 4.15). Nevertheless, the same reaction procedure with Fmoc-tyrosine was not so efficient (Figures 4.16 and 4.17). After the addition of tyrosinase the color change went from white to pink in approximatively 6 h and stayed pink overnight. The addition of  $FeCl_2$  only gave a brown color to the solution, characteristic of the Fe(III) dissolution in aqueous medium. The UV-Vis spectrum confirmed the absence of coordination with no LMCT peak observed at 650 nm. The Fmoc protection seems to highly influence the oxidation reaction of the phenol group to catechol, thus preventing the coordination with iron. To confirm this observation, we tried the same procedure with dopamine hydrochloride, a small molecule with phenol group fairly similar to L-tyrosine (Figures 4.18 and 4.19).

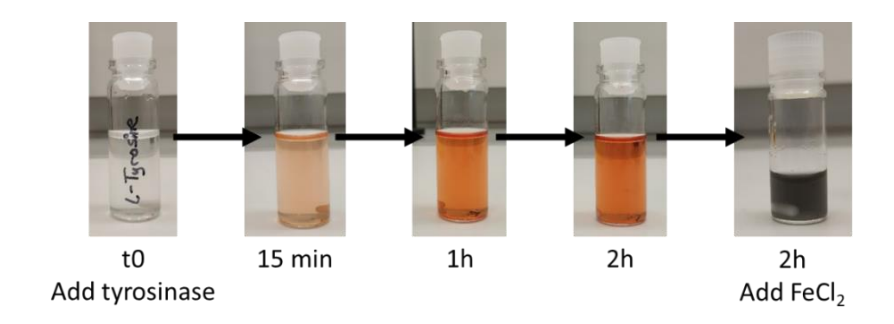


Figure 4.14. Photographs of L-tyrosine in presence of tyrosinase and FeCl<sub>2</sub>.

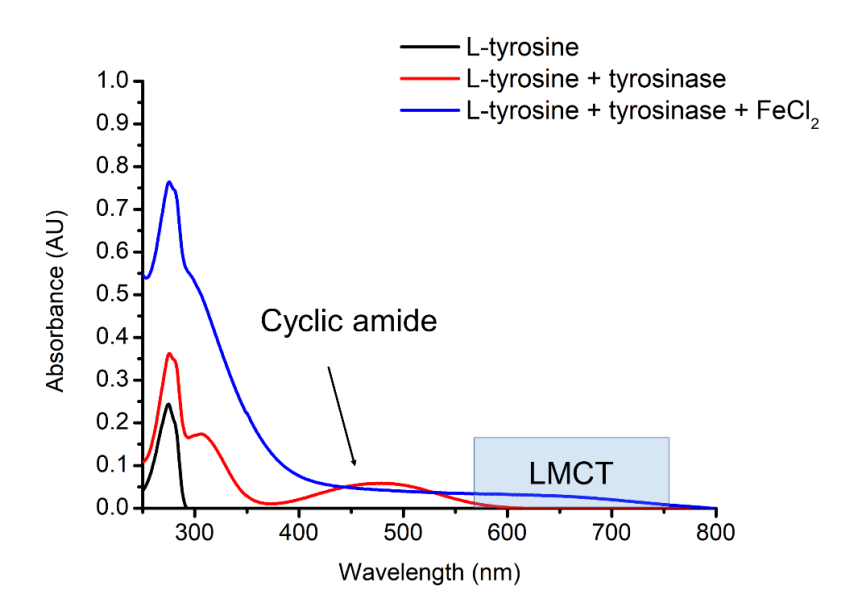


Figure 4.15. UV-Vis absorbance spectra of L-tyrosine in presence of tyrosinase and FeCl<sub>2</sub>.

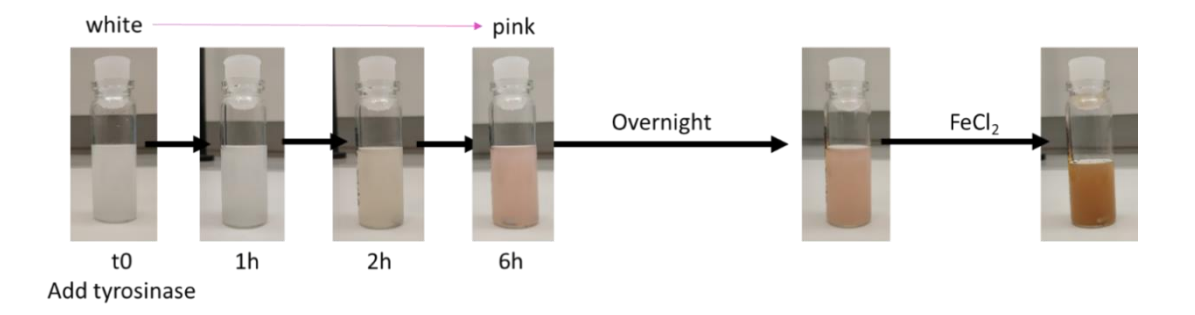


Figure 4.16. Photographs of Fmoc-tyrosine in presence of tyrosinase and FeCl<sub>2</sub>.

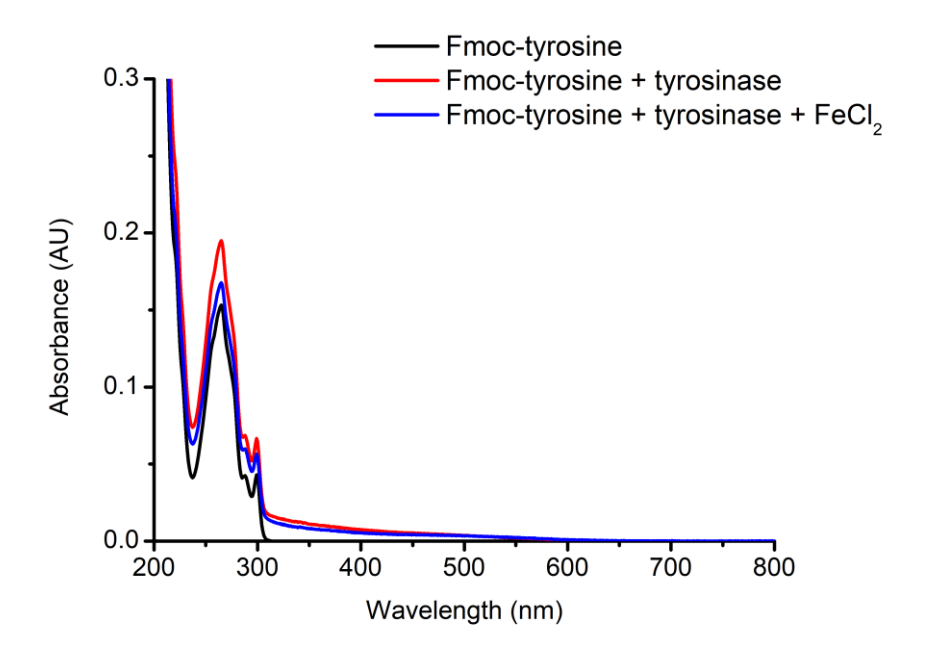


Figure 4.17. UV-Vis absorbance spectra of Fmoc-tyrosine in presence of tyrosinase and FeCl<sub>2</sub>.

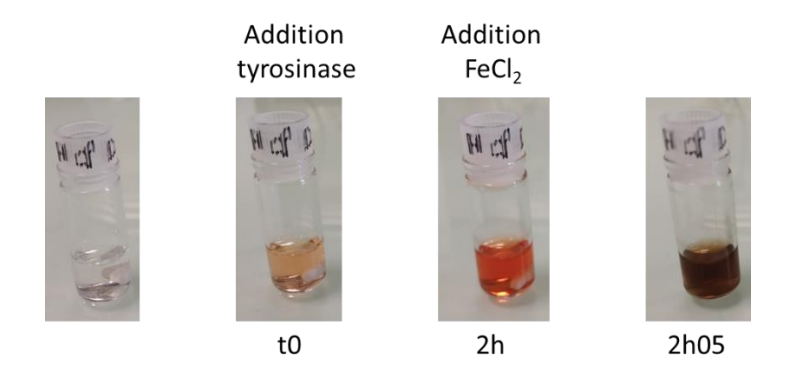
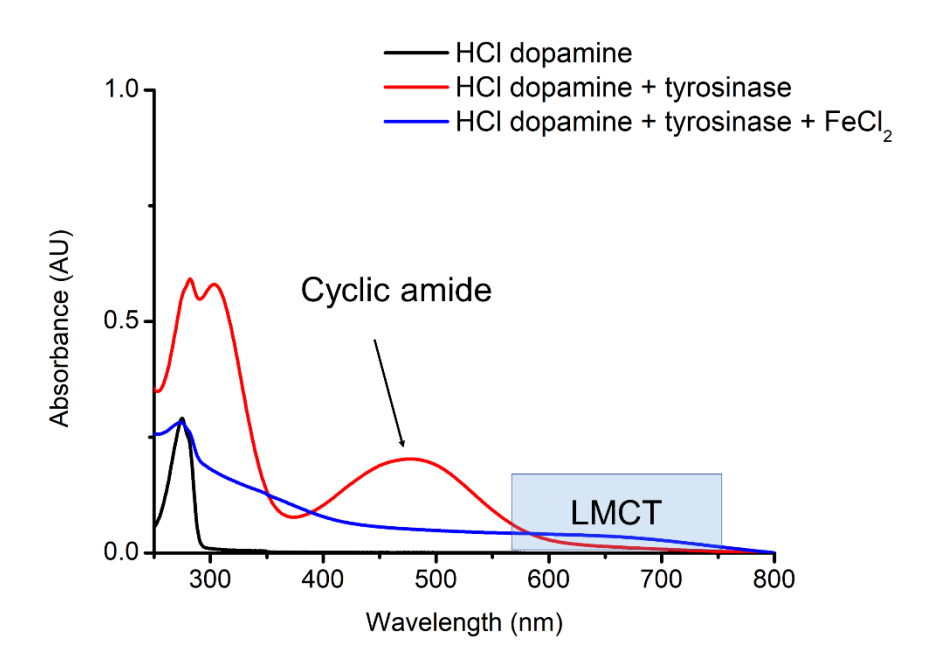


Figure 4.18. Photographs of dopamine hydrochloride in presence of tyrosinase and FeCl<sub>2</sub>.



**Figure 4.19.** UV-Vis absorbance spectra of dopamine hydrochloride in the presence of tyrosinase and FeCl<sub>2</sub>.

The solution turned to orange after 2 h in the presence of tyrosinase and to black after the addition of FeCl<sub>2</sub>. The UV-Vis spectra also confirmed the oxidation step and the coordination with Fe(III). All these preliminary tests seem to suggest that the presence of Fmoc protecting group prevents enzymatic or chemical cross-linking reactions.

#### 4.3.5 Photo cross-linking using phenylalanine and tyrosine derivatives

As another alternative to form covalent bonds into our supramolecular hydrogels, we studied the photo-cross-linking of phenylalanine and tyrosine derivatives, namely Fmoc-Phe(4-azido)-OH and Fmoc-Tyr(propargyl)-OH. UV light irradiation can induce the formation of reactive species of the aryl azide<sup>31</sup> that will react with C-H bonds, while it can initiate radical polymerization of alkynes.<sup>32</sup> Alternatively, a click chemistry reaction between the azide and alkyne groups could also be used to cross-link the amino acids through Cu(I) catalysis or heating. In order to study the interest of photo-cross-linkable groups, we have added 4-azido-Phe, Fmoc-4-azidophe and Fmoc-Tyr(propargyl)-OH derivatives to the screening. Binary mixtures with Fmoc-Tyr-OH, Fmoc-Phe-OH or Fmoc-Tyr(Bzl)-OH were made following strictly the same protocol as that used in chapter 2 Following this method four hydrogels could be obtained with at least one of the derivatives carrying a photo-cross-linkable group as shown in Table 4.1.

**Table 4.1.** Co-assembly of L-Tyr and L-Phe derivatives in 2% DMSO/ $H_2O$  (v/v). Pink color = Liquid; red color = Gel + gelation time in brackets.

	Fmoc- azidophe	4-azido- Phe	Fmoc- Tyr(propargyl)- OH	Fmoc- Tyr-OH	Fmoc- Phe-OH	Fmoc- Tyr(BzI)- OH
Fmoc- Azidophe				GEL (min)		GEL (hours)
4-azido-Phe				GEL (hours)		
Fmoc- Tyr(propargyl)- OH						GEL (days)
Fmoc-Tyr-OH						
Fmoc-Phe-OH						
Fmoc-Tyr(Bzl)- OH						

From these hydrogels, different tests of photo-crosslinking under UV irradiation have been performed. The preformed gels were irradiated under a UV lamp at 254 nm and characterized by HPLC to assess if new products formed or if one of the starting gel components was degraded. Tests were also carried out in the liquid phase before gelation by varying various parameters such as the type of solvent or the concentration of amino acids. The different tests performed are presented in Table 4.2. None of the studied conditions allowed the formation of new products formed by crosslinking of the amino acid derivatives. Different tests including 4-azido-Phe in aqueous medium showed the degradation of the amino acid derivatives under irradiation at 254 nm with the disappearance of their characteristic peak by HPLC. However, in the presence of DMSO the degradation of 4-azido-Phe did not occur. According to all these results, the cross-linking of tyrosine and phenylalanine derivatives, in particular protected by a Fmoc group, under our reaction conditions remains challenging. Therefore, we decided to test other approaches to improve the mechanical stability of our supramolecular gels.

**Table 4.2.** Presentation of the different tests of photo-cross-linking performed with 4-aAzido-Phe, Fmoc-L-azidophe and Fmoc-Tyr(propargyl)-OH.

Samples	Solvent	Liquid or Gel state	Degradation of amino acid derivatives	New products
4-Azido-Phe 2.45 mM + Fmoc-Tyr-OH 2.45 mM	H <sub>2</sub> O/2%DMSO	Gel	No	No
4-Azido-Phe 0.1 mg·mL <sup>-1</sup> + Fmoc-Tyr-OH 4.9 mM	H <sub>2</sub> O/2%DMSO	Gel	No	No
Fmoc-Tyr(propargyl)-OH 2.45 mM + Fmoc-Tyr(Bzl)-OH 2.45 mM	H <sub>2</sub> O/2%DMSO	Gel	No	No
Fmoc-4-azidophe 2.45 mM + Fmoc-Tyr-OH	H <sub>2</sub> O/2%DMSO	Gel	No	No
Fmoc-4-azidophe 2.45 mM + Fmoc-Tyr(Bzl)-OH	H <sub>2</sub> O/2%DMSO	Gel	No	No
4-Azido-Phe 0.01 mg·mL <sup>-1</sup> + Fmoc-Tyr-OH 4.9 mM	H <sub>2</sub> O/2%DMSO	Gel	No	No
4-Azido-Phe 0.5 mg·mL⁻¹ + Fmoc-Tyr-OH 2.45 mM	H <sub>2</sub> O/2%DMSO	Liquid	No	No
4-Azido-Phe 0.015 mg·mL <sup>-1</sup> + Fmoc-Tyr-OH 2.45 mM	H <sub>2</sub> O/2%DMSO	Liquid	No	No
4-Azido-Phe 2.45 mM	H <sub>2</sub> O/2%DMSO	Liquid	No	No
4-Azido-Phe 0.015 mg·mL <sup>-1</sup>	H <sub>2</sub> O	Liquid	Yes	No
Fmoc-Tyr-OH 0.05 mg·mL <sup>-1</sup>	H <sub>2</sub> O	Liquid	No	No
4-Azido-Phe 0.015 mg·mL <sup>-1</sup> + Fmoc-Tyr-OH 0.2 mg·mL <sup>-1</sup>	H <sub>2</sub> O	Liquid	Yes	No
4-Azido-Phe 0.015 mg·mL <sup>-1</sup> + Fmoc-Tyr-OH 0.1 mg·mL <sup>-1</sup>	H <sub>2</sub> O	Liquid	Yes	No
4-Azido-Phe 0.015 mg·mL <sup>-1</sup> + L-Tyr 0.1 mg·mL <sup>-1</sup>	H <sub>2</sub> O	Liquid	Yes	No
L-Tyr 0.1 mg⋅mL <sup>-1</sup>	H <sub>2</sub> O	Liquid	No	No

### 4.3.6 Synthesis of double network hydrogel based on amino acids and polyacrylamide

Rather than creating new covalent bonds inside the supramolecular structure, another approach to formulate tough hydrogels is to add a polymer into the first supramolecular network to form unique multi-component materials. We firstly tried simultaneous formation of DN hydrogels in which the precursors of the networks are mixed and synthesized simultaneously by independent noninterfering route using amino acids in DMSO for the first supramolecular network and acrylamide/bis-acrylamide monomer for the second chemical network. The chemically cross-linked polyacrylamide (PAA) network was obtained by free radical polymerization of acrylamide/bis-acrylamide in the presence tetramethylethylenediamine (TEMED) and ammonium persulfate (APS) 10 % (Figure 4.19). Polyacrylamide gels are formed by copolymerization of acrylamide monomers, CH<sub>2</sub>=CH-C(O)–NH<sub>2</sub>, and a cross-linking comonomer, N,N'-methylenebisacrylamide, CH<sub>2</sub>=CH–C(O)–NH– CH<sub>2</sub>-NH-C(O)-CH=CH<sub>2</sub> (also named bisacrylamide).<sup>33,34</sup> The mechanism of gel formation is a vinyl addition polymerization and is catalyzed by a free radical-generating system composed of APS as the initiator and an accelerator TEMED that induces the formation of free radicals from APS and catalyzes the polymerization. As the supramolecular amino acid hydrogel network is formed through the addition of water into the amino acids dissolved in DMSO, we first tried the DN gel formation by addition of fresh polyacrylamide aqueous solution at the desired concentration into the Fmoc-Tyr-OH/Fmoc-Tyr(Bzl)-OH (gel 1 of Chapter 2) or Fmoc-Phe-OH/Fmoc-Tyr(Bzl)-OH (gel 2 of Chapter 2) amino acids diluted in DMSO. However, when we directly added the polyacrylamide solution into the amino acids diluted in DMSO we observed a rapid precipitation. The presence of polyacrylamide, TEMED and persulfate solution was immediately disturbing the supramolecular network formation. To prevent this phenomenon, we used a two-step dilution method. A solution of 9.8 mM amino acids in 4 % DMSO/H<sub>2</sub>O was directly mixed to an equal volume of concentrated polyacrylamide solution to obtain the desired concentration of 4.9 mM amino acids in 2 % DMSO/polyacrylamide solution (Figure 4.20).

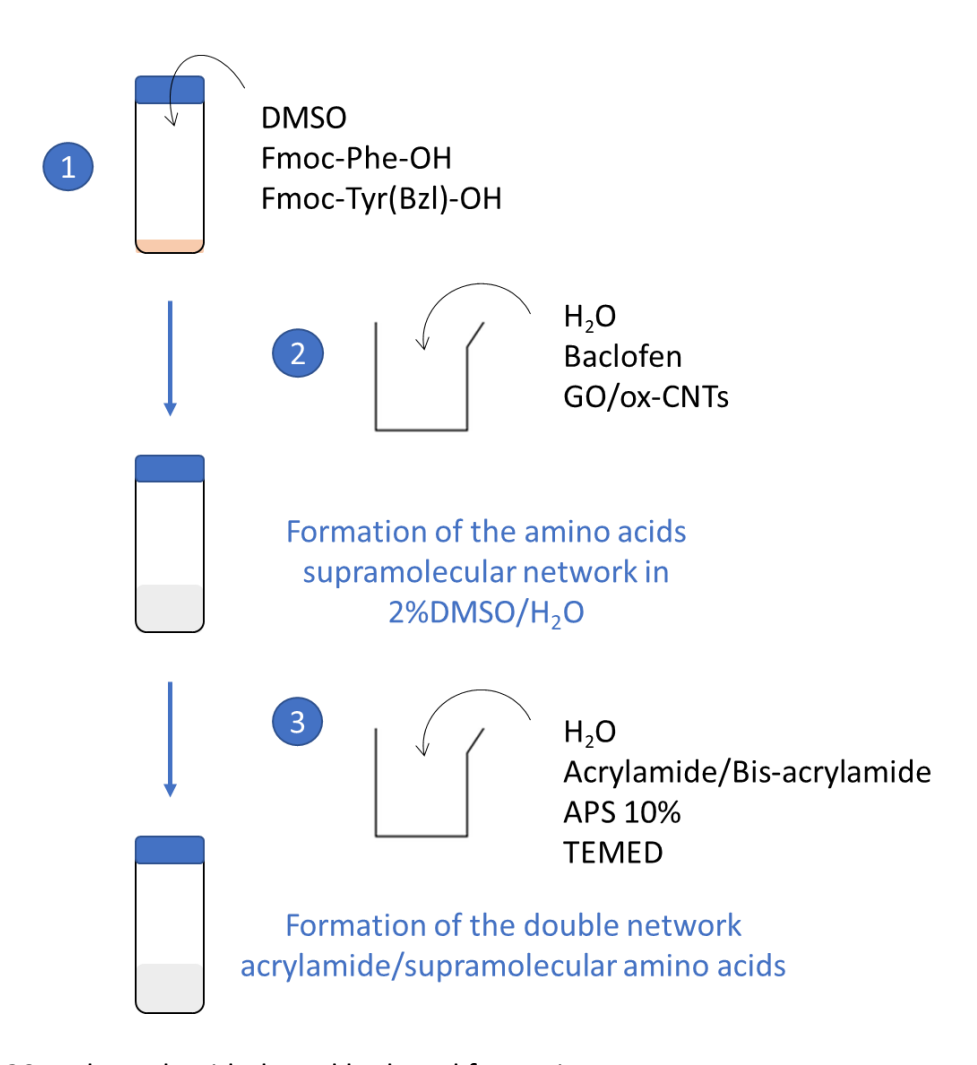
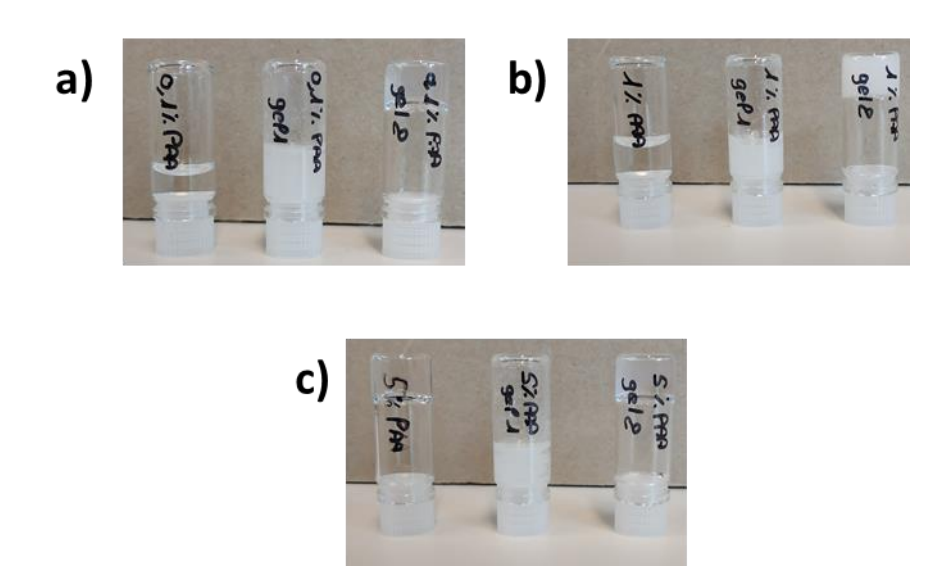


Figure 4.20. Polyacrylamide-based hydrogel formation.

Different final concentrations of polyacrylamide (PAA) were tested from 0.1 % to 10 % and the gelation of the samples was confirmed by the vial inversion test. For all the polyacrylamide concentration tested, the gel 1 was totally destructured with absence of gelation while the gel 2 formed stable hydrogels (Figure 4.21). Polyacrylamide gels are known to form quickly in less than 1 h for a concentration up to 4 %. We performed control experiments with only polyacrylamide at the concentration studied (Figure 4.21). At 0.1 % and 1 % polyacrylamide gels were not formed whereas with at 5 % and 10 % the polyacrylamide gels were well formed and stable to the inversion test. As the extent of swelling is inversely related to the extent of cross-linking, a concentration of 0.1 % or 1 % of acrylamide is too low to obtain a gel state in our conditions. The supramolecular gel 2 had a gelation time of approximatively 2 h but in presence of 1 % to 10 % acrylamide/bisacrylamide the gelation was longer (up to 24 h). Control samples with 5 % and 10 % single network without amino acids formed gels quickly in approximatively 30 min. In the PAA

gelation process, the kinetics is influenced by several factors such as the concentration of monomers, the amount of initiator or temperature. The presence of the supramolecular network affected the gelation kinetics of PAA by increasing the gelation time. As acrylamide is a neurotoxic substance, further tests should be carried out to confirm the absence of residual monomers after gelation.



**Figure 4.21.** Photographs of hydrogels developed with a) 0.1 % PAA, b) 1 % PAA and c) 5 % PAA. From left to right on each photograph: PAA gel, DN gel 1 + PAA and DN gel 2 + PAA.

#### 4.3.7 Synthesis of double network hydrogel based on amino acids and agarose

Another procedure to develop DN hydrogels consists in the incorporation of a pre-formed polymer, such as agarose, that does not require any polymerization step. Agarose gels are easily formed by a simple heating and cooling process. Agarose is a polysaccharide composed of D-galactose and 3,6-anhydro-L-galactopyranose forming a porous gel structure though non-covalent interactions like hydrogen bonds and electrostatic interactions in aqueous media. DN network hydrogels containing supramolecular amino acids and agarose networks were easily developed using the similar two-step dilution method. The gel was formed by mixing 1 mL of a hot agarose solution and a solution of Fmoc-Tyr-OH/Fmoc-Tyr(Bzl)-OH (gel 1) or Fmoc-Phe-OH/Fmoc-Tyr(Bzl)-OH (gel 2) at 9.8 mM in 1 mL 4 % DMSO/H<sub>2</sub>O and cooling them to room temperature. Different concentrations of agarose at 0.1 %, 0.5 % and 1 % were tested and all gels were stable to the inversion test (Figure 4.22). Whereas the supramolecular gel 1 and gel 2 developed in chapter 2 were formed in 2 h, DN hydrogels containing gel 1 or gel 2 with 0.1 % of agarose were formed more rapidly in 1 h.

The DN hydrogels obtained with a higher agarose concentration (0.5 % and 1 %) were formed in few seconds. Control samples with only agarose at the different concentrations formed gels with similar kinetics in the presence or in the absence of amino acid supramolecular network. These results indicated that the gelation time was driven by the agarose gelation process.

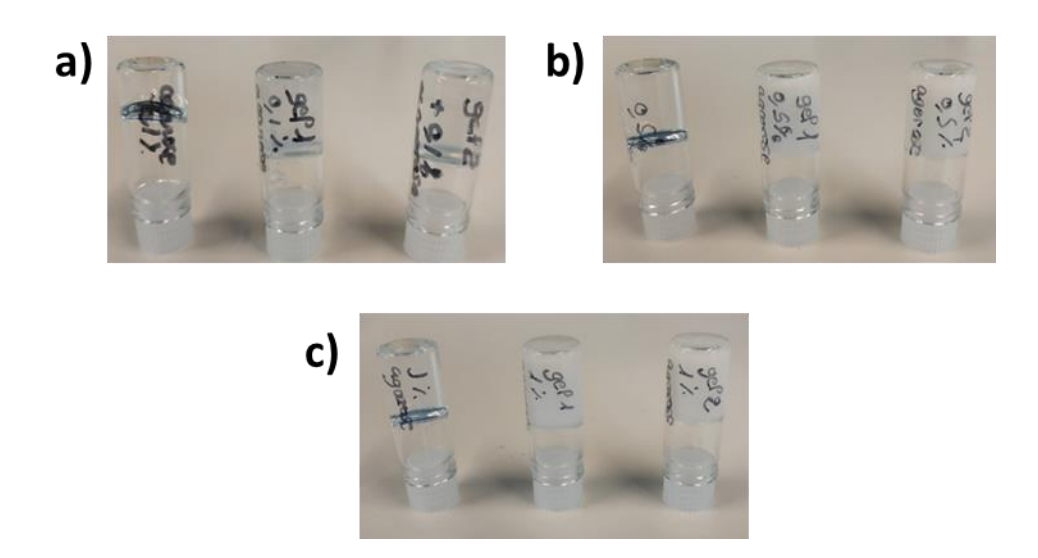


**Figure 4.22.** Photographs of hydrogels developed with a) 0.1 % agarose, b) 0.5 % agarose and c) 1 % agarose. From left to right on each photograph: agarose gel, DN gel 1 + agarose and DN gel 2 + agarose.

# 4.3.8 Formation of hybrid DN hydrogels containing carbon nanomaterials

To develop hybrid hydrogels with carbon nanomaterials we incorporated ox-CNTs and GO at the concentration of 0.025 wt% into the DN hydrogels. For the formation of both DN hydrogels with PAA or agarose, the amino acids were mixed in DMSO and diluted in water before the addition of the acrylamide/bis-acrylamide monomer or hot agarose solution (Figure 4.20). Carbon nanomaterials were dispersed in water by sonication before addition to the solution of amino acids (Fmoc-Tyr-OH/Fmoc-Tyr(Bzl)-OH for gel 1, Fmoc-Phe-OH/Fmoc-Tyr(Bzl)-OH for gel 2) in DMSO to initiate the formation of the supramolecular network. Fresh PAA or hot agarose solution were then mixed with the carbon nanomaterials and amino acids in DMSO to form the DN hybrid hydrogels. The gel 1 with PAA at the different concentrations studied were not stable in presence of carbon nanomaterials, similarly to the native gel without carbon nanomaterials. The gel 2 with PAA at the three concentrations were homogenous and stable in presence of both ox-CNTs or GO at the

concentration used. The photographs of the gel 1 (unstable) and gel 2 (stable) + PAA 1 % + carbon nanomaterials are shown in Figure 4.23. All the hybrid gels developed with agarose at the different concentrations studied were also homogenous and stable (Figure 4.24). The incorporation of carbon nanomaterials did not impact the stability or the gelation behavior of the different DN agarose hydrogels made.





**Figure 4.23.** Photographs of the DN gels PAA 1 % with a) gel 1 and b) gel 2. From left to right: no carbon nanomaterials, 0.025 wt% of ox-CNTs and 0.025 wt% of GO.





**Figure 4.24.** Photographs of the DN gels agarose 0.5 % and a) gel 1 and b) gel 2. From left to right: no carbon nanomaterials, 0.025 wt% of ox-CNTs and 0.025 wt% of GO.

# 4.3.9 Incorporation of the drug baclofen

In order to study the drug release properties of the newly developed double network hydrogels, we incorporated baclofen (Figure 4.25). This drug, also known as Lioresal®, is a muscle relaxant that acts on the spinal cord as a GABA-B receptor agonist.<sup>35,36</sup>

Figure 4.25. Chemical structure of baclofen.

It is prescribed for the muscular spasticity found in many neurological disorders such as strokes, head injuries, spinal cord injuries, multiple sclerosis and cerebral palsy with varying degrees. Symptoms of spasticity include muscle tightness, joint stiffness, involuntary movements, muscle spasms and pain in the affected muscles and joints. In a severe state, spasticity can also interfere with daily function and cause extreme discomfort or pain for patients with urinary tract infections, risk of developing pressure ulcers or bone fractures and luxation.<sup>37</sup> However, orally administered baclofen suffers from poor crossing of the blood-brain barrier and non-selective distribution in the central nervous system. Achieving an adequate therapeutic response therefore requires high doses of 30 to 80 mg per day with a risk of significant side effects. The only current alternative to reduce the doses is the administration of a programmable intrathecal pump positioned in the patient spinal cord (Figure 4.26).<sup>36-38</sup>

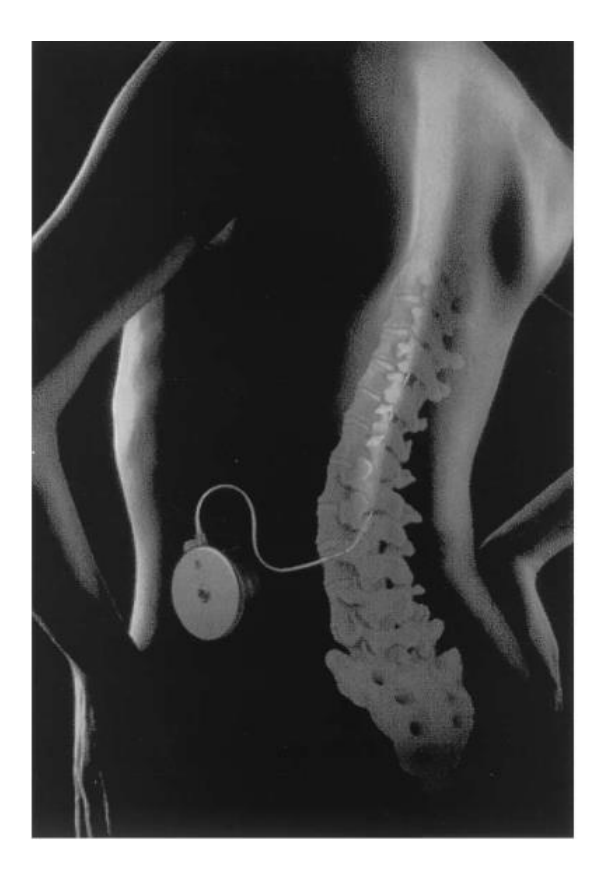


**Figure 4.26.** Scheme of baclofen pump implanted under the skin of the abdomen linked to the spinal cord with a catheter.<sup>39</sup>

The daily dose for an adult is then reduced to a concentration of 300  $\mu$ g to 800  $\mu$ g per day by continuous injection, but this mode of administration remains very invasive. Intrathecal

baclofen therapy can also present several complications such as catheter fracture, dislocation or occlusion, wound complications (*e.g.*, cerebrospinal fluid leak, fistula) or infections.<sup>39</sup> The development of injectable hydrogels for controlled release of baclofen appears to be a promising new therapeutic alternative. With this objective, baclofen was incorporated into the DN hydrogels developed at a concentration of 1.0 mg·mL<sup>-1</sup>. In both procedures, the drug was dissolved in water and mixed to the amino acids in DMSO before the addition of the second chemical network PAA or agarose (Figure 4.20). The incorporation of baclofen did not show any impact on the gelation kinetic or gel state.

With the development of these new DN hydrogels and the incorporation of carbon nanomaterials and baclofen, we then analyzed their photothermal profile and drug release properties.

#### 4.3.10 Photothermal profile of PAA/amino acid DN hydrogels

The photothermal response of PAA/gel 2 hydrogels were investigated using NIR irradiation at 808 nm under 2 W·cm<sup>-2</sup> for 10 min. For the three PAA concentrations the hybrid DN PAA/gel 2 hydrogels showed similar behavior to gel 2 + ox-CNTs and GO with shrinkage after NIR light irradiation (see part 2.3.10.2). The temperature increases were lower than the one observed for the supramolecular hydrogels alone (Figure 4.27). The highest increases of temperature were around 44.3 °C and 44.2 °C obtained for the hybrid gels in presence ox-CNTs with 1 % and 5 % of PAA, respectively. The lowest increase was obtained for the hybrid gels in presence of GO + 1 % PAA with an increase of 37.5 °C and GO + PAA 10 % with an increase of 38.6 °C, which is still largely sufficient. This can be due to the less well-dispersed GO in the gel matrix because of its shape compared to the ox-CNTs as previously observed for the supramolecular gel 1 and 2. The photothermal response of blank PAA hydrogels and PAA/supramolecular DN hydrogels without carbon nanomaterials were also monitored under similar conditions as controls showing a negligible temperature rise. The change in temperature with PAA at 1 %, 5 % or 10 % was very low with an increase of 5.7 °C, 2.6 °C and 3.7 °C, respectively. For the DN PAA/gel 2 without carbon nanomaterials, the temperature increase was slightly higher reaching 7.5 °C, 4.3 °C and 4.2 °C with 1 %, 5 % and 10 % PAA respectively. The blank samples stayed intact with no water release after irradiation.

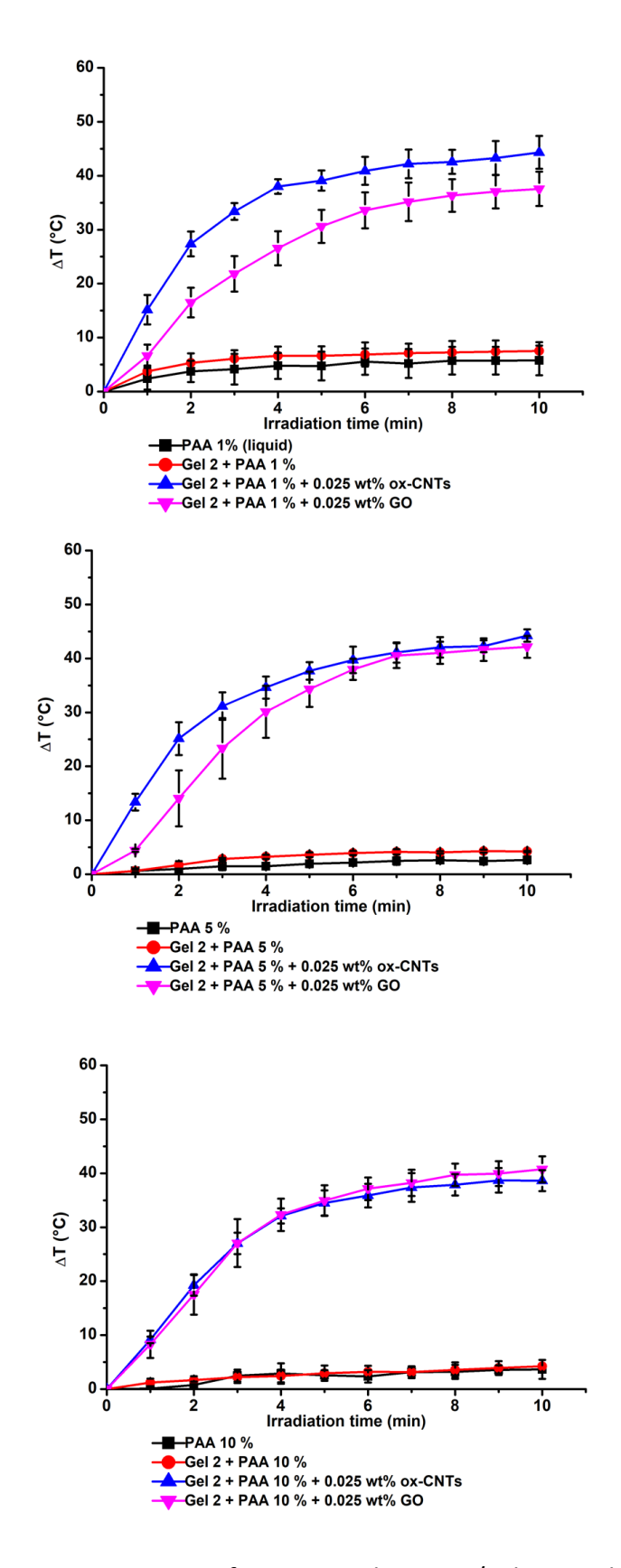


**Figure 4.27.** Temperature increase of PAA samples, PAA/gel 2 DN hydrogels and hybrid hydrogels with ox-CNTs and GO when exposed to a NIR laser (at 808 nm, under 2 W⋅cm<sup>-2</sup>) as a function of the laser irradiation time.

#### 4.3.11 Water and drug release from PAA/amino acid DN hydrogels

In the presence of carbon nanomaterials, we observed a high amount of water and drug released for the three concentrations (Figure 4.28). The highest release of water was obtained for the DN PAA 1 %/gel 2 network with 64 % and 62.6 % of water released in the presence of ox-CNTs and GO, respectively, probably due to the low cross-linking extent at this concentration of acrylamide/bis-acrylamide monomers.

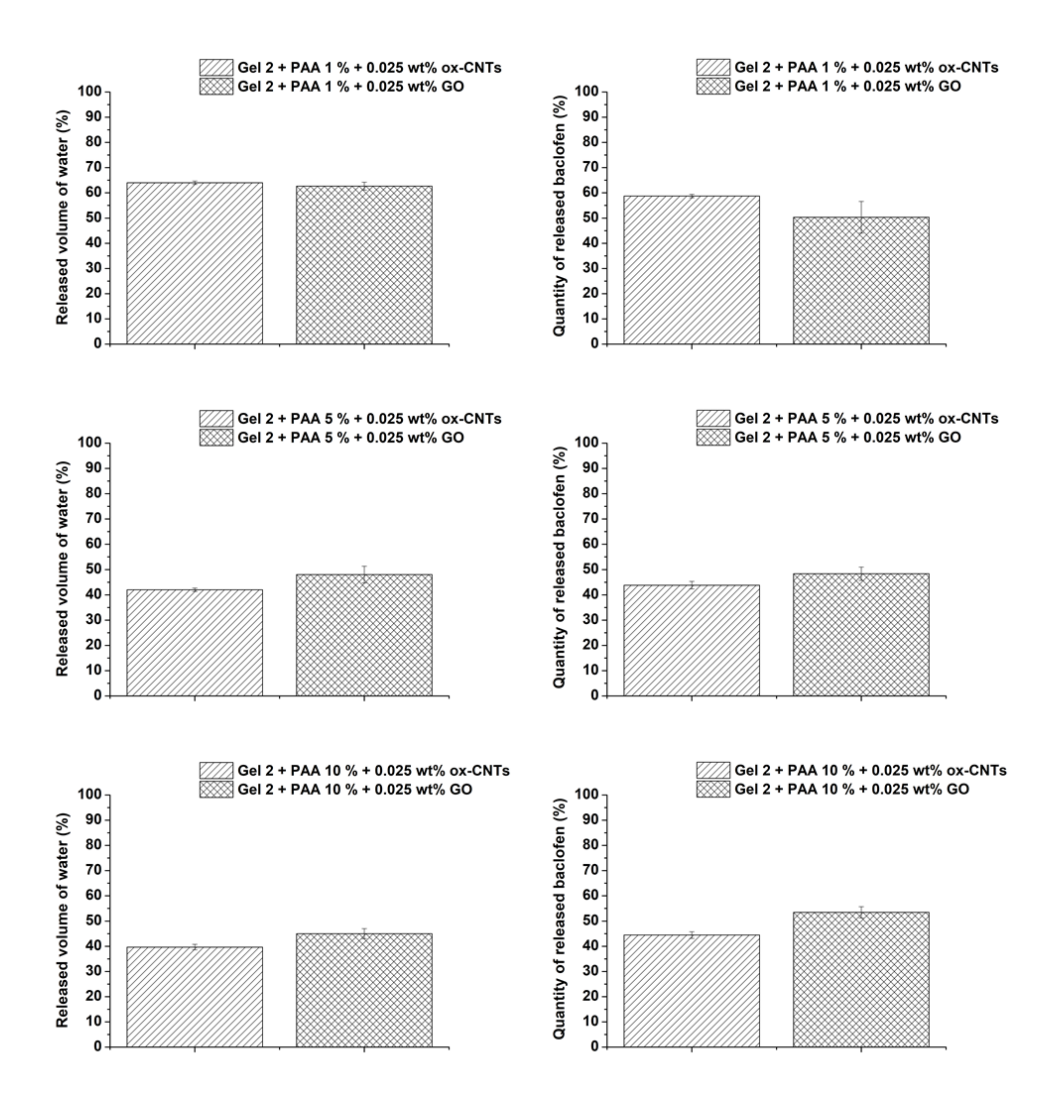


**Figure 4.28.** Release of water (left, n=3) and baclofen (right, n=3) from the hybrid DN gels containing PAA under NIR light irradiation.

The quantity of water released was reduced with the increase of PAA concentration: 42 % (ox-CNTs) and 48 % (GO) with PAA 5 %, 39.6 % (ox-CNTs) and 45% (GO) with PAA 10 %. The increase in the amount of polyacrylamide in the DN led to an increase in the gel stability during heating under NIR light irradiation reducing the amount of water released. The

amount of released baclofen was assessed by HPLC and calculated from the calibration curve of baclofen obtained with varying concentrations ( $0.2-1~{\rm mg\cdot mL^{-1}}$ ) at 220 nm. The drug release was estimated from the total drug loaded. Surprisingly, the quantity of drug released was similar for the three concentrations of PAA and the two different types of carbon nanomaterials added: 43.8 % obtained for DN PAA 5 %/gel 2 with ox-CNTs and 58.7 % obtained for DN PAA 1 %/gel 2 with ox-CNTs. The quantity of baclofen released from 1 mL samples hydrogels is in the range of the daily dose needed for an adult (300-800 µg per day) by pump injection. By varying the quantity of polyacrylamide in the double network, it is therefore possible to modify the stability of the gel while maintaining adequate release properties.

#### 4.3.12 Photothermal profile of agarose/amino acid DN hydrogels

The photothermal properties of the agarose gels and agarose/supramolecular DN hydrogels in presence and in absence of carbon nanomaterials were investigated under NIR irradiation following the same procedure (Figure 4.29). The highest increases of temperature were obtained for the three concentrations with the DN agarose/gel 2 in presence of GO: 46.6 °C, 49.4 °C, and 47.5 °C with 0.1 %, 0.25 % and 0.5 % of agarose, respectively. In presence of 0.5 % agarose, the lowest temperature increase was measured for the DN agarose 0.5 %/gel 1 + GO (33.6 °C). With a lower concentration of agarose (0.1 % and 0.25 %), the lowest temperature increases were measured for the gels without supramolecular network containing GO (39.3 °C for 0.1 % and 38 °C for 0.25 %). Similarly to the results obtained in presence of PAA, the lowest increase of temperature obtained in presence of GO can be due to its limited dispersibility in the gel matrix compared to ox-CNTs. In absence of carbon nanomaterials, the photothermal behavior of the blank agarose gels and DN was very low (< 10 °C) after 10 min irradiation, as expected. However, the blank DN hydrogels showed a lower increase (3.9 °C for gel 2 + agarose 0.25 % and 6.6 °C for gel 1 + agarose 0.5 %) than the pure agarose gels with an increase of 7 °C (0.1 %), 7.2 °C (0.25 %) and 8.4 °C (0.5 %). Here also, the DN slightly reduced the temperature increase, but the temperatures reached are still sufficient for our application. Here also, the gels in absence of carbon nanomaterials stayed totally intact after 10 min NIR irradiation with the absence of water release.

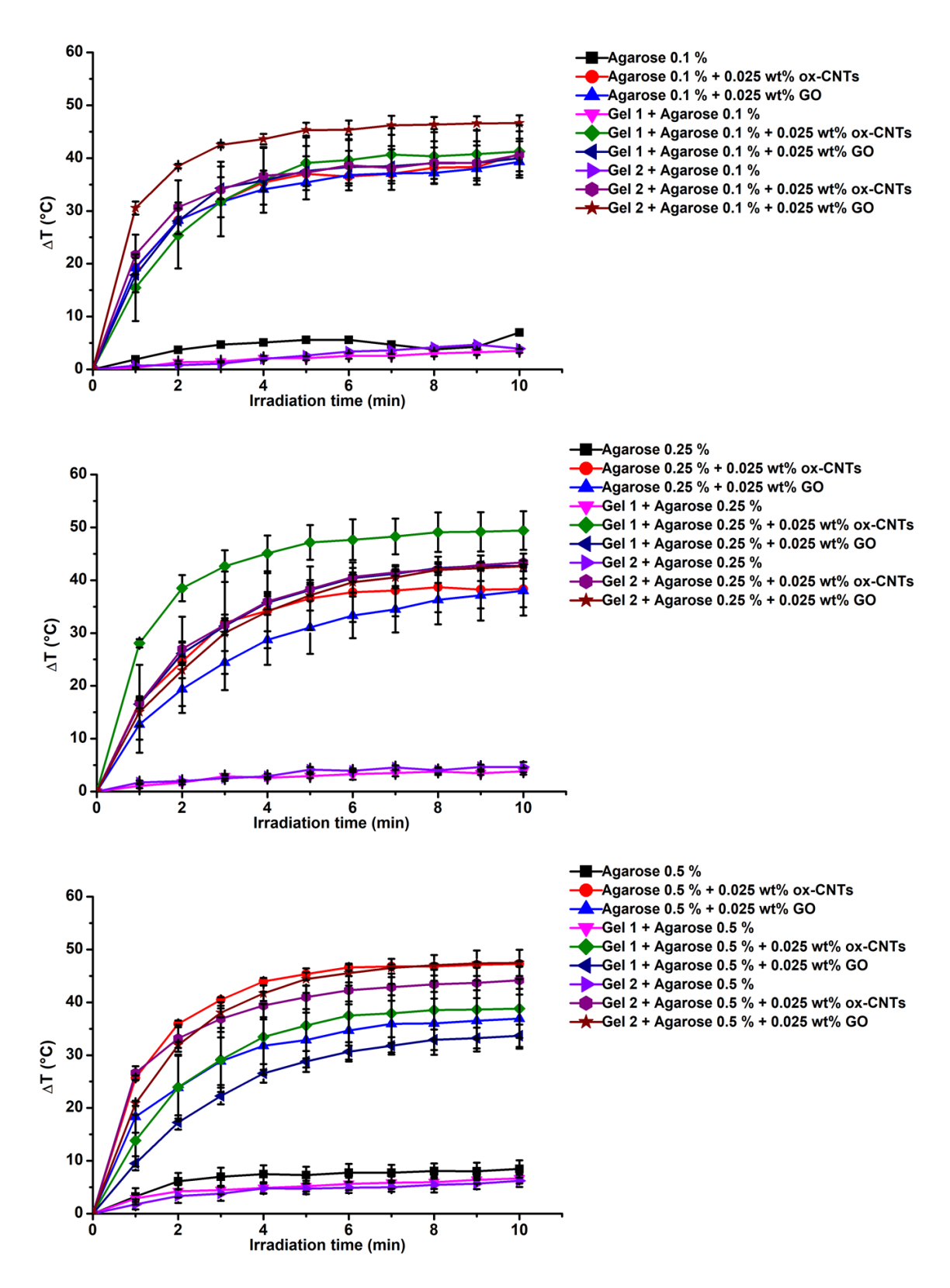


**Figure 4.29.** Temperature increase of agarose hydrogels (n=3), agarose/gel 2 DN hydrogels (n=3) and hybrid hydrogels with ox-CNTs and GO (n=3) when exposed to a NIR laser (at 808 nm, under 2 W·cm<sup>-2</sup>) as a function of the laser irradiation time.

#### 4.3.13 Water and drug release of agarose/amino acid DN hydrogels

Upon NIR irradiation the DN agarose/supramolecular hybrid gel containing carbon nanomaterials showed a destructuration of the gel matrix. The quantity of water and drug released decreased with an increase of the agarose percentage (Figure 4.30). With 0.1 % of agarose we measured a released water amount from 48 % (agarose/gel 2 + ox-CNTs) to 75 % (agarose/gel 1 + ox-CNTs). In contrast, the maximum amount of water released was 35 % with 0.25 % of agarose (agarose 0.25 %/gel 1 + ox-CNTs) and 6.7 % with 0.5 % of agarose (agarose/gel 1 + ox-CNTs). The amount of baclofen released assessed by HPLC was proportional to the water released quantity for the three agarose concentrations. We measured the highest drug released amount with DN agarose 0.1 %/gel 1 hybrid hydrogels with 73.5 % with ox-CNTs and 57.4 % with GO. The DN agarose 0.1 %/gel 2 hybrid hydrogels also presented a high amount of baclofen released with 52.9 % with GO and 48.1 % with ox-CNTs. By increasing the agarose concentration to 0.25 %, the release was reduced to values between 10.6 % (agarose 0.25 %/gel 2 + ox-CNTs) to 35 % (for agarose 0.25 %/gel 1 + GO). With the highest agarose concentration of 0.5 %, the quantity of baclofen released was less than 6.6 % (agarose 0.5 %/gel 1 + ox-CNTs). Control experiments were performed on the agarose gels with carbon nanomaterials but without the amino acid supramolecular network. With 0.1 % agarose the gels in presence of ox-CNTs and GO became totally liquid after the irradiation but formed again a gel upon cooling. With 0.25 % and 0.5 % of agarose the gels lost a low amount of water during the irradiation (less than 10 %) but they totally reformed a gel after cooling.

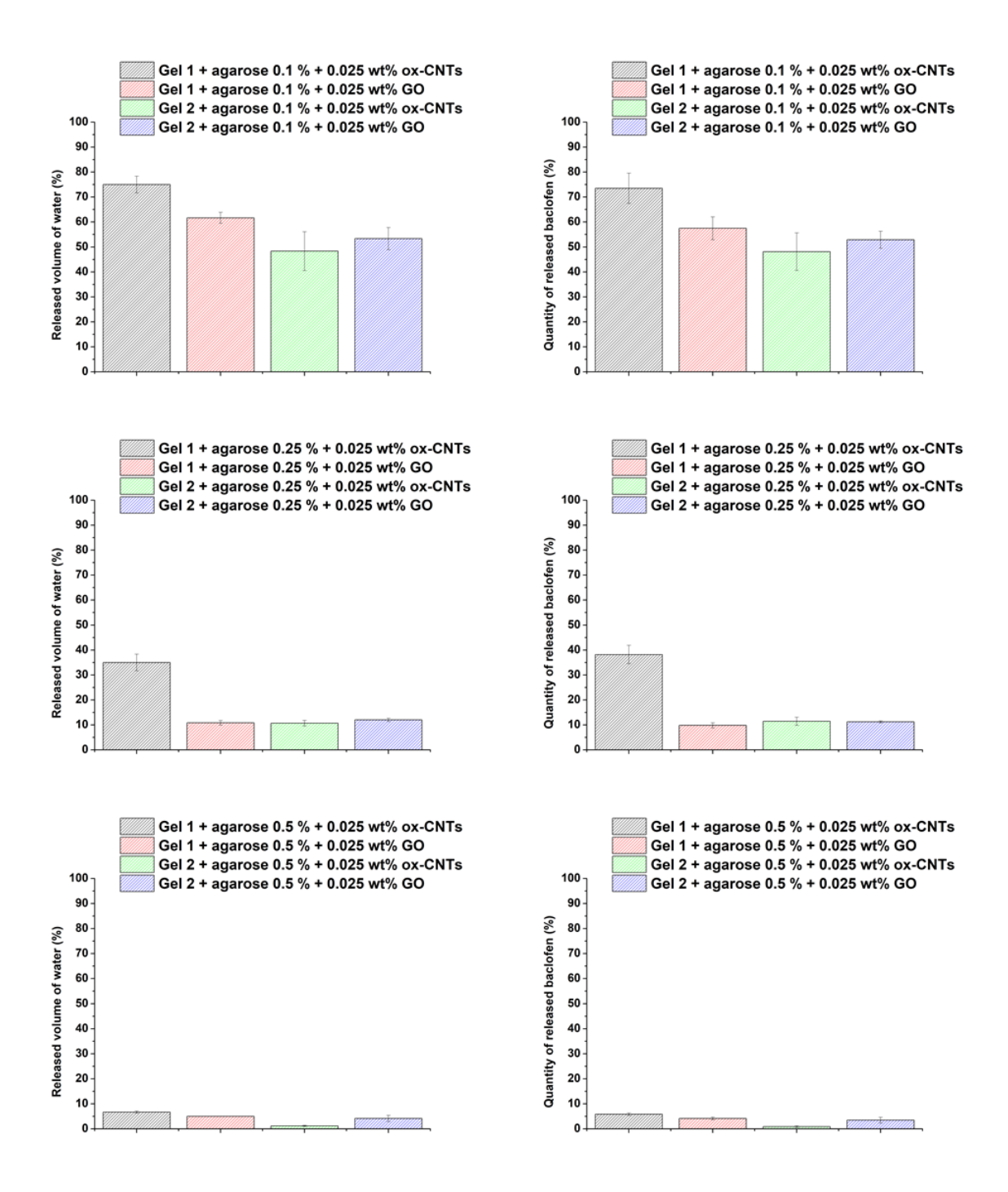


**Figure 4.30.** Release of water (left, n=3) and b) baclofen (right, n=3) from the hybrid DN gels containing agarose under NIR light irradiation.

The amount of drug released from the DN hydrogels was influenced by the quantity of agarose or PAA, the nature of the amino acids and the type of carbon nanomaterials present into the hydrogels. Among all the different PAA concentrations studied, we observed a high amount of drug released from approximatively 40 % to 60 %. In contrast, by slightly modulating the agarose concentration (from 0.1 % to 0.5 %) we were able to control the

drug release from less than 10 % to more than 50 %. In both cases, the concentration of baclofen released would be sufficient regarding the quantity needed per day. These observations make it possible to envisage the use of these gels, in particular double network agarose-based gels, as drug delivery devices that can be better adapted to specific patient dosage. With this purpose, the double network hydrogels containing baclofen will probably be tested into spasticity murine model in collaboration with the group of the Professor Luc Dupuis in Strasbourg (INSERM U 1118). In order to characterize the mechanical properties of the DN hydrogels, rheological studies were performed in collaboration with Dr. Maria Elena Valle Medina from iCube (Strasbourg) but the apparatus was not appropriate for the study of our gels.

#### 4.4 Conclusion

In this work, a series of cross-linking protocols were tested on different tyrosine derivatives in order to apply the procedure to the cross-linking of gel 1 and gel 2. HRP was used as an enzyme catalyst to induce the polymerization of tyrosine derivatives in water. Fe(III) and Cu(II) were used to form complexes through metal-ligand coordination. Oxidative crosslinking procedure were also tried with Fremy's salt and tyrosinase. The reactions were followed by UV-Vis spectroscopy, fluorescence spectroscopy and HPLC. All these tests suggested that the presence of a protecting group such as the Fmoc moiety prevents enzymatic or chemical cross-linking reactions. However, additional analyses should be performed to characterize some by-products formed in some conditions. Additionally, understanding the influence of various parameters such as concentration, temperature, reaction time, on the reactions may be helpful. The photo-cross-linking of phenylalanine and tyrosine derivatives was also studied. Different tests including 4-azido-phenylalanine carried out in water showed the degradation of this derivative under irradiation at 254 nm but none of the conditions studied revealed the appearance of new cross-linking products. Several other methods could be tried as the use of other enzymes like laccase or papain, or HRP mimetics like hematin or Fe-salen. Incorporating Fmoc-Phe-(NH<sub>2</sub>)-OH as hydrogelators would allowusing genipin or glutaraldehyde as cross-linking reagent as they are highly reactive with amine groups. As already demonstrated in literature, ruthenium catalyst, or riboflavin as a more biocompatible alternative, could also be tested for the photo-cross-linking of tyrosine derivatives through the generation of highly reactive radicals.

Alternatively, we designed two novel polymer/supramolecular double network hydrogels with polyacrylamide or agarose. Oxidized carbon nanomaterials were added to the DN hydrogels to study the drug release properties under NIR irradiation with the aim of developing new advanced controlled drug delivery systems. The formation of a polymer network in the supramolecular systems increased the mechanical properties by reducing the amount of water released under NIR light irradiation while allowing effective drug release. The quantity of drugs released were modulated according to the amount of polymer added to the system. The polyacrylamide DN hydrogels with a concentration of 5 % and 10 % displayed good stability and a baclofen release rate corresponding to current daily needed dose. For agarose DN hydrogels, the lowest agarose concentrations of 0.1 % and 0.25 % showed very good stability and drug release under irradiation. A higher concentration of 0.5 % gave too robust hydrogels and drastically reduced the amount of drug released. We anticipate that these new classes of DN hydrogels can find applications in the development of new treatment for spasticity to complement or replace current treatment methods.

Additional analysis by UV-Vis and thermogravimetric analysis could be performed on the DN hydrogels developed to further characterize the polymer formation and stability. Complementary tests followed by HPLC and LC-MS should be done to confirm the absence of residual neurotoxic acrylamide monomers into the gel matrix. The mechanical properties should also be studied by rheology. We will study the morphology of the DN hydrogels by electron microscopy and perform circular dichroism to determine if the presence of polyacrylamide or agarose has an influence on the amino acid self-assembly. Finally, we will also analyze the stability of the gels under physiological conditions.

#### 4.5 References

- 1. Partlow, B. P.; Applegate, M. B.; Omenetto, F. G.; Kaplan, D. L. Dityrosine Cross-Linking in Designing Biomaterials. ACS Biomater. Sci. Eng. 2016, 2 (12), 2108–2121.
- 2. Roberts, J. J.; Naudiyal, P.; Lim, K. S.; Poole-Warren, L. A.; Martens, P. J. A Comparative Study of Enzyme Initiators for Crosslinking Phenol-Functionalized Hydrogels for Cell Encapsulation. Biomater. Res. 2016, 20 (1), 30.
- 3. Ding, Y.; Li, Y.; Qin, M.; Cao, Y.; Wang, W. Photo-Cross-Linking Approach to Engineering Small Tyrosine-Containing Peptide Hydrogels with Enhanced Mechanical Stability. Langmuir 2013, 29 (43), 13299–13306.

- 4. Rosu, C.; Cueto, R.; Russo, P. S. Poly(Colloid)s: "Polymerization" of Poly(I-Tyrosine)-Silica Composite Particles through the Photoinduced Cross-Linking of Unmodified Proteins Method. Langmuir 2016, 32 (33), 8392–8402.
- 5. Brassinne, J.; Fustin, C.-A.; Gohy, J.-F. Polymer Gels Constructed Through Metal–Ligand Coordination. J. Inorg. Organomet. Polym. Mater. 2013, 23, 24.
- 6. Atwood, C. S.; Perry, G.; Zeng, H.; Kato, Y.; Jones, W. D.; Ling, K.-Q.; Huang, X.; Moir, R. D.; Wang, D.; Sayre, L. M.; Smith, M. A.; Chen, S. G.; Bush, A. I. Copper Mediates Dityrosine Cross-Linking of Alzheimer's Amyloid-β. Biochemistry 2004, 43 (2), 560–568.
- 7. Choi, J.; McGill, M.; Raia, N. R.; Hasturk, O.; Kaplan, D. L. Silk Hydrogels Crosslinked by the Fenton Reaction. Adv. Healthcare Mater. 2019, 8 (17), 1900644.
- 8. Fuchs, S.; Shariati, K.; Ma, M. Specialty Tough Hydrogels and Their Biomedical Applications. Adv. Healthcare Mater. 2020, 9 (2), 1901396.
- 9. Hao, J.; Gao, Y.; Liu, J.; Hu, J.; Ju, Y. Tough, Stretchable, Compressive Double Network Hydrogel Using Natural Glycyrrhizic Acid Tailored Low-Molecular-Weight Gelator Strategy: In Situ Spontaneous Formation of Au Nanoparticles To Generate a Continuous Flow Reactor. ACS Appl. Mater. Interfaces 2020, 12 (4), 4927–4933.
- 10. Sun, W.; Xue, B.; Li, Y.; Qin, M.; Wu, J.; Lu, K.; Wu, J.; Cao, Y.; Jiang, Q.; Wang, W. Polymer-Supramolecular Polymer Double-Network Hydrogel. Adv. Healthcare Mater. 2016, 26 (48), 9044–9052.
- 11. Gong, J. P.; Katsuyama, Y.; Kurokawa, T.; Osada, Y. Double-Network Hydrogels with Extremely High Mechanical Strength. Adv. Mater. 2003, 15 (14), 1155–1158.
- 12. Nakajima, T.; Sato, H.; Zhao, Y.; Kawahara, S.; Kurokawa, T.; Sugahara, K.; Gong, J. P. A Universal Molecular Stent Method to Toughen Any Hydrogels Based on Double Network Concept. Adv. Funct. Mater. 2012, 22 (21), 4426–4432.
- 13. Chen, Q.; Zhu, L.; Zhao, C.; Wang, Q.; Zheng, J. A Robust, One-Pot Synthesis of Highly Mechanical and Recoverable Double Network Hydrogels Using Thermoreversible Sol-Gel Polysaccharide. Adv. Mater. Weinheim 2013, 25 (30), 4171–4176.
- 14. Bakarich, S. E.; Balding, P.; Iii, R. G.; Spinks, G. M.; Panhuis, M. in het. Printed Ionic-Covalent Entanglement Hydrogels from Carrageenan and an Epoxy Amine. RSC Adv. 2014, 4 (72), 38088–38092.
- 15. Zhao, Y.; Nakajima, T.; Yang, J. J.; Kurokawa, T.; Liu, J.; Lu, J.; Mizumoto, S.; Sugahara, K.; Kitamura, N.; Yasuda, K.; Daniels, A. U. D.; Gong, J. P. Proteoglycans and Glycosaminoglycans Improve Toughness of Biocompatible Double Network Hydrogels. Adv. Mater. 2014, 26 (3), 436–442.
- 16. Chang, A.; Babhadiashar, N.; Barrett-Catton, E.; Asuri, P. Role of Nanoparticle—Polymer Interactions on the Development of Double-Network Hydrogel Nanocomposites with High Mechanical Strength. Polymers 2020, 12 (2), 470.
- 17. Wang, Q.; Hou, R.; Cheng, Y.; Fu, J. Super-Tough Double-Network Hydrogels Reinforced by Covalently Compositing with Silica-Nanoparticles. Soft Matter 2012, 8 (22), 6048–6056.
- 18. Yang, W.; Furukawa, H.; Gong, J. P. Highly Extensible Double-Network Gels with Self-Assembling Anisotropic Structure. Adv. Mater. 2008, 20 (23), 4499–4503.
- 19. Liang, S.; Yu, Q. M.; Yin, H.; Wu, Z. L.; Kurokawa, T.; Gong, J. P. Ultrathin Tough Double Network Hydrogels Showing Adjustable Muscle-like Isometric Force Generation Triggered by Solvent. Chem. Commun. 2009, 48, 7518–7520.

- 20. Michon, T.; Chenu, M.; Kellershon, N.; Desmadril, M.; Guéguen, J. Horseradish Peroxidase Oxidation of Tyrosine-Containing Peptides and Their Subsequent Polymerization: A Kinetic Study. Biochemistry 1997, 36 (28), 8504–8513.
- 21. Sarma, R.; Alva, K. S.; Marx, K. A.; Tripathy, S. K.; Akkara, J. A.; Kaplan, D. L. Enzymatic Polymerization of Amphiphilic Alkyl Tyrosine Derivatives from Emulsions. Materials Science and Engineering: C 1996, 4 (3), 189–192.
- 22. Al-Hilaly, Y. K.; Biasetti, L.; Blakeman, B. J. F.; Pollack, S. J.; Zibaee, S.; Abdul-Sada, A.; Thorpe, J. R.; Xue, W.-F.; Serpell, L. C. The Involvement of Dityrosine Crosslinking in α-Synuclein Assembly and Deposition in Lewy Bodies in Parkinson's Disease. Sci. Rep. 2016, 6 (1), 39171.
- 23. Fukuoka, T.; Tachibana, Y.; Tonami, H.; Uyama, H.; Kobayashi, S. Enzymatic Polymerization of Tyrosine Derivatives. Peroxidase- and Protease-Catalyzed Synthesis of Poly(Tyrosine)s with Different Structures. Biomacromolecules 2002, 3 (4), 768–774.
- 24. Akkara, J. A.; Wang, J.; Yang, D.-P.; Gonsalves, K. E. Hematin-Catalyzed Polymerization of Phenol Compounds. Macromolecules 2000, 33 (7), 2377–2382.
- 25. Ke, Z.; Huang, Q. Effect of Protein Structure and/or Conformation on the Dityrosine Cross-Linking Induced by Haem-Hydrogen Peroxide. Biochim. Biophys. Acta (BBA) General Subjects 2016, 1860 (10), 2232–2238.
- 26. Fukuoka, T.; Uyama, H.; Kobayashi, S. Synthesis of Ultrahigh Molecular Weight Polyphenols by Oxidative Coupling. Macromolecules 2003, 36 (22), 8213–8215.
- 27. Qu, N.; Guo, L.-H.; Zhu, B.-Z. An Electrochemical Biosensor for the Detection of Tyrosine Oxidation Induced by Fenton Reaction. Biosens. Bioelectron. 2011, 26 (5), 2292–2296.
- 28. Pignatello, J. J. Dark and Photoassisted Iron(3+)-Catalyzed Degradation of Chlorophenoxy Herbicides by Hydrogen Peroxide. Environ. Sci. Technol. 1992, 26 (5), 944–951.
- 29. Wilchek, M.; Miron, T. Mussel-Inspired New Approach for Polymerization and Cross-Linking of Peptides and Proteins Containing Tyrosines by Fremy's Salt Oxidation. Bioconjugate Chem. 2015, 26 (3), 502–510.
- 30. Zhong, Q.-Z.; Richardson, J. J.; Li, S.; Zhang, W.; Ju, Y.; Li, J.; Pan, S.; Chen, J.; Caruso, F. Expanding the Toolbox of Metal—Phenolic Networks via Enzyme-Mediated Assembly. Angew. Chem., Int. Ed. 2020, 59 (4), 1711–1717.
- 31. Gritsan, N. P.; Platz, M. S. Kinetics, Spectroscopy, and Computational Chemistry of Arylnitrenes. Chem. Rev. 2006, 106 (9), 3844–3867.
- 32. Kovar, R. F.; Ehlers, G. F. L.; Arnold, F. E. Thermosetting Acetylene-Terminated Polyphenylquinoxalines. J. Polym. Sci., Polym. Chem. 1977, 15 (5), 1081–1095.
- 33. Weiss, N.; Vliet, T. van; Silberberg, A. Influence of Polymerization Initiation Rate on Permeability of Aqueous Polyacrylamide Gels. J. Polym. Sci., Polym. Phys. 1981, 19 (10), 1505–1512.
- 34. Sabbagh, F.; Muhamad, I. I. Acrylamide-Based Hydrogel Drug Delivery Systems: Release of Acyclovir from MgO Nanocomposite Hydrogel. J. Taiwan Inst. Chem. Eng. 2017, 72, 182–193.
- 35. Pucks-Faes, E.; Dobesberger, J.; Hitzenberger, G.; Matzak, H.; Mayr, A.; Fava, E.; Genelin, E.; Saltuari, L. Intrathecal Baclofen in Hereditary Spastic Paraparesis. Front. Neurol. 2019, 10.
- 36. Sammaraiee, Y.; Yardley, M.; Keenan, L.; Buchanan, K.; Stevenson, V.; Farrell, R. Intrathecal Baclofen for Multiple Sclerosis Related Spasticity: A Twenty-Year Experience. Mult. Scler. Relat. Disord. 2019, 27, 95–100.

- 37. Adams, M. M.; Ginis, K. A. M.; Hicks, A. L. The Spinal Cord Injury Spasticity Evaluation Tool: Development and Evaluation. Arch Phys Med Rehabil 2007, 88 (9), 1185–1192.
- 38. Kao, L. W.; Amin, Y.; Kirk, M. A.; Turner, M. S. Intrathecal Baclofen Withdrawal Mimicking Sepsis. J. Emerg. Med. 2003, 24 (4), 423–427.
- 39. Vender, J. R.; Hester, S.; Waller, J. L.; Rekito, A.; Lee, M. R. Identification and Management of Intrathecal Baclofen Pump Complications: A Comparison of Pediatric and Adult Patients. J. Neurosurg. Pediatrics 2006, 104 (1), 9–15.

#### **CHAPTER 5. CONCLUSION AND PERSPECTIVES**

#### 5.1 Conclusion

In this work, the development of new types of hybrid hydrogels made of aromatic amino acids and di-peptides in combination with carbon nanomaterials have been performed to develop new drug delivery systems.

Two stable gels made of a binary mixture of Fmoc-Y-OH/Fmoc-Y(Bzl)-OH and Fmoc-F-OH/Fmoc-Y(Bzl)-OH were investigated in detail. By circular dichroism and molecular dynamics simulations we highlighted the key role of  $\pi$ - $\pi$  interactions between aromatic groups that drive the self-assembly process leading to hydrogel formation. Oxidized CNTs and GO were incorporated in these hydrogels to induce drug release using NIR light irradiation. The physical and structural properties of the gels were studied by different microscopic techniques and by rheology. During hydrogelation, the amino acids organized into fibrils and we observed a homogenous dispersion of oxidized carbon nanomaterials into the hydrogel matrix. Oxidized carbon nanotubes (ox-CNTs) and graphene oxide (GO) showed good interfacing with the fibrils. The ox-CNTs had an impact on the hydrogelation kinetics by accelerating the gelation. The temperature of the hydrogels was increased by the heat generated by the carbon nanomaterials upon NIR light irradiation. The type of selected drug model appeared to be an important parameter for the drug loading and release properties. Indeed, aromatic molecules remained trapped in the gel structures limiting the drug release over time. On the contrary, L-ascorbic acid was loaded in a high quantity and was released very efficiently after only 10 min of NIR light irradiation thanks to the temperature increase induced by the carbon nanomaterials leading to gel destabilization.

We also investigated the self-assembly in water and the formation of hydrogels using dipeptides, in particular Boc-diphenylalanine and Boc-dityrosine and their  $\beta$  and  $\gamma$  homologues. Several hydrogelation protocols were studied by modifying different parameters such as temperature, pH or concentration. Transmission electron microscopy showed that the three Boc-dityrosine peptides formed aggregates in water. They were not able to form hydrogels in all the conditions tested. In contrast, Boc-diphenylalanine peptides self-organized in nanospheres (Boc- $\alpha$ -Phe- $\alpha$ -Phe-OH) or nanofibers (Boc- $\beta$ -Phe- $\beta$ -Phe-OH and Boc- $\gamma$ -Phe- $\gamma$ -Phe-OH) in water and the three homologues formed hydrogels using a pH-

switch protocol. The hydrogels were characterized by electron microscopy and circular dichroïsm spectroscopy. Fibrillar structures were observed in the gel state for the three Bocdiphenylalanine peptides. Carbon nanomaterials (ox-CNTs or GO) and L-ascorbic acid were incorporated into the hydrogels. Boc-γ-Phe-γ-Phe-OH containing carbon nanotubes was destabilized when incorporating the drug, whereas the other gels were stable in presence of the carbon nanomaterials and the drug. L-ascorbic acid was released at high concentration due to the destabilization of the gel structure caused by the photothermal effect of the carbon nanomaterials. We performed preliminary toxicity tests on human skin in view of topical applications showing no apparent negative effects on the epidermis with no difference between the epidermis of the skin in absence of the dipeptide hydrogels and the epidermis of the skin in presence of the gels.

To design more robust hydrogels from supramolecular gel 1 and gel 2, we tried to create covalent bonds within tyrosine derivatives to form dityrosine and potentially poly-tyrosine products. The different procedures tried on tyrosine derivatives suggested that the presence of a protective group such as the Fmoc moiety prevents enzymatic or chemical cross-linking reactions. As alternative, new supramolecular hydrogels were explored containing photocross-linkable phenylalanine or tyrosine derivatives. Different protocols of UV irradiation were performed in the gel states and in solution, but none of the conditions studied revealed the appearance of new products obtained by photo-cross-linking. As the crosslinking strategy appeared more challenging than expected, we decided to test the incorporation of a polymer into our supramolecular systems. Novel double network (DN) hydrogels were successfully designed by incorporating polyacrylamide or agarose at different concentrations into the supramolecular gels Fmoc-Y-OH/Fmoc-Y(Bzl)-OH (gel 1) and Fmoc-F-OH/Fmoc-(Bzl)-OH (gel 2). Carbon nanomaterials and baclofen, a drug used in the treatment of spasticity in the case of multiple sclerosis for instance, were loaded into the gels. In comparison to the supramolecular gels 1 and 2, DN hydrogels showed improved mechanical properties. Due to the presence of polyacrylamide or agarose, the amount of water released was reduced under NIR light irradiation while allowing effective drug release. The quantity of released drug was modulated by the amount of polymer added to the system. These new classes of DN hydrogels could find applications in the development of new treatment for spasticity to complement or replace current treatment methods.

#### **5.2** Perspectives

After the promising results obtained with the development of diphenylalanine hydrogels, some computational studies could be performed to give additional information about the self-assembly behavior such as the number and the nature of the interactions involved in the fibrillar formation with the Boc-diphenylalanine homologues.

Regarding the cross-linking of gel 1 and gel 2, other methods can be tried such as the use of HRP mimetics like hematin or Fe-salen. We can also explore the cross-linking of gels containing Fmoc-Phe-(NH<sub>2</sub>)-OH using amino-reactive cross-linkers including genipin and glutaraldehyde. We will study the morphology of the DN hydrogels by electron microscopy and perform circular dichroism to determine if the presence of polyacrylamide or agarose has an influence on the amino acid self-assembly behavior. The mechanical properties will be studied by rheology. We will also analyze the stability of the gels under physiological conditions. The double network hydrogels containing baclofen may be tested into spasticity murine model of amyotrophic lateral sclerosis.

Finally, to consider their use as subcutaneous drug delivery systems, the behavior of the different gels will be tested via syringe injection. For topical applications, we will investigate the potential toxicity of the different hydrogels on human skin. We will also quantify the sensitizing or irritating potential of our gels by measuring the presence or absence of TNF- $\alpha$  released in the culture medium.

#### **CHAPTER 6. EXPERIMENTAL SECTION**

#### 6.1 Materials and Methods

#### 6.1.1 Amino acids

The amino acids L-tyrosine, L-histidine, L-tryptophan, Fmoc-Tyr(tBu)-OH, H-Tyr(Bzl)-OBzl·HCl, Z-Tyr-OMe, and Fmoc-Trp-OH were purchased from Sigma-Aldrich, and L-phenylalanine from Neo-MPS, respectively. H-Tyr-OBzl, Fmoc-Tyr(Bzl)-OH, and Z-Tyr(Bzl)-OH were acquired from Bachem, and Fmoc-Phe-OH, Fmoc-Tyr-OH, and Fmoc-His-OH from PolyPeptide Group. 4-azido-L-phenylalanine, Fmoc-4-azido-phenylalanine and Fmoc-Tyr(propargyl)-OH were purchased from Combi-block.

#### 6.1.2 Dipeptides

The dipeptides  $Boc-\alpha$ -Phe- $\alpha$ -Phe-OH,  $Boc-\beta$ -Phe- $\beta$ -Phe-OH and  $Boc-\gamma$ -Phe- $\gamma$ -Phe-OH were synthesized by Dr. Dinesh Bhimareddy, post-doctoral fellow in the group. The dityrosine derivatives  $Boc-\alpha$ -Tyr- $\alpha$ -Tyr-OH,  $Boc-\beta$ -Tyr- $\beta$ -Tyr-OH and  $Boc-\gamma$ -Tyr- $\gamma$ -Tyr-OH were synthesized by Dr. Olivier Chaloin, research engineer in the research unit.

#### 6.1.3 Carbon nanomaterials

The pristine multi-walled CNTs (20-30 nm diameter, 0.5-2  $\mu$ m length, 95% purity; batch 1240XH) were purchased from Nanostructured and Amorphous Materials. These CNTs were oxidized by Dr. B. Dinesh and Rym Soltani, PhD student in the group, following the protocol we reported in a previous work.<sup>1</sup> GO was obtained from Grupo Antolin.

#### 6.1.4 Chemicals and solvents

L-ascorbic acid, methylene blue, rhodamine B and baclofen was purchased from Sigma-Aldrich. Solvents such as DMSO, HCl, NaOH, HFIP and MeOH were used as analytical grade. RPMI-1640 Medium and Dulbecco's Modified Eagle Medium were purchased from Sigma-Aldrich and Lonza, respectively, and fetal bovine serum from Dominique Dutscher. Basic Agarose Premier MP Biomedicals was acquired from Fischer Scientist. Acrylamide/Bisacrylamide (40%), Tetramethylethylenediamine (TEMED) and ammonium persulfate (APS) were purchased from Euromedex (ref EU0062-B), Roth (2367.1) and Merck (ref A3678-100G) respectively. Paraformaldehyde aqueous solution was acquired from

Electron Microscopy Sciences (15710), Triton 100 X detergent from Bio-rad (1610407), Fixation/Permeabilization Solution Kit (RUO), BD Cytofix/Cytoperm™ from BD Biosciences (554714), PBS 1X from Lonza (BE17-516F/12) and Fluoromount-G® mounting medium from Electron Microscopy Sciences, Hatfield, PA. The antibodies were purchased from BD Biosciences.

#### 6.1.5 Characterization methods and instruments

#### a. <u>Sonication</u>

Sonication was performed in an ultrasonic bath Elmasonic P (100 W, 37 kHz).

#### b. <u>High performance liquid chromatography</u>

HPLC was performed using a Nucleosil 100-5 Waters  $C_{18}$  reverse phase HPLC column and a Waters Alliance e2695 separation module. The column was used with 1.2 mL·min<sup>-1</sup> flow rate of a gradient from 0 to 100% of B (A =  $H_2O/0.1\%$  TFA; B =  $CH_3CN/0.08\%$  TFA) for 20 min.

#### c. <u>UV-Vis-NIR spectroscopy</u>

UV-Vis-NIR spectra were recorded using a Varian Cary 5000 spectrophotometer, using 1 cm path quartz glass cuvettes.

#### d. <u>Transmission electron microscopy</u>

TEM analysis was performed with a Hitachi 7500 transmission electron microscope (Hitachi High Technologies Corporation, Tokyo, Japan) with an accelerative voltage of 80 kV equipped with an AMT Hamamatsu digital camera (Hamamatsu Photonics, Hamamatsu City, Japan). To prepare the TEM grids, 10 μL of each hydrogel or self-assembly tests were deposited onto a carbon-coated copper grid (Formvar/Carbon 300 Mesh; Cu from Delta Microscopies). The grids were allowed to dry under ambient condition. The observations were performed by Cathy Royer "Plateforme Imagerie in vitro" at the Center of Neurochemistry (INCI, Strasbourg, France).

#### e. <u>Scanning electron microscopy</u>

SEM analysis was performed on a SEM S-800 (Hitachi High Technologies Corporation, Tokyo, Japan) with an accelerative voltage of 5 kV. The samples were placed onto glass slides and

then allowed to stand for 1 h, after which the excess sample was removed with a filter paper. Samples were metallized by sputtering with Au/Pt (SCD030 BALZERS). The observations were performed by Cathy Royer "Plateforme Imagerie in vitro" at the Center of Neurochemistry (INCI, Strasbourg, France).

#### f. <u>Circular dichroism</u>

The binary mixture of amino acids in 2 % DMSO/H2O (v/v) were prepared and after sonication the solutions were directly transferred into a 0.05 mm path length quartz cuvette. The dipeptides gels were formed using the pH-switch method and after HCl addition, samples were transferred into a 0.05 mm path length quartz cuvette. CD spectra were recorded on a JASCO J-810 spectropolarimeter at room temperature from 350-190 nm with 1.0 nm step, a scanning speed of 100 nm/min and 1 s integration time.

#### g. <u>Rheological study</u>

Rheological properties were investigated by D. Collin at the Institut Charles Sadron (ICS, Strasbourg, France) using a controlled-stress rheometer (Haake, Mars III) working in oscillatory mode. The measuring cell used was concentric cylinders (Couette cell type). For the rheological study, the same protocol was followed for the sample preparation and for the shear measurements. Once prepared, the sample still in its liquid state, was introduced in the Couette cell and measurements of the complex shear modulus were performed over time to follow the evolution of the shear response from the liquid state to the gel state. The frequency f and the stress to the sample applied  $\sigma$  were 1 Hz and 0.2 Pa, respectively. After 20 h, these measurements were followed by shear measurements performed as a function of frequency. All the measurements were carried out at room temperature (20°C).

#### h. <u>Computational analysis</u>

#### Computational methods

The binary mixtures have been simulated by classical MD simulations using the AMBER16 software,<sup>2</sup> in which the potential energy U is empirically represented by a sum of bond, angle and dihedral deformations and by pair wise additive 1-6-12 (electrostatic + van der Waals) interactions between non-bonded atoms:

$$\begin{split} U &= \sum_{\text{bonds}} k_b (r-r_0)^2 + \sum_{\text{angles}} k_\theta (\theta-\theta_0)^2 + \sum_{\text{dihedrals}} V_n [1 + \cos(n\varphi-\gamma)] \\ &+ \sum_{i=1}^{N-1} \sum_{j=i+1}^{N} \left[ \frac{A_{ij}}{R_{ij}^{12}} - \frac{B_{ij}}{R_{ij}^6} + \frac{q_i \, q_j}{\epsilon_0 r_{i,j}} \right] \end{split}$$

Cross terms in van der Waals interactions were constructed using the Lorentz-Berthelot rules. Water was represented with the TIP3P model<sup>3</sup> and DMSO by the model developed by Fox and Kollman.<sup>4</sup> Fmoc molecules were represented with the parameters from AMBER99 force field and RESP charges. The 1-4 van der Waals and 1-4 coulombic interactions were scaled down by 2.0 and 1.2, respectively. The solutions were simulated with 3D-periodic boundary conditions, using an atom-based cutoff of 12 Å for non-bonded interactions, and correcting for the long-range electrostatics by using the Ewald summation method. The MD simulations were performed at 300 K starting with random velocities. The temperature was monitored via a coupling to a thermal bath using the Berendsen algorithm<sup>5</sup> with a relaxation time of 0.2 ps. In the (NPT) simulations, the pressure was similarly coupled to a barostat with a relaxation time of 0.2 ps. A time step of 2 fs was used to integrate the equations of motion via the Verlet leapfrog algorithm. For each system, a "random" mixture of the two amino acids was prepared in a box of water:DMSO 98:2. After 1000 steps of energy minimization, 0.25 ns of dynamics were performed with ions in order to allow the solvent to relax around the solute. This was followed by a dynamics of 0.25 ns at constant volume and of 1 ns at a constant pressure of 1 atm. The evolution of the mixture was then followed for 50 to 300 ns of dynamics (NVT ensemble).

#### **Analysis of the results**

The trajectories were analyzed using our MD simulations software.<sup>6</sup> Snapshots were drawn with the VMD software.<sup>7</sup>

#### 6.2 Experimental section

#### 6.2.1 Self-assembly

The samples were dissolved in MilliQ® water or in MeOH at a concentration of 0.5 mg.mL $^{-1}$ . Samples were sonicated 10 sec into an ultrasonic bath and left for 1 h before deposition of 10  $\mu$ L on a TEM grid, followed by evaporation of the drop at room temperature.

#### 6.2.2 Gelation

#### a. Gelation test using solvent-triggered method with amino acids

Each monomer was dissolved in DMSO to make stock solutions of 247 mM. Single amino acid solutions were prepared by dilution of the amino acids from the stock solutions in MilliQ® water to reach a concentration of 4.9 mM in 2 % DMSO/H<sub>2</sub>O (v/v). Binary mixtures were prepared by mixing each amino acid from the stock solutions in a 1:1 ratio followed by dilution in MilliQ® water to a final concentration of 4.9 mM (2.45 mM of each amino acid) in 2 % DMSO/H<sub>2</sub>O (v/v). After dilution each sample was sonicated in a water bath for 10 sec and left under ambient conditions. The gelation of the samples was confirmed by the vial inversion test by turning the vials upside down to observe whether the hydrogel is stable or not.

#### b. Gelation test using the solvent-triggered method with di-peptides

The dipeptide Boc- $\alpha$ -Phe- $\alpha$ -Phe-OH, Boc- $\beta$ -Phe- $\beta$ -Phe-OH or Boc- $\gamma$ -Phe- $\gamma$ -Phe-OH was dissolved in organic solvent (DMSO, HFIP or MeOH) at a concentration of 247 mM via 10 sec sonication to help the dissolution process. Then, the solution was diluted using MilliQ® water to reach a final concentration of 2.45, 4.9 or 9.8 mM in 2 % organic solvent/water (v/v), or 10 % organic solvent/water (v/v) and left under ambient conditions. The gelation of the samples was confirmed by the vial inversion test to observe if the hydrogel was stable.

#### c. <u>Gelation test using the pH-switch method with dipeptides</u>

The dipeptide was dissolved in a solution of 10 mM NaOH to reach a final concentration of 4.9 mM. Stirring and sonication were used to help the dissolution process. To turn the solution transparent to opaque, the minimum amount of HCl 0.5 M was added, 1 % (v/v) for Boc- $\alpha$ -Phe- $\alpha$ -Phe-OH and Boc- $\gamma$ -Phe-OH and 7 % (v/v) for Boc- $\beta$ -Phe- $\beta$ -Phe-OH. After gentle stirring, the samples were left under ambient conditions. The gelation was confirmed by the vial inversion test to observe if the gel was stable.

#### d. Double network hydrogel polyacrylamide/amino acid synthesis

Blank polyacrylamide hydrogels were prepared using acrylamide as the main monomer, bisacrylamide as the cross-linker, ammonium persulfate as the initiator and TEMED as catalyst. A precalculated volume of acrylamide/bisacrylamide (40%) were dissolved in MilliQ® water and vortexed to obtain the desired final concentration. APS was added to the solution and vortexed for a few seconds to homogenize the solution. TEMED was finally added to the solution before vortexing to initiate the polymerization.

The volume of acrylamide/bisacrylamide stock solution (40%) required in order to obtain the desired gel concentration (<40%) can be calculated as follow:

$$V = C \times \frac{V_{tot}}{40 \%}$$

Where V is the required volume of 40 % stock solution, C is the desired concentration and  $V_{tot}$  the total desired volume.

The amounts of each product are presented in the table below:

Final concentration in percentage	0.1 %	0.5 %	1 %	10 %
Acrylamide/Bisacrylamide 40 % (mL)	0.025	0.125	0.25	2.5
milliQ® water (mL)	9.975	9.875	9.75	7.5
10 % APS (μL)	50	50	50	50
TEMED (μL)	5	5	5	5
Total volume (mL)	10	10	10	10

The PAA/amino acid supramolecular hydrogels were formed by mixing 1 mL of a fresh solution of polyacrylamide and a solution of Fmoc-Y-OH/Fmoc-Y(BzI)-OH or Fmoc-F-OH/Fmoc-Y(BzI)-OH (4.9/4.9 mM) in 1 mL 4 % DMSO/ $H_2O$  (v/v) The full solution was gently homogenized and let under ambient conditions for hydrogelation.

#### e. <u>Double network hydrogel agarose/amino acid synthesis</u>

Blank agarose hydrogel 0.1% was obtained by heating a solution of 1 mg of agarose into 1 mL of MilliQ® water until obtaining a limpid solution and then cooling the mixture to room temperature to induce the hydrogelation. Same procedures were used with the different concentrations studied.

The agarose/amino acid supramolecular hydrogels were formed by mixing a hot solution of agarose in 1 mL of MilliQ® water and a hot solution of Fmoc-Y-OH/Fmoc-Y(BzI)-OH or Fmoc-F-OH/Fmoc-Y(BzI)-OH (4.9/4.9 mM) in 1 mL 4 % DMSO/H<sub>2</sub>O (v/v) and cooling the mixture to room temperature.

#### f. Gelation tests using phenylalanine derivatives for photo cross-linking procedures

Fmoc-Tyr(propargyl)-OH, Fmoc-4-azido-phenylalanine, 4-L-azido-phenylalanine, Fmoc-Tyr-OH, Fmoc-Phe-OH and Fmoc-Tyr(Bzl)-OH were dissolved in DMSO to make stock solutions of 247 mM. Binary mixtures were prepared by mixing each monomer from the stock solutions in a 1:1 ratio followed by dilution in MilliQ $^{\circ}$  water to a final concentration of 4.9 mM (2.45 mM of each monomer) in 2 % DMSO/H<sub>2</sub>O (v/v). After dilution, each sample was sonicated in a water bath for 10 sec and left under ambient conditions. The gelation of the samples was confirmed by the vial inversion test by turning the vials upside down to observe whether the hydrogel is stable or not.

#### **6.2.3** Incorporation of carbon nanomaterials

#### a. Amino acid hydrogels

The pristine CNTs, ox-CNTs, or GO were dispersed in MilliQ® water at three different concentrations: 255  $\mu g \cdot m L^{-1}$  (0.025 wt%), 1.26  $m g \cdot m L^{-1}$  (0.1 wt%), and 6.3  $m g \cdot m L^{-1}$  (0.5 wt%). The suspensions were added to the amino acid solution of gel 1 or gel 2 in DMSO (247 mM) to reach a final concentration of monomer of 4.9 mM in 2 % DMSO/H<sub>2</sub>O (v/v). The suspensions were sonicated for 10 sec in a water bath and left under ambient conditions.

#### b. Dipeptide hydrogels

GO and ox-CNTs were incorporated in the hydrogels prepared using the pH-switch method. Before the addition of HCl, 100  $\mu$ g of ox-CNTs or GO powder were dispersed in the basic dipeptide solution of 400  $\mu$ L by sonication in a water bath for 10 and 3 min, respectively (final concentration of carbon nanomaterials was 255  $\mu$ g·mL<sup>-1</sup>). The gelation in presence of carbon nanomaterials was performed as previously described by the acidification of the basic dipeptide solution.

#### c. Double network hydrogels

GO and ox-CNTs were first dispersed in MilliQ® water at a 255  $\mu g \cdot m L^{-1}$  by sonication in a water bath and added to the amino acid solution of gel 1 or gel 2 in DMSO to reach a final concentration of monomer of 4.9/4.9 mM in 1 mL 4 % DMSO/H<sub>2</sub>O. A volume of 1 mL of a fresh acrylamide solution or hot agarose solution was mixed with the fresh amino acid supramolecular solution containing carbon nanomaterials and left under ambient condition for hydrogelation.

#### 6.2.4 Drug loading

#### a. <u>Amino acid hydrogels</u>

To prepare the methylene blue-loaded hydrogels, the amino acid solutions of Fmoc-Tyr-OH/Fmoc-Tyr(Bzl)-OH (gel 1) or Fmoc-Phe-OH/Fmoc-Tyr(Bzl)-OH (gel 2) in DMSO were diluted in a solution of methylene blue in MilliQ® water at different concentrations from 30  $\mu g \cdot m L^{-1}$  to 300  $\mu g \cdot m L^{-1}$ . The stability of the gels was tested by the vial inversion procedure. The hybrid gels were obtained by dispersing the ox-CNTs or GO at a concentration of 255  $\mu g \cdot m L^{-1}$  (0.025 wt%) in a solution of methylene blue in MilliQ® water (0.1  $m g \cdot m L^{-1}$ ). After sonication for 10 min in a water bath, the amino acid solution in DMSO was added. The suspensions were sonicated for 10 sec in a water bath and left under ambient conditions.

To prepare the rhodamine B base-loaded hydrogels, the amino acid solutions of Fmoc-Tyr-OH/Fmoc-Tyr(Bzl)-OH (gel 1) or Fmoc-Phe-OH/Fmoc-Tyr(Bzl)-OH (gel 2) in DMSO were diluted in a solution of rhodamine B base in MilliQ® water at different concentrations from 1 mg.mL $^1$  to 1.5 mg·mL $^{-1}$ . The stability of the gels was tested by the vial inversion procedure. The hybrid gels were obtained by dispersing the ox-CNTs or GO at a concentration of 255  $\mu$ g·mL $^{-1}$  (0.025 wt%) in a solution of methylene blue in MilliQ® water (1 mg·mL $^{-1}$ ). After sonication for 10 min in a water bath, the amino acid solution in DMSO was added. The suspensions were sonicated for 10 sec in a water bath and left under ambient conditions.

To prepare the L-ascorbic acid-loaded hydrogels, the amino acid solutions of Fmoc-Tyr-OH/Fmoc-Tyr(BzI)-OH (gel 1) or Fmoc-Phe-OH/Fmoc-Tyr(BzI)-OH (gel 2) in DMSO were diluted in a solution of L-ascorbic acid in MilliQ® water (0.7 mg·mL $^{-1}$ ). The hybrid gels were obtained by dispersing the ox-CNTs or GO at a concentration of 255  $\mu$ g·mL $^{-1}$  (0.025 wt%) in a

solution of L-ascorbic acid in MilliQ® water (0.7 mg·mL<sup>-1</sup>). After sonication for 10 min in a water bath, the amino acid solution in DMSO was added. The suspensions were sonicated for 10 sec in a water bath and left under ambient conditions.

#### b. <u>Dipeptide hydrogels</u>

The Boc-diphenylalanine homologues were dissolved in 10 mM NaOH at a final concentration of 4.9 mM. Stirring and sonication helped the dissolution process. Then, ox-CNTs or GO were incorporated into the gels and dispersed thanks to sonication (final concentration of the nanomaterials: 0.025 wt%). L-ascorbic acid was finally incorporated at a final concentration of 0.7 mg·mL<sup>-1</sup> and HCl 0.5 M was added to trigger the gelation.

#### c. <u>Double network hydrogels</u>

Baclofen was dissolved in MilliQ® water at an initial concentration of 2 mg·mL $^{-1}$ . GO and ox-CNTs were dispersed in the baclofen aqueous solution at a concentration of 255 µg·mL $^{-1}$  and added to the amino acid solution of gel 1 or gel 2 in DMSO to reach a final concentration of monomer of 4.9/4.9 mM in 1 mL 4 % DMSO/H<sub>2</sub>O. A volume of 1 mL of a fresh acrylamide solution or hot agarose solution were mixed with the fresh amino acid supramolecular solution containing the carbon nanomaterials and baclofen and left under ambient condition for hydrogelation.

#### 6.2.5 Cross-linking

#### a. <u>Cross-linking of ι-tyrosine with HRP followed by UV-Vis spectroscopy</u>

1.065 g of ammonium acetate was diluted in 250 mL of MilliQ® (50 mM) water. The pH was adjusted to 8.7 using an aqueous solution of NaOH. An amount of 25 mg of L-tyrosine (0.5 mM) was dissolved in the buffer solution which was left to stand for 1 h under agitation. 6 mg of HRP were added (final concentration of 0.5  $\mu$ M). The reaction was initiated by the addition of 53.5  $\mu$ L (2 mM) of hydrogen peroxide (H<sub>2</sub>O<sub>2</sub> 35 wt%). The reaction was monitored by UV/Vis spectroscopy every hour for 4 hours.

# b. <u>Cross-linking of L-tyrosine and tyrosine derivatives with HRP followed by</u> fluorescence spectroscopy

Stock solutions of 2.47 mM of L-tyrosine in water, 1 mM of HRP and 2.5 mM of  $H_2O_2$  were prepared in water, kept on ice, and protected from light. 10  $\mu$ L of HRP were added to 990  $\mu$ L of L-tyrosine in a 1 cm quartz cuvette to keep the final concentration of L-tyrosine at 2.45 mM. To test the influence of  $H_2O_2$  concentration, 2  $\mu$ L of the hydrogen peroxide stock solution were added by successive additions every 5 or 10 min from 0 to 40  $\mu$ L with mixing. The emission spectra were recorded with  $\lambda_{ex}$  = 260 nm and  $\lambda_{em}$  = [270-500] nm for L-tyrosine and  $\lambda_{ex}$  = 325 nm and  $\lambda_{em}$  = [350-580] nm for dityrosine at 350 V within a few sec to 1 min after the addition of hydrogen peroxide. Similar procedures were used with Fmoc-tyrosine, N-acetyl-L-tyrosine, and N-tert-butyl-L-tyrosine with a unique addition of 2  $\mu$ L N-202 (5  $\mu$ M). The emission spectra were recorded with N-201 nm and N-210 nm for the tyrosine derivatives and N-211 nm and N-212 nm and N-213 nm for dityrosine at 350 V within a few sec to 1 min after the addition of hydrogen peroxide.

#### c. <u>Cross-linking of L-tyrosine and Fmoc-tyrosine with HRP followed by HPLC</u>

HPLC chromatograms of L-tyrosine (tr = 4.65 min), L-tyrosine + 0.1 mM of HRP, L-tyrosine + 0.1 mM of HRP + 5  $\mu$ M of H<sub>2</sub>O<sub>2</sub> in water and Fmoc-tyrosine (tr = 13.25 min), Fmoc-tyrosine + 0.1 mM HRP + 5  $\mu$ M of H<sub>2</sub>O<sub>2</sub> in water were record at 220 nm using a 0-100 gradient on C<sub>18</sub> column with 10  $\mu$ L injection.

# d. <u>Cross-linking of L-tyrosine by Fenton and photo-Fenton reactions followed by</u> <u>fluorescence spectroscopy</u>

From stock solution freshly prepared in water, 100  $\mu$ L of L-tyrosine, 10  $\mu$ L of FeSO<sub>4</sub> or CuCl<sub>2</sub> and 890  $\mu$ L of H<sub>2</sub>O<sub>2</sub> were mixed in a 1 cm quartz cuvette to obtain final concentrations of 2.45 mM of L-tyrosine, 1 mM of FeSO<sub>4</sub> or CuCl<sub>2</sub> and 3.4 mM of H<sub>2</sub>O<sub>2</sub>. The emission spectra were recorded with  $\lambda_{ex}$  = 260 nm and  $\lambda_{em}$  = [270-500] nm for L-tyrosine and  $\lambda_{ex}$  =325 nm and  $\lambda_{em}$  = [350-580] nm for dityrosine at 350 V. The same procedures were performed using UV irradiation of 254 nm for 1 h with FeSO<sub>4</sub> or CuCl<sub>2</sub>.

#### e. <u>Cross-linking of L-tyrosine by Fenton and photo-Fenton reactions followed by HPLC</u>

HPLC chromatograms of L-tyrosine (tr = 4.65 min) and L-tyrosine + 1 mM of  $CuCl_2$  + 3.4 mM of  $H_2O_2$  in water after 1 h of irradiation at 254 nm were recorded at 220 nm using a 0-100 gradient on  $C_{18}$  column with 10  $\mu L$  injection.

# f. <u>Cross-linking of Fmoc-tyrosine by Fenton and photo-Fenton reactions followed by</u> fluorescence spectroscopy

From stock solution freshly prepared in water, 100  $\mu$ L of Fmoc-tyrosine, 10  $\mu$ L of FeSO<sub>4</sub> or CuCl<sub>2</sub> and 890  $\mu$ L of H<sub>2</sub>O<sub>2</sub> were mixed in a 1 cm quartz cuvette to obtain final concentrations of 2.45 mM of Fmoc-tyrosine, 1 mM of FeSO<sub>4</sub> or CuCl<sub>2</sub> and 3.4 mM of H<sub>2</sub>O<sub>2</sub>. The emission spectra were recorded every hours during 6 h with  $\lambda_{ex}$  = 300 nm and  $\lambda_{em}$  = [310-550] nm for Fmoc-tyrosine at 350 V. The same procedures were performed using UV irradiation of 365 nm or 254 nm for 6 h with FeSO<sub>4</sub> or an irradiation of 254 nm for 3 h with CuCl<sub>2</sub>.

#### g. <u>Cross-linking of Fmoc-tyrosine by Fenton and photo-Fenton reactions followed HPLC</u>

HPLC chromatograms of Fmoc-tyrosine, and Fmoc-tyrosine + FeSO<sub>4</sub> or CuCl<sub>2</sub> 1 mM +  $H_2O_2$  3.4 mM under 3 h irradiation at 254 nm in water were recorded at 220 nm using a 0-100 gradient on  $C_{18}$  column with 10  $\mu$ L injection.

#### h. Cross-linking using Fremy's salt

Fremy's salt was dissolved in water and i) added to Fmoc-Y-OH dissolved in DMSO to obtain a final concentration of 2.45 mM Fmoc-Y-OH for 7.35 mM Fremy's salt (ratio 1:3) in 2 % DMSO/H<sub>2</sub>O, or ii) added to the binary mixture Fmoc-Y-OH/Fmoc-Y(BzI)-OH to obtain a final concentration of 2.45 mM/2.45 mM of Fmoc-Y-OH/Fmoc-Y(BzI)-OH for 14.7 mM Fremy's salt (ratio 1:3) in 2 % DMSO/H<sub>2</sub>O. The sample were left under ambient condition until precipitation and analyzed by HPLC at 220 nm using a 0-100 gradient on C18 column with 10  $\mu$ L injection with retention times of Fmoc-Y-OH = 13.25 min and Fmoc-Y(BzI)-OH = 16.8 min.

#### i. <u>Cross-linking using tyrosinase</u>

L-Tyrosine (0.4 mg) was dissolved in 1 mL of MilliQ® water, sonicated until dissolution and mixed with 10 μL of tyrosinase solution (10 kU·mL<sup>-1</sup> in PBS). After incubation for 2 h under stirring 4 mg of FeCl<sub>2</sub> in 10 μL of MilliQ® water were added. The reaction was monitored by

UV/Vis spectroscopy. The same procedure was performed with Fmoc-tyrosine with an overnight incubation and dopamine·HCl with 2 h of incubation before the addition of FeCl<sub>2</sub>.

#### j. Photo cross-linking using phenylalanine derivatives

Single or binary mixture of 4-azido-L-Phe, Fmoc-4-azido-phenylalanine, Fmoc-Tyr(propargyl)-OH, Fmoc-Tyr-OH or L-tyrosine were dissolved in water or in water + 2 % DMSO in a 1 cm quartz cuvette. The sample were left under ambient condition or under UV irradiation using a UV lamp of 254 nm or 365 nm. The reactions were followed by UV-Vis spectroscopy and HPLC. Different tests mixing two amino acid derivatives in different proportions were also performed. For the tests performed on gels 4-azido-Phe/Fmoc-Tyr-OH, Fmoc-4-azido-phenylalanine/Fmoc-Tyr-OH the UV irradiation at 254 nm and 365 nm was applied during the gelation process, directly after the addition of water to the amino acids in DMSO. For the gels 4-azido-Phe/Fmoc-Tyr-OH and Fmoc-Tyr(propargyl)-OH/Fmoc-Y(Bzl)-OH the UV-Vis irradiation was applied on the pre-formed gel after the 2 h of gelation.

#### 6.2.6 Photothermal studies

#### a. <u>Carbon nanomaterials</u>

Different concentrations of ox-CNTs and GO in MilliQ® water (0.005 wt%, 0.01 wt%, and 0.025 wt%) were sonicated for 10 min to obtain highly dispersed suspensions. Native and hybrid gels were synthesized and left for gelation for 2 h under ambient conditions. The photothermal conversion of the carbon nanomaterial suspensions and the heating profile of the gels were examined by monitoring the temperature increase during exposure to 808 nm laser with a power of 2 W·cm<sup>-2</sup> for 10 min. Each photothermal measurement was repeated three times. Maximum temperatures and infrared thermographic maps were recorded by an infrared thermal imaging camera.

#### b. <u>Hydrogels</u>

Heating profiles were obtained by monitoring the temperature increase during exposure to 808 nm laser with a power of 2 W·cm<sup>-2</sup> for 10 min. Each photothermal measurement was repeated three times. Maximum temperatures and infrared thermographic maps were recorded by an infrared thermal imaging camera FLIR.

#### 6.2.7 Drug release

#### a. <u>Amino acid hydrogels</u>

#### Release of methylene blue or rhodamine B base

NIR light irradiation (at 808 nm, under 2 W·cm- $^2$  for 10 min, at a distance of 3 cm from the gels) was applied on the gels after 2 h of gelation to avoid any significant drug degradation. The volume of released water was withdrawn, centrifuged (12300 rpm, 10 min), and the amount of methylene blue (Figure 6.1) or rhodamine B base (Figure 6.2) was assessed by UV-Vis spectroscopy (Abs = 664 nm for methylene blue and Abs = 554 nm for rhodamine B base).

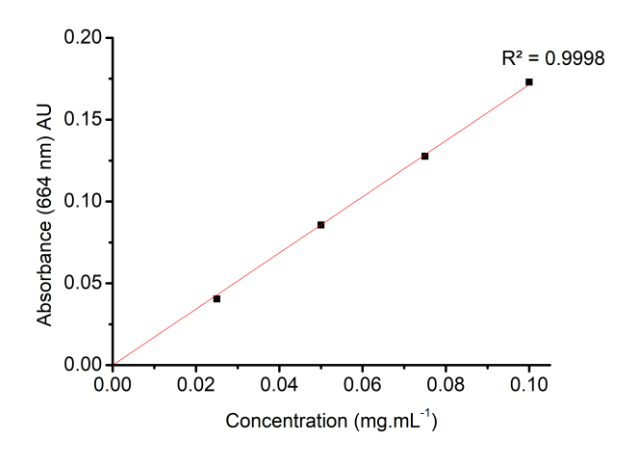


Figure 6.1 Calibration curve of methylene blue at 664 nm by UV-Vis absorbance

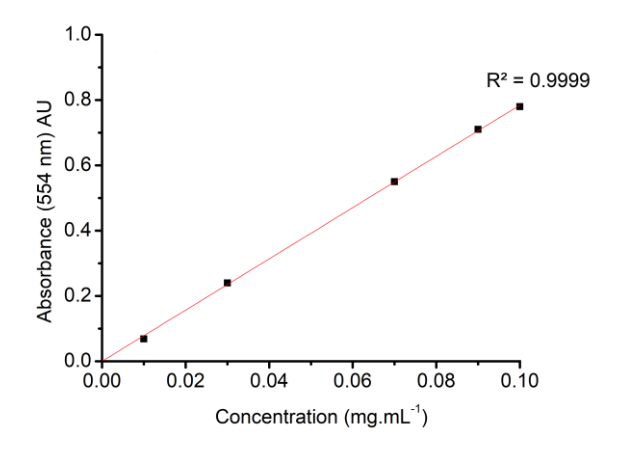


Figure 6.2. Calibration curve of rhodamine B base at 554 nm by UV-Vis absorbance

#### Release of I-ascorbic acid

NIR light irradiation (at 808 nm, under 2 W for 10 min, at a distance of 3 cm from the gels) was applied on the gels after 2 h of gelation to avoid any significant drug degradation. The volume of released water was withdrawn, centrifuged (12300 rpm, 10 min), and the amount of L-ascorbic acid (Figure 6.3) was assessed by HPLC ( $t_r$  = 2.3 min at  $\lambda$  = 254 nm for L-ascorbic acid). Statistical analysis was performed with Prism 7.0 (GraphPad Software). Data were analyzed with one-way-ANOVA (including Bonferroni multiple comparison test). A p value of < 0.05 was considered as significant.

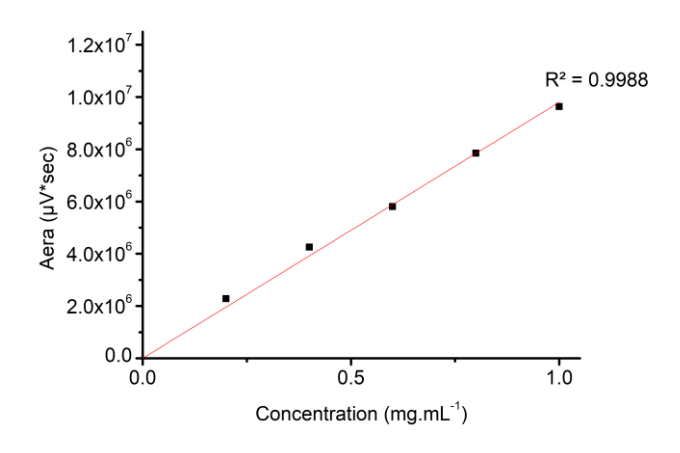


Figure 6.3. Calibration curve of for L-ascorbic acid (tr = 2.3 min) at 220 nm by HPLC

#### b. <u>Dipeptide hydrogels</u>

NIR light irradiation (808 nm, 2 W.cm<sup>-2</sup> for 10 min) was applied on the gels. The volume of released water was withdrawn, centrifuged (12300 rpm, 10 min), and the amount of L-ascorbic acid was assessed by HPLC (tr = 2.08 min at  $\lambda$  = 220 nm for L-ascorbic acid).

#### c. Double network hydrogels

NIR light irradiation (808 nm, 2 W·cm<sup>-2</sup> for 10 min) was applied on the gels. The volume of released water was withdrawn, centrifuged (12300 rpm, 10 min), and the amount of baclofen (Figure 6.4) was assessed by HPLC (tr = 7.2 min at  $\lambda$  = 220 nm for baclofen).

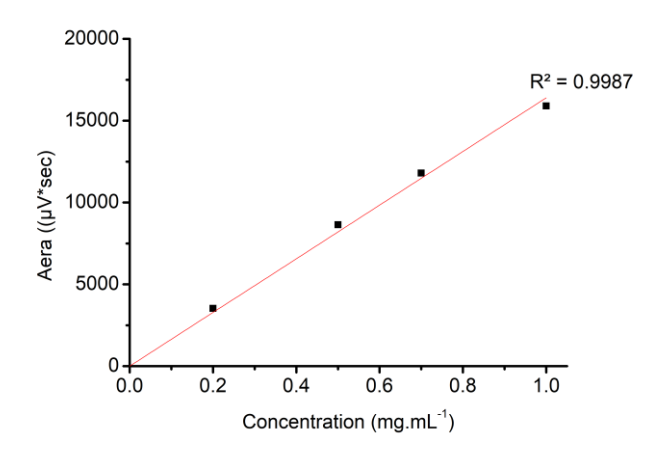


Figure 6.4. Calibration curve of baclofen (tr = 7.2 min) at 220 nm by HPLC

#### 6.2.8 Stability studies in physiological conditions

A volume of 100  $\mu$ L of physiological saline solution (0.9% NaCl in MilliQ® water) or RPMI or DMEM supplemented with 10% fetal bovine serum was added on top of each hydrogel (400  $\mu$ L). After 15 h the solution was withdrawn, centrifuged (12300 rpm, 5 min), and the amount of L-ascorbic acid was determined by HPLC (gradient 0-100 in C<sub>18</sub> column at 220 nm).

#### 6.2.9 Skin sensibilisation

Skin sensibilization experiments were performed in collaboration with the Dr. Q. Muller and A. Hoste in our unit at the Molecular and Cellular Biology Institute (IBMC, Strasbourg, France). An explant of normal human skin, with a surface area of 4 cm² and a thickness of 800 μm, was placed on a nylon filter in RPMI at 37 °C for 24 hours. After the settling time of 24 h the skin samples were fixed in 4 % paraformaldehyde for 20 min at room temperature. Skin samples were permeabilized and saturated for 1 h with a 2 % bovine serum albumin solution (bovine serum albumin, BSA), supplemented with 0.1% Triton 100X in PBS 1X, then washed in PBS 1X. Primary antibodies, at optimal dilution (around 100 and 200 ng·mL<sup>-1</sup>) in PBS 1X + BSA 2 % were incubated overnight at 4 °C. After a series of PBS washings, the secondary antibodies, at optimal dilution (between 0.5 and 2 μg·mL<sup>-1</sup>, according to the supplier's recommendations) in PBS 1X + BSA 2 %, were incubated on the samples for 1-2 h at room temperature, protected from light. Cell nuclei labelling with 4',6-diamidino-2-phenylindole (DAPI) was done at the same time as the secondary antibody at 0.5 μg·mL<sup>-1</sup> and left for 20 min at room temperature, protected from light at 5 μg·mL<sup>-1</sup> in PBS.

The samples were observed with the Confocal LSM700 microscope from Zeiss and the images were acquired by the proprietary ZEN 2010 software. The raw images with the .zvi or .lsm extension were analyzed by the royalty-free software ImageJ in its version ImageJ-2 Fiji. After multiple PBS washings, the samples were included in Fluoromount-G® mounting medium. Indirect immunofluorescence labeled skin samples were included between two glass slides to allow proper orientation when observing under the microscope. Incubation for 24 to 48 h at room temperature and protected from light, was necessary for complete polymerization of the mounting medium.

#### **6.3** References

- Samorì, C.; Sainz, R.; Ménard-Moyon, C.; Toma, F. M.; Venturelli, E.; Singh, P.; Ballestri, M.; Prato, M.; Bianco, A. Potentiometric Titration as a Straightforward Method to Assess the Number of Functional Groups on Shortened Carbon Nanotubes. *Carbon* 2010, 48, 2447–2454.
- Case, D. A.; Cerutti, D. S.; Cheatham, T. E.; Darden, T. A.; Duke, R. E.; Giese, T. J.; Gohlke, H.; Goetz, A. W.; Greene, D.; Homeyer, N.; Izadi, S.; Kovalenko, A.; Lee, T. S.; LeGrand, S.; Li, P.; Lin, C.; Liu, J.; Luchko, T.; Luo, R.; Mermelstein, D.; Merz, K. M.; Monard, G.; Nguyen, H.; Omelyan, I.; Onufriev, A.; Pan, F.; Qi, R.; Roe, D. R.; Roitberg, A.; Sagui, C.; Simmerling, C. L.; Botello-Smith, W. M.; Swails, J.; Walker, R. C.; Wang, J.; Wolf, R. M.; Wu, X.; Xiao, L.; York, D. M.; Kollman, P. A. Amber 2017, Reference Manual Principal Contributors to the Current Codes, University of California, San Francisco, 2017.
- 3. Jorgensen, W. L.; Chandrasekhar, J.; Madura, J. D.; Impey, R. W.; Klein, M. L. Comparison of Simple Potential Functions for Simulating Liquid Water. J. Chem. Phys. 1983, 79, 926–935.
- 4. Fox, T.; Kollman, P. A. Application of the RESP Methodology in the Parametrization of Organic Solvents. J. Phys. Chem. B 1998, 102, 8070–8079.
- 5. Berendsen, H. J. C.; Postma, J. P. M.; van Gunsteren, W. F.; DiNola, A.; Haak, J. R. Molecular Dynamics with Coupling to an External Bath. J. Chem. Phys. 1984, 81, 3684–3690.
- 6. Engler, E.; Wipff, G. MD-DRAW Software. Display of Dynamic Structures from MD Simulations. In Crystallography of Supramolecular Compounds, Kluwer Dordrecht.; Tsoucaris, G., Ed.; Nato Science Series C; 1996.
- 7. Humphrey, W.; Dalke, A.; Schulten, K. VMD: Visual Molecular Dynamics. J. Mol. Graph. 1996, 14, 33–38.

#### LIST OF PUBLICATIONS AND COMMUNICATIONS

#### **Publications**

- <u>Guilbaud-Chéreau, C.</u>; Dinesh, B.; Schurhammer, R.; Collin, D.; Bianco, A.; Ménard-Moyon, C. Protected Amino Acid-Based Hydrogels Incorporating Carbon Nanomaterials for Near-Infrared Irradiation-Triggered Drug Release. ACS Appl. Mater. Interfaces 2019, 11 (14), 13147–13157.
- Aloisi, A.; Christensen, N. J.; Sørensen, K. K.; <u>Guilbaud-Chéreau, C.;</u> Jensen, K. J.; Bianco, A. Synthesis and Characterization of Adamantane-Containing Heteropeptides with a Chirality Switch. European Journal of Organic Chemistry 2020, 2020 (7), 815–820.

#### **Communications**

- <u>Guilbaud-Chéreau, C.</u>, Bianco, A., Ménard-Moyon. Amino acids based hydrogels in combination with carbon nanomaterials for controlled drug released, Colloque Francophone du Carbone, Obernai, 15-18 may 2018,
- <u>Guilbaud-Chéreau, C.</u>, Bianco, A., Ménard-Moyon. Self-assembled amino acids- and peptides-based hydrogels in combination with carbon nanomaterials, Journée des doctorants de l'école doctorale des Sciences Chimiques, Strasbourg, 3 december 2019



### Chloé GUILBAUD-CHÉREAU



# Development of supramolecular medical hydrogels based on amino acids and dipeptides in combination with carbon nanomaterials

## Résumé

Les hydrogels supramoléculaires à base d'acides aminés ou de petits peptides ont fait l'objet d'une grande attention ces dernières années pour diverses applications médicales grâce à leur biocompatibilité.

Dans ce contexte, nous avons développé des gels supramoléculaires à base d'acides aminés aromatiques protégés par le groupement Fmoc et d'homologues de Boc-diphénylalanine. Nous avons étudié en détail la gélification des gels obtenus et leurs propriétés.

Des nanotubes de carbone oxydés et de l'oxyde de graphène ont également été incorporés dans ces hydrogels et la chaleur générée par les nanomatériaux carbonés lors de l'irradiation dans le proche infrarouge a induit la libération d'acide L-ascorbique à un taux élevé.

Nous avons essayé plusieurs stratégies de cross-linking pour améliorer les propriétés mécaniques des gels supramoléculaires. Comma alternative, des gels à double réseau ont été développés par introduction de polyacrylamide ou d'agarose. Nous avons réalisé l'incorporation de baclofène dans les gels et étudié son relargage sous irradiation infrarouge. Le baclofène est prescrit contre la spasticité musculaire qui accompagne de nombreux troubles neurologiques comme la sclérose latérale amyotrophique ou la sclérose en plaques.

Mots clés : hydrogel, acides aminés, diphénylalanine, auto-assemblage, nanotubes de carbone, oxyde de graphène, relargage de médicaments, double réseau, baclofène

## Résumé en anglais

Supramolecular hydrogels made of amino acids or small peptides have received a lot of attention in recent years for various medical applications due to their biocompatibility.

In this context, we have developed supramolecular gels based on aromatic amino acids protected by the Fmoc moiety and Boc-diphenylalanine analogs. We have studied in detail the gelation process of and the gel properties.

Oxidized carbon nanotubes and graphene oxide were also incorporated in these hydrogels and the heat generated by the carbon nanomaterials during near-infrared irradiation induced the release of L-ascorbic acid at a high rate.

We have tried several cross-linking strategies to improve the mechanical properties of the supramolecular hydrogels. As an alterntaive, we developed double-network gels by introducing polyacrylamide and agarose. We performed the incorporation of baclofen and studied its release under infrared irradiation. Baclofen is prescribed against muscle spasticity associated with many neurological disorders such as amyotrophic lateral sclerosis or multiple sclerosis.

Keywords: hydrogel, amino acids, diphenylalanine, self-assembly, carbon nanotubes, graphene oxide, drug delivery, double network, baclofen